



UvA-DARE (Digital Academic Repository)

Arterial spin labeling perfusion MRI: Inter-vendor reproducibility and clinical applicability

Mutsaerts, H.J.M.M.

Publication date

2015

Document Version

Final published version

[Link to publication](#)

Citation for published version (APA):

Mutsaerts, H. J. M. M. (2015). *Arterial spin labeling perfusion MRI: Inter-vendor reproducibility and clinical applicability*.

General rights

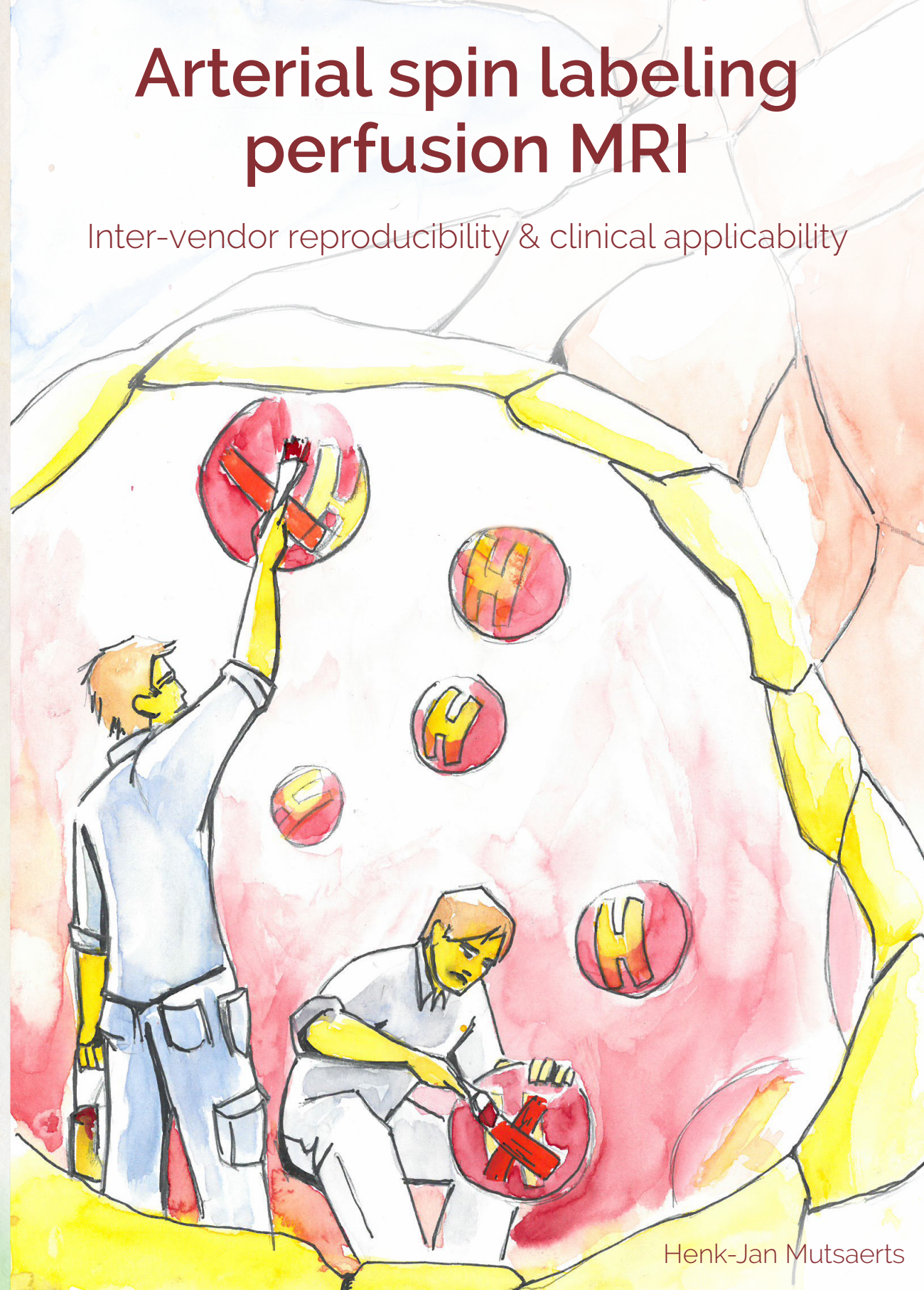
It is not permitted to download or to forward/distribute the text or part of it without the consent of the author(s) and/or copyright holder(s), other than for strictly personal, individual use, unless the work is under an open content license (like Creative Commons).

Disclaimer/Complaints regulations

If you believe that digital publication of certain material infringes any of your rights or (privacy) interests, please let the Library know, stating your reasons. In case of a legitimate complaint, the Library will make the material inaccessible and/or remove it from the website. Please Ask the Library: <https://uba.uva.nl/en/contact>, or a letter to: Library of the University of Amsterdam, Secretariat, Singel 425, 1012 WP Amsterdam, The Netherlands. You will be contacted as soon as possible.

Arterial spin labeling perfusion MRI

Inter-vendor reproducibility & clinical applicability



Arterial spin labeling perfusion MRI

Inter-vendor reproducibility & clinical applicability

The printing of this thesis was financially supported by the department of Radiology, Academic Medical Center, Amsterdam, the Netherlands and by NutsOhra Foundation grant 1002-031.

Copyright © HJMM Mutsaerts, Amsterdam, The Netherlands

No part of this thesis may be reproduced, stored or transmitted in any form or by any means, without prior permission by the author.

Cover design by F van Meurs. This Figure shows a transversal slice of a single carotid artery during labeling (control image not shown).

Printed by: Off Page

ISBN: 978-94-6182-542-1

ARTERIAL SPIN LABELING PERFUSION MRI
Inter-vendor reproducibility and clinical applicability

ACADEMISCH PROEFSCHRIFT

ter verkrijging van de graad van doctor
aan de Universiteit van Amsterdam
op gezag van de Rector Magnificus
prof. dr. D.C. van den Boom
ten overstaan van een door het College voor Promoties
ingestelde commissie,
in het openbaar te verdedigen in de Agnietenkapel
op 26 maart 2015, te 14:00 uur

door

Henri Jean Maximilien Marie Mutsaerts
geboren te 's-Hertogenbosch

Promotiecommissie

Promotor:	Prof. dr. C.B.L.M. Majoie	Universiteit van Amsterdam
Copromotor:	Dr. ir. A.J. Nederveen	Universiteit van Amsterdam
Overige leden:	Prof. dr. E.T. van Bavel	Universiteit van Amsterdam
	Prof. dr. X. Golay	University College London
	Dr. J. Hendrikse	UMC Utrecht
	Prof. dr. A. Bjørnerud	Oslo University Hospital
	Dr. L. Reneman	Universiteit van Amsterdam
	Prof. dr. J. Booiij	Universiteit van Amsterdam
Faculteit:	Geneeskunde	

Contents

Contents

Chapter 1	7
General introduction and outline	
<u>Part I Inter-vendor reproducibility of arterial spin labeling</u>	
Chapter 2	39
Inter-vendor reproducibility of pseudo-continuous arterial spin labeling at 3 Tesla	
Chapter 3	59
Reproducibility of pharmacological ASL using sequences from different vendors: implications for multi-center drug studies	
Chapter 4	79
Quantitative functional arterial spin labeling (fASL) MRI – sensitivity and reproducibility of regional CBF changes using pseudo-continuous ASL product sequences	
Chapter 5	102
Multi-vendor reliability of arterial spin labeling perfusion MRI using a near-identical sequence: implications for multi-center studies	
<u>Part II Clinical applicability of arterial spin labeling</u>	
Chapter 6	128
Gray matter contamination in arterial spin labeling white matter perfusion measurements in patients with dementia	
Chapter 7	143
Cerebral perfusion measurements in the elderly using arterial spin labeling	
Chapter 8	157
White matter hyperintensities in hypertension are not related to general perfusion deficits	
Chapter 9	175
Risk factor analysis of cerebral white matter hyperintensities in children with sickle cell disease	

Chapter 10	195
General discussion, conclusions and implications	
Chapter 11	211
Summary	
Appendix	
List of abbreviations	218
Portfolio	224
List of publications	227
Curriculum Vitae	230
Acknowledgments	232

1

General introduction and outline

Cerebral perfusion

Blood flow is one of the most fundamental physiological parameters, being responsible for the delivery of oxygen and nutrients to biological tissue. Maintenance of adequate cerebral blood flow (CBF) is of vital importance for the health, growth and repair of brain tissue². CBF is commonly expressed as the volume of blood that flows through 100 grams of brain tissue each minute (mL/100g/min). CBF is determined by the cerebral perfusion pressure (CPP) and cerebrovascular resistance (CVR), with the following relationship^{2,3}:

$$\text{CBF} = \frac{\text{CPP}}{\text{CVR}} \quad [1]$$

CPP is the net pressure gradient, causing blood to flow from the proximal supplying vasculature to distal vasculature in the brain. CVR is the resistance offered by the cerebral vasculature to the CPP. The vessel walls of intra-cerebral arteries contain smooth muscle tissue that enable vasoconstriction upon contraction and vasodilation upon relaxation⁴. By transitionally varying the tone of the smooth muscles, the cerebral vasculature can regulate the CBF locally⁵. If CPP falls - within the autoregulatory CPP range (CPP>60 mm Hg, Figure 1) - the cerebral arteries dilate, reducing CVR, increasing cerebral blood volume (CBV) and bringing CBF back to its original level within seconds. These rapid vascular adaptations to changes in CPP are known as the dynamic cerebral autoregulation³. A second compensatory mechanism is the variation of the oxygen extraction fraction (OEF), which is the fraction of oxygen which is extracted from blood for metabolic use. If CBF decreases, the OEF will increase. These two mechanisms simultaneously keep the cerebral metabolic rate of oxygen (CMRO₂) at a constant level, which is important to keep in mind when interpreting CBF values.

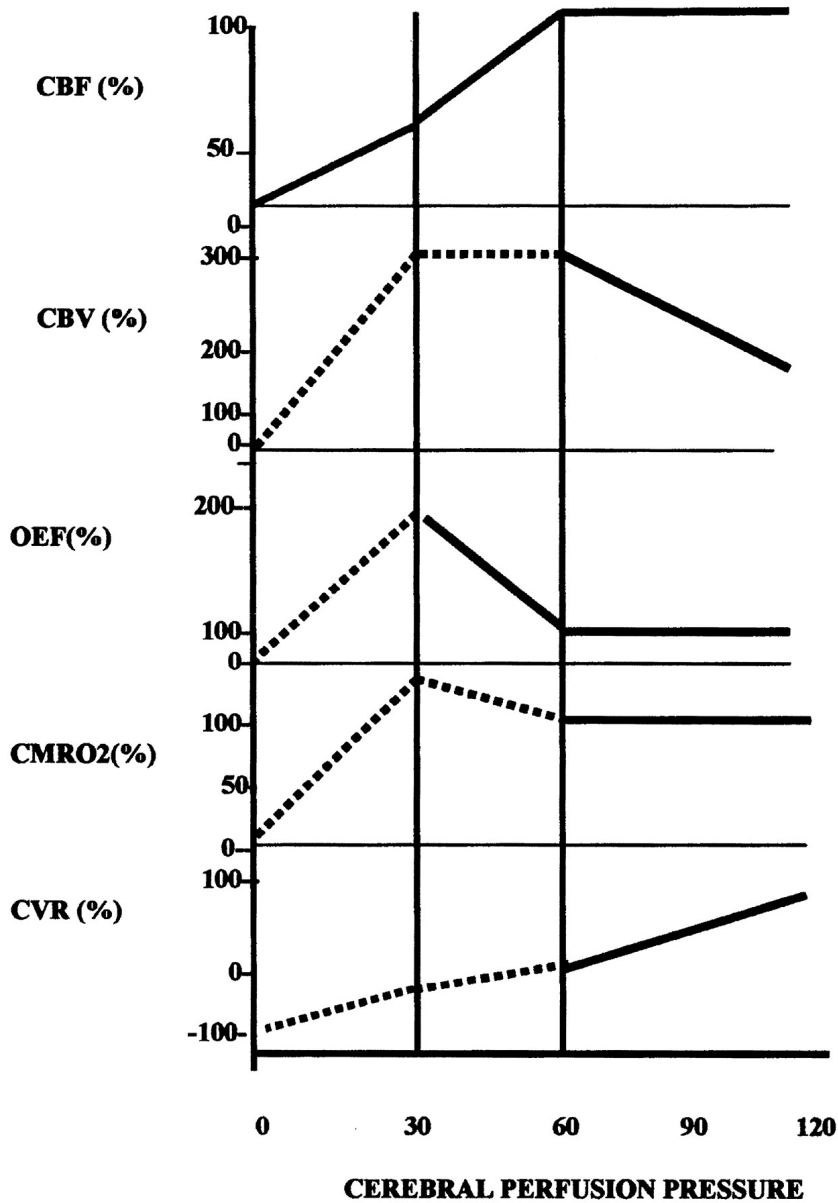


Figure 1 shows the relationship between several perfusion parameters. CBF = cerebral blood flow, CBV = cerebral blood volume, OEF = oxygen extraction fraction, CMRO₂ = cerebral metabolic rate of oxygen, CVR = cerebrovascular resistance. 60 mmHg is the lower border of healthy cerebral perfusion pressure (CPP) values. 30 mmHg is the border at which autoregulation and OEF have reached their maximum and further CBF decline will cause disruption of normal cellular metabolism and function.

Perfusion modifiers

A multitude of factors influence cerebral perfusion⁶. These are not only important to account for in the interpretation of CBF values, but can also be employed as challenges to evoke changes in cerebral perfusion⁷. One important class of perfusion modifiers is neuronal action secondary to cognitive performance, which is the basis of task-based functional MRI (fMRI)⁸. A variety of tasks exist that can induce perfusion changes. One class of tasks that are easy to perform is motor activity, such as finger tapping. When a subject performs a finger tapping task (Figure 2a), CBF will increase in the sensorimotor cortex (Figure 2b), and return to its original value after the task has ended and the hand is idle⁹. Task-based fMRI can be of particular interest to neurobiologically map the psychiatric brain¹⁰⁻¹².

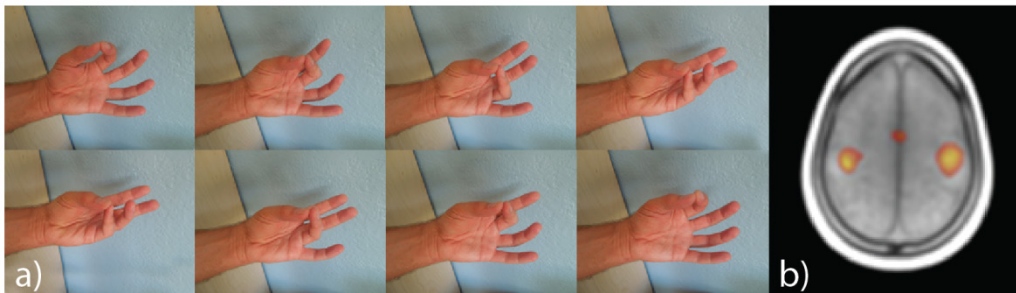


Figure 2. Sequential opposition finger-tapping task (a) inducing an increase in CBF in the sensorimotor cortex, here projected on a T1 image (b)

Drugs form another important class of perfusion modifiers¹³. The study of CBF changes induced by medication or recreational drugs may not only serve to gain a better understanding of the effects of drugs on perfusion, but also of the neurobiology of psychiatric pathologies and the pathophysiology of craving¹⁴⁻¹⁶. Caffeine is an example of a drug that can be considered a first choice pharmacological challenge for explorative studies in healthy volunteers, as it is one of the most socially accepted and widely consumed neuro-stimulants in the world^{16, 17}. Caffeine has two paradoxical effects on hemodynamics, as it is both a cognitive enhancer - potentially increasing CBF similar to finger-tapping as described above - and a potent vaso-constrictive agent - decreasing CBF^{18, 19}. Because the vaso-constrictive effect of caffeine outweighs its cognition enhancing effect in terms of CBF changes, CBF decreases with 20%-30% approximately 30 minutes after the intake of 200 mg caffeine (equivalent to 1-5 cups of coffee)¹⁷. Consequentially, OEF will increase to sustain CMRO₂ levels (Figure 1). As this example shows, the range over which CBF can fluctuate over the day while sustaining healthy neuronal

function is large. Other main perfusion modifiers include patient characteristics such as age²⁰, gender²¹ and stress²² as well as lifestyle factors such as food consumption²³, exercise²⁴, alcohol²⁵ and smoking²⁶.

If the perfusion changes of interest are subtle, they can be easily dominated by perfusion fluctuations arising from this multitude of perfusion modifiers. Therefore, only a handful of pathologies, including cerebral infarction or tumors, may induce perfusion changes that are sufficiently large to be reliably measured on the single subject level²⁷⁻³⁰. Most of the perfusion changes of interest in clinical, psychological or pharmacological studies are subtle, and can frequently only be reliably detected on a group level^{31,32}. For this reason, most applications of arterial spin labeling (ASL) perfusion MRI are still in the research setting³³⁻³⁵.

Short history of ASL

In the first few years of the existence of ASL^{36,37}, investigators were exploring its possibilities in rodents³⁸, mainly focusing on fundamental improvements of its implementation³⁹. Around 1997 clinical applications in humans began to appear, although these were limited to a few specialized research centers⁴⁰⁻⁴³. Main developments that helped to increase the clinical reliability of ASL include the implementation of background suppression in 2000⁴⁴, the increasing availability of 3T MRI⁴⁵ and the invention of pseudo-continuous ASL in 2005⁴⁶. Simultaneously, more and more clinical applications of ASL were tested^{47,48}. These developments promoted a broader applicability of ASL and from 2000 up until now, ASL-related publications have been exponentially increasing from 19 PubMed® hits in 2000 to 252 in 2013 (US National Library of Medicine) (Figure 3).

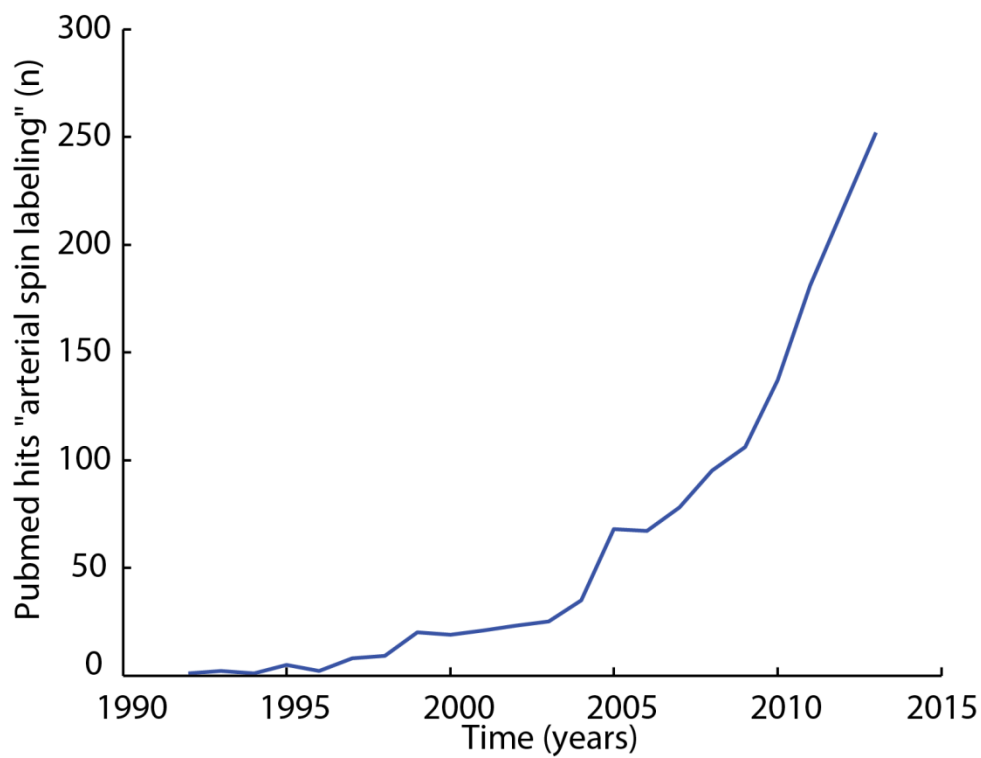


Figure 3 shows the exponential increase of peer reviewed arterial spin labeling studies, after its inception in 1992.

Useful MRI terminology

Spin Elementary particles such as water protons carry a physical property which is called spin. Spin can be represented by a vector and resembles a very small compass needle in many aspects. Under the influence of the strong magnetic field of the MR scanner, spin vectors will tend to align with the main magnetic field. Magnetization is the net effect of the magnetic vectors of all spins within an imaging voxel.

Sequence A single MRI scan or experiment. This name stems from the fact that a single MRI measurement consists of a series of actions such as the application of radiofrequency (RF) pulses. Each sequence consists of a preparation phase and a readout phase.

Magnetic resonance imaging During the preparation phase of an MRI sequence, the magnetization is modulated by RF pulses. Subsequently, the magnetization will recover to its original value and emit RF waves. These RF waves are then measured - during the readout phase - and reconstructed into an image¹.

Point spread function Describes the spatial response of an imaging system to a point source. A large point spread function translates to a large extent of spatial smoothing of the acquired image.

Readout The part of the sequence during which the emitted RF waves are being measured.

Signal-to-noise ratio (SNR) Mean (signal) divided by its variation (noise). A ratio that describes to which extent the values on an MR image are determined by actual signal of interest compared to random noise. Provides an estimate of image quality.

Voxel Volume pixel, where pixel stands for picture element. An MR image is composed of a grid of voxels, where each voxel is a cube with its own value or intensity. All voxels together form an image, which can appear mosaic-like (Figure 8c).

Arterial spin labeling

ASL is a relatively new MRI perfusion modality that changes the magnetization of blood water protons to use them as an endogenous tracer ⁴⁹. ASL is a completely non-invasive imaging modality, meaning that it requires neither ionizing radiation nor the administration of an exogenous contrast agent. Non-invasiveness has several advantages for clinical research: it is possible to repeat the CBF measurement as frequently as desired and the measurement can be applied in vulnerable populations such as patients with renal failure or children ⁵⁰.

In ASL, a labeling plane is first positioned perpendicular to the cervical arteries ⁵¹. Throughout labeling, the positive magnetization of blood water protons that flow through the labeling plane is inverted by a radiofrequency (RF) pulse. The blood will then have a negative magnetization ^{37, 52}. During the subsequent post-labeling delay (PLD), the labeled blood will travel downstream to the brain tissue (Figure 4). After this PLD, an image of the brain is acquired during the readout. This image will contain both the original positive magnetization of the stationary brain tissue as well as the negative magnetization from the inflowing labeled blood ³⁹. In a second image, an identical MRI experiment is carried out without the labeling of blood. Hence, in this second image, the magnetization of both the brain tissue and the blood will be positive. The subtraction of these two images provides an image that is weighted by perfusion, because the magnetization of stationary brain tissue is the same in both images but the signal of blood is different (Figure 5). Noteworthy, this subtractive nature of ASL cancels out scanner signal drift (i.e. longitudinal changes in MRI signal related to MRI hardware), rendering ASL preferable to blood-oxygen-level-dependent (BOLD)-contrast for the study of longitudinal changes of cerebral physiology ¹³.

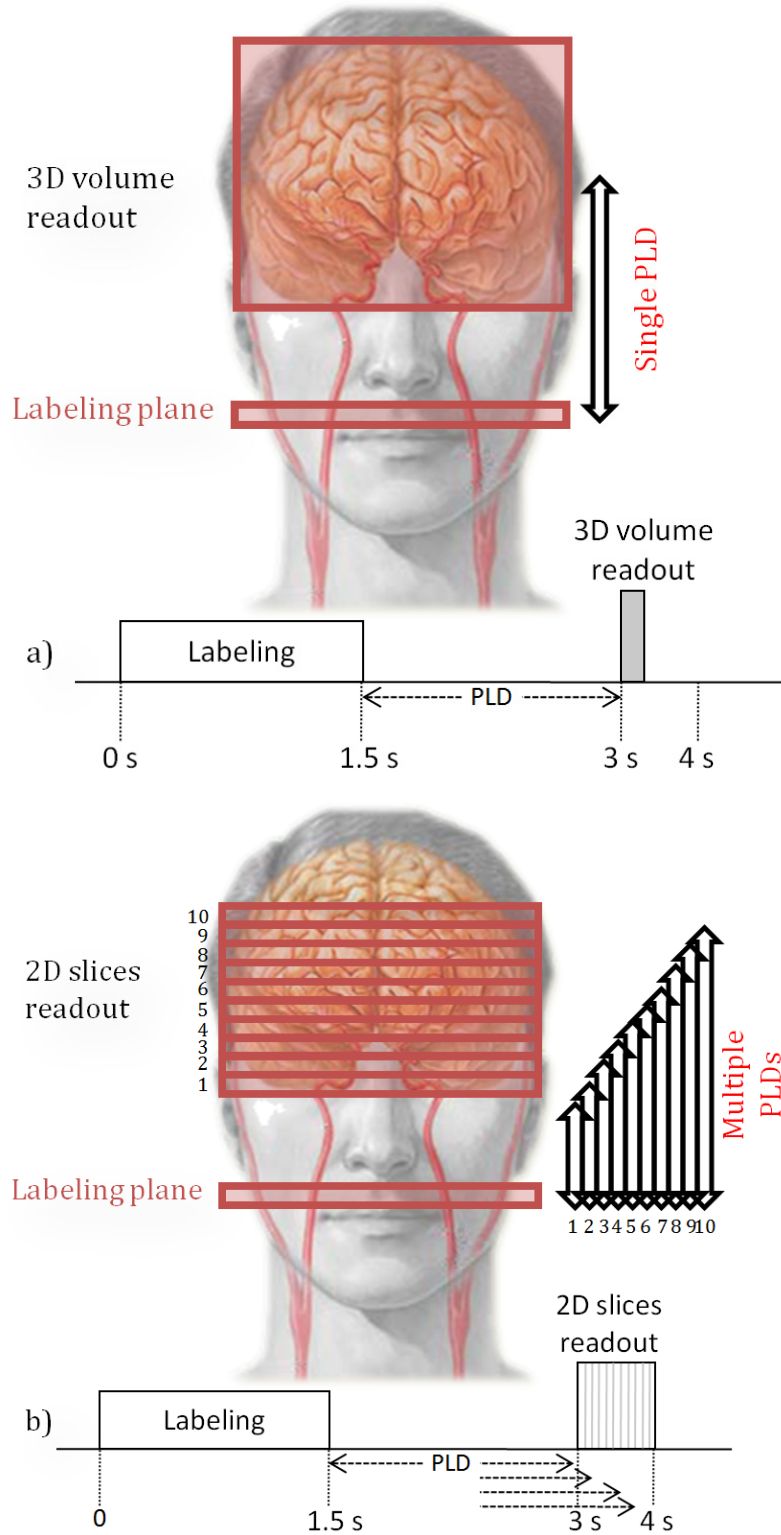


Figure 4 illustrates the timeline and spatial setup of a single ASL experiment schematically, for a 3D (a) and 2D (b) readout. The 3D readout module (a) occurs on a single time point for the whole brain, with a single effective post-labeling delay (PLD). For a 2D readout module (b), multiple slices are imaged consecutively, and the effective PLD increases with the slice readout duration for each slice in ascending mode. s = second, PLD = post-labeling delay. For illustrative purposes, only 10 slices are depicted here.

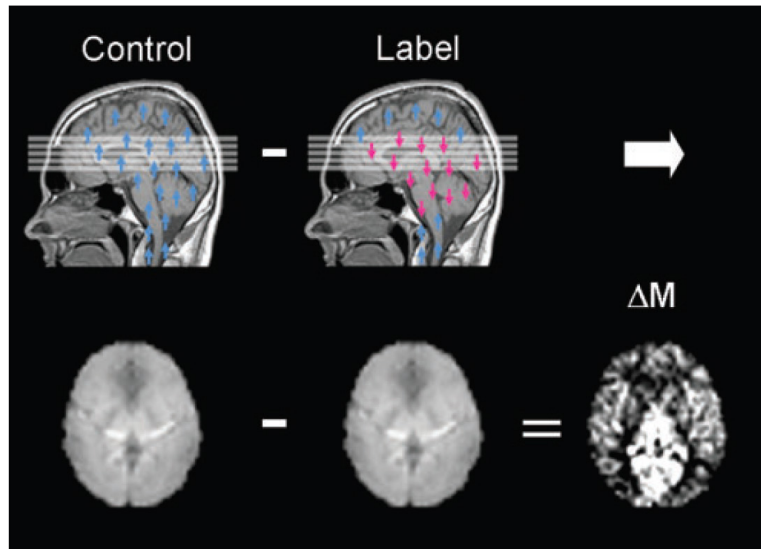


Figure 5 demonstrates how the subtraction of MR images with and without labeling yields perfusion-weighted images. Both the control and label images contain the positive magnetization of static brain tissue (blue arrows), whereas only the label image contains the negative magnetization of labeled blood (red arrows). Since the majority of the brain volume is composed of brain tissue, the control and label images themselves will appear as low resolution anatomical images, whereas the subtraction image (ΔM) is weighted for the magnetization difference between the control and label images, hence for perfusion.

One major caveat of the use of blood as an endogenous perfusion tracer, is that blood only forms 0-2% of brain volume within an imaging voxel, the other 98% being stationary brain tissue⁵³. In addition, the lifetime of the endogenous tracer is short: the inverted magnetization of the blood protons will return to its original positive magnetization with a T1 relaxation time (abbreviated as T1). In the context of ASL, T1 is defined as the time after which the inverted magnetization recovers to approximately 63% of its original value. At 3T MRI, the T1 of blood is 1.65 s^{54,55}, whereas the T1 of tissue is even shorter (1.2 s for gray matter (GM), 0.9 s for white matter (WM))⁵⁶. For these reasons, the signal-to-noise ratio (SNR) of ASL can be regarded as 50-100 times as small as the SNR of conventional anatomical MRI³⁴. In order to account for this low SNR, ASL experiments - 8 seconds for a single control-label pair (in case of a 2D EPI readout) - are typically repeated 20-40 times and the image resolution is kept low (in each dimension, ASL voxels are typically 3-4 times as large as anatomical MRI voxels)^{57,58}.

Reproducibility

Before any new measurement method can be applied clinically or in clinical research^{59,60}, it is important to assess its accuracy and precision (Figure 6)⁶¹⁻⁶³. Accuracy states how close the mean of all measurements is to the "real" value. High accuracy is also referred to as low offset, bias or low systematic error. Precision, on the other hand, states how close each individual measurement is to the mean of all measurements. High precision is also referred to as low variation. In other words, the accuracy concerns a comparison of the means of all measurements from two different ASL sequences, preferably in comparison to a gold standard measurement, whereas the precision concerns a comparison of the variation between the measurements within one ASL sequence and the variation between measurements within another ASL sequence.

Likewise, if we perform repeated measurement sessions with different methods, we can compare between methods either 1) the mean of the repeated measurements - analogous to accuracy - or 2) the variation between the repeated measurements - analogous to precision. To this end, we can compare multiple measurements of baseline resting CBF values, assuming that the effects of perfusion modifiers are randomly divided across different the measurement sessions⁶⁴⁻⁶⁹. In addition, it is of interest to compare the mean and variation of a perfusion change - which is the outcome variable of many clinical and psychopharmacological perfusion studies^{7, 70, 71}. For the assessment of reproducibility in healthy volunteers, finger tapping can be considered a first choice fMRI task because is it easily performed and highly validated, whereas caffeine can be considered a convenient drug for reproducibility assessments because of its large whole-brain effect, wide availability and socially and medical-ethically accepted status.

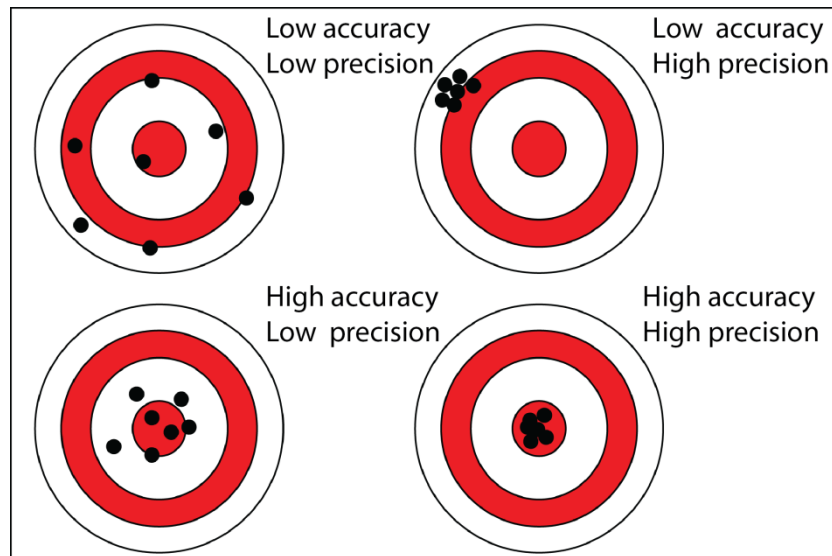


Figure 6. Four situations with different combinations of high or low accuracy and/or precision.

Sources of variability

Two main components of variability of ASL-based CBF measurements can be distinguished: measurement noise and perfusion fluctuations⁷². Measurement noise can be considered the first and most important to deal with, especially since the temporal SNR of ASL is intrinsically low. Because the temporal SNR of ASL is proportional to CBF, the reproducibility of ASL can vary significantly between patients and between different brain regions. In patients with high CBF - such as children - SNR optimizations may have low priority⁵⁰. On the other hand, in patients with low CBF - such as elderly with cerebrovascular or neurodegenerative disease - it is important to focus on improving SNR of ASL. Factors that can improve the SNR of ASL - and consequently its reproducibility - can be subdivided into MRI scanner hardware (including field strength and head coil design) and sequence optimization (including higher labeling efficiency or efficient readout strategies, as discussed below)⁷³.

The relative influence of the perfusion fluctuations component increases as ASL technology advances and becomes increasingly robust - especially since averaging several voxels within a region of interest (ROI) - which is referred to as spatial averaging - can decrease the measurement noise. This follows from the assumption that the actual mean CBF within a ROI is constant but the variability between different voxels within a ROI is high because of the low SNR of ASL. In this case, the contribution of the measurement noise to the variability of CBF values can be greatly decreased by averaging CBF-values of multiple voxels within an ROI. Since long-term perfusion fluctuations are relatively large^{74, 75}, these can easily dominate the variability for a large ROI such as the total GM^{64, 65, 76, 77}. Hence, if the

variability differs between different head coils or ASL readouts, this difference may be clearly apparent on an individual voxel level but much less when multiple voxels within a large ROI are averaged for a mean CBF value.

Confounding effect of transit time

"Conventional" ASL sequences that are commonly used in clinical research employ a single time point at which the readout is performed, directly following the PLD (Figure 4)⁵³. With a single time point ASL experiment, the validity of the measurement relies on the assumption that all the labeled blood has reached the brain tissue or its capillaries within the imaging voxel after the PLD^{39,78}. If the label has not arrived in the imaging voxel at the time of imaging, the CBF will be underestimated. Paradoxically, if the label has already arrived in the imaging voxel but still resides within large blood vessels and has not arrived in the tissue or its capillaries yet, CBF will be overestimated. This is the consequence of the differences in T1 between blood and static tissue (GM or WM): when the label has not arrived in brain tissue yet, it has decayed slower than label that has already been in brain tissue for a period of time (Figure 7). Therefore, the time it takes for the labeled blood to travel to the tissue - which is called transit time (TT), also known as arrival time - can have a large effect on the quantification of ASL-based CBF values⁵³: it may introduce a bias (systematically under- or over-estimating CBF) or it may contribute to the variability of the measurement⁶⁷.

Since TTs are similar to the T1 of blood on 3T MRI and the label signal decays exponentially (Figure 7), the selection of labeling duration and PLD can have a major effect on the accuracy and precision of the ASL measurement⁷⁹. E.g., if TT is short, the labeled blood has resided longer in the tissue and more signal will have decayed at the time of the readout, compared to if it had been residing in blood vessels only in case of a long TT (Figure 7). Although a-priori assumptions of TT can be inferred from literature⁸⁰, these may still vary within- and between populations^{66, 81}. Therefore, the measurement of TT in addition to CBF may improve the accuracy and precision of ASL-based CBF values. In addition, there may be situations in which TT values carry information additional to - or even more important than - CBF values alone⁸²⁻⁸⁵.

Although this may not always be the case, a good rule of thumb is that TTs are inversely proportional to CBF^{80, 86}. In GM, TT is generally lower and CBF generally higher compared to TT and CBF in WM tissue^{87, 88}. Children have shorter TT and higher CBF than adults⁷⁹, perhaps to compensate for their increased brain metabolism during brain development. Moreover, in children with sickle cell disease (SCD), TTs are even shorter and CBF even higher to compensate for their anemia. This can be visually

appreciated on the perfusion-weighted images in children, where label has already arrived in the sagittal and transverse sinus at the readout time point ⁷⁹. In contrast, elderly with neurodegenerative or cerebrovascular disease, have longer TTs and lower CBF, which may be the consequence of the extra-cranial and cerebral arteries becoming more tortuous (hence prolonging TT) ⁸⁹. In addition, perfusion modifiers such as drugs (e.g. caffeine) ⁹⁰ or neuronal activation (e.g. finger tapping) ^{88, 91, 92} also modify TT. Therefore, it is important to take into account that TT differences may add to the bias and variability of CBF values measured by a single time point ASL sequence ⁶⁷. For these reasons, several methods have been developed to measure TT using ASL ^{93, 94} and current efforts are focused on developing a simultaneous measurement of CBF and TT without SNR penalty for the single time point CBF measurement ⁹⁵⁻⁹⁷.

Parameter	Value
GM CBF children with SCD	80-100 mL/100g/min
GM CBF children	60-80 mL/100g/min
GM CBF adults	50-60 mL/100g/min
GM CBF elderly	40-50 mL/100g/min
GM CBF elderly with cognitive decline	30-40 mL/100g/min
WM CBF	15-20 mL/100g/min
T1 blood	1650 ms
T1 GM tissue	1240 ms
T1 WM tissue	900 ms

Table 1 provides an impression of the range of gray matter (GM) cerebral blood flow (CBF)-values that can be expected in different populations. For the white matter (WM), a single range is shown, since this value does not differ much between populations ⁷⁴, and is not reported as frequently as GM CBF-values. These CBF-values are typical values and may vary strongly with the employed ASL and quantification techniques.

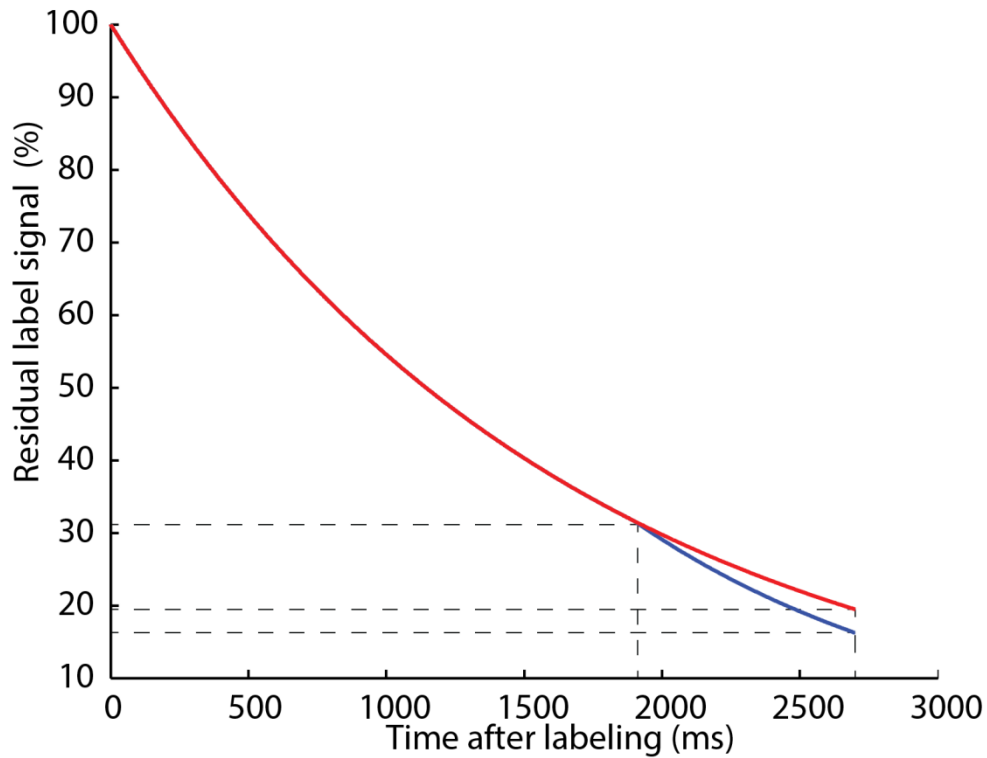


Figure 7. Schematic view of label signal evolution. Consider a typical ASL experiment with a 3D readout, 1800 ms labeling duration and 1800 ms post-labeling delay⁵³, in a healthy young volunteer with a transit time of 1900 ms for a proximal voxel and 2700 ms for a distal voxel. The average blood water proton is labeled at 900 ms ($0.5 \times$ labeling duration). This label will then have had $900 \text{ ms} + 1800 = 2700$ ms between labeling and readout. If the label would arrive in the distal voxel, its signal has decayed with the T1 of blood only (red line). If the label would arrive in the proximal voxel, the signal has decayed the first 1900 ms with the T1 of blood and upon its arrival in tissue for another 800 ms with the T1 of GM tissue (blue line).

Pseudo-continuous labeling strategy

Since the inception of ASL in 1992, a plethora of labeling and readout strategies have been proposed³⁷. Recently, a review has been published providing a consensus on the clinical application of single time point ASL⁵³. From all existing labeling strategies, pseudo-continuous ASL (PCASL) has been selected as the most robust and widely available labeling strategy for single time point ASL^{76, 98}. This labeling strategy relies upon continuous labeling - i.e. during a relatively long labeling duration - of blood flowing through a relatively thin labeling plane (Figure 4). The prefix "pseudo" is added because in PCASL labeling is not performed in a single continuous RF pulse but rather as a train of very short discrete RF pulses (around 1000 Hz)⁹⁹. The effect and CBF quantification of PCASL can be regarded the same as continuous labeling (CASL) but PCASL has several advantages compared to CASL, including higher labeling efficiency and better compatibility with existing MRI hardware - as it requires no extra coil^{46, 98, 99}. An important disadvantage of PCASL - although this may also apply for ASL in general - is that the 1000 Hz labeling produces a sound that can be highly uncomfortable for patients. There have been initiatives to adapt the PCASL sequence to produce more patient-friendly sounds, which can be especially important for clinical research applications in which it is important that the subject lies still for a prolonged period of time¹⁰⁰.

Readout strategies

Whereas most previous ASL experiments have been performed with a 2D readout^{57, 58} such as 2D gradient-echo echo-planar imaging (EPI), it has been agreed upon that a 3D readout - such as 3D fast-spin echo stack-of-spirals - is preferable for clinical applications of ASL⁵³. The main difference between a 2D and 3D readout for whole-brain imaging, is that a 2D readout is composed of multiple sequential single-slice readouts, whereas a 3D readout measures the magnetization in the whole brain at a single time point (Figure 4a). One important difference between reading out the magnetization of the whole brain at a single time point or ascendingly at sequential time points, is that the PLD is fixed for 3D whereas it becomes longer for each slice that is being read out later in time in the case of a 2D readout (Figure 4b). The main advantage of a 3D readout is its larger SNR compared to a 2D readout, translating into higher reproducibility¹⁰¹. One of the main reasons why the SNR of a 3D readout is higher, is its improved implementation of background suppression¹⁰¹.

Background suppression

Ideally, the magnetization of stationary brain tissue is identical for the control and label experiments and will not contribute to the perfusion-weighted values of the subtraction image. In practice this is not the case, since the control and label experiments are performed at different time points and perfusion- and MRI-related artifacts change in time ¹⁰². Differences in stationary brain tissue magnetization between control and label images lead to subtraction errors that can be referred to as pseudo-perfusion ¹⁰³. One of the largest subtraction errors is formed by head motion between the control and label scans, which can be visually appreciated as a bright edge around the brain on the perfusion-weighted image ⁵³. Since subtraction errors increase the noise of the mean perfusion-weighted image, the suppression of background magnetization - i.e. the magnetization of stationary brain tissue - can greatly increase the SNR of ASL ^{44, 104}.

Background suppression minimizes the magnetization of stationary brain tissue during the readout. Since the magnetization - and hence the signal - of stationary brain tissue does not have a stable value but rather follows an exponential recovery curve ¹⁰⁵ (Figure 8), it is not feasible to alter the magnetization of brain tissue in such a way that it is as low as possible at all time points in a multi-slice 2D readout ¹⁰⁴. The magnetization of brain tissue will be lowest in the caudal slices, but will recover to its original values as more cranial slices are being readout later in time (Figure 8) ¹⁰⁶. Hence, background suppression is only optimal for the first slice of a 2D readout, and suboptimal for the remaining superior slices. On the other hand, for the single time point of a 3D whole-brain readout, the magnetization of stationary brain tissue can be carefully altered by RF pulses to be as low as possible at the single readout time point ¹⁰⁵. Therefore, the efficiency of background suppression is optimal for the whole brain in 3D whereas a standard 2D readout background suppression implementation is only optimal for a few caudal slices ^{104, 106}. However, this suboptimal noise reduction is still considered preferable to no noise reduction ^{53, 65}. Since the accuracy and precision of ASL can suffer much from the intrinsically low SNR of ASL, improvements of SNR are highly desirable. This is especially the case in clinical applications with long TT and low CBF, such as in elderly with cerebrovascular or neurodegenerative disease ¹⁰⁷.

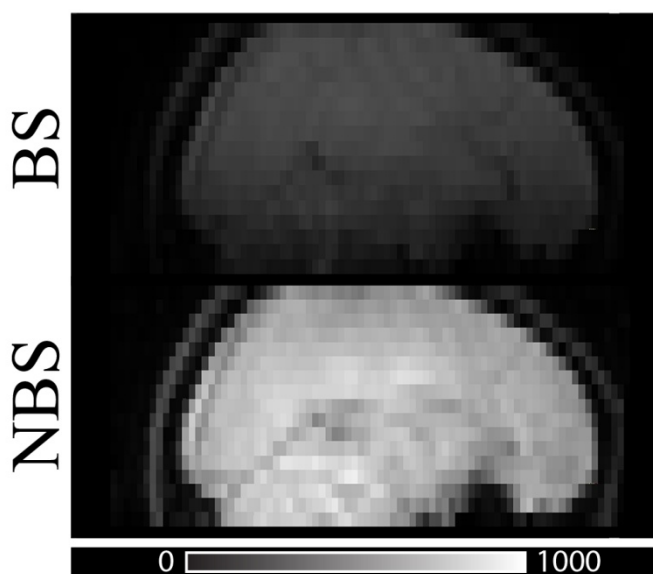
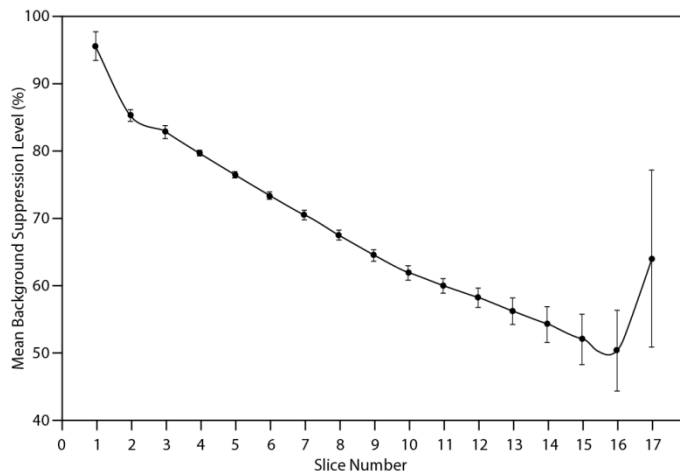
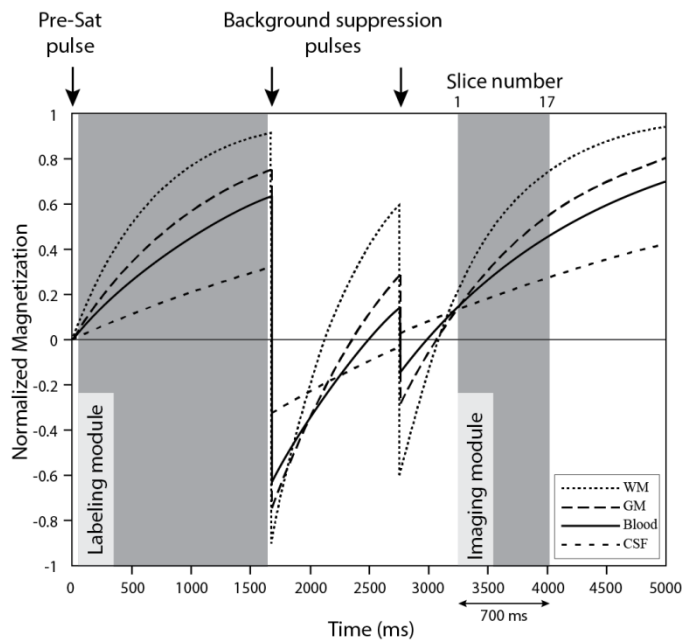


Figure 8 demonstrates the effect of background suppression. a) shows its implementation for a pseudo-continuous labeling module with a multi-slice 2D readout and the resulting evolution of tissue magnetization over time for gray matter (GM), white matter (WM), blood and cerebrospinal fluid (CSF). The second gray surface represents the readout phase during which all slices are consecutively readout, during which the "background" tissue signal returns to its original positive magnetization, reducing the background suppression level (b). This can be visually appreciated in (c), in which sagittal projections of raw EPI images are shown with (BS, upper Figure) and without background suppression (NBS, lower Figure). The bar below the picture indicates the signal intensity.

Spatial smoothing

An important disadvantage of a 3D readout module is its larger point spread function (PSF)^{53, 101}, resulting in a higher degree of spatial smoothing compared to a 2D readout, as illustrated by Figure 9. Other factors that can contribute to spatial smoothing include head motion and registration and interpolation errors in the post-processing stage¹⁰⁸. Furthermore, it is common practice to apply additional smoothing before statistical group analyses are carried out with ASL data¹⁰⁹. These origins of spatial smoothing contribute to a lower effective spatial resolution. A degree of smoothing can be desirable since it decreases random noise, similar to averaging multiple voxels¹⁰⁹. Nevertheless, considering the large perfusion differences between GM, WM and CSF tissue types, it is important to restrict the amount of smoothing to retain information that is beneficial for post-processing (e.g. non-linear registration)^{108, 110} or for the detection of small focal CBF changes¹¹¹. It should be noted that the PSF of a 3D sequence can vary much between different implementations of 3D readouts¹⁰¹. Currently, efforts are directed towards decreasing the PSF of 3D sequences⁷⁵.

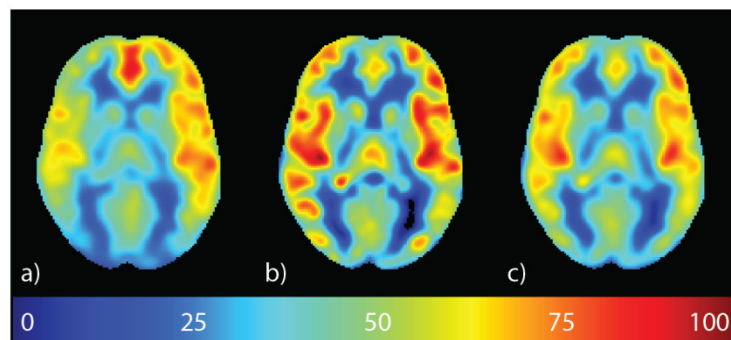


Figure 9. Illustration of spatial smoothness differences in cerebral blood flow (CBF) data acquired in the same subject with a 3D spiral (a) and 2D EPI (b) readout module, after post-processing and

normalization to standard space. There is a clear difference in the visual differentiation between gray and white matter CBF, which can be strongly reduced by smoothing the 2D EPI CBF map to the same smoothness as the 3D spiral image (c). This illustrates how smoothing can be understood as a way of "ironing out" differences between neighboring voxels. The color scale shows CBF-values between 0 and 100 mL/100g/min.

White matter perfusion

WM CBF may carry more information than GM CBF for certain pathologies¹¹²⁻¹¹⁴. In the elderly, early hemodynamic changes related to small vessel disease are frequently observed as white matter lesions (WML)^{115, 116}. These lesions are thought to arise from a combination of focal and general perfusion deficits, and it has been suggested that WM CBF can represent a micro-vascular biomarker to investigate the interplay between aging and neurodegenerative and cerebrovascular pathology¹¹⁴. WML are frequently observed on MRI scans in the elderly, and are regarded as clinically silent lesions, having no direct neurological or cognitive consequence. Despite being clinically silent, WML are associated with cognitive impairment and with an increased risk of neurodegenerative disease, stroke and even mortality¹¹⁷⁻¹²⁰. Despite the vast interest in these lesions, the pathophysiology is still not well known^{121, 122}. There may be similarities as well as differences in the pathophysiology of these lesions in various diseases, including aging, cerebrovascular disease, neurodegeneration, multiple sclerosis (MS) or SCD¹²³.

As most of the WM tissue lies at the end of the cerebrovascular tree, it has been postulated that transient moments of low perfusion pressure may affect the WM perfusion more than the GM perfusion, which lies more proximally in the vascular tree¹²⁴. Small vessel disease and WML are strongly correlated with hypertension¹²². The general hypothesis is that as hypertension becomes chronic, the cerebral autoregulation will adapt to chronically sustain higher perfusion pressures. This adapted autoregulation will have a lower ability to respond to lower perfusion pressures, leaving patients more vulnerable to transient moments of low perfusion pressure¹²⁵.

Despite the pathophysiological interest of WM CBF as an early micro-vascular marker of vascular pathology^{113, 114}, the reliability of ASL in WM is relatively poor¹²⁶. Because of the long TT in the WM (Figure 10), the majority of the signal will have decayed at the time of readout and the SNR of WM CBF becomes very poor. However, with recent ASL advances it seems possible to measure WM CBF in the majority of voxels with longer measurement times and preferably longer labeling duration and PLD¹²⁷. If CBF is averaged across the total WM ROI, SNR may even be sufficient for patient groups¹²⁸. Another challenge for WM perfusion imaging is its close proximity to GM. Since the GM CBF is 3 to 4-fold as

high and varies more than WM CBF, even minor contamination of WM signal by GM perfusion signal can distort WM CBF measurements¹²⁶. This is especially problematic considering the low spatial resolution and various sources of smoothing in ASL¹²⁹. In a worst case scenario, an apparent change in WM CBF is nothing more than a change in GM CBF that has been detected in the WM because of signal contamination¹²⁶.

Sickle cell disease

Children with SCD form a population in which WMLs occur at a low age^{130, 131}. Similar to WML in the elderly, these WML have no direct clinical consequences and are referred to as silent cerebral infarcts (SCIs), but are associated with progressive cognitive decline¹³² and increased stroke risk in the long-term^{133, 134}. SCD is a hereditary disorder in which hemoglobin is developed abnormally, leading to anemia due to chronic hemolysis¹³⁵. In order to sustain brain metabolism - which is high in developing children¹³⁶ - CBF is elevated in these patients to compensate for their lower hemoglobin level. Because the higher CBF of children with SCD translates to much higher SNR for ASL than in elderly patients¹³⁷, it is more feasible to study WM CBF in patients with SCD than in elderly with low ASL SNR. Because not only the WML but also the patterns of other cerebral lesions are similar in patients with SCD as in elderly with small vessel disease¹³⁸, it has been suggested that the cerebrovascular pathophysiology in both populations may have similarities as well. Therefore, the study of WM CBF in patients with SCD with ASL may not only benefit the understanding of cerebrovascular pathology in SCD but may eventually also improve the understanding of the pathophysiology of SVD¹³⁹.

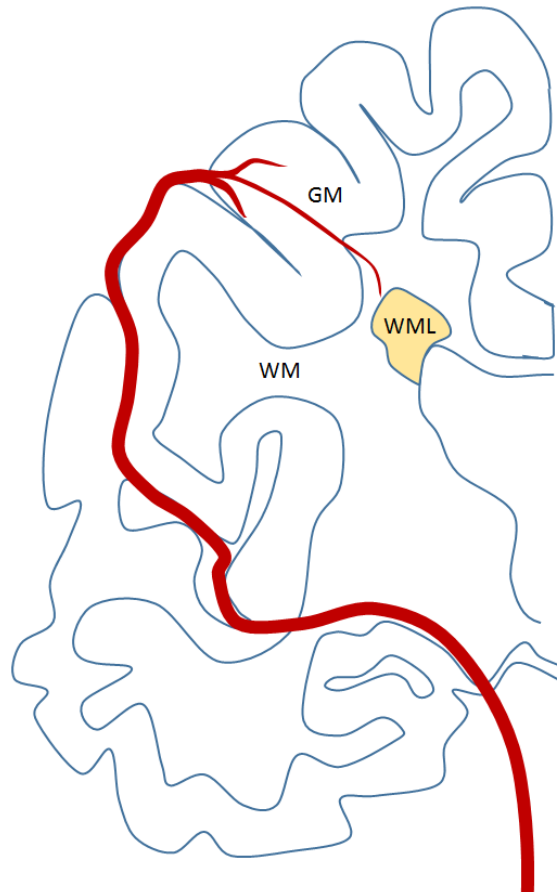


Figure 10. Schematic overview of the vasculature within one cerebral hemisphere, showing the route blood travels to reach the white matter (WM), resulting in longer transit times for white matter than for the gray matter (GM). Transit time is longest for regions prone to development of white matter lesion (WML).

Outline of this thesis

The overall aim of this thesis was to investigate the inter-vendor reproducibility of ASL sequences in healthy volunteers at 3 Tesla (Part I) and to investigate its applicability for clinical research in several patient populations (Part II).

Part I Inter-vendor reproducibility of ASL

Firstly, using the ASL product sequences of General Electric (GE) and Philips, the inter-vendor reproducibility of ASL was investigated for baseline ASL measurements (**Chapter 2**), pharmacological ASL (**Chapter 3**) and functional ASL (**Chapter 4**). Although it was known that the readout strategies of these vendors were different, the question remained how different the results of these measurements were in comparison to long-term physiological fluctuations of CBF. Secondly, the inter-vendor reproducibility was assessed between GE, Philips and Siemens for nearly identical custom-made sequences on three scanners from these major MRI vendors (**Chapter 5**). It was hypothesized that the inter-vendor reproducibility was more comparable to the intra-vendor reproducibility for these near-identical sequences in comparison to the abovementioned dissimilar ASL product sequences.

Part II Clinical research applications of ASL

The possibility to measure uncontaminated WM CBF in elderly patients with cognitive decline was investigated in **Chapter 6**. It was hypothesized that a large part of WM voxels are contaminated by GM CBF and that care is needed to isolate pure WM CBF signal. In **Chapter 7**, the feasibility of an alternative ASL sequence was assessed in elderly patients with hypertension. This sequence acquires both micro-vascular CBF and a mix of micro- and macro-vascular CBF, the ratio of which is inversely proportional to micro-vascular TT. Although the SNR of this sequence may be too low on an individual level, it was hypothesized that could be sufficient for group level analyses. In **Chapter 8**, the clinical applicability of ASL to detect associations between CBF and WML was investigated in elderly patients with hypertension. It was hypothesized that WMLs were not only correlated to WM CBF but also to GM CBF, reflecting widespread perfusion deficits rather than focally reduced perfusion within the lesion. In **Chapter 9**, the clinical applicability of ASL to detect associations between CBF, WML and hematological parameters was investigated in children with SCD. The aim was to investigate whether ASL-based CBF measurements can help to estimate the contribution of endothelial dysfunction and CBF insufficiency to the development of WML in children with SCD.

Reference list

1. Bernstein MA, King K.F., Zhou X.J. *Handbook of MRI pulse sequences*. Amsterdam, Boston, Heidelberg: Elsevier; 2004.
2. Powers WJ. Cerebral hemodynamics in ischemic cerebrovascular disease. *Ann Neurol* 1991; **29(3)**:231-240.
3. van Beek AH, Claassen JA, Rikkert MG, Jansen RW. Cerebral autoregulation: an overview of current concepts and methodology with special focus on the elderly. *J Cereb Blood Flow Metab* 2008; **28(6)**:1071-1085.
4. Vanhoutte PM, Rubanyi GM, Miller VM, Houston DS. Modulation of vascular smooth muscle contraction by the endothelium. *Annu Rev Physiol* 1986; **48**:307-320.
5. Aaslid R, Lindegaard KF, Sorteberg W, Normes H. Cerebral autoregulation dynamics in humans. *Stroke* 1989; **20(1)**:45-52.
6. Clement P, Mutsaerts H, Ghariq E, Smits M, Acou M, Rostrup E, *et al*. Review of confounding effects on perfusion measurements. In: Belgian Brain Council 2014 Modulating the brain: facts, fiction, future; 2014.
7. Heijtel DF, Mutsaerts HJ, Bakker E, Schober P, Stevens MF, Petersen ET, *et al*. Accuracy and precision of pseudo-continuous arterial spin labeling perfusion during baseline and hypercapnia: a head-to-head comparison with (1)(5)O H(2)O positron emission tomography. *Neuroimage* 2014; **92**:182-192.
8. Sadaghiani S, Hesselmann G, Friston KJ, Kleinschmidt A. The relation of ongoing brain activity, evoked neural responses, and cognition. *Front Syst Neurosci* 2010; **4**:20.
9. Biswal B, Yetkin FZ, Haughton VM, Hyde JS. Functional connectivity in the motor cortex of resting human brain using echo-planar MRI. *Magn Reson Med* 1995; **34(4)**:537-541.
10. Walther S, Federspiel A, Horn H, Razavi N, Wiest R, Dierks T, *et al*. Resting state cerebral blood flow and objective motor activity reveal basal ganglia dysfunction in schizophrenia. *Psychiatry Res* 2011; **192(2)**:117-124.
11. Walther S, Hofle O, Federspiel A, Horn H, Hugli S, Wiest R, *et al*. Neural correlates of disbalanced motor control in major depression. *J Affect Disord* 2012; **136(1-2)**:124-133.
12. Andreescu C, Gross JJ, Lenze E, Edelman KD, Snyder S, Tanase C, *et al*. Altered cerebral blood flow patterns associated with pathologic worry in the elderly. *Depress Anxiety* 2011; **28(3)**:202-209.
13. Wang DJ, Chen Y, Fernandez-Seara MA, Detre JA. Potentials and challenges for arterial spin labeling in pharmacological magnetic resonance imaging. *J Pharmacol Exp Ther* 2011; **337(2)**:359-366.
14. Handley R, Zelaya FO, Reinders AA, Marques TR, Mehta MA, O'Gorman R, *et al*. Acute effects of single-dose aripiprazole and haloperidol on resting cerebral blood flow (rCBF) in the human brain. *Hum Brain Mapp* 2013; **34(2)**:272-282.
15. Chen Y, Wan HI, O'Reardon JP, Wang DJ, Wang Z, Korczykowski M, *et al*. Quantification of cerebral blood flow as biomarker of drug effect: arterial spin labeling phMRI after a single dose of oral citalopram. *Clin Pharmacol Ther* 2011; **89(2)**:251-258.
16. Field AS, Laurienti PJ, Yen YF, Burdette JH, Moody DM. Dietary caffeine consumption and withdrawal: confounding variables in quantitative cerebral perfusion studies? *Radiology* 2003; **227(1)**:129-135.
17. Fredholm BB, Battig K, Holmen J, Nehlig A, Zvartau EE. Actions of caffeine in the brain with special reference to factors that contribute to its widespread use. *Pharmacol Rev* 1999; **51(1)**:83-133.
18. Mulderink TA, Gitelman DR, Mesulam MM, Parrish TB. On the use of caffeine as a contrast booster for BOLD fMRI studies. *Neuroimage* 2002; **15(1)**:37-44.

19. Vidyasagar R, Greyling A, Draijer R, Corfield DR, Parkes LM. The effect of black tea and caffeine on regional cerebral blood flow measured with arterial spin labeling. *J Cereb Blood Flow Metab* 2013; **33(6)**:963-968.
20. Chen JJ, Rosas HD, Salat DH. Age-associated reductions in cerebral blood flow are independent from regional atrophy. *Neuroimage* 2011; **55(2)**:468-478.
21. Gur RE, Gur RC. Gender differences in regional cerebral blood flow. *Schizophr Bull* 1990; **16(2)**:247-254.
22. Wang J, Rao H, Wetmore GS, Furlan PM, Korczykowski M, Dinges DF, *et al.* Perfusion functional MRI reveals cerebral blood flow pattern under psychological stress. *Proc Natl Acad Sci U S A* 2005; **102(49)**:17804-17809.
23. Arbelaez AM, Su Y, Thomas JB, Hauch AC, Hershey T, Ances BM. Comparison of regional cerebral blood flow responses to hypoglycemia using pulsed arterial spin labeling and positron emission tomography. *PLoS One* 2013; **8(3)**:e60085.
24. Herholz K, Buskies W, Rist M, Pawlik G, Hollmann W, Heiss WD. Regional cerebral blood flow in man at rest and during exercise. *J Neurol* 1987; **234(1)**:9-13.
25. Tolentino NJ, Wierenga CE, Hall S, Tapert SF, Paulus MP, Liu TT, *et al.* Alcohol effects on cerebral blood flow in subjects with low and high responses to alcohol. *Alcohol Clin Exp Res* 2011; **35(6)**:1034-1040.
26. Shinohara T, Nagata K, Yokoyama E, Sato M, Matsuoka S, Kanno I, *et al.* Acute effects of cigarette smoking on global cerebral blood flow in overnight abstinent tobacco smokers. *Nicotine Tob Res* 2006; **8(1)**:113-121.
27. Deibler AR, Pollock JM, Kraft RA, Tan H, Burdette JH, Maldjian JA. Arterial spin-labeling in routine clinical practice, part 2: hypoperfusion patterns. *AJNR Am J Neuroradiol* 2008; **29(7)**:1235-1241.
28. Deibler AR, Pollock JM, Kraft RA, Tan H, Burdette JH, Maldjian JA. Arterial spin-labeling in routine clinical practice, part 3: hyperperfusion patterns. *AJNR Am J Neuroradiol* 2008; **29(8)**:1428-1435.
29. Wolf RL, Detre JA. Clinical neuroimaging using arterial spin-labeled perfusion magnetic resonance imaging. *Neurotherapeutics* 2007; **4(3)**:346-359.
30. Telischak NA, Detre JA, Zaharchuk G. Arterial spin labeling MRI: Clinical applications in the brain. *J Magn Reson Imaging* 2014.
31. Murphy K, Harris AD, Diukova A, Evans CJ, Lythgoe DJ, Zelaya F, *et al.* Pulsed arterial spin labeling perfusion imaging at 3 T: estimating the number of subjects required in common designs of clinical trials. *Magn Reson Imaging* 2011; **29(10)**:1382-1389.
32. Detre JA, Wang J, Wang Z, Rao H. Arterial spin-labeled perfusion MRI in basic and clinical neuroscience. *Curr Opin Neurol* 2009; **22(4)**:348-355.
33. Golay X, Guenther M. Arterial spin labelling: final steps to make it a clinical reality. *MAGMA* 2012; **25(2)**:79-82.
34. Detre JA, Rao H, Wang DJ, Chen YF, Wang Z. Applications of arterial spin labeled MRI in the brain. *J Magn Reson Imaging* 2012; **35(5)**:1026-1037.
35. Wierenga CE, Hays CC, Zlatar ZZ. Cerebral blood flow measured by arterial spin labeling MRI as a preclinical marker of Alzheimer's disease. *J Alzheimers Dis* 2014; **42(0)**:S411-S419.
36. Koretsky AP. Early development of arterial spin labeling to measure regional brain blood flow by MRI. *Neuroimage* 2012; **62(2)**:602-607.
37. Williams DS, Detre JA, Leigh JS, Koretsky AP. Magnetic resonance imaging of perfusion using spin inversion of arterial water. *Proc Natl Acad Sci U S A* 1992; **89(1)**:212-216.
38. Detre JA, Zhang W, Roberts DA, Silva AC, Williams DS, Grandis DJ, *et al.* Tissue specific perfusion imaging using arterial spin labeling. *NMR Biomed* 1994; **7(1-2)**:75-82.
39. Alsop DC, Detre JA. Reduced transit-time sensitivity in noninvasive magnetic resonance imaging of human cerebral blood flow. *J Cereb Blood Flow Metab* 1996; **16(6)**:1236-1249.

40. Wong EC, Buxton RB, Frank LR. Implementation of quantitative perfusion imaging techniques for functional brain mapping using pulsed arterial spin labeling. *NMR Biomed* 1997; **10(4-5)**:237-249.
41. Alsop DC, Detre JA. Multisection cerebral blood flow MR imaging with continuous arterial spin labeling. *Radiology* 1998; **208(2)**:410-416.
42. Zaharchuk G, Mandeville JB, Bogdanov AA, Jr., Weissleder R, Rosen BR, Marota JJ. Cerebrovascular dynamics of autoregulation and hypoperfusion. An MRI study of CBF and changes in total and microvascular cerebral blood volume during hemorrhagic hypotension. *Stroke* 1999; **30(10)**:2197-2204.
43. Detre JA, Alsop DC. Perfusion magnetic resonance imaging with continuous arterial spin labeling: methods and clinical applications in the central nervous system. *Eur J Radiol* 1999; **30(2)**:115-124.
44. Ye FQ, Frank JA, Weinberger DR, McLaughlin AC. Noise reduction in 3D perfusion imaging by attenuating the static signal in arterial spin tagging (ASSIST). *Magn Reson Med* 2000; **44(1)**:92-100.
45. Wang J, Alsop DC, Li L, Listerud J, Gonzalez-At JB, Schnall MD, *et al.* Comparison of quantitative perfusion imaging using arterial spin labeling at 1.5 and 4.0 Tesla. *Magn Reson Med* 2002; **48(2)**:242-254.
46. Garcia D, de Bazelaire C., Alsop DC. Pseudo-continuous flow driven adiabatic inversion for arterial spin labeling. In: ISMRM. Miami Beach, FL, USA; 2005.
47. Detre JA, Samuels OB, Alsop DC, Gonzalez-At JB, Kasner SE, Raps EC. Noninvasive magnetic resonance imaging evaluation of cerebral blood flow with acetazolamide challenge in patients with cerebrovascular stenosis. *J Magn Reson Imaging* 1999; **10(5)**:870-875.
48. Alsop DC, Dai W, Grossman M, Detre JA. Arterial spin labeling blood flow MRI: its role in the early characterization of Alzheimer's disease. *J Alzheimers Dis* 2010; **20(3)**:871-880.
49. Golay X, Hendrikse J, Lim TC. Perfusion imaging using arterial spin labeling. *Top Magn Reson Imaging* 2004; **15(1)**:10-27.
50. Gevers S, Nederveen AJ, Fijnvandraat K, van den Berg SM, van OP, Heijtel DF, *et al.* Arterial spin labeling measurement of cerebral perfusion in children with sickle cell disease. *J Magn Reson Imaging* 2012; **35(4)**:779-787.
51. Hartkamp NS, Petersen ET, De Vis JB, Bokkers RP, Hendrikse J. Mapping of cerebral perfusion territories using territorial arterial spin labeling: techniques and clinical application. *NMR Biomed* 2013; **26(8)**:901-912.
52. Detre JA, Leigh JS, Williams DS, Koretsky AP. Perfusion imaging. *Magn Reson Med* 1992; **23(1)**:37-45.
53. Alsop DC, Detre JA, Golay X, Gunther M, Hendrikse J, Hernandez-Garcia L, *et al.* Recommended implementation of arterial spin-labeled perfusion MRI for clinical applications: A consensus of the ISMRM perfusion study group and the European consortium for ASL in dementia. *Magn Reson Med* 2014.
54. Lu H, Clingman C, Golay X, van Zijl PC. Determining the longitudinal relaxation time (T1) of blood at 3.0 Tesla. *Magn Reson Med* 2004; **52(3)**:679-682.
55. Zhang X, Petersen ET, Ghariq E, De Vis JB, Webb AG, Teeuwisse WM, *et al.* In vivo blood T(1) measurements at 1.5 T, 3 T, and 7 T. *Magn Reson Med* 2012; **70(4)**:1082-1086.
56. Weiskopf N, Suckling J, Williams G, Correia MM, Inkster B, Tait R, *et al.* Quantitative multi-parameter mapping of R1, PD(*), MT, and R2(*) at 3T: a multi-center validation. *Front Neurosci* 2013; **7**:95.
57. Edelman RR, Siewert B, Darby DG, Thangaraj V, Nobre AC, Mesulam MM, *et al.* Qualitative mapping of cerebral blood flow and functional localization with echo-planar MR imaging and signal targeting with alternating radio frequency. *Radiology* 1994; **192(2)**:513-520.
58. Yang Y, Frank JA, Hou L, Ye FQ, McLaughlin AC, Duyn JH. Multislice imaging of quantitative cerebral perfusion with pulsed arterial spin labeling. *Magn Reson Med* 1998; **39(5)**:825-832.

59. Golay X. How to do an ASL multicenter neuroimaging study. In: International Society of Magnetic Resonance in Medicine; 2009.
60. Bland JM, Altman DG. Measuring agreement in method comparison studies. *Stat Methods Med Res* 1999; **8(2)**:135-160.
61. WG2 Joint Committee for Guides in Metrology, Bureau International des Poids et Mesures. International vocabulary of metrology - Basic and general concepts and associated terms. *Joint Committee for Guides in Metrology* 2008.
62. Bland JM, Altman DG. Measurement error proportional to the mean. *BMJ* 1996; **313(7049)**:106.
63. Bland JM, Altman DG. Agreement between methods of measurement with multiple observations per individual. *J Biopharm Stat* 2007; **17(4)**:571-582.
64. Floyd TF, Ratcliffe SJ, Wang J, Resch B, Detre JA. Precision of the CASL-perfusion MRI technique for the measurement of cerebral blood flow in whole brain and vascular territories. *J Magn Reson Imaging* 2003; **18(6)**:649-655.
65. Gevers S, van Osch MJ, Bokkers RP, Kies DA, Teeuwisse WM, Majoie CB, *et al.* Intra- and multicenter reproducibility of pulsed, continuous and pseudo-continuous arterial spin labeling methods for measuring cerebral perfusion. *J Cereb Blood Flow Metab* 2011.
66. Petersen ET, Mouridsen K, Golay X. The QUASAR reproducibility study, Part II: Results from a multi-center Arterial Spin Labeling test-retest study. *Neuroimage* 2010; **49(1)**:104-113.
67. Wu B, Lou X, Wu X, Ma L. Intra- and interscanner reliability and reproducibility of 3D whole-brain pseudo-continuous arterial spin-labeling MR perfusion at 3T. *J Magn Reson Imaging* 2013.
68. Wu WC, Jiang SF, Yang SC, Lien SH. Pseudocontinuous arterial spin labeling perfusion magnetic resonance imaging--a normative study of reproducibility in the human brain. *Neuroimage* 2011; **56(3)**:1244-1250.
69. Xu G, Rowley HA, Wu G, Alsop DC, Shankaranarayanan A, Dowling M, *et al.* Reliability and precision of pseudo-continuous arterial spin labeling perfusion MRI on 3.0 T and comparison with 15O-water PET in elderly subjects at risk for Alzheimer's disease. *NMR Biomed* 2010; **23(3)**:286-293.
70. Winter JD, Fierstra J, Dorner S, Fisher JA, St Lawrence KS, Kassner A. Feasibility and precision of cerebral blood flow and cerebrovascular reactivity MRI measurements using a computer-controlled gas delivery system in an anesthetised juvenile animal model. *J Magn Reson Imaging* 2010; **32(5)**:1068-1075.
71. Yen YF, Field AS, Martin EM, Ari N, Burdette JH, Moody DM, *et al.* Test-retest reproducibility of quantitative CBF measurements using FAIR perfusion MRI and acetazolamide challenge. *Magn Reson Med* 2002; **47(5)**:921-928.
72. Friston K. Ten ironic rules for non-statistical reviewers. *Neuroimage* 2012; **61(4)**:1300-1310.
73. Vidorreta M, Balteau E, Wang Z, De VE, Pastor MA, Thomas DL, *et al.* Evaluation of segmented 3D acquisition schemes for whole-brain high-resolution arterial spin labeling at 3 T. *NMR Biomed* 2014; **27(11)**:1387-1396.
74. Parkes LM, Rashid W, Chard DT, Tofts PS. Normal cerebral perfusion measurements using arterial spin labeling: reproducibility, stability, and age and gender effects. *Magn Reson Med* 2004; **51(4)**:736-743.
75. Hodkinson DJ, O'Daly O, Zunszain PA, Pariante CM, Lazurenko V, Zelaya FO, *et al.* Circadian and homeostatic modulation of functional connectivity and regional cerebral blood flow in humans under normal entrained conditions. *J Cereb Blood Flow Metab* 2014; **34(9)**:1493-1499.
76. Chen Y, Wang DJ, Detre JA. Test-retest reliability of arterial spin labeling with common labeling strategies. *J Magn Reson Imaging* 2011; **33(4)**:940-949.
77. Liu T, Wierenga C, Mueller B, F-BIRN. Reliability and Reproducibility of Arterial Spin Labeling Perfusion Measures Assessed with a Multi-Center Study. In: International Society of Magnetic Resonance in Medicine; 2008. p. 3338.

78. Petersen ET, Zimine I, Ho YC, Golay X. Non-invasive measurement of perfusion: a critical review of arterial spin labelling techniques. *Br J Radiol* 2006; **79(944)**:688-701.
79. Wu WC, St Lawrence KS, Licht DJ, Wang DJ. Quantification issues in arterial spin labeling perfusion magnetic resonance imaging. *Top Magn Reson Imaging* 2010; **21(2)**:65-73.
80. Mezue M, Segerdahl AR, Okell TW, Chappell MA, Kelly ME, Tracey I. Optimization and reliability of multiple postlabeling delay pseudo-continuous arterial spin labeling during rest and stimulus-induced functional task activation. *J Cereb Blood Flow Metab* 2014; **34(12)**:1919-1927.
81. Bokkers RP, van Laar PJ, van de Ven KC, Kapelle LJ, Klijn CJ, Hendrikse J. Arterial spin-labeling MR imaging measurements of timing parameters in patients with a carotid artery occlusion. *AJNR Am J Neuroradiol* 2008; **29(9)**:1698-1703.
82. MacIntosh BJ, Graham SJ. Magnetic resonance imaging to visualize stroke and characterize stroke recovery: a review. *Front Neurol* 2013; **4**:60.
83. Donahue J, Sumer S, Wintermark M. Assessment of collateral flow in patients with cerebrovascular disorders. *J Neuroradiol* 2013.
84. MacIntosh BJ, Swardfager W, Robertson AD, Tchistiakova E, Saleem M, Oh PI, *et al.* Regional Cerebral Arterial Transit Time Hemodynamics Correlate with Vascular Risk Factors and Cognitive Function in Men with Coronary Artery Disease. *AJNR Am J Neuroradiol* 2014.
85. Al-Bachari S, Parkes LM, Vidyasagar R, Hanby MF, Tharaken V, Leroi I, *et al.* Arterial spin labelling reveals prolonged arterial arrival time in idiopathic Parkinson's disease. *Neuroimage Clin* 2014; **6**:1-8.
86. Wang R, Yu S, Alger JR, Zuo Z, Chen J, Wang R, *et al.* Multi-delay arterial spin labeling perfusion MRI in moyamoya disease--comparison with CT perfusion imaging. *Eur Radiol* 2014; **24(5)**:1135-1144.
87. van Gelderen P, de Zwart JA, Duyn JH. Pitfalls of MRI measurement of white matter perfusion based on arterial spin labeling. *Magn Reson Med* 2008; **59(4)**:788-795.
88. Qiu M, Paul MR, Arora J, Planeta-Wilson B, Weinzimmer D, Wang J, *et al.* Arterial transit time effects in pulsed arterial spin labeling CBF mapping: insight from a PET and MR study in normal human subjects. *Magn Reson Med* 2010; **63(2)**:374-384.
89. Brown WR, Thore CR. Review: cerebral microvascular pathology in ageing and neurodegeneration. *Neuropathol Appl Neurobiol* 2011; **37(1)**:56-74.
90. MacIntosh BJ, Pattinson KT, Gallichan D, Ahmad I, Miller KL, Feinberg DA, *et al.* Measuring the effects of remifentanyl on cerebral blood flow and arterial arrival time using 3D GRASE MRI with pulsed arterial spin labelling. *J Cereb Blood Flow Metab* 2008; **28(8)**:1514-1522.
91. Gonzalez-At JB, Alsop DC, Detre JA. Cerebral perfusion and arterial transit time changes during task activation determined with continuous arterial spin labeling. *Magn Reson Med* 2000; **43(5)**:739-746.
92. Yang Y, Engelen W, Xu S, Gu H, Silbersweig DA, Stern E. Transit time, trailing time, and cerebral blood flow during brain activation: measurement using multislice, pulsed spin-labeling perfusion imaging. *Magn Reson Med* 2000; **44(5)**:680-685.
93. Yang Y, Engelen W, Xu S, Gu H, Silbersweig DA, Stern E. Transit time, trailing time, and cerebral blood flow during brain activation: measurement using multislice, pulsed spin-labeling perfusion imaging. *Magn Reson Med* 2000; **44(5)**:680-685.
94. Wang J, Alsop DC, Song HK, Maldjian JA, Tang K, Salvucci AE, *et al.* Arterial transit time imaging with flow encoding arterial spin tagging (FEAST). *Magn Reson Med* 2003; **50(3)**:599-607.
95. Dai W, Shankaranarayanan A, Alsop DC. Volumetric measurement of perfusion and arterial transit delay using hadamard encoded continuous arterial spin labeling. *Magn Reson Med* 2013; **69(4)**:1014-1022.

96. Teeuwisse WM, Schmid S, Ghariq E, Veer IM, van Osch MJ. Time-encoded pseudocontinuous arterial spin labeling: Basic properties and timing strategies for human applications. *Magn Reson Med* 2014.
97. Petersen ET, De Vis JB, Van den Berg CAT, Hendrikse J. Turbo-QUASAR: a signal-to-noise optimal arterial spin labeling and sampling strategy. In: International Society for Magnetic Resonance in Medicine; 2013.
98. Wu WC, Fernandez-Seara M, Detre JA, Wehrli FW, Wang J. A theoretical and experimental investigation of the tagging efficiency of pseudocontinuous arterial spin labeling. *Magn Reson Med* 2007; **58(5)**:1020-1027.
99. Dai W, Garcia D, de BC, Alsop DC. Continuous flow-driven inversion for arterial spin labeling using pulsed radio frequency and gradient fields. *Magn Reson Med* 2008; **60(6)**:1488-1497.
100. van der Meer JN, Heijtel DF, van HG, Plattel GJ, van Osch MJ, van Someren EJ, *et al.* Acoustic noise reduction in pseudo-continuous arterial spin labeling (pCASL). *MAGMA* 2014; **27(3)**:269-276.
101. Vidorreta M, Wang Z, Rodriguez I, Pastor MA, Detre JA, Fernandez-Seara MA. Comparison of 2D and 3D single-shot ASL perfusion fMRI sequences. *Neuroimage* 2012; **66C**:662-671.
102. Aguirre GK, Detre JA, Zarahn E, Alsop DC. Experimental design and the relative sensitivity of BOLD and perfusion fMRI. *Neuroimage* 2002; **15(3)**:488-500.
103. Wang Z, Aguirre GK, Rao H, Wang J, Fernandez-Seara MA, Childress AR, *et al.* Empirical optimization of ASL data analysis using an ASL data processing toolbox: ASLtbx. *Magn Reson Imaging* 2008; **26(2)**:261-269.
104. St Lawrence KS, Frank JA, Bandettini PA, Ye FQ. Noise reduction in multi-slice arterial spin tagging imaging. *Magn Reson Med* 2005; **53(3)**:735-738.
105. Maleki N, Dai W, Alsop DC. Optimization of background suppression for arterial spin labeling perfusion imaging. *MAGMA* 2012; **25(2)**:127-133.
106. Ghariq E, Chappell MA, Schmid S, Teeuwisse WM, van Osch MJ. Effects of background suppression on the sensitivity of dual-echo arterial spin labeling MRI for BOLD and CBF signal changes. *Neuroimage* 2014; **103C**:316-322.
107. Hartkamp NS, van Osch MJ, Kappelle J, Bokkers RP. Arterial spin labeling magnetic resonance perfusion imaging in cerebral ischemia. *Curr Opin Neurol* 2014; **27(1)**:42-53.
108. Ashburner J. A fast diffeomorphic image registration algorithm. *Neuroimage* 2007; **38(1)**:95-113.
109. Skup M. Longitudinal fMRI analysis: A review of methods. *Stat Interface* 2010; **3(2)**:232-252.
110. Dai W, Carmichael OT, Lopez OL, Becker JT, Kuller LH, Gach HM. Effects of image normalization on the statistical analysis of perfusion MRI in elderly brains. *J Magn Reson Imaging* 2008; **28(6)**:1351-1360.
111. Ridgway GR, Litvak V, Flandin G, Friston KJ, Penny WD. The problem of low variance voxels in statistical parametric mapping; a new hat avoids a 'haircut'. *Neuroimage* 2012; **59(3)**:2131-2141.
112. Yamaji S, Ishii K, Sasaki M, Imamura T, Kitagaki H, Sakamoto S, *et al.* Changes in cerebral blood flow and oxygen metabolism related to magnetic resonance imaging white matter hyperintensities in Alzheimer's disease. *J Nucl Med* 1997; **38(9)**:1471-1474.
113. Brickman AM, Zahra A, Muraskin J, Steffener J, Holland CM, Habeck C, *et al.* Reduction in cerebral blood flow in areas appearing as white matter hyperintensities on magnetic resonance imaging. *Psychiatry Res* 2009; **172(2)**:117-120.
114. Zhang Q, Stafford RB, Wang Z, Arnold SE, Wolk DA, Detre JA. Microvascular Perfusion Based on Arterial Spin Labeled Perfusion MRI as a Measure of Vascular Risk in Alzheimer's Disease. *J Alzheimers Dis* 2012; **32(3)**:677-687.
115. Longstreth WT, Jr., Arnold AM, Beauchamp NJ, Jr., Manolio TA, Lefkowitz D, Jungreis C, *et al.* Incidence, manifestations, and predictors of worsening white matter on serial cranial magnetic resonance imaging in the elderly: the Cardiovascular Health Study. *Stroke* 2005; **36(1)**:56-61.

116. de Leeuw FE, de Groot JC, Bots ML, Wittteman JC, Oudkerk M, Hofman A, *et al.* Carotid atherosclerosis and cerebral white matter lesions in a population based magnetic resonance imaging study. *J Neurol* 2000; **247(4)**:291-296.
117. Gunning-Dixon FM, Brickman AM, Cheng JC, Alexopoulos GS. Aging of cerebral white matter: a review of MRI findings. *Int J Geriatr Psychiatry* 2009; **24(2)**:109-117.
118. Longstreth WT, Jr., Manolio TA, Arnold A, Burke GL, Bryan N, Jungreis CA, *et al.* Clinical correlates of white matter findings on cranial magnetic resonance imaging of 3301 elderly people. The Cardiovascular Health Study. *Stroke* 1996; **27(8)**:1274-1282.
119. Bernick C, Kuller L, Dulberg C, Longstreth WT, Jr., Manolio T, Beauchamp N, *et al.* Silent MRI infarcts and the risk of future stroke: the cardiovascular health study. *Neurology* 2001; **57(7)**:1222-1229.
120. Gunning-Dixon FM, Raz N. The cognitive correlates of white matter abnormalities in normal aging: a quantitative review. *Neuropsychology* 2000; **14(2)**:224-232.
121. Greenberg SM. Small vessels, big problems. *N Engl J Med* 2006; **354(14)**:1451-1453.
122. Erten-Lyons D, Woltjer R, Kaye J, Mattek N, Dodge HH, Green S, *et al.* Neuropathologic basis of white matter hyperintensity accumulation with advanced age. *Neurology* 2013; **81(11)**:977-983.
123. Garcia-Lorenzo D, Francis S, Narayanan S, Arnold DL, Collins DL. Review of automatic segmentation methods of multiple sclerosis white matter lesions on conventional magnetic resonance imaging. *Med Image Anal* 2013; **17(1)**:1-18.
124. Nowinski WL, Chua BC, Marchenko Y, Puspitsari F, Volkau I, Knopp MV. Three-dimensional reference and stereotactic atlas of human cerebrovasculature from 7T Tesla. *Neuroimage* 2011; **55(3)**:986-998.
125. Paulson OB, Strandgaard S, Edvinsson L. Cerebral autoregulation. *Cerebrovasc Brain Metab Rev* 1990; **2(2)**:161-192.
126. van Gelderen P, de Zwart JA, Duyn JH. Pitfalls of MRI measurement of white matter perfusion based on arterial spin labeling. *Magn Reson Med* 2008; **59(4)**:788-795.
127. van Osch MJ, Teeuwisse WM, van Walderveen MA, Hendrikse J, Kies DA, van Buchem MA. Can arterial spin labeling detect white matter perfusion signal? *Magn Reson Med* 2009; **62(1)**:165-173.
128. Wu WC, Lin SC, Wang DJ, Chen KL, Li YD. Measurement of cerebral white matter perfusion using pseudocontinuous arterial spin labeling 3T magnetic resonance imaging--an experimental and theoretical investigation of feasibility. *PLoS One* 2013; **8(12)**:e82679.
129. Pohmann R. Accurate, localized quantification of white matter perfusion with single-voxel ASL. *Magn Reson Med* 2010; **64(4)**:1109-1113.
130. Pegelow CH, Macklin EA, Moser FG, Wang WC, Bello JA, Miller ST, *et al.* Longitudinal changes in brain magnetic resonance imaging findings in children with sickle cell disease. *Blood* 2002; **99(8)**:3014-3018.
131. Ohene-Frempong K, Weiner SJ, Sleeper LA, Miller ST, Embury S, Moohr JW, *et al.* Cerebrovascular accidents in sickle cell disease: rates and risk factors. *Blood* 1998; **91(1)**:288-294.
132. Steen RG, Miles MA, Helton KJ, Strawn S, Wang W, Xiong X, *et al.* Cognitive impairment in children with hemoglobin SS sickle cell disease: relationship to MR imaging findings and hematocrit. *AJNR Am J Neuroradiol* 2003; **24(3)**:382-389.
133. Prohovnik I, Hurler-Jensen A, Adams R, De VD, Pavlakis SG. Hemodynamic etiology of elevated flow velocity and stroke in sickle-cell disease. *J Cereb Blood Flow Metab* 2009; **29(4)**:803-810.
134. Miller ST, Macklin EA, Pegelow CH, Kinney TR, Sleeper LA, Bello JA, *et al.* Silent infarction as a risk factor for overt stroke in children with sickle cell anemia: a report from the Cooperative Study of Sickle Cell Disease. *J Pediatr* 2001; **139(3)**:385-390.
135. Adams RJ. Big strokes in small persons. *Arch Neurol* 2007; **64(11)**:1567-1574.

136. London K, Howman-Giles R. Voxel-based analysis of normal cerebral [F]FDG uptake during childhood using statistical parametric mapping. *Neuroimage* 2014.
137. Helton KJ, Paydar A, Glass J, Weirich EM, Hankins J, Li CS, *et al.* Arterial spin-labeled perfusion combined with segmentation techniques to evaluate cerebral blood flow in white and gray matter of children with sickle cell anemia. *Pediatr Blood Cancer* 2009; **52(1)**:85-91.
138. Van der Land V., Zwanenburg JJ, Biemond BJ, Hendrikse J, Mutsaerts HJMM, Engelen M, *et al.* Cerebral small vessel disease in patients with sickle cell disease: initial findings with ultra-high field 7T MRI. In: Annual Meeting and Exposition. New Orleans: Blood; 2013.
139. Hendrikse J, Petersen ET, Golay X. Vascular disorders: insights from arterial spin labeling. *Neuroimaging Clin N Am* 2012; **22(2)**:259-2xi.

Part I

Inter-vendor reproducibility of ASL

2

Inter-vendor reproducibility of pseudo-continuous arterial spin labeling at 3 Tesla

HJMM Mutsaerts

RME Steketee

DFR Heijtel

JPA Kuijjer

MJP van Osch

CBLM Majoie

M Smits

AJ Nederveen

PlosOne 9; 2014. In press

Abstract

Purpose Prior to the implementation of arterial spin labeling (ASL) in clinical multi-center studies, it is important to establish its status quo inter-vendor reproducibility. This study evaluates and compares the intra- and inter-vendor reproducibility of pseudo-continuous ASL (pCASL) as clinically implemented by GE and Philips.

Material and Methods 22 healthy volunteers were scanned twice on both a 3T GE and a 3T Philips scanner. The main difference in implementation between the vendors was the readout module: spiral 3D fast spin echo vs. 2D gradient-echo echo-planar imaging respectively. Mean and variation of cerebral blood flow (CBF) were compared for the total gray matter (GM) and white matter (WM), and on a voxel-level.

Results Whereas the mean GM CBF of both vendors was almost equal ($p=1.0$), the mean WM CBF was significantly different ($p<0.01$). The inter-vendor GM variation did not differ from the intra-vendor GM variation ($p=0.3$ and $p=0.5$ for GE and Philips respectively). Spatial inter-vendor CBF and variation differences were observed in several GM regions and in the WM.

Conclusion These results show that total GM CBF-values can be exchanged between vendors. For the inter-vendor comparison of GM regions or WM, these results encourage further standardization of ASL implementation among vendors.

Introduction

Arterial spin labeling (ASL) is an emerging magnetic resonance imaging (MRI) perfusion modality that enables non-invasive cerebral perfusion measurements. Since ASL is virtually harmless, not hampered by the blood-brain barrier and enables absolute quantification of cerebral blood flow (CBF), it is an attractive tool compared to other perfusion imaging modalities^{1, 2}. Through several methodological advances, ASL perfusion MRI has matured to the point where it can provide high quality whole-brain perfusion images in only a few minutes of scanning³. Its reproducibility has been established and its CBF-maps are comparable with imaging methods based on exogenous tracers^{4,7}. ASL is commercially available on all major MRI systems and clinical applications are under rapid development. ASL-based CBF measurements are of clinical value in a number of cerebral pathologies, such as brain tumors, cerebrovascular pathology, epilepsy and neurodegeneration^{8, 9}. Therefore, the initiation of large-scale multi-center ASL studies is a next step to extend our understanding of the pathophysiology of many common disorders.

However, it is essential to first establish the inter-vendor reproducibility of ASL^{10,11}. One main obstacle that impedes multi-center studies, is that fundamental differences exist between ASL implementations of different vendors. Each MRI vendor has implemented a different labeling-readout combination, which may seriously hamper the comparison of multi-vendor ASL-data¹². Since each labeling and readout strategy exhibits specific advantages and disadvantages, a substantial technical heterogeneity is introduced¹³. Therefore, it remains unclear to which degree ASL-based CBF-maps from centers with scanners of different vendors are comparable. The aim of the current study is to assess and compare the intra- and inter-vendor reproducibility of pseudo-continuous ASL (pCASL) CBF measurements as currently clinically implemented by two major vendors: i.e. GE and Philips.

Materials and Methods

Subject recruitment and study design

Twenty-two healthy volunteers (9 men, 13 women, mean age 22.6 ± 2.1 (SD) years) were included. In addition to standard MRI exclusion criteria, subjects with history of brain or psychiatric disease or use of medication - except for oral contraceptives - were excluded. No consumption of vasomotor substances such as alcohol, cigarettes, coffee, licorice and tea was allowed on the scan days. On the day prior to the examination, alcohol and nicotine consumption was restricted to three units and cigarettes respectively.

All subjects were scanned twice at two academic medical centers in the Netherlands: Erasmus MC – University Medical Center Rotterdam (center 1) and Academic Medical Center Amsterdam (center 2). The inter-session time interval was kept at 1-4 weeks. MRI experiments were performed on a 3T GE scanner at center 1 (Discovery MR750, GE Healthcare, Milwaukee, WI, US) and on a 3T Philips scanner at center 2 (Intera, Philips Healthcare, Best, the Netherlands), both equipped with an 8-channel head coil (InVivo, Gainesville, FL, US). Foam padding inside the head coil was used to restrict head motion during scanning¹⁰. Subjects were awake and had their eyes closed during all ASL scans.

Ethics statement

All subjects provided written informed consent and the study was approved by the ethical review boards of both centers.

Acquisition

Each scan session included a pCASL and 1 mm isotropic 3D T1-weighted scan for segmentation and registration purposes. For the acquisition of a single time-point CBF-map, pCASL has become the preferred labeling strategy because of its relatively high signal-to-noise ratio (SNR) and wide availability across all platforms^{3, 14}. On both scanners we employed the clinically implemented pCASL protocols that are currently used in clinical studies^{15, 16}. Table 1 and Figure 1 summarize the protocol details and show the timing diagrams for both sequences respectively. The main difference between the GE and Philips implementations was the readout module: multi-shot spiral 3D fast spin-echo vs. single-shot 2D gradient-echo echo-planar imaging respectively.

Post-processing: quantification

Matlab 7.12.0 (MathWorks, MA, USA) and Statistical Parametric Mapping (SPM) 8 (Wellcome Trust Center for Neuroimaging, University College London, UK) were used for post-processing and statistical analyses. For the Philips data, label and control pCASL images were pair-wise subtracted and averaged to obtain perfusion-weighted images. For the GE data, the perfusion-weighted images as directly provided by the scanner were used. Since the images as provided by GE did not incorporate motion correction, this was not applied to the Philips data. The perfusion-weighted maps of both vendors were quantified into CBF maps using a single compartment model^{3, 17}:

$$CBF(mL/100g/min) = \frac{6000\Delta M e^{PLD/T_{1a}}}{2\alpha\alpha_{inv}M_{0a}T_{1a}(1 - e^{-\tau/T_{1a}})} \quad [1]$$

where ΔM represents the difference images between control and label and M_{0a} the equilibrium magnetization of arterial blood. In Philips, ΔM was corrected for the transversal magnetization decay time (T_2^*) of arterial blood (48 ms) during the 17 ms echo time (TE) by e^{TE/T_2^*} ¹⁸. PLD is the post-labeling delay (1.525 s), T_{1a} is the longitudinal relaxation time of arterial blood (1.650 s), α is the labeling efficiency (0.8), where α_{inv} corrects for the decrease in labeling efficiency due to the 5 and 2 background suppression pulses at GE (0.75) and Philips (0.83) respectively and τ represents the labeling duration (1.450 s and 1.650 s for GE and Philips respectively)¹⁹⁻²¹. The increase in label decay in the ascending acquired 2D slices in Philips-data was accounted for. GE has, but Philips has not, implemented a standard M_0 -acquisition where proton density maps are obtained with a saturation recovery acquisition using readout parameters identical to the ASL readout. These maps were converted to M_{0a} by the following equation:

$$M_{0a} = \frac{PD}{\lambda_{GM}(1 - e^{-\frac{t_{sat}}{T_{1GM}}})} \quad [2]$$

where t_{sat} is the saturation recovery time (2 s), T_{1GM} is the relaxation time of gray matter (GM) tissue (1.2 s) and λ_{GM} is the GM brain-blood water partition coefficient (0.9 mL/g)^{15, 22, 23}. For the Philips data, a single M_{0a} -value was used for all subjects. This value was obtained in a previous study with the same center, scanner, head coil, pCASL protocol and a similar population (n=16, 56% M, age 20-24 years)²⁴. In short, cerebrospinal fluid T1 recovery curves were fitted on the control images of multiple time-point pCASL measurements, with the same readout, without background suppression. The acquired M_0 was converted to M_{0a} by multiplication with the blood water partition coefficient (0.76) and the density of brain tissue (1.05 g/mL)^{23, 25}. No difference was made between the quantification of GM and WM CBF.

Post-processing: spatial normalization

A single 3D T1-weighted anatomical scan from each scanner for each subject (n=44) was segmented into GM and white matter (WM) tissue probability maps. All CBF maps were transformed into anatomical space by a rigid-body registration on the GM tissue probability maps. The tissue probability maps were spatially normalized using the Diffeomorphic Anatomical Registration analysis using Exponentiated Lie algebra (DARTEL) algorithm, and the resulting normalization fields were applied to

the CBF maps as well ²⁶. Finally, all normalized images were spatially smoothed using an 8 x 8 x 8 mm full-width-half-maximum Gaussian kernel, to minimize registration and interpolation errors.

Data analysis

All intra-vendor reproducibility analyses were based on a comparison of session 1 with session 2 within each vendor (n=22). All inter-vendor reproducibility analyses were based on a comparison of GE session 1 with Philips session 2, and GE session 2 with Philips session 1 (n=44). In this way, the temporal physiological variation is expected to have an equal contribution to the intra- and inter-vendor reproducibility. All reproducibility analyses were based on the mean CBF of the two sessions, and on the mean and standard deviation of the paired inter-session CBF difference, denoted as ΔCBF and $SD_{\Delta CBF}$ respectively. The within-subject coefficient of variation (wsCV) - a normalized parameter of variation - was defined as the ratio of $SD_{\Delta CBF}$ to the mean CBF of both sessions:

$$wsCV = 100\% \frac{SD_{\Delta CBF}}{meanCBF} \quad [3]$$

Reproducibility was assessed on a total GM and WM level, and on a voxel-level.

Data analysis: total supratentorial GM and WM

Mean CBF-values of each session were obtained for the total supratentorial GM and WM. GM and WM masks were obtained by thresholding GM and WM probability maps at 70% and 95% tissue probabilities respectively. GM-WM CBF ratios were calculated individually. The significance of paired inter-session CBF differences (ΔCBF) was tested with a paired two-tailed Student's t-test. The Levene's test was used to test the significance of the difference between GE $SD_{\Delta CBF}$ and Philips $SD_{\Delta CBF}$, as well as between the inter-vendor $SD_{\Delta CBF}$ and both intra-vendor $SD_{\Delta CBF}$ ²⁷. Limits of agreement - defining the range in which 95% of future measurements is expected to lie - were defined as $\Delta CBF \pm 1.96 SD_{\Delta CBF}$ ²⁸.

Data analysis: voxel-level comparison

To assess spatial inter-vendor differences, CBF- and wsCV-values were computed for each voxel. For CBF, both sessions and all subjects were averaged. To test significant voxel-wise inter-vendor CBF differences, a Bonferroni-corrected paired two-tailed Student's t-test was performed (using both sessions, n=44). Individual histograms of CBF (25 bins, range 0-160 mL/100g/min) were averaged to generate a group-level histogram. A wsCV histogram (25 bins, range 5-45%) was generated from the

wsCV-maps. Both CBF and wsCV histograms were generated for the total supratentorial GM and WM of each vendor. Statistical significance was set to $p < 0.05$ for all tests.

	GE	Philips
Labeling module	pseudo-continuous	pseudo-continuous
Labeling pulse shape	Hanning	Hanning
Labeling pulse duration	0.5 ms	0.5 ms
Labeling pulse flip angle	23°	18°
Mean gradient strength	0.7 mT/m	0.6 mT/m
Maximal gradient strength	7 mT/m	6 mT/m
Labeling duration	1450 ms	1650 ms
Post-labeling delay (PLD) (initial)	1525 ms	1525 ms
PLD increase per slice	n.a.	28.3 ms
PLD (average)	1525 ms	1770 ms
Labeling plane planning	Fixed 22 mm below lower edge	89 mm below, parallel to AC-PC line
Labeling plane distance*	72 mm	89 mm
Readout module	3D fast spin-echo interleaved stack-of-spirals	2D gradient-echo single-shot echo-planar imaging SENSE 2.5, CLEAR
Acquisition matrix	8 spirals x 512 sampling points	80 x 80
Field of view	24 cm ³	24 cm ²
Number of slices	36	17
Slice thickness	4 mm	7 mm
Acquisition voxel size (volume)	3.8 x 3.8 x 4 mm (57.8 mm ³)	3.0 x 3.0 x 7.0 mm (63 mm ³)
Reconstruction voxel size	1.9 x 1.9 x 4.0 mm	3.0 x 3.0 x 7.0 mm
Slice gap	n.a.	0 mm
Echo time/repetition time	10.5/4600 ms	17/4000 ms
Number of signal averages	3	33
Readout planning	True axial, lower edge fixed at lower boundary pons	Parallel to AC-PC line
Background suppression (n pulses)	yes (5)	yes (2)
Vascular crushing	no	no
Acquisition duration	4:29 min	4:33 min

Table 1 Acquisition protocols. *Labeling plane distance represents distance from the anterior commissure-posterior commissure (ACPC) line in the head-feet direction ²⁰. n.a. = not applicable

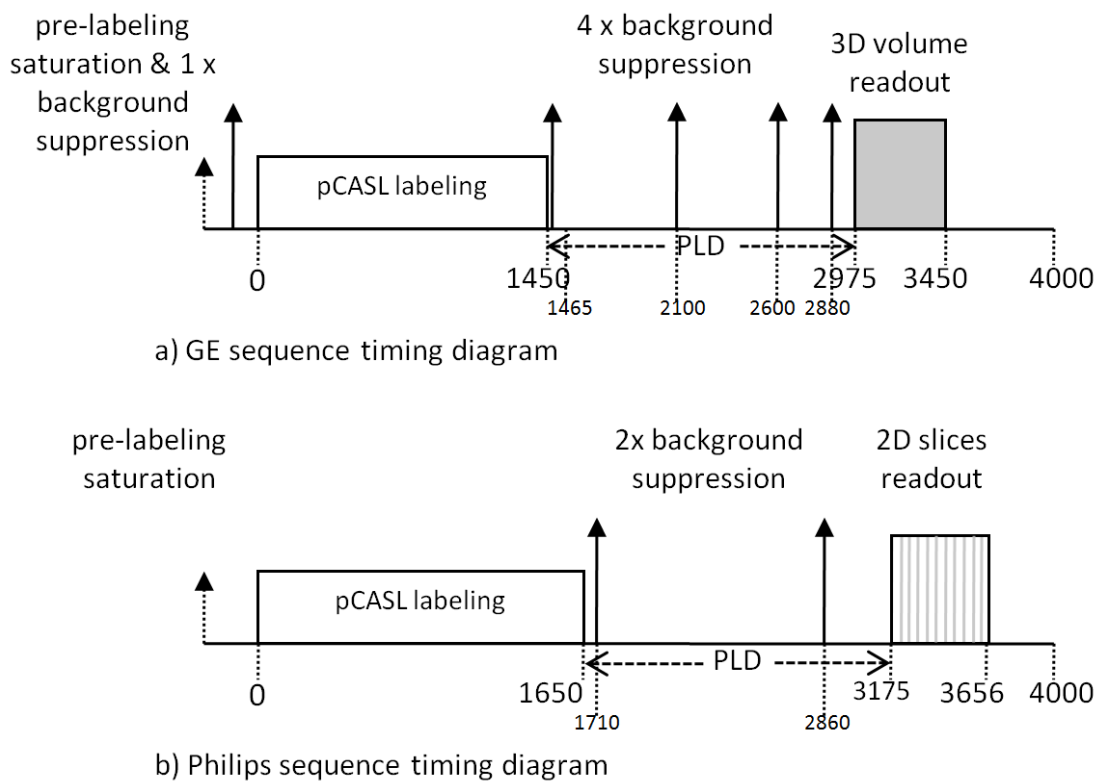


Figure 1. Sequence timing diagrams of a) General Electric (GE) and b) Philips, shown at the same time scale (ms). pCASL = pseudo-continuous arterial spin labeling, PLD = post-labeling delay.

Results

Session timing

The number of days between intra-vendor sessions did not differ between vendors: 18.3 ± 6.5 and 19.7 ± 7.2 for GE and Philips respectively (independent sample Student's t-test, $p=0.5$). However, GE session 1 and session 2 took place earlier in the day compared to the Philips sessions ($15\text{h}26 \pm 4\text{h}00$ and $15\text{h}55 \pm 3\text{h}34$ compared to $20\text{h}16 \pm 2\text{h}06$ and $19\text{h}47 \pm 2\text{h}38$ respectively, $p<0.01$).

Total GM and WM

The intra- and inter-vendor statistics are summarized in Table 2 and visualized by the Bland-Altman plots in Figure 2. GM CBF did not differ significantly between both vendors ($p=1.0$), but WM CBF did ($p<0.01$). Likewise, the intra-vendor GM variances of the paired CBF differences did not differ between the two vendors whereas the WM variances did ($p=0.6$ and $p=0.02$ respectively). The GM-WM CBF ratios of both vendors differed significantly, the 2D readout (Philips) GM-WM ratio being approximately twice as large as the ratio of the 3D readout (GE) ($p<0.01$). Both the GM and WM intra-vendor wsCVs were similar to the inter-vendor wsCVs (Table 2), which is confirmed by the Levene's

test. The variance of GM inter-vendor CBF differences did not differ significantly from the variance of intra-vendor differences ($p=0.3$ and $p=0.5$ for GE and Philips respectively). For the WM, however, the variance of inter-vendor CBF differences did differ significantly from the Philips variance but not from the GE variance ($p=0.02$ and $p=0.8$ respectively).

	GE	CI (n=22)	Philips	CI (n=22)	inter- vendor	CI (n=44)
GM mean CBF (mL/100g/min)	65.9	48.4 ··· 83.4	65.9	42.0 ··· 89.8	65.9	45.4 ··· 86.4
GM Δ CBF	-0.4	-3.5 ··· 2.8	3.9	0.6 ··· 7.2	0.0	-2.7 ··· 2.7
GM $SD_{\Delta CBF}$	7.1	4.8 ··· 9.4	7.5	5.1 ··· 9.8	8.9	7.0 ··· 10.9
GM lower LOA	-14.3	-18.2 ··· -10.4	-10.7	-14.8 ··· -6.6	-17.5	-20.9 ··· -14.2
GM upper LOA	13.6	9.7 ··· 17.5	18.5	14.4 ··· 22.6	17.5	14.2 ··· 20.9
GM wsCV (%)	10.8	6.2 ··· 15.3	11.3	5.4 ··· 17.2	13.6	9.8 ··· 17.3
WM mean CBF (mL/100g/min)	30.5	22.0 ··· 39.0	15.4	9.1 ··· 21.7	22.9	15.6 ··· 30.3
WM Δ CBF	-0.6	-2.2 ··· 1.0	1.0	0.1 ··· 2.0	15.0	14.0 ··· 16.1
WM $SD_{\Delta CBF}$	3.6	2.4 ··· 4.7	2.1	1.4 ··· 2.8	3.5	2.7 ··· 4.2
WM lower LOA	-7.6	-9.6 ··· -5.7	-3.1	-4.3 ··· -2.0	8.3	7.0 ··· 9.6
WM upper LOA	6.4	4.4 ··· 8.3	5.2	4.1 ··· 6.4	21.8	20.5 ··· 23.1
WM wsCV (%)	11.7	9.5 ··· 13.9	13.8	12.2 ··· 15.4	15.0	13.7 ··· 16.4
GM-WM CBF ratio	2.2	1.9 ··· 2.5	4.3	3.4 ··· 5.2	2.9	2.4 ··· 3.4

Table 2 Inter-session statistics. Mean and Δ CBF represent the inter-session CBF mean and paired difference respectively. The limits of agreement (LOA) represent Δ CBF \pm 1.96 standard deviation of the paired difference ($SD_{\Delta CBF}$). CI = confidence interval, CBF = cerebral blood flow, GE = General Electric, GM = gray matter, WM = white matter, wsCV = within-subject coefficient of variation.

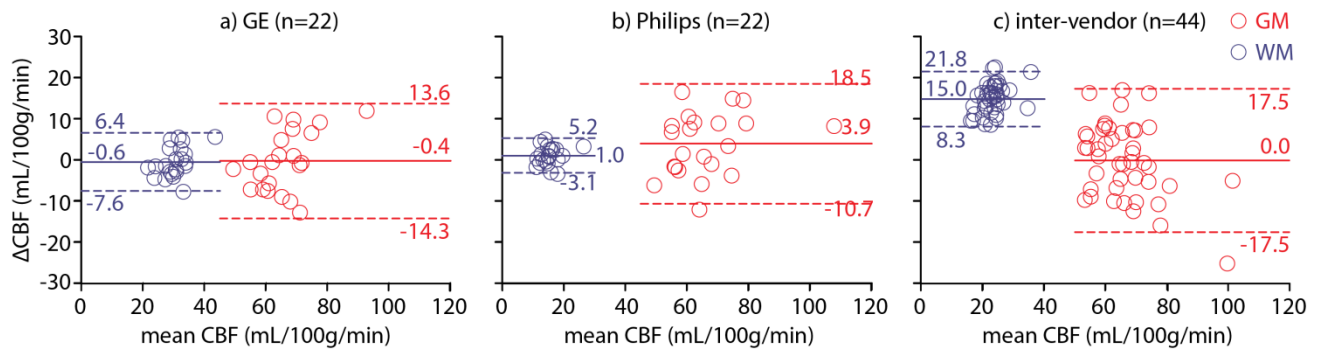


Figure 2. Bland-Altman plots. Intra-vendor a) GE (n=22) and b) Philips (n=22) and c) inter-vendor (n=44) GM (red) and WM (blue) CBF differences are plotted against mean CBF. Continuous and broken lines indicate mean difference and limits of agreement (mean difference \pm 1.96 standard deviation of the paired difference) respectively. CBF= cerebral blood flow, GM=gray matter, WM=white matter.

Voxel-level comparison

Spatial CBF differences between GE and Philips are illustrated for a single subject and on group level in Figure 3 and 4 respectively. The spatial wsCV distribution is shown in Figure 5. In addition, Figure 6 provides an overview of spatial CBF differences between subjects, sessions and vendors for a single transversal slice. The main visual difference on all these maps was the homogeneity of GE compared to the heterogeneity of Philips, especially in the WM and in the z-direction. More specifically, the contrast between GM and WM was higher on the Philips CBF and wsCV-maps. Also within the GM, the CBF was more heterogeneous on the Philips maps compared to the GE maps. A CBF decrease and wsCV increase was observed in the posterior and superior regions on the GE maps and in the anterior-inferior and superior regions on the Philips maps. The GM CBF histograms were comparable between vendors (Figure 4d). The GE WM CBF histogram had a higher mean, but had the same shape as the Philips WM CBF histogram. The wsCV histograms, on the other hand, were less comparable (Figure 5d). The spatial GM wsCV distribution of Philips had a higher mean and was wider compared to GE. This difference in mean and spread was even larger for the WM.

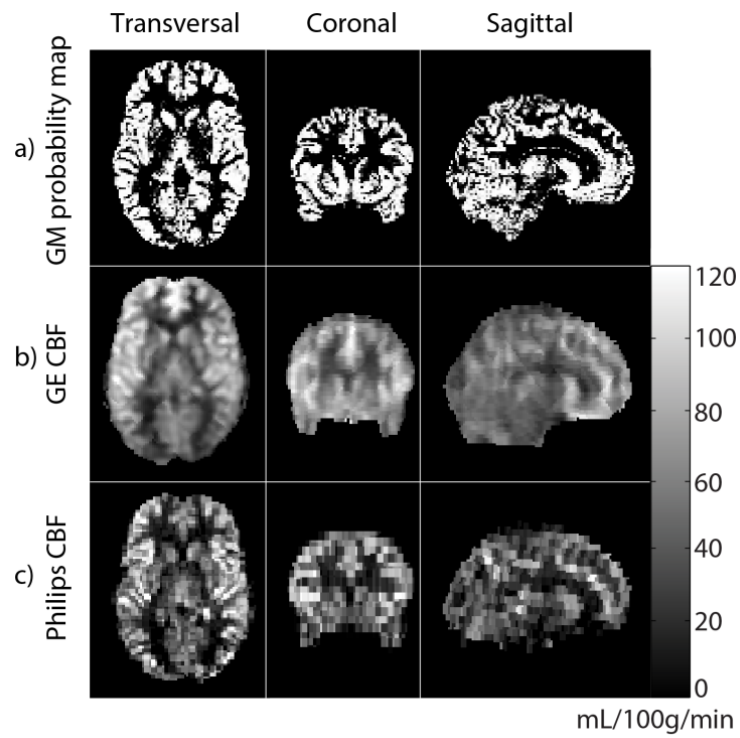


Figure 3. Cerebral blood flow maps of a representative subject of GE (b) and Philips (c), as compared to gray matter (GM) tissue probability map (a; for this example the GE 3D T1-weighted image was used). Maps are registered, re-sliced, skull-stripped and shown in native space.

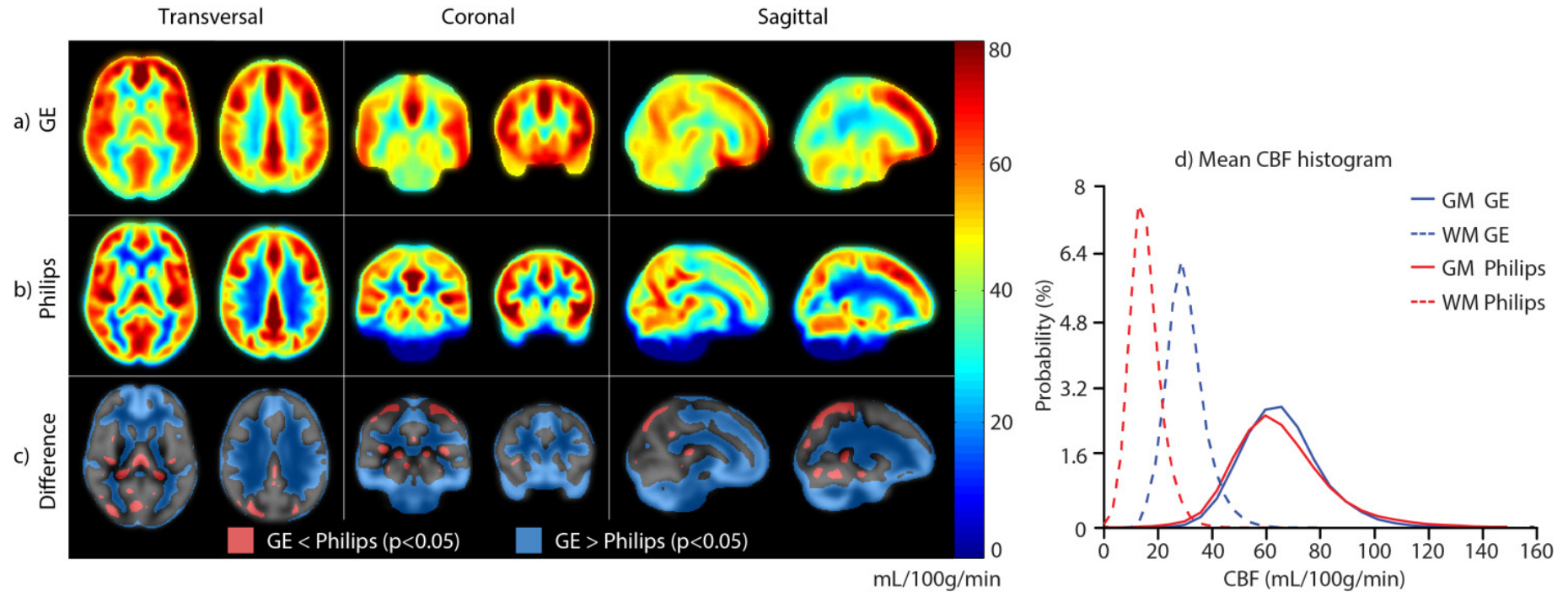


Figure 4. Mean cerebral blood flow (CBF) maps of all subjects ($n=22$) are shown for GE (a) and Philips (b), averaged for both sessions. Voxel-wise significant inter-vendor differences are visualized by a binary parametric map projected on the gray matter (GM) probability map (c). Red voxels represent where $GE < Philips$, blue voxels represent where $GE > Philips$ (Bonferroni corrected $p < 0.05$). On the right, mean CBF histograms are shown for the total GM and white matter (WM) (d).

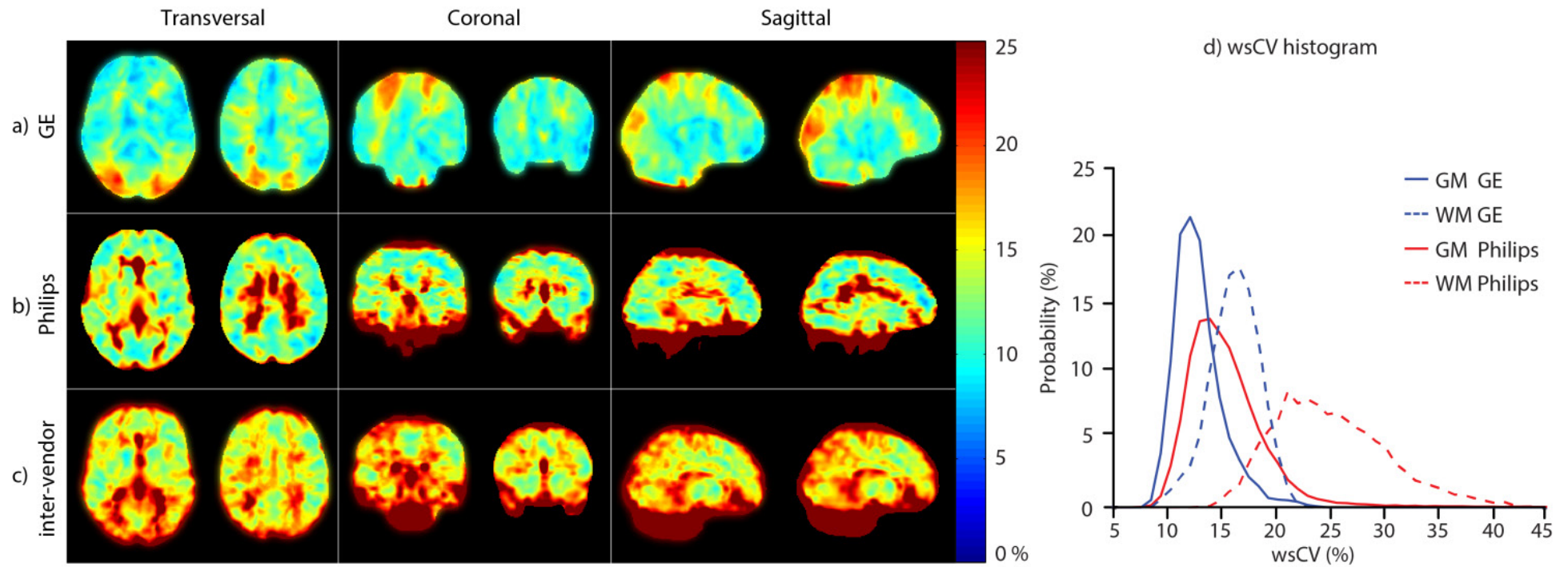


Figure 5. a) GE and b) Philips intra- and c) inter-vendor within-subject coefficient of variability (wsCV)-maps. d) wsCV histograms are shown on the right for the total gray matter (GM) and white matter (WM).

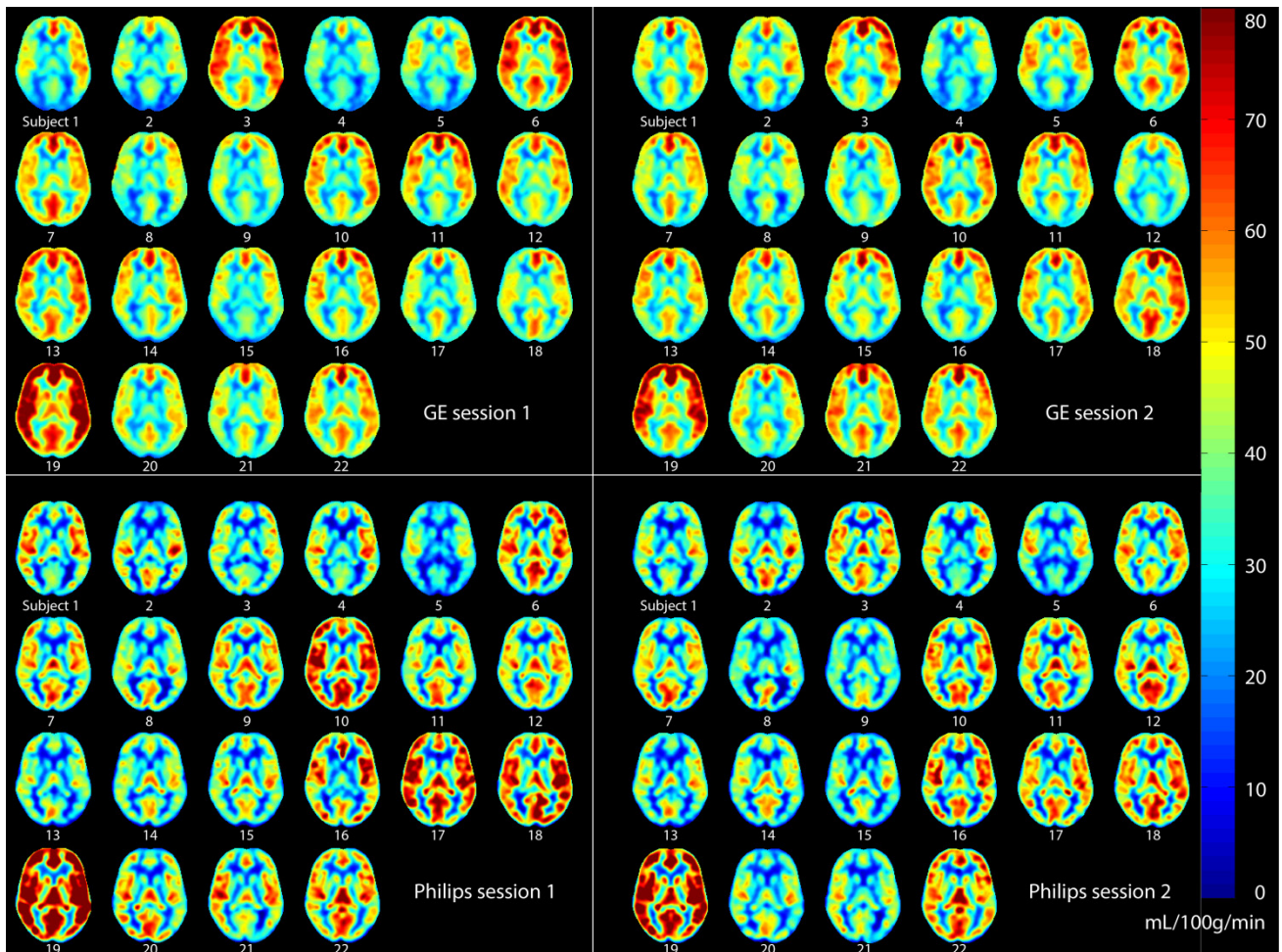


Figure 6. Single transversal cerebral blood flow slice of all subjects ($n=22$) for GE (upper quadrants) and Philips (lower quadrants), session 1 (left quadrants) and session 2 (right quadrants), after spatial normalization.

Discussion

The most important result of this study is that - despite several voxel-wise differences between vendors - there were no inter-vendor differences in mean CBF or wsCV on a total GM level. This can be explained by the fact that the variation between the sessions can for a large part be attributed to physiological factors, as was previously noted in single-vendor reproducibility studies^{11, 29-31}. For clinical studies that focus on the GM in total, it may therefore be more important to minimize and account for physiological variation than to account for inter-vendor differences in ASL implementation.

A different picture arises for smaller GM regions or for the total WM. We observed several spatial differences between vendors which can mainly be explained by differences in the readout module. The most visually striking inter-vendor difference on all CBF- and wsCV-maps was in the WM. The GM-

WM CBF ratio of the 2D readout (Philips) was twice as large as the ratio of the 3D readout (GE), which is in agreement with a previous readout comparison on a single Siemens scanner¹³. This can be explained by the larger extent of spatial smoothing of a spiral 3D readout (GE) compared to the 2D readout (Philips), which leads to more contamination of the GM signal into the WM and vice versa. Therefore, a 2D readout seems most suitable when the goal is to acquire uncontaminated GM or WM CBF – although the ability of ASL to measure WM CBF is debatable due to the long transit time of WM³².

This difference in spatial smoothing may also explain the homogeneous GM appearance of the mean CBF and wsCV maps acquired with GE as compared to the more heterogeneous appearance of those acquired with Philips. In addition, it may explain the significant inter-vendor CBF difference within the subcortical GM since this area is surrounded by WM and therefore suffers more from smoothing with WM signal in GE (Figure 4c). Another explanation for the smaller spatial variation of GE, is its higher SNR compared to Philips. The SNR at GE is most probably higher because of the intrinsically high SNR of a 3D readout and because background suppression is more efficient for a single-volume readout as compared to a multi-slice readout¹³. In addition, parallel imaging was not available in the GE sequence, but was turned on in the Philips sequence. To what extent the heterogeneous appearance of the Philips CBF maps has a physiological origin or is rather the result of a too low SNR, cannot be differentiated with these data.

In regions with long arrival times - i.e. the posterior vascular territory and posterior watershed area - lower CBF and higher wsCV was observed in GE but not in Philips (Figures 4 and 5)⁵. This inter-vendor difference can be explained by differences in the effective post-labeling delay (PLD) between the readouts, even though both acquisitions had the same initial PLD (1525 ms). Whereas the 3D readout obtains all ASL signal for the total 3D volume at a single time-point - i.e. after 1525 ms PLD - the 2D readout obtains signal from each slice sequentially. With this multi-slice acquisition, each slice exhibits a longer effective PLD compared to its previous slice. This inferior-superior PLD increase of the 2D readout (Philips) allows the labeled blood more time to reach the superior slices compared to the homogeneous PLD of the 3D readout (GE). Therefore, the PLD may have been too short for the label to reach the superior slices in 3D (GE), whereas the effective PLD for the superior slices in 2D (Philips) was sufficient. These inter-vendor CBF differences and higher wsCV for GE in superior regions with long transit times are probably resolved by selecting a longer PLD for the 3D readout, such as 2000 ms

³.

Other prominent spatial inter-vendor CBF (Figure 4) and wsCV (Figure 5) differences were observed on the brain edges. We observed higher CBF and lower wsCV in anterior and inferior regions in Philips but not in GE. The prominent inferior CBF and wsCV differences (Figure 4c and Figure 5c) are partly due to the fact that these slices were simply not acquired by the 2D readout (Philips). With a 2D sequence, it is common practice to scan cerebral slices only as well as to optimize the PLD, T1 decay and background suppression for the cerebral slices. These issues do not apply for a 3D sequence, whose 3D slab usually has whole-brain coverage. The differences in the other areas can be explained by susceptibility artifacts from bone-air transitions at the paranasal sinuses and mastoid air cells present in the gradient-echo T2*-weighted readout implemented by Philips³³. In addition, it is expected that the echo-planar imaging readout (Philips) exhibits geometric distortion in these regions³³. The T2-weighted spin-echo readout employed by GE is much less sensitive to these artifacts, in comparison to the gradient-echo readout employed by Philips. For these reasons, a 3D readout is superior in regions such as the orbito-frontal lobe and cerebellum compared to a 2D readout. This especially favors the use of a 3D readout for clinical applications of ASL, since pathologies in these regions could remain undetected on a 2D readout³⁴⁻³⁶.

A limitation of the current study is that we did not acquire spatial M_0 -maps with the same readout in Philips. By employing a voxel-wise normalization of the ASL-signal, these maps would have opposed the T_2^* susceptibility effects, since these will be approximately equally large for the ΔM and M_0 -map. Therefore, Philips spatial M_{0a} -maps could have improved quantification in regions of air-tissue transitions, which may have diminished the inter-vendor variation to a certain extent. However, the added value of spatial M_0 -maps is limited since they cannot improve the lower SNR of the gradient-echo readout (Philips) near the air-tissue transitions. Therefore, the inter-vendor reproducibility in these regions is expected to remain low.

The current study may also be limited by the inter-vendor calibration of quantification parameters. These may remain arbitrary, mostly because they have been derived from simulations rather than measurements. One example is the inter-vendor differences in labeling efficiency due to a different number of background suppression pulses (5 and 2 for GE and Philips respectively)²¹. One way to deal with this is to scale to a phase-contrast MRI sequence of the main feeding arteries²⁰. However, this would shift the inter-vendor CBF variation from the ASL-sequence towards the phase-contrast MRI measurements.

Inter-vendor CBF and wsCV differences were observed on a voxel-level but not on the total GM level. Apparently, the effects of the abovementioned readout differences do cancel out when sufficient GM voxels are averaged. There are several explanations for this observation. First, the higher SNR of the 3D module may be important on a voxel-level, but if sufficient GM voxels are averaged physiological variation seems to outnumber the SNR differences between the readout modules. Second, the smoothing of the GE 3D readout averages signal from multiple GM voxels which increases SNR and subsequently decreases the wsCV within a single voxel. This effect is similar to averaging signal from multiple GM voxels of the 2D readout in post-processing. Therefore, this difference of spatial signal averaging between both readouts becomes apparent on a voxel-level but is negligible when all GM voxels are averaged.

It should be acknowledged that this study evaluated healthy controls only. The abovementioned inter-vendor readout differences could become more or less important in patients, considering the different spatial CBF variation in patients compared to healthy controls. Furthermore, these inter-vendor differences should not be generalized to all MRI vendors. Visual readout differences between GE and Siemens, who both use a 3D approach, may be smaller than the readout differences in the current study

¹³.

In conclusion, the current study shows that pCASL results do not differ between vendors on a total GM level. Therefore, the reliability of averaged CBF-values for the total GM can be expected to be equal in single- and multi-vendor studies. However, the reliability of measurements in GM regions or in the WM, is impeded by differences between the readout modules of both vendors. Therefore, our results strongly encourage the standardization of ASL implementations among vendors, which was also advocated by the recent ASL consensus paper³.

Reference list

1. Golay X, Hendrikse J, Lim TC. Perfusion imaging using arterial spin labeling. *Top Magn Reson Imaging* 2004; **15(1)**:10-27.
2. Williams DS, Detre JA, Leigh JS, Koretsky AP. Magnetic resonance imaging of perfusion using spin inversion of arterial water. *Proc Natl Acad Sci U S A* 1992; **89(1)**:212-216.
3. Alsop DC, Detre JA, Golay X, Gunther M, Hendrikse J, Hernandez-Garcia L, *et al.* Recommended implementation of arterial spin-labeled perfusion MRI for clinical applications: A consensus of the ISMRM perfusion study group and the European consortium for ASL in dementia. *Magn Reson Med* 2014.
4. Chen Y, Wolk DA, Reddin JS, Korczykowski M, Martinez PM, Musiek ES, *et al.* Voxel-level comparison of arterial spin-labeled perfusion MRI and FDG-PET in Alzheimer disease. *Neurology* 2011; **77(22)**:1977-1985.
5. Petersen ET, Mouridsen K, Golay X. The QUASAR reproducibility study, Part II: Results from a multi-center Arterial Spin Labeling test-retest study. *Neuroimage* 2010; **49(1)**:104-113.
6. Xu G, Rowley HA, Wu G, Alsop DC, Shankaranarayanan A, Dowling M, *et al.* Reliability and precision of pseudo-continuous arterial spin labeling perfusion MRI on 3.0 T and comparison with 15O-water PET in elderly subjects at risk for Alzheimer's disease. *NMR Biomed* 2010; **23(3)**:286-293.
7. Jahng GH, Song E, Zhu XP, Matson GB, Weiner MW, Schuff N. Human brain: reliability and reproducibility of pulsed arterial spin-labeling perfusion MR imaging. *Radiology* 2005; **234(3)**:909-916.
8. Detre JA, Rao H, Wang DJ, Chen YF, Wang Z. Applications of arterial spin labeled MRI in the brain. *J Magn Reson Imaging* 2012; **35(5)**:1026-1037.
9. Hendrikse J, Petersen ET, Golay X. Vascular disorders: insights from arterial spin labeling. *Neuroimaging Clin N Am* 2012; **22(2)**:259-2xi.
10. Golay X. How to do an ASL multicenter neuroimaging study. In: International Society of Magnetic Resonance in Medicine; 2009.
11. Liu T, Wierenga C, Mueller B, F-BIRN. Reliability and Reproducibility of Arterial Spin Labeling Perfusion Measures Assessed with a Multi-Center Study. In: International Society of Magnetic Resonance in Medicine; 2008. p. 3338.
12. Kilroy E, Apostolova L, Liu C, Yan L, Ringman J, Wang DJ. Reliability of two-dimensional and three-dimensional pseudo-continuous arterial spin labeling perfusion MRI in elderly populations: Comparison with 15o-water positron emission tomography. *J Magn Reson Imaging* 2013.
13. Vidorreta M, Wang Z, Rodriguez I, Pastor MA, Detre JA, Fernandez-Seara MA. Comparison of 2D and 3D single-shot ASL perfusion fMRI sequences. *Neuroimage* 2012; **66C**:662-671.
14. Chen Y, Wang DJ, Detre JA. Test-retest reliability of arterial spin labeling with common labeling strategies. *J Magn Reson Imaging* 2011; **33(4)**:940-949.
15. Binnewijzend MA, Kuijer JP, Benedictus MR, van der Flier WM, Wink AM, Wattjes MP, *et al.* Cerebral blood flow measured with 3D pseudocontinuous arterial spin-labeling MR imaging in Alzheimer disease and mild cognitive impairment: a marker for disease severity. *Radiology* 2013; **267(1)**:221-230.
16. Donahue MJ, Ayad M, Moore R, van OM, Singer R, Clemmons P, *et al.* Relationships between hypercarbic reactivity, cerebral blood flow, and arterial circulation times in patients with moyamoya disease. *J Magn Reson Imaging* 2013.
17. Alsop DC, Detre JA. Reduced transit-time sensitivity in noninvasive magnetic resonance imaging of human cerebral blood flow. *J Cereb Blood Flow Metab* 1996; **16(6)**:1236-1249.
18. St Lawrence KS, Wang J. Effects of the apparent transverse relaxation time on cerebral blood flow measurements obtained by arterial spin labeling. *Magn Reson Med* 2005; **53(2)**:425-433.

19. Lu H, Clingman C, Golay X, van Zijl PC. Determining the longitudinal relaxation time (T1) of blood at 3.0 Tesla. *Magn Reson Med* 2004; **52(3)**:679-682.
20. Aslan S, Xu F, Wang PL, Uh J, Yezhuvath US, van OM, *et al.* Estimation of labeling efficiency in pseudocontinuous arterial spin labeling. *Magn Reson Med* 2010; **63(3)**:765-771.
21. Garcia DM, Duhamel G, Alsop DC. Efficiency of inversion pulses for background suppressed arterial spin labeling. *Magn Reson Med* 2005; **54(2)**:366-372.
22. Lu H, Nagae-Poetscher LM, Golay X, Lin D, Pomper M, van Zijl PC. Routine clinical brain MRI sequences for use at 3.0 Tesla. *J Magn Reson Imaging* 2005; **22(1)**:13-22.
23. Herscovitch P, Raichle ME. What is the correct value for the brain--blood partition coefficient for water? *J Cereb Blood Flow Metab* 1985; **5(1)**:65-69.
24. Heijtel DF, Mutsaerts HJ, Bakker E, Schober P, Stevens MF, Petersen ET, *et al.* Accuracy and precision of pseudo-continuous arterial spin labeling perfusion during baseline and hypercapnia: a head-to-head comparison with O HO positron emission tomography. *Neuroimage* 2014.
25. Chalela JA, Alsop DC, Gonzalez-Atavales JB, Maldjian JA, Kasner SE, Detre JA. Magnetic resonance perfusion imaging in acute ischemic stroke using continuous arterial spin labeling. *Stroke* 2000; **31(3)**:680-687.
26. Ashburner J. A fast diffeomorphic image registration algorithm. *Neuroimage* 2007; **38(1)**:95-113.
27. Levene, Howard, Olkin I, Hotelling H. *Contributions to Probability and Statistics: Essays in Honor of Harold Hotelling*. Stanford University Press; 1960.
28. Bland JM, Altman DG. Measuring agreement in method comparison studies. *Stat Methods Med Res* 1999; **8(2)**:135-160.
29. Floyd TF, Ratcliffe SJ, Wang J, Resch B, Detre JA. Precision of the CASL-perfusion MRI technique for the measurement of cerebral blood flow in whole brain and vascular territories. *J Magn Reson Imaging* 2003; **18(6)**:649-655.
30. Parkes LM, Rashid W, Chard DT, Tofts PS. Normal cerebral perfusion measurements using arterial spin labeling: reproducibility, stability, and age and gender effects. *Magn Reson Med* 2004; **51(4)**:736-743.
31. Gevers S, van Osch MJ, Bokkers RP, Kies DA, Teeuwisse WM, Majoie CB, *et al.* Intra- and multicenter reproducibility of pulsed, continuous and pseudo-continuous arterial spin labeling methods for measuring cerebral perfusion. *J Cereb Blood Flow Metab* 2011; **31(8)**:1706-1715.
32. van Gelderen P, de Zwart JA, Duyn JH. Pitfalls of MRI measurement of white matter perfusion based on arterial spin labeling. *Magn Reson Med* 2008; **59(4)**:788-795.
33. Deichmann R, Josephs O, Hutton C, Corfield DR, Turner R. Compensation of susceptibility-induced BOLD sensitivity losses in echo-planar fMRI imaging. *Neuroimage* 2002; **15(1)**:120-135.
34. Timmann D, Konczak J, Ilg W, Donchin O, Hermsdorfer J, Gizewski ER, *et al.* Current advances in lesion-symptom mapping of the human cerebellum. *Neuroscience* 2009; **162(3)**:836-851.
35. Wolf RC, Thomann PA, Sambataro F, Vasic N, Schmid M, Wolf ND. Orbitofrontal cortex and impulsivity in borderline personality disorder: an MRI study of baseline brain perfusion. *Eur Arch Psychiatry Clin Neurosci* 2012; **262(8)**:677-685.
36. Walther S, Federspiel A, Horn H, Razavi N, Wiest R, Dierks T, *et al.* Resting state cerebral blood flow and objective motor activity reveal basal ganglia dysfunction in schizophrenia. *Psychiatry Res* 2011; **192(2)**:117-124.

3

Reproducibility of pharmacological ASL using sequences from different vendors: implications for multi-center drug studies

HJMM Mutsaerts

RME Steketee

DFR Heijtel

JPA Kuijer

MJP van Osch

CBLM Majoie

M Smits

AJ Nederveen

In submission

Abstract

Object The current study assesses the multi-center feasibility of pharmacological arterial spin labeling (ASL) by comparing a caffeine-induced relative cerebral blood flow decrease (%CBF↓) measured with two pseudo-continuous ASL sequences as provided by two major vendors.

Material and Methods Twenty-two healthy volunteers were scanned twice with both a 3D spiral (GE) and a 2D EPI (Philips) sequence. The inter-session reproducibility was evaluated by comparisons of the mean and within-subject coefficient of variability (wsCV) of the %CBF↓, both for the total cerebral gray matter and on a voxel level.

Results The %CBF↓ was larger when measured with the 3D spiral sequence ($23.9\% \pm 5.9\%$) than when measured with the 2D EPI sequence ($19.2\% \pm 5.6\%$) on a total gray matter level ($p=0.02$), and on a voxel level in the posterior watershed area ($p<0.001$). There was no difference between the gray matter wsCV of the 3D spiral (57.3%) and 2D EPI sequence (66.7%, $p=0.3$), whereas on a voxel level the wsCV was visibly different between the sequences.

Conclusion The observed differences between ASL sequences of both vendors can be explained by differences in the employed readout modules. These differences may seriously hamper multi-center pharmacological ASL, which strongly encourages standardization of ASL implementations.

Introduction

Pharmacological magnetic resonance imaging (phMRI) is increasingly used as a tool to study hemodynamic changes in response to a pharmaceutical substance ¹. Cerebral blood flow (CBF) as a marker of drug effects has potential use at various stages of human drug research and may even enable to monitor or predict therapeutic efficacy ^{2,3}.

Arterial spin labeling (ASL) is an attractive MRI perfusion modality that exhibits several advantages compared to modalities that have previously been used to study pharmacological effects on the brain ⁴. The use of blood as an endogenous perfusion tracer renders ASL non-invasive, making it preferable to modalities based on exogenous tracers such as positron emission tomography (PET) ⁵. Because ASL is based on a subtraction method, scanner signal drift is cancelled out, which renders ASL preferable to blood-oxygen-level-dependent (BOLD) pharmacological MRI for the study of longitudinal changes ⁴. Moreover, ASL enables absolute CBF quantification as compared to the complex contrast provided by BOLD. This exact quantification is a key advantage of ASL for the assessment of drug effects on CBF during both resting and task activation states ⁴.

Through several methodological advances, ASL perfusion MRI has matured to the point where it can provide whole brain perfusion images in only a few minutes of scanning ⁶. The reproducibility of baseline measurements has been thoroughly assessed and initial pharmacological ASL (phASL) results are promising ⁷⁻¹⁰. Therefore, the initiation of large-scale multi-center pharmacological ASL (phASL) trials is the next step to extend our understanding of the effects of drugs on cerebral hemodynamics ⁴.

One main obstacle that may impede multi-center studies, is that fundamental differences exist between ASL implementations of different vendors ¹¹⁻¹³. It is currently unknown to what extent these differences limit the interpretation and/or power of phASL. Therefore, we performed a multi-vendor reproducibility study in which we employed caffeine as a pharmacological challenge, of which the baseline results have been reported elsewhere ¹³.

Caffeine is an adenosine antagonist that not only acts as a neuro-stimulant (adenosine A1) but is also a strong vasoconstrictor (adenosine A2), reducing CBF by 13–30% ^{14,15}. Furthermore, caffeine is one of the most socially accepted and widely consumed neuro-stimulants in the world, which facilitates its use

in explorative studies in healthy volunteers^{16, 17}. For these reasons, caffeine has been the research topic in many pharmacological MRI studies and can be considered a first choice challenge to gain knowledge and experience with phASL⁴.

The current study assesses the inter-session reproducibility of a caffeine-induced CBF decrease as measured with pseudo-continuous ASL (pCASL) and compares this reproducibility between the different pCASL sequences of two MRI vendors. The mean and variation of the CBF decrease are compared on a total GM level and on a voxel level, to compare the reproducibility of phASL between the sequences on a global and on a spatial level. In addition, the obtained reproducibility measures are employed in a sample size calculation to illustrate their implications for future phASL studies.

Materials and Methods

Subject recruitment

Twenty-two healthy volunteers (9 men, 13 women, mean age 22.6 ± 2.1 years standard deviation (SD)) were included. All subjects provided written informed consent and the study was approved by the institutional review boards of both centers. In addition to standard MRI exclusion criteria, subjects with a history of neurologic or psychiatric disease or the use of prescription medication (except for oral contraceptives) were excluded. No consumption of vasoactive substances such as alcohol, cigarettes, coffee, licorice and tea was allowed on the scan days. On the day prior to the examination, alcohol and nicotine consumption was restricted to three units and cigarettes respectively.

Ethical standards

All subjects provided written informed consent and the study was approved by the institutional review boards of both centers. The current study has been performed in accordance with the ethical standards laid down in the 1964 Declaration of Helsinki and its later amendments.

Study design

Figure 1 provides a schematic overview of the study design. All subjects were scanned twice at two academic medical centers in the Netherlands. MRI experiments were performed at center 1 on a 3T GE scanner (Discovery MR750, GE Healthcare, Milwaukee, WI, US) and at center 2 on a 3T Philips scanner

(Intera, Philips Healthcare, Best, the Netherlands), both equipped with an 8-channel head coil (InVivo, Gainesville, FL, US), in random order to avoid order effects. The inter-session time interval was kept at 1–4 weeks. pCASL scans were performed before and 30 minutes after the oral intake of four 50 mg caffeine tablets, from a single preparation batch from a single supplier (Fagron, Capelle aan den IJssel, The Netherlands). This resulted in an average administered dose of 2.9 ± 0.4 mg/kg at an average subject weight of 69.2 ± 9.6 kg. For the intake of caffeine, subjects were removed from the scanner gantry, remained seated on the scanner couch and were returned in the scanner gantry after which localizer and reference scans were repeated. Care was taken to keep the head position in relation to the coil as identical as possible. Foam padding was used to restrict head motion during scanning.

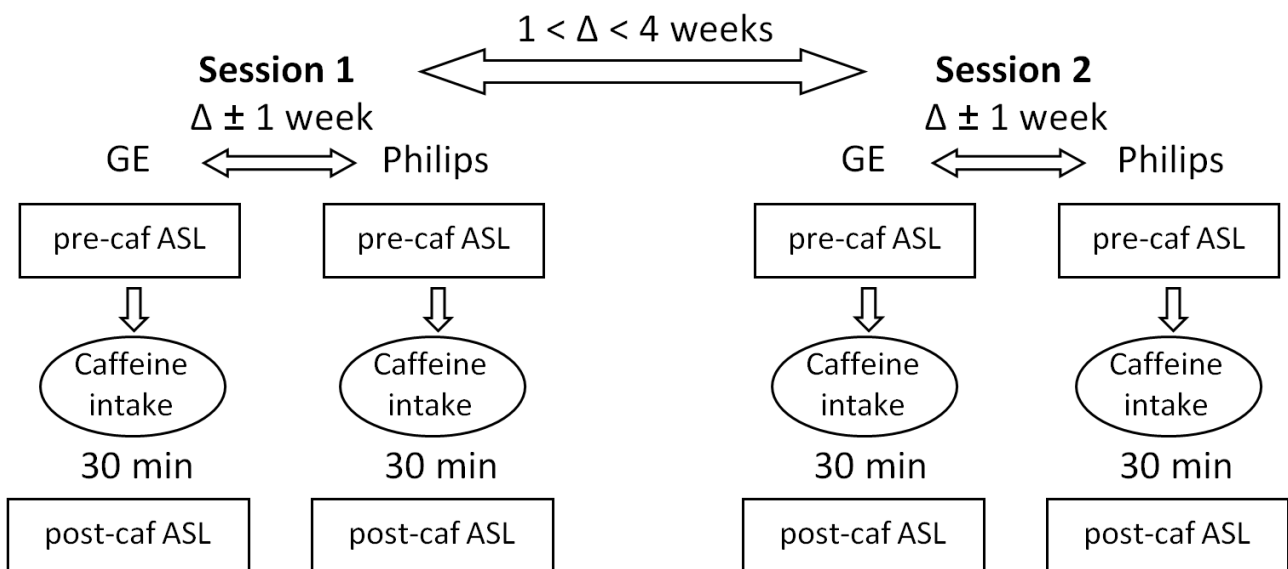


Figure 1. A schematic view of the study design. ASL = arterial spin labeling, caf = caffeine, Δ = inter-session time difference.

Acquisition

Each scan session included a pCASL and a 1 mm^3 isotropic 3D T1-weighted scan for segmentation, registration and normalization purposes. On both scanners we employed the standard clinical pCASL protocols as provided by the vendors, which are currently used in clinical research^{18, 19}. Table 1 summarizes the similarities and differences between the two pCASL protocols. The main difference

between the pCASL sequences implemented by GE and Philips is the readout module: multi-shot spiral 3D fast spin-echo versus single-shot 2D gradient-echo echo-planar imaging (EPI) respectively.

	3D spiral sequence	2D EPI sequence
Labeling module	pseudo-continuous	pseudo-continuous
Labeling pulse shape	Hanning	Hanning
Labeling pulse duration	0.5 ms	0.5 ms
Labeling pulse flip angle	23°	18°
Mean gradient strength	0.7 mT/m	0.6 mT/m
Maximal gradient strength	7 mT/m	6 mT/m
Labeling duration	1450 ms	1650 ms
Post-labeling delay (PLD) (initial)	1525 ms	1525 ms
PLD increase per slice	n.a.	28.3 ms
PLD (average)	1525 ms	1770 ms
Labeling plane planning	Fixed 22 mm below lower edge	89 mm below, parallel to AC-PC line
Labeling plane distance*	72 mm	89 mm
Readout module	3D fast spin-echo interleaved stack-of-spirals	2D gradient-echo single-shot echo-planar imaging SENSE 2.5, CLEAR
Acquisition matrix	8 spirals x 512 sampling points	80 x 80
Field of view	24 cm ³	24 cm ²
Number of slices	36	17
Slice thickness	4 mm	7 mm
Acquisition voxel size (volume)	3.8 x 3.8 x 4 mm (57.8 mm ³)	3.0 x 3.0 x 7.0 mm (63 mm ³)
Reconstruction voxel size	1.9 x 1.9 x 4.0 mm	3.0 x 3.0 x 7.0 mm
Slice gap	n.a.	0 mm
Echo time/repetition time	10.5/4600 ms	17/4000 ms
Number of signal averages	3	33
Readout planning	True axial, lower edge fixed at lower boundary pons	Parallel to AC-PC line
Background suppression (n pulses)	yes (5)	yes (2)
Vascular crushing	no	no
Acquisition duration	4:29 min	4:33 min

Table 1 Acquisition protocols. *Labeling plane distance represents distance from the anterior commissure-posterior commissure (ACPC) line in the head-feet direction²¹. n.a. = not applicable

CBF quantification

Matlab 7.12.0 (MathWorks, MA, USA) and Statistical Parametric Mapping (SPM) 8 (Wellcome Trust Center for Neuroimaging, University College London, UK) were used for post-processing and statistical analyses. For the 2D EPI data, label and control pCASL images were pair-wise subtracted and averaged to obtain perfusion-weighted images. For the 3D spiral data, the perfusion-weighted images as directly provided by the scanner were used. Since the 3D spiral data did not incorporate motion correction, this was also not applied to the 2D EPI data. The quantification of CBF from the acquired perfusion-weighted scans was based on a single compartment model ⁶:

$$CBF(mL / 100g / min) = \frac{6000\Delta M e^{PLD/T_{1a}}}{2\alpha\alpha_{inv}M_{0a}T_{1a}(1 - e^{-\tau/T_{1a}})} \quad [1]$$

where ΔM represents the difference images between control and label and M_{0a} the equilibrium magnetization of arterial blood. PLD is the post-label delay (1.525 s), T_{1a} is the longitudinal relaxation time of arterial blood (1.650 s), α is the labeling efficiency (0.8), where α_{inv} corrects for the decrease in labeling efficiency due to the 5 and 2 background suppression pulses for the 3D spiral (0.75) and the 2D EPI sequence (0.83) respectively and τ represents the labeling duration (1.450 s and 1.650 s for 3D spiral and 2D EPI respectively) ²⁰⁻²². The inferior-superior increase in post-label delay in the 2D EPI multi-slice data was accounted for. GE has, but Philips has not, implemented a standard M_0 -acquisition where proton density (PD) maps are obtained with a saturation recovery acquisition using readout parameters identical to the ASL readout. These maps were converted to M_{0a} by the following equation:

$$M_{0a} = \frac{PD}{\lambda_{GM}(1 - e^{-\frac{t_{sat}}{T_{1GM}}})} \quad [2]$$

where t_{sat} is the saturation recovery time (2 s), T_{1GM} is the relaxation time of gray matter (GM) tissue (1.2 s) and λ_{GM} is the GM brain-blood water partition coefficient (0.9 mL/g) ^{23, 24}. For the 2D EPI data, a single M_{0a} -value was used for all subjects. This value was obtained in a previous study within the same center, with the same scanner, head coil, pCASL protocol and a similar population (n=16, 56% M, age 20–24 years), by fitting cerebrospinal fluid T1 recovery curves on the control images of multiple time-point pCASL measurements ²⁵. M_0 was converted to M_{0a} by multiplication with the blood water

partition coefficient (0.76), the density of brain tissue (1.05 g/mL) and by correction for the transversal magnetization decay time (T_2^*) of arterial blood (48 ms) during the 17 ms echo time (TE) by e^{TE/T_2^*} 24, 26, 27.

Spatial normalization

A single 3D T1-weighted anatomical scan from each scanner for each subject (n=44) was segmented into GM and white matter tissue probability maps. All CBF maps were transformed into anatomical space by a rigid-body registration to the GM tissue probability maps. The tissue probability maps were spatially normalized using the Diffeomorphic Anatomical Registration analysis using Exponentiated Lie algebra (DARTEL) algorithm²⁸. The resulting normalization fields were then applied to the CBF maps as well.

Statistics

Reproducibility parameters

The inter-session intra-vendor reproducibility was evaluated by a comparison of the relative CBF decrease (%CBF↓) of session 1 with %CBF↓ of session 2 (n=22). %CBF↓ was defined as:

$$\%CBF \downarrow = 100\% \frac{CBF_{pre} - CBF_{post}}{CBF_{pre}} \quad [3]$$

where CBF_{pre} and CBF_{post} represent the CBF maps acquired before and 30 minutes after caffeine intake respectively. Reproducibility analyses were based on the mean %CBF↓ of the sessions (i.e. the measured phASL effect), and on the standard deviation (SD) of the inter-session difference ($\Delta_{\%CBF\downarrow}$) in %CBF↓ ($SD\Delta_{\%CBF\downarrow}$, i.e. the variation of the phASL effect). The within-subject coefficient of variability (wsCV), a normalized parameter of variation, was defined as the ratio of $SD\Delta_{\%CBF\downarrow}$ to the mean %CBF↓ of both sessions.

Total cerebral GM

To assess global differences in the phASL effect between both sequences, mean %CBF↓ was calculated for the total cerebral GM (tissue probability thresholded >70%), for each single session separately and for both sessions averaged. The %CBF↓ of each session and the differences between sessions ($\Delta_{\%CBF\downarrow}$)

were tested for normality using the Shapiro-Wilk test. A paired two-tailed Student's t-test was used to test whether the %CBF↓ (both sessions pooled, n=44) and whether the intra-session $\Delta_{\%CBF\downarrow}$ (n=22) differed between the sequences. The Levene's test was used to test whether there was an inter-sequence difference in $SD\Delta_{\%CBF\downarrow}$. Limits of agreement were defined as $\Delta_{\%CBF\downarrow} \pm 1.96 SD\Delta_{\%CBF\downarrow}$ ²⁹. To compare results with previous ASL reproducibility studies, the absolute cerebral GM CBF decrease was calculated as well.

Spatial comparison

To assess spatial phASL differences between both sequences, both %CBF↓- and wsCV-values were computed for each cerebral GM voxel. To test in which voxels the %CBF↓ was different from 0, a two-tailed t-test was performed on the %CBF↓ maps of each session. To test in which voxels the %CBF↓ differed between the sequences, a two-tailed t-test was performed for both sessions pooled per vendor (n=44). To be sensitive for subtle differences between sequences, statistical significance was not defined strictly ($p < 0.001$, not corrected for multiple comparisons). Individual histograms of the %CBF↓ maps (50 bins, range -30–60%) were averaged to generate a group-level histogram of each session. Histograms were generated from the wsCV-maps (40 bins, range 0–150%). Both %CBF↓ and wsCV histograms were generated for the total cerebral GM. To investigate the effect of differences in data smoothness between the 3D spiral and 2D EPI sequences, the 2D EPI data were smoothed with an anisotropic Gaussian kernel to achieve the same smoothness as the 3D spiral data. Data smoothness was estimated with SPM according to a previously described method³⁰. %CBF↓ and wsCV maps and histograms were also generated from these smoothed 2D EPI data.

Sample size calculation for future studies

The cerebral GM $SD\Delta_{\%CBF\downarrow}$ from the data of both vendors were used to calculate the required sample size (n) for future phASL studies. Calculations were performed for a within-subject cross-over experimental design with a desired effect size of 15%. This effect size was chosen in a previous study that determined the sample size for ASL baseline studies³¹. Two sample sizes were calculated, to detect 1) a 15% CBF decrease caused by caffeine and 2) a 15% change in the caffeine-induced %CBF↓. A study design example where the second calculation would be applicable, is to test whether a caffeine-induced %CBF↓ changes if the measurement is repeated with a different condition (e.g. with a different drug

dose). For a one-tailed t-test in which we have a hypothesis about the direction of the CBF change (CBF is expected to decrease with caffeine) the following equation applies:

$$n = (Z_{1-\alpha/2} + Z_{1-\beta})^2 \left(\frac{SD\Delta_{\%CBF\downarrow}}{effect_size} \right)^2 \quad [4]$$

where $Z_{1-\alpha/2}$ is the Z-value related to the significance level ($p < 0.05$), $Z_{1-\beta}$ the Z-value corresponding to the detection power (80%) and $SD\Delta_{\%CBF\downarrow}$ is used for the SD in the sample size calculation of a within-subject design³¹. 15% of the mean baseline CBF and 15% of the mean $\%CBF\downarrow$ from both vendors were used as effect size for the first and second sample size calculation respectively.

Results

Total GM

The inter-session statistics are summarized in Table 2 and visualized in Bland-Altman plots in Figure 2. For both vendors, the $\%CBF\downarrow$ of both sessions and the inter-session $\Delta_{\%CBF\downarrow}$ were normally distributed according to the Shapiro-Wilk test. The mean $\%CBF\downarrow$ measured with 3D spiral was larger than the mean $\%CBF\downarrow$ measured with 2D EPI ($p=0.02$). The $\Delta_{\%CBF\downarrow}$ ($p=0.3$) and $SD\Delta_{\%CBF\downarrow}$ ($p=0.3$) did not differ between both vendors, resulting in similar wsCVs (57.3% and 66.7% for 3D spiral and 2D EPI respectively).

The mean absolute CBF decrease was 15.9 ± 5.1 and 13.1 ± 6.5 mL/100g/min for the 3D spiral and 2D EPI data respectively. The SD of the inter-session difference of the absolute CBF decrease was 9.5 and 8.7 mL/100g/min for the 3D spiral and 2D EPI data respectively.

	3D spiral	CI (n=22)	2D EPI	CI (n=22)
%CBF↓ session 1 (%)	* 21.4	-0.8 ··· 43.6	18.8	3.4 ··· 34.2
%CBF↓ session 2 (%)	* 26.4	11.1 ··· 41.8	19.6	-1.0 ··· 40.2
Mean %CBF↓ (%)	* 23.9	10.3 ··· 37.5	19.2	6.0 ··· 32.4
$\Delta_{\%CBF\downarrow}$ (%)	5.0	-1.1 ··· 11.1	0.8	-4.9 ··· 6.4
$SD\Delta_{\%CBF\downarrow}$ (%)	13.7	9.3 ··· 18.1	12.8	8.7 ··· 16.9
Lower LOA (%)	-21.8	-29.3 ··· -14.3	-24.4	-31.4 ··· -17.3
Upper LOA (%)	31.9	24.4 ··· 39.4	25.9	18.9 ··· 32.9
wsCV (%)	57.3	51.9 ··· 62.7	66.7	61.7 ··· 71.8

Table 2. Inter-session statistics. Inter-session statistics for the total cerebral gray matter, as illustrated in the Bland-Altman plots in Figure 2. Values represent mean and difference of mean %CBF↓ of both sessions respectively. %CBF↓ = relative cerebral blood flow decrease, wsCV = within-subject coefficient of variability. Asterisk (*) denotes significant ($p < 0.05$) difference between sequences. The limits of agreement (LOA) represent $\Delta_{\%CBF\downarrow} \pm 1.96$ standard deviation of the paired inter-session difference ($SD\Delta_{\%CBF\downarrow}$).

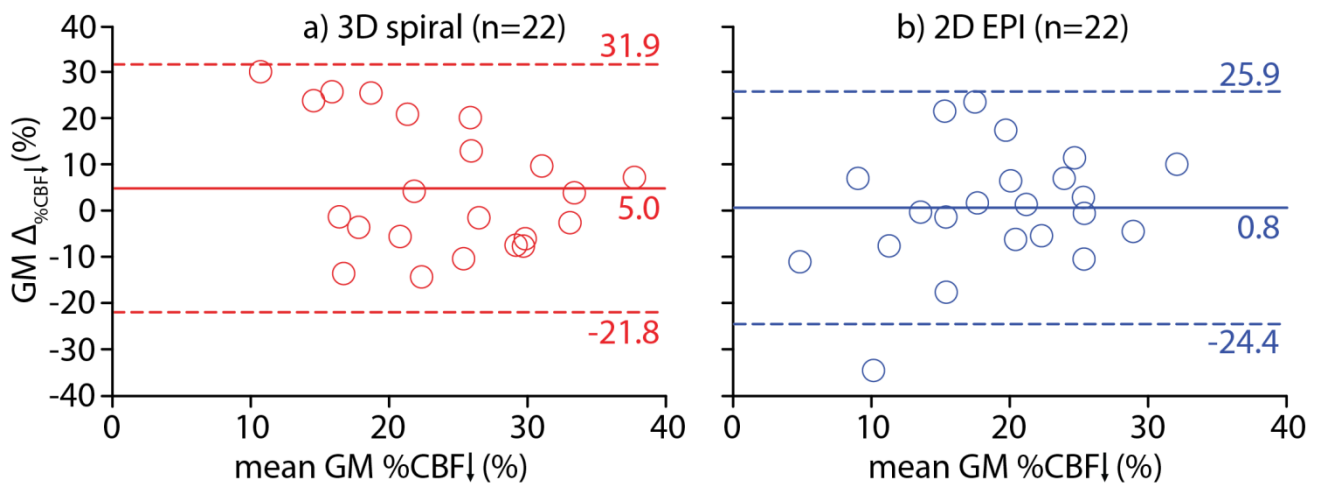


Figure 2. a–b Bland Altman plots of inter-session statistics, as summarized in Table 2. Total cerebral gray matter (GM) inter-session differences in relative cerebral blood flow decrease ($\Delta_{\%CBF\downarrow}$) are plotted

against the mean GM %CBF↓ for the a) 3D spiral (n=22) and b) 2D EPI sequence (n=22). Dotted lines indicate limits of agreement (mean difference \pm 1.96 standard deviation).

Spatial comparison

Figures 3 and 4 illustrate the spatial distribution of the caffeine-induced statistically significant %CBF↓ and wsCV respectively. The significant caffeine-induced %CBF↓ was higher for the 3D spiral sequence than for the 2D EPI sequence on visual comparison, especially in the posterior watershed region (Figure 3a and 3d). The wsCV-maps showed a homogeneous distribution for the 3D spiral data but heterogeneous for the 2D EPI data, which approached the homogeneity of the 3D spiral data after additional smoothing. The shapes of the %CBF↓ histograms of 3D spiral session 1 and both 2D EPI sessions were similar, although 3D spiral session 1 had a higher peak location (Figure 3e). The peak location of the histogram of 3D spiral session 2 was comparable to 3D spiral session 1, but the distribution was narrower. The wsCV histogram of 3D spiral had a lower peak location and a narrower distribution compared to the 2D EPI wsCV histogram (Figure 4d). After additional smoothing, the 2D EPI wsCV histogram approached the 3D spiral wsCV histogram.

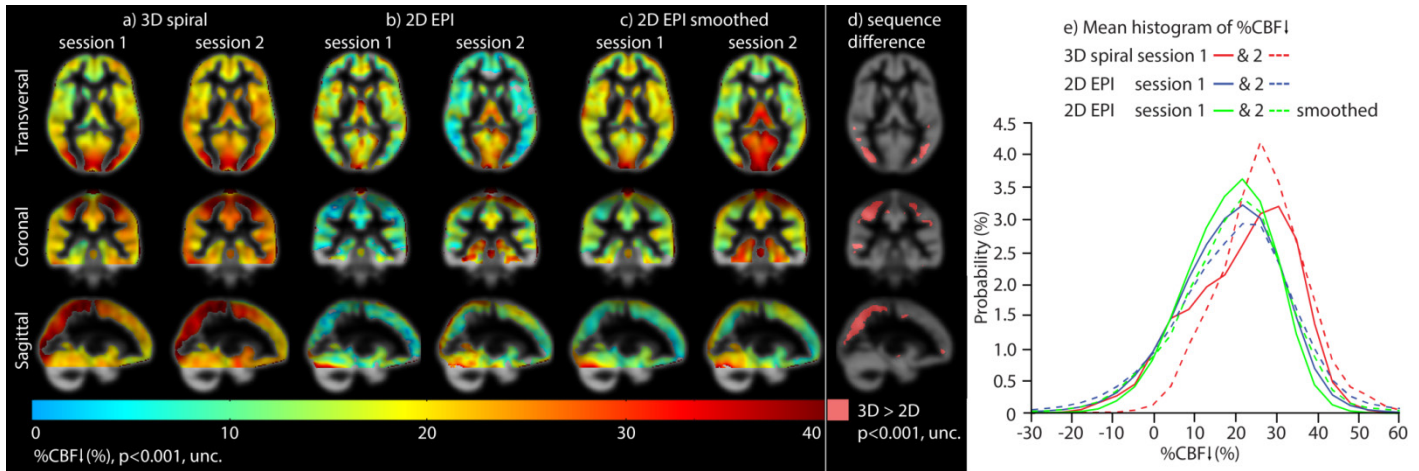


Figure 3. Parametric maps showing voxels with significant cerebral blood flow (CBF) decrease ($\%CBF\downarrow$, $p < 0.001$ uncorrected) for the 3D spiral (a) and 2D EPI sequences (b), as well as for the additionally smoothed 2D EPI data (c). There were no voxels showing a significant CBF increase. d) Parametric maps depicting voxels with significant inter-sequence $\%CBF\downarrow$ differences ($p < 0.001$ uncorrected). All maps are projected on gray matter probability maps. On the right (e), mean individual histograms of the $\%CBF\downarrow$ are shown for all sessions.

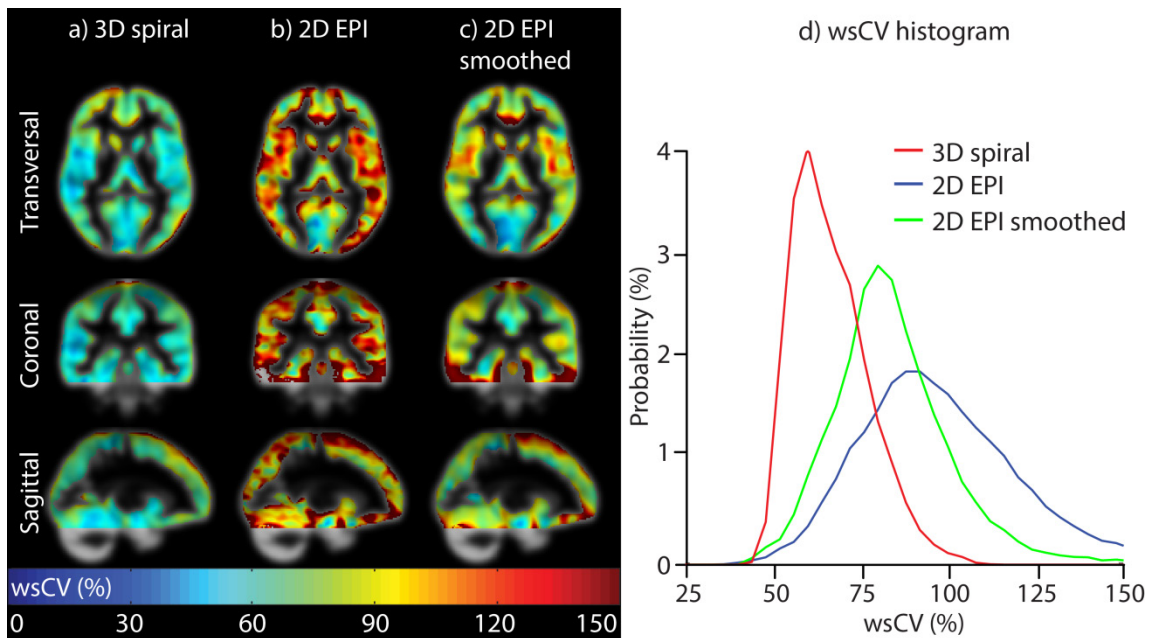


Figure 4. Within-subject coefficient of variation (wsCV)-maps of a) 3D spiral and b) 2D EPI sequences. c) Here, the same 2D EPI wsCV maps are shown after smoothing them to the smoothness of the 3D spiral maps. d) wsCV histograms are shown on the right.

Sample size calculation for future studies

To detect a caffeine-induced 15% GM decrease in CBF – equivalent to 9.9 mL/100g/min for both vendors – the calculated sample sizes were $n=7$ and $n=6$ for 3D spiral and 2D EPI measurements respectively¹³. To detect a 15% change of caffeine-induced GM %CBF↓ ($15\% * 23.9\% = 3.6\%$ (3D spiral) and $15\% * 19.2\% = 2.9\%$ (2D EPI)) the calculated sample sizes were $n=115$ and $n=155$ for 3D spiral and 2D EPI respectively.

Discussion

The main results of this study were threefold: 1) the mean but not the variation of the global %CBF↓ differed between the pCASL sequences of both vendors, 2) both the mean and variation of %CBF↓ spatially differed between the sequences, and 3) the sample size for future studies was much larger to detect a *change* in the caffeine effect than to detect whether there *is* a caffeine effect.

It has previously been suggested that the inter-session variation of ASL measurements is dominated by the physiological variability of baseline CBF³². For the measurement of caffeine-induced %CBF↓, different or additional sources of physiological variability can be expected, including those related to the absorption of caffeine from the gastrointestinal tract, as well as the pharmaco-kinetics and cardiovascular effects of caffeine^{16, 33, 34}. Nevertheless, the inter-session variation of the caffeine-induced CBF change was not much larger than the previously reported baseline CBF variation of the current study, or than baseline CBF variation from previous studies^{13, 32, 35}. This can be attributed to the presence of covariance between baseline and post-caffeine CBF measurements, which may have decreased the influence of baseline CBF variability on the %CBF↓ variation. In addition, the normalization of the absolute CBF difference by the baseline CBF (equation 3) may have reduced the contribution of baseline CBF variability to the %CBF↓ variation even further.

Whereas the baseline reproducibility of ASL has been thoroughly investigated, only one previous study has reported on the inter-session reproducibility of ASL for the measurement of a pharmaceutically induced CBF change³⁶. This study assessed the reproducibility of perfusion changes induced by an oral 16 mg citalopram administration as measured with pulsed ASL. Whereas the inter-session variation was similar (SD 10.1 versus 9.5 [3D spiral] or 8.7 mL/100g/min [2D EPI]), the effect size of citalopram was

roughly 3 times as small as caffeine (mean absolute CBF change 4.4 versus 15.9 [3D spiral] or 13.1 mL/100g/min [2D EPI]). As a result, the reproducibility of CBF changes induced by citalopram (expressed by wsCV) can be expected to be roughly 3 times as low as the reproducibility of caffeine-induced CBF changes. This comparison shows that pharmaceuticals with a specific affinity, such as citalopram, have a lower effect size but not necessarily a lower inter-session variation than less specific pharmaceuticals, such as caffeine. This again points to the fact that the variation of phASL is dominated by physiological CBF fluctuations. The recently reported inter-session reproducibility of ASL for a CO₂ inhalation challenge supports this point, since the baseline and hypercapnia wsCV were equal (12.8% versus 12.7% respectively)²⁵.

Surprisingly, we found a significant difference in total GM effect size between sequences, whereas our previous baseline results showed perfect agreement¹³. One explanation for this difference in the phASL effect size could be the confounding effect of transit times on the measurement of CBF. A caffeine-induced vaso-constriction is not only expected to result in a decrease in CBF, but also in an increase in arterial transit time³⁷. Therefore, the post-caffeine transit time can be expected to be longer than the pre-caffeine transit time, which could have led to a post-caffeine CBF underestimation and subsequently a %CBF↓ overestimation. This confounding effect will be larger for a shorter PLD and will be most pronounced in the brain region with the longest transit times, which is the posterior watershed area³⁸.

Although the same initial PLD was applied for both sequences (1525 ms), the effective PLD is longer for superior slices in the 2D EPI readout. The sequential multi-slice 2D EPI readout results in an infero-superior increase of the effective PLD as compared to the homogeneous PLD of a single time-point 3D spiral readout. Therefore, with the same initial PLD applied, the 2D EPI readout will be less sensitive to the confounding effect of prolonged transit times on the measurement of %CBF↓. This can explain the inter-sequence difference in effect size, both globally as well as in the posterior watershed area. In addition, the higher sensitivity of the 3D spiral readout for transit times may have increased the variation of the 3D spiral data. This is not supported by the homogeneous 3D spiral wsCV-maps. However, any larger variation in the superior regions could be masked by the high degree of smoothing in the Z-direction of the 3D spiral readout. These sequence differences in CBF and in wsCV in superior regions with long transit times are probably resolved by selecting a longer PLD for the 3D spiral readout, such as 2000 ms⁶.

There was a large difference between the calculated sample sizes to either 1) detect the effect of phASL or to 2) detect a change in the effect of phASL. Whereas the first was comparable with baseline sample size recommendations to detect a 15% GM CBF change ($n=4$), the second was much larger³¹. It is worth noting that the sample size calculation is quadratically dependent on the ratio of the variation to the effect size (equation 4). For the first sample size, the inter-session variation of caffeine-induced CBF changes was not much larger than baseline, and the effect size is the same as for baseline sample size calculations – i.e. 15% of the mean baseline CBF. For the second sample size, however, the inter-session variation is the same but the effect size is one fifth of baseline sample size calculations – i.e. 15% of the %CBF \downarrow . This shows that the number of subjects required to detect the effect of a pharmaceutical on CBF, does not necessarily have to be large. However, to detect changes of the phASL effect size, statistical power seems mainly limited by a relatively small effect size of phASL. One important example in which changes of phASL effect size are of interest, is the investigation of a drug dose response³⁹.

It should be acknowledged that our study design choice - comparing two different ASL product sequences on two different vendors - is both a major strength and major weakness of this study. The major strength is that it represents the current status of multi-center phASL: each center will most likely use the ASL product sequence with its optimal settings as implemented on their MRI system. However, this design choice limits the ability to differentiate to what extent the observed differences were caused by differences in ASL readout and the corresponding sequence parameters, by MRI hardware or site effects. Fortunately, we were able to compare our results with previous studies that isolated the effects of different labeling or readout strategies on a single vendor^{11,32}.

The observation that the variation of phASL was comparable between sequences on a total GM level but not on a voxel level is in agreement with our baseline results¹³. However, when identical sequences are implemented, the voxel level variation of ASL is comparable between vendors¹². This strongly suggests that the spatial phASL variability differences between vendors can be mainly explained by sequence differences and much less by hardware or site effects. A 3D spiral readout has a higher SNR and a higher degree of spatial smoothing than a 2D EPI readout¹¹. Both are expected to have decreased the spatial variation as observed in the 3D spiral data. This is supported by Figure 3 and 4, showing that it is possible to approach the voxel level effect size and variability of 3D spiral by additionally smoothing the 2D EPI data.

One previous study compared voxel-wise group-level activation after a sensory-motor task between a 3D spiral and 2D EPI readout on a single scanner, with and without the addition of background suppression to the 3D spiral sequence ¹¹. With background suppression, the 3D spiral readout showed much larger areas of activation compared to the 2D EPI readout, which is in agreement with our results. Without background suppression, however, the performance of both readouts was not very different. This suggests that the residual differences between the wsCV histograms of the 3D spiral and smoothed 2D EPI data can be mainly explained by differences in background suppression efficiency between the 3D and 2D readout ²². Another factor that may have contributed to the smaller variation of the 3D spiral data compared to the 2D EPI data is the higher SNR resulting from the shorter TE of the 3D spiral sequence compared to the 2D EPI sequence.

The positioning of the label plane differed between both sequences (Table 1). Whereas it is common practice for the Philips 2D EPI sequence to plan the labeling plane parallel to, and 9 cm lower than, the anterior commissure-posterior commissure-line (ACPC), the GE 3D spiral sequence has a fixed labeling plane, which is closer to the brain. This may have decreased the transit times for the 3D spiral sequence, although it has been previously shown that signal intensity differences are small when the labeling plane distance is varied between 74-94 mm ²¹. Another difference between the standard implementation of both sequences was the labeling duration (1450 ms versus 1650 ms at 3D spiral and 2D EPI respectively). This 13% longer bolus may have added SNR for the 2D EPI sequence, which may have slightly counterbalanced the large SNR difference due to the intrinsic SNR difference between 2D and 3D and the higher efficiency of background suppression for the 3D spiral sequence.

The differences in M_0 acquisitions between the vendors could potentially have an effect on the quantification of CBF. However, any M_0 quantification differences between sequences will most likely be similar for the pre- and post-caffeine scans and will not contribute to the differences in %CBF↓ between the 3D spiral and 2D EPI sequences.

Conclusion

Using the current clinical ASL product sequences, only the inter-session variation of the phASL total GM effect size can be compared. The mean total GM effect size, as well as the spatial mean and

variation of the phASL effect size differed between the sequences. This may seriously impede multi-center phASL studies, especially in cases with locally restricted effects. These sequence differences strongly encourage the standardization of ASL implementations.

Reference list

1. Donahue M, Jezzard P. MR perfusion imaging in neuroscience. In: *Clinical Perfusion MRI: Techniques and Applications*. Barker P, Golay X, Zaharchuk G (editors). Cambridge: Cambridge University Press; 2013. pp. 114-117.
2. George E, Becerra L, Upadhyay J, Schmidt U, Borsook D. Evaluation of novel drugs using fMRI in early-phase clinical trials: safety monitoring. *Drug Discov Today* 2010; **15(15-16)**:684-689.
3. Handley R, Zelaya FO, Reinders AA, Marques TR, Mehta MA, O'Gorman R, *et al.* Acute effects of single-dose aripiprazole and haloperidol on resting cerebral blood flow (rCBF) in the human brain. *Hum Brain Mapp* 2013; **34(2)**:272-282.
4. Wang DJ, Chen Y, Fernandez-Seara MA, Detre JA. Potentials and challenges for arterial spin labeling in pharmacological magnetic resonance imaging. *J Pharmacol Exp Ther* 2011; **337(2)**:359-366.
5. Golay X, Hendrikse J, Lim TC. Perfusion imaging using arterial spin labeling. *Top Magn Reson Imaging* 2004; **15(1)**:10-27.
6. Alsop DC, Detre JA, Golay X, Gunther M, Hendrikse J, Hernandez-Garcia L, *et al.* Recommended implementation of arterial spin-labeled perfusion MRI for clinical applications: A consensus of the ISMRM perfusion study group and the European consortium for ASL in dementia. *Magn Reson Med* 2014.
7. Petersen ET, Mouridsen K, Golay X. The QUASAR reproducibility study, Part II: Results from a multi-center Arterial Spin Labeling test-retest study. *Neuroimage* 2010; **49(1)**:104-113.
8. Zelaya FO, Zois E, Muller-Pollard C, Lythgoe DJ, Lee S, Andrews C, *et al.* The response to rapid infusion of fentanyl in the human brain measured using pulsed arterial spin labelling. *Magn Reson Mater Phys* 2012; **25(2)**:163-175.
9. Khalili-Mahani N, van Osch MJ, Baerends E, Soeter RP, de KM, Zoethout RW, *et al.* Pseudocontinuous arterial spin labeling reveals dissociable effects of morphine and alcohol on regional cerebral blood flow. *J Cereb Blood Flow Metab* 2011; **31(5)**:1321-1333.
10. Chen Y, Wan HI, O'Reardon JP, Wang DJ, Wang Z, Korczykowski M, *et al.* Quantification of cerebral blood flow as biomarker of drug effect: arterial spin labeling phMRI after a single dose of oral citalopram. *Clin Pharmacol Ther* 2011; **89(2)**:251-258.
11. Vidorreta M, Wang Z, Rodriguez I, Pastor MA, Detre JA, Fernandez-Seara MA. Comparison of 2D and 3D single-shot ASL perfusion fMRI sequences. *Neuroimage* 2012; **66C**:662-671.
12. Mutsaerts HJMM, Van Osch MJP, Zelaya FO, Wang DJJ, Nordhoy W, Wang Y, *et al.* Multi-vendor comparison of arterial spin labeling with same labeling and readout modules. In: International Society for Magnetic Resonance in Medicine; 2014. p. 4569.
13. Mutsaerts HJ, Steketee RM, Heijtel DF, Kuijer JP, van Osch MJ, Majoie CB, *et al.* Inter-vendor reproducibility of pseudo-continuous arterial spin labeling at 3 tesla. *PLoS One* 2014; **9(8)**:e104108.
14. Mulderink TA, Gitelman DR, Mesulam MM, Parrish TB. On the use of caffeine as a contrast booster for BOLD fMRI studies. *Neuroimage* 2002; **15(1)**:37-44.

15. Vidyasagar R, Greyling A, Draijer R, Corfield DR, Parkes LM. The effect of black tea and caffeine on regional cerebral blood flow measured with arterial spin labeling. *J Cereb Blood Flow Metab* 2013; **33(6)**:963-968.
16. Fredholm BB, Battig K, Holmen J, Nehlig A, Zvartau EE. Actions of caffeine in the brain with special reference to factors that contribute to its widespread use. *Pharmacol Rev* 1999; **51(1)**:83-133.
17. Field AS, Laurienti PJ, Yen YF, Burdette JH, Moody DM. Dietary caffeine consumption and withdrawal: confounding variables in quantitative cerebral perfusion studies? *Radiology* 2003; **227(1)**:129-135.
18. Binnewijzend MA, Kuijer JP, Benedictus MR, van der Flier WM, Wink AM, Wattjes MP, *et al.* Cerebral blood flow measured with 3D pseudocontinuous arterial spin-labeling MR imaging in Alzheimer disease and mild cognitive impairment: a marker for disease severity. *Radiology* 2013; **267(1)**:221-230.
19. Donahue MJ, Ayad M, Moore R, van OM, Singer R, Clemmons P, *et al.* Relationships between hypercarbic reactivity, cerebral blood flow, and arterial circulation times in patients with moyamoya disease. *J Magn Reson Imaging* 2013.
20. Lu H, Clingman C, Golay X, van Zijl PC. Determining the longitudinal relaxation time (T₁) of blood at 3.0 Tesla. *Magn Reson Med* 2004; **52(3)**:679-682.
21. Aslan S, Xu F, Wang PL, Uh J, Yezhuvath US, van OM, *et al.* Estimation of labeling efficiency in pseudocontinuous arterial spin labeling. *Magn Reson Med* 2010; **63(3)**:765-771.
22. Garcia DM, Duhamel G, Alsop DC. Efficiency of inversion pulses for background suppressed arterial spin labeling. *Magn Reson Med* 2005; **54(2)**:366-372.
23. Lu H, Nagae-Poetscher LM, Golay X, Lin D, Pomper M, van Zijl PC. Routine clinical brain MRI sequences for use at 3.0 Tesla. *J Magn Reson Imaging* 2005; **22(1)**:13-22.
24. Herscovitch P, Raichle ME. What is the correct value for the brain-blood partition coefficient for water? *J Cereb Blood Flow Metab* 1985; **5(1)**:65-69.
25. Heijtel DF, Mutsaerts HJ, Bakker E, Schober P, Stevens MF, Petersen ET, *et al.* Accuracy and precision of pseudo-continuous arterial spin labeling perfusion during baseline and hypercapnia: a head-to-head comparison with (1)(5)O H(2)O positron emission tomography. *Neuroimage* 2014; **92**:182-192.
26. St Lawrence KS, Wang J. Effects of the apparent transverse relaxation time on cerebral blood flow measurements obtained by arterial spin labeling. *Magn Reson Med* 2005; **53(2)**:425-433.
27. Chalela JA, Alsop DC, Gonzalez-Atavales JB, Maldjian JA, Kasner SE, Detre JA. Magnetic resonance perfusion imaging in acute ischemic stroke using continuous arterial spin labeling. *Stroke* 2000; **31(3)**:680-687.
28. Ashburner J. A fast diffeomorphic image registration algorithm. *Neuroimage* 2007; **38(1)**:95-113.
29. Bland JM, Altman DG. Measuring agreement in method comparison studies. *Stat Methods Med Res* 1999; **8(2)**:135-160.
30. Worsley KJ, Marrett S, Neelin P, Vandal AC, Friston KJ, Evans AC. A unified statistical approach for determining significant signals in images of cerebral activation. *Hum Brain Mapp* 1996; **4(1)**:58-73.
31. Murphy K, Harris AD, Diukova A, Evans CJ, Lythgoe DJ, Zelaya F, *et al.* Pulsed arterial spin labeling perfusion imaging at 3 T: estimating the number of subjects required in common designs of clinical trials. *Magn Reson Imaging* 2011; **29(10)**:1382-1389.
32. Chen Y, Wang DJ, Detre JA. Test-retest reliability of arterial spin labeling with common labeling strategies. *J Magn Reson Imaging* 2011; **33(4)**:940-949.
33. Arnaud MJ. The pharmacology of caffeine. *Prog Drug Res* 1987; **31**:273-313.

34. Blanchard J, Sawers SJ. The absolute bioavailability of caffeine in man. *Eur J Clin Pharmacol* 1983; **24(1)**:93-98.
35. Gevers S, van Osch MJ, Bokkers RP, Kies DA, Teeuwisse WM, Majoie CB, *et al.* Intra- and multicenter reproducibility of pulsed, continuous and pseudo-continuous arterial spin labeling methods for measuring cerebral perfusion. *J Cereb Blood Flow Metab* 2011; **31(8)**:1706-1715.
36. Klomp A, Caan MW, Denys D, Nederveen AJ, Reneman L. Feasibility of ASL-based phMRI with a single dose of oral citalopram for repeated assessment of serotonin function. *Neuroimage* 2012; **63(3)**:1695-1700.
37. MacIntosh BJ, Pattinson KT, Gallichan D, Ahmad I, Miller KL, Feinberg DA, *et al.* Measuring the effects of remifentanyl on cerebral blood flow and arterial arrival time using 3D GRASE MRI with pulsed arterial spin labelling. *J Cereb Blood Flow Metab* 2008; **28(8)**:1514-1522.
38. Hendrikse J, Petersen ET, van Laar PJ, Golay X. Cerebral border zones between distal end branches of intracranial arteries: MR imaging. *Radiology* 2008; **246(2)**:572-580.
39. Chen Y, Parrish TB. Caffeine dose effect on activation-induced BOLD and CBF responses. *Neuroimage* 2009; **46(3)**:577-583.

4

Quantitative functional arterial spin labeling (fASL) MRI – sensitivity and reproducibility of regional CBF changes using pseudo-continuous ASL product sequences

RME Steketee
HJMM Mutsaerts
EE Bron
MJP van Osch
CBLM Majoie
A van der Lugt
AJ Nederveen
M Smits

In submission

Abstract

Arterial spin labeling (ASL) magnetic resonance imaging is increasingly used to quantify task-related brain activation. This study assessed functional ASL (fASL) using pseudo-continuous ASL (pCASL) product sequences from two vendors. By scanning healthy participants twice with each sequence while they performed a motor task, this study assessed functional ASL for 1) its sensitivity to detect task-related cerebral blood flow (CBF) changes, and 2) its reproducibility of resting CBF and absolute CBF changes (delta CBF) in the motor cortex. Whole-brain voxel-wise analyses showed that sensitivity for motor activation was sufficient with each sequence, and comparable between sequences. Reproducibility was assessed with within-subject coefficients of variation (wsCV) and intraclass correlation coefficients (ICC). Reproducibility of resting CBF was reasonably good within (wsCV: 12.1-14.9%; ICC: 0.68-0.80) and between sequences (wsCV: 14.0%; ICC: 0.71). Reproducibility of delta CBF was relatively low, both within (wsCV: 209-259%; ICC: 0.29-0.35) and between sequences (wsCV: 214%; ICC: 0.39), while inter-session variation was low. This may be due to delta CBF's small mean effect (0.06-0.86 mL/100g gray matter/min). In conclusion, fASL seems sufficiently sensitive to detect task-related changes on a group level, with acceptable inter-sequence differences. Resting CBF may provide a consistent baseline to compare task-related activation to, but absolute regional CBF changes are more variable, and should be interpreted cautiously when acquired with two pCASL product sequences.

Introduction

Arterial spin labeling (ASL) perfusion magnetic resonance imaging (MRI) is being increasingly used for imaging of task-related brain activation. Such functional ASL (fASL) has been used to study the neural correlates of a multitude of cognitive domains, including attention,¹ memory,² language,³ visual,⁴ and sensorimotor processing,⁵ and is increasingly considered as an alternative to blood oxygen level-dependent (BOLD) functional MRI (fMRI), which has been predominantly used as a marker for neural activation during the last two decades.

ASL has several advantages over BOLD imaging with respect to acquisition and interpretation. First, ASL has better sensitivity in low frequency paradigms. The BOLD signal has been shown to be confounded by slow ‘drift’ effects in baseline signal, which are reduced in ASL imaging as a result of the pair wise subtraction of labeled and unlabeled images⁵. Second, despite the intrinsically low signal-to-noise ratio (SNR) of ASL, spatial localization of neuronal activity seems more accurate when measured with ASL than with BOLD. The BOLD signal is affected by macrovascular venous effects⁶ whereas ASL is more sensitive to the microvasculature⁷. The interpretation of the BOLD signal is more complex as it reflects a combination of cerebral blood flow (CBF), cerebral blood volume (CBV) and cerebral metabolic rate of oxygen consumption (CMRO₂),^{8, 9} whereas ASL provides a measure of CBF that is relatively less sensitive to other hemodynamic parameters. Furthermore, ASL provides an in principle quantitative measure of CBF, whereas the BOLD signal is relative. These advantages favor the application of fASL over fMRI BOLD for task-related brain imaging.

The quantitative aspect of ASL in particular could facilitate the comparison and exchange of CBF values across multiple sites and enable multicenter studies, for instance, to pool data. However, before fASL can be used as such, its variability needs to be determined, not only within sessions and scanners, but also between product sequences of different vendors, as each vendor provides its own particular ASL implementation. Reproducibility of ASL in general is affected by intrinsic properties, such as low SNR and relative sensitivity to hemodynamics such as arterial transit time (ATT)¹⁰. In addition, although within-sequence reproducibility is sufficient for the commonly available labeling schemes,¹¹⁻²² pseudo-continuous arterial spin labeling (pCASL) has been shown to be best reproducible within session, scanner, and vendor, being more stable and less variable than continuous ASL (CASL) and pulsed ASL (PASL)^{23, 24}. Even if vendors do employ the same labeling scheme, variability is introduced by differences between MR scanners, such as gradient design, radiofrequency transmit chain, receive-filters and reconstruction algorithms.

Nevertheless, not every user is aware of the potential impact of these factors and may assume that any ASL implementation will provide the same information, as can be expected from a quantitative technique. This may seem particularly appealing for the quantification of brain activation in functional imaging studies. The extent to which different vendor implementations affect these data is not known. We will therefore compare two pCASL product sequences of two different vendors, by limiting adjustment of sequence parameters to within the constraints imposed by the vendor-specific implementation.

Baseline or resting CBF values have been found to be well reproducible within sessions, within scanners, and between scanners of the same vendor on a whole-brain level, whereas on a regional level reproducibility was lower^{23, 24}. We previously assessed the reproducibility of whole-brain resting CBF within and between pCASL product sequences at 3T scanners of two different vendors²⁵. Mean global CBF did not differ between vendors, i.e. between product sequences, but voxel-by-voxel assessment revealed regional differences. Regional variability presents a challenge for fASL, where local effects are of particular interest. In addition to the variability in regional CBF changes, the variability in the detection of such CBF changes needs to be assessed. Sufficient and similar sensitivity to detect local task-induced CBF changes is a prerequisite for multicenter fASL implementations, and essential to good reproducibility.

As of yet, variability of quantitative fASL and variation of sensitivity for task-induced CBF changes between product sequences of different vendors have not been studied. Not only is this information essential for exchanging and comparing fASL data, but results generated by one product sequence can only be generalized to another if variability between them is known. The aim of the present study was to assess quantitative fASL by 1) assessing sensitivity to detect regional CBF changes in a voxel-wise whole-brain analysis, and 2) by investigating regional reproducibility of both resting CBF and task-induced CBF changes in the primary motor cortex, within and between pCASL product sequences from two major vendors. We investigated this by means of paced finger tapping, a simple behavioral paradigm that is known to elicit robust and consistent regional activation in the primary motor cortex in a multitude of activation studies using BOLD as well as fASL⁵⁻⁷. We employed this paradigm in healthy volunteers using vendor-supplied ASL sequences.

Methods

1.1 Participants

Twenty-two healthy volunteers, aged 18-40 years, were recruited as part of a larger study on ASL reproducibility²⁶. Participants were recruited through advertisement at the University of Amsterdam. Only participants with no history of neurological or psychiatric disease were included. Participants that used medication other than contraceptives, or had contraindications for MRI were excluded.

Participants were asked to limit their consumption of alcohol, nicotine and caffeine to a maximum of three units 12-24 hours prior to scanning, and to refrain from consuming alcohol, nicotine and caffeine 12 hours prior to scanning. The study was approved by the local medical research ethics committees of both sites: the Erasmus MC – University Medical Center Rotterdam and the Academic Medical Center, Amsterdam and was conducted according to the Declaration of Helsinki. All participants gave written informed consent and received financial compensation for participation.

1.2 Image acquisition

Imaging was performed on a 3T Inera (Philips Healthcare, Best, the Netherlands) and a 3T Discovery MR750 (GE Healthcare, WI, USA) scanner, using an 8 channel receive head coil. Participants were scanned twice on both scanners, i.e. four times in total, in no specific order. Scanning sessions were separated by at least one week, but no more than four weeks.

A high resolution 3D T1-weighted (T1w) scan for anatomical reference was acquired during one of the two sessions on each scanner. Perfusion data were acquired using pCASL product sequences that were provided by the vendor of each scanner. As we aimed to assess the reproducibility of the currently implemented (i.e. product) sequences, we chose to employ vendor-supplied sequences rather than to reprogram the sequences to make them match completely. Hence, parameters were only adjusted within the given limits of the clinical scanning sequences. Imaging data of the two sites were acquired by two different researchers. Strict agreements were made about the complete process of instructing and positioning participants in order to minimize differences between researchers and subsequently between sequences. Details of both pCASL sequences are listed in Table 1. Note that on the GE scanner a segmented 3D readout was employed, whereas on the Philips scanner single-shot multi-slice 2D imaging was combined with averaging to obtain a temporal resolution similar to the GE-sequence. Another difference between sequences was that on the GE scanner perfusion data are averaged during acquisition, whereas for Philips data is averaged after acquisition, after pair-wise subtraction of label and

control images during post-processing. As the GE sequence only provides three fixed post-labeling delays (1 025, 1 525 and 2 025 ms for respectively children, adults, and older adults or adults with cerebrovascular disease), a delay of 1 525 ms, considered most suitable for the current population, was selected for all ASL imaging.

	GE	Philips
Readout sequence	3D FSE stack-of-spirals	2D gradient-echo single-shot EPI
Acquisition matrix	8 arms with 512 sampling points	80 * 80
Parallel imaging	No	SENSE factor = 2.5
Voxel size	3.75 * 3.75 * 4 mm	3 * 3 * 7 mm
Field of view (FOV)	24 * 24 cm ²	24 * 24 cm ²
Number of slices	36	17
Echo time	10.5 ms	17 ms
Repetition time	4 600 ms	4 000 ms
Flip angle	111°	90°
Labeling duration	1 450 ms	1 650 ms
Post-labeling delay	1 525 ms	1 525 ms
Labeling plane (distance from AC-PC line ^a in head-feet direction)	89 mm	72 mm
Background suppression	Yes	Yes
Vascular crushers	No	No
Total scanning time	2:01 min	2:08 min
NEX; no. of excitations (GE)	1	16
NSA; no. of repetitions (Philips)		

Table 1. Vendor-specific parameters of the pCASL product sequences. ^a anterior commissure – posterior commissure line

1.3 Motor activation paradigm

Eight ASL scans were acquired, during which participants performed a blocked motor activation task. Block length was equal to acquisition time of one scan, i.e. 2 minutes. Participants were instructed to tap the fingers of both hands to the thumbs in random order (finger tapping, FT) during the odd scans and to keep their hands still (rest) during even scans. FT was auditorily paced at a frequency of 1 Hz.

1.4 Data processing

The imaging data were processed according to the methods described in full in Bron *et al.*, 2014²⁶.

1.4.1. Tissue segmentation

The unified tissue segmentation method (Ashburner and Friston, 2005) of SPM8 (Statistical Parametric Mapping 8, Wellcome Trust Centre for Neuroimaging, University College London, UK) was used to obtain gray matter (GM), white matter (WM) and cerebrospinal fluid (CSF) probability maps from the T1w image.

1.4.2 ASL post-processing

For Philips data, label and control pCASL images were pair-wise subtracted (without motion correction) and averaged to obtain perfusion weighted images. For GE data, the perfusion-weighted images, as provided by the scanner, were used. For each participant, the perfusion-weighted image and the GM probability map were rigidly registered (Elastix registration software²⁸). The results of the registration were visually inspected.

1.4.3 Quantification

To quantify the perfusion-weighted maps of both pCASL sequences as cerebral blood flow (CBF) maps, a single-compartment model was used¹⁰:

$$CBF \text{ (ml/100g/min)} = \frac{6000 \lambda \Delta M e^{PLD/T1a}}{2 \alpha T1a M0a (1 - e^{-\tau/T1a})} \quad [1]$$

Parameters used in this model and their values are summarized in Table 2. Differences in effective post-labeling delay for different slices resulting from the 2D multi-slice readout were accounted for in the Philips data (Table 2).

Symbol	Variable	Value
	blood-brain partition	
λ	coefficient for gray matter	0.9 mL/g
ΔM	perfusion-weighted image	Philips: corrected for transversal magnetization decay time (T_2^*) for arterial blood (50 ms) during the 17 ms echo time (TE) by e^{TE/T_2^*} (St Lawrence and Wang, 2005)
M_{0a}	equilibrium magnetization of arterial blood	GE: obtained by individual proton density maps, adjusted for T1 decay time of gray matter tissue ($T1_{GM}$, 1.2 s) during saturation recovery time (t_{sat} , 2 s) by $1 - e^{-t_{sat}/T1_{GM}}$ Philips: scanner average ($3.7 \cdot 10^6$ a.u.) from previous study (Heijtel et al., 2014)
PLD	post-labeling delay	1 525 ms
T_{1a}	longitudinal relaxation time of arterial blood	1 650 ms (Lu et al., 2004)
a	labeling efficiency	0.8 (Aslan et al., 2010). In order to correct for background suppression pulses (Garcia et al., 2005): GE: $a * 0.75$ Philips: $a * 0.83$
τ	labeling duration	GE: 1 450 ms Philips: 1 650 ms

Table 2. variables of the single-compartment model used for quantification (based Alsop et al., 2014)

1.5 Whole-brain voxel-wise preprocessing and activation sensitivity

Registered T1w images and CBF maps were transformed to a common template space based on the T1w images of all participants;²⁶ CBF maps were smoothed using an isotropic 8 mm full width at half maximum (FWHM) kernel.

Voxel-wise differences within and between sequences in relation to finger tapping were assessed using SPM8. Averaged CBF maps per block of finger tapping (FT) and rest were convolved with the hemodynamic response function and modeled on an individual level using a General Linear Model (GLM), yielding parameter estimates for the main effects of FT and rest and the contrast [FT > rest]

which were subsequently used in group analyses. Task-induced changes were assessed per session per sequence by pair-wise comparison of main effects of FT and rest for each participant during each session. As participants were scanned in a random order, we chose to assess inter-sequence differences by means of a repeated measures ANOVA on the contrast [FT > rest] for GE (session) 1 compared to Philips 2 and GE 2 to Philips 1 (n=44). By comparing sessions this way, we can assume that temporal physiological variation affected intra-sequence and inter-sequence reproducibility to a similar extent. All voxel-wise results were thresholded at $p < 0.001$ without correction for multiple comparisons, to be maximally sensitive to intra- and inter-sequence differences in the detection of CBF changes.

1.6 ROI preprocessing and regional reproducibility analysis

1.6.1 ROI labeling and selection

Individual CBF maps were transformed to individual T1w image space for region of interest (ROI) analysis. ROIs for each participant were defined using a multi-atlas approach by registering thirty labeled T1w images, each containing 83 ROIs,^{29,30} to the participants' T1w images, using a rigid, affine, and non-rigid model consecutively. For the current study, we focused on the bilateral primary motor cortex (precentral gyri). Analysis of CBF in the primary motor cortex was performed in GM only.

1.6.2 CBF post-processing in the primary motor cortex

For every pCASL scan, mean GM CBF values were obtained from the left and right precentral gyrus (primary motor cortex). CBF values were averaged per session over the four FT blocks and over the four rest blocks, and then over the primary motor cortex bilaterally, such that for every session we obtained one mean GM CBF value in the bilateral primary motor cortex for the FT condition and one for the rest condition.

1.6.3. Task-induced regional CBF changes within sessions

To assess task-induced CBF changes in the primary motor cortex, mean FT CBF (CBF_{FT}) and resting CBF (CBF_{rest}) within sessions were compared with paired t-tests ($p < .05$). Absolute CBF changes as a result of finger tapping are referred to as delta CBF: $[CBF_{FT} - CBF_{rest}]$. Delta CBF within sessions was normalized by expressing it as a percentage of resting CBF: $[CBF_{FT} - CBF_{rest}] / CBF_{rest}$.

1.6.4. Reproducibility of regional resting CBF and regional task-induced CBF changes

Intra- and inter-sequence reproducibility were assessed by the following measures:

1. Within-subject coefficients of variation (wsCV) were calculated as the ratio of the standard deviation of the CBF difference (SD_{diff}) between sessions to the mean CBF value of those sessions: $wsCV = 100\% (SD_{diff}/\text{mean value})$. The SD_{diff} , rather than the SD of the mean, was used to reflect the extent of variability in differences in relation to the mean. Mean CBF values over sessions, mean CBF differences between sessions, SD_{diff} , and wsCVs and their 95% confidence intervals (CIs) are reported for CBF_{rest} , CBF_{FT} , and delta CBF.

Intra-sequence measures were calculated between the two sessions per sequence. Inter-sequence measures were calculated by comparing GE (session) 1 to Philips 2 and GE 2 to Philips 1 (n=44).

2. Intraclass correlation coefficients (ICC) and 95% CIs were calculated for CBF_{rest} , CBF_{FT} , and delta CBF. A two way-random model and absolute agreement were employed to allow for generalization of the results and to take into account systematic variability between sequences, respectively. ICCs were defined as function of ANOVA mean squares using the following formula: ³¹

$$\frac{BMS - EMS}{BMS + (k - 1)EMS + k/n(JMS - EMS)} \quad [2]$$

in which BMS refers to the between-targets mean square (i.e. variance between participants), JMS refers to the between-judges mean square (i.e. variance between intra- or inter-sequence sessions) and EMS to the residual mean square (i.e. residual sources of variance), in a two-way ANOVA with $n = 22$ (intra-sequence) or 44 (inter-sequence) targets and $k = 2$ judges.

Intravendor ICCs were calculated between the two sessions per sequence by comparing GE (session) 1 to Philips 2 and GE 2 to Philips 1 (n=44).

3. Bland-Altman plots and 95% limits of agreement (mean difference $\pm 1.96 SD_{diff}$) were created for CBF_{rest} and delta CBF to visualize agreement between sessions and between sequences respectively.

Statistical analyses were carried out in IBM SPSS Statistics, version 20.0 (New York, USA).

Results

2.1 Participant characteristics

Nine male and 13 female volunteers with a mean age of 22.1 ± 2.1 years (range: 19-27 years) participated in the study. It should be noted that one participant had CBF values that were 2 – 3 standard deviations higher than the group mean, but this participant was retained in the analysis as data were normally distributed (Kolmogorov-Smirnov tests did not detect significant deviations from normality in any session, $p > .05$). Scan sessions were separated by 2.8 ± 1.0 weeks on the GE and 2.6 ± 0.9 weeks on the Philips scanner (not significant (n.s.)). Inter-sequence sessions were separated by 3.1 ± 1.1 weeks (GE 1 – Philips 2) and 2.6 ± 1.9 weeks (GE 2 – Philips 1), n.s.. Sessions on the GE scanner took place at an earlier time of day than sessions on the Philips scanner: $3:26\text{pm} \pm 4\text{h}00\text{min}$ and $3:55\text{pm} \pm 3\text{h}34\text{min}$ versus $8:16\text{pm} \pm 2\text{h}06\text{min}$ and $7\text{h}47\text{pm} \pm 2\text{h}38\text{min}$ respectively, $p < .05$.

2.2 Whole-brain voxel-wise activation sensitivity of pCASL sequences

Voxel-wise CBF changes in relation to FT are illustrated with t-statistic maps in Figure 1. Both with GE (fig. 1A) and Philips (fig. 1B) CBF increases were observed in the bilateral primary motor cortex in both sessions. Additional activation was observed in the supplementary motor area and the left cerebellum in GE session 2; and in the thalamus, and supplementary motor area in both Philips sessions. As can be appreciated visually, Philips (fig. 1B) seems to be more sensitive to detect activation than GE (fig. 1A). Upon formal assessment with repeated measures ANOVA (fig. 1C), differences between pCASL sequences were found in the right primary motor cortex, left precuneus, right posterior cingulate, and in the bilateral thalamus.

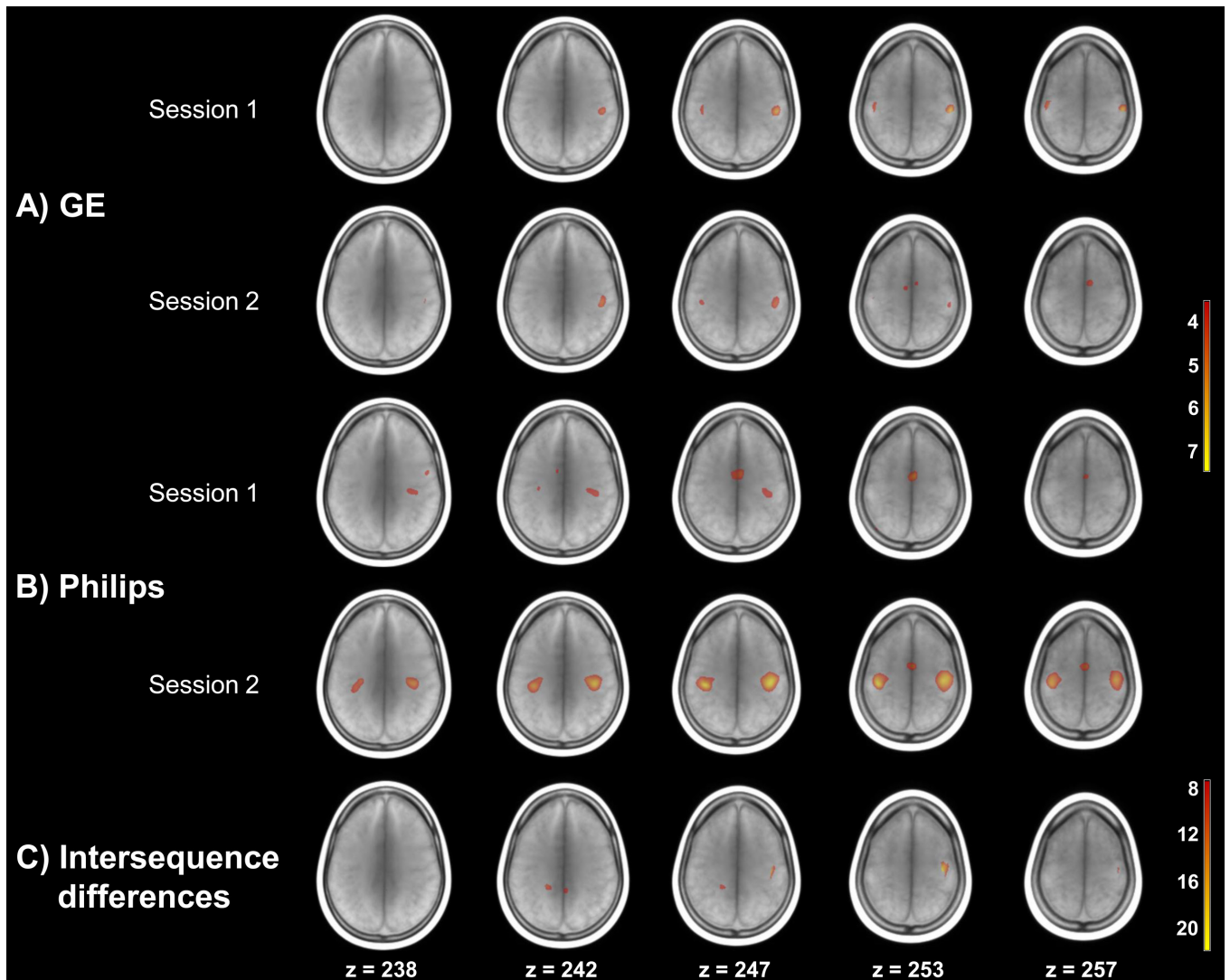


Figure 1. Whole-brain voxel-wise CBF differences associated with finger tapping compared to rest, overlaid on a mean T1w scan. Intra-sequence T-maps of A) GE and B) Philips are thresholded at $T=3.52$, $p<.001$ (uncorrected). C) shows the F-map depicting differences in activation between pCASL sequences, thresholded at $F(2,63) = 7.7$, $p<.001$ (uncorrected).

2.3 Task-induced regional CBF changes within sessions

Absolute CBF values differed systematically between pCASL sequences, with mean CBF_{rest} values being 3.1 mL/100g GM/min higher as measured with GE than with Philips. The increase in CBF in the motor cortex as a result of FT was significant for both sequences and all sessions (Table 3). Normalized CBF changes showed a larger increase in CBF for the two GE sessions (4.65 and 3.31%) than for the two Philips sessions (2.46 and 2.65%).

		CBF (mL/100g GM/min)		<i>p</i> -value	Normalized delta CBF (%)
		Mean	SD		
GE	Session 1	FT	68.2	.033	4.65
		R	65.2		
	Session 2	FT	68.2	.049	3.31
		R	66.0		
Philips	Session 1	FT	71.9	.012	2.46
		R	70.1		
	Session 2	FT	69.0	.027	2.65
		R	67.2		

Table 3. Mean CBF (mL/100g GM/min) and standard deviations (SD) in the motor cortex during finger tapping and rest, and respective *p*-values and normalized delta CBF, per sequence per session. CBF: cerebral blood flow, SD: standard deviation, FT: finger tapping, R: rest.

2.4 Reproducibility of regional resting CBF and regional task-induced CBF changes

WsCV, SD_{diff} , mean CBF values and ICCs and 95% CIs are reported for CBF_{rest} , CBF_{FT} , and delta CBF in Table 4. WsCVs were comparable within and between pCASL sequences for CBF_{rest} and CBF_{FT} . WsCVs for delta CBF were much higher as the mean effect of delta CBF is much smaller than that of CBF_{rest} or CBF_{FT} .

Reproducibility of CBF_{rest} and CBF_{FT} in terms of ICCs was moderate to good for both sequences, with ICCs of .68 and .66 for GE and .80 and .77 for Philips, respectively. Reproducibility of absolute delta CBF was poor for both sequences with ICCs of .35 (GE) and .29 (Philips), and CIs being 1.5 – 2.4 times larger than for CBF_{rest} and CBF_{FT} . Between sequences, reproducibility was reasonable for CBF_{rest} (.71) and CBF_{FT} (.65) and poor for absolute delta CBF (ICC: .39). Inter-sequence CIs for delta CBF were approximately 1.5 times larger than for CBF_{rest} and CBF_{FT} .

	GE	95% CI	Philips	95% CI	Inter- sequence	95% CI	
CBF_{rest}	Mean CBF	65.6	60.7 – 70.5	68.7	62.9 – 74.4	67.1	63.5 – 70.7
	Mean CBF difference	-0.80	-5.14 – 3.54	2.94	-0.74 – 6.61	-3.11	-5.96 – -0.25
	SD difference	9.79	6.65 – 12.9	8.28	5.63 – 10.9	9.38	7.33 – 11.42
	wsCV (%)	14.9	9.10 – 20.8	12.1	5.72 – 18.4	14.0	9.81 – 18.13
	ICC	0.68	0.37 – 0.86	0.80	0.58 – 0.91	0.71	0.53 – 0.84
CBF_{FT}	Mean CBF	68.2	64.1 – 72.3	70.4	65.5 – 75.3	69.3	66.3 – 72.3
	Mean CBF difference	0.04	-3.72 – 3.81	2.88	-0.57 – 6.34	-2.25	-5.01 – 0.50
	SD difference	8.48	5.76 – 11.2	7.80	5.29 – 10.3	9.04	7.07 – 11.02
	wsCV (%)	12.4	7.53 – 17.4	11.1	5.55 – 16.6	13.1	9.44 – 16.7
	ICC	0.66	0.34 – 0.85	0.77	0.52 – 0.90	0.65	0.44 – 0.79
Delta CBF	Mean CBF	2.61	0.88 – 4.33	1.75	0.42 – 3.09	2.18	1.10 – 3.26
	Mean CBF	0.85	-1.57 – 3.26	-0.06	-2.06 – 1.95	0.86	-0.56 – 2.28
	SD difference	5.45	3.70 – 7.20	4.53	3.08 – 5.98	4.67	3.65 – 5.68
	wsCV (%)	209	207 – 212	259	257 – 261	214	213 – 216
	ICC	0.35	-0.08 – 0.67	0.29	-0.16 – 0.63	0.39	0.12 – 0.62

Table 4. Mean CBF measurements and reproducibility estimates between sessions and sequences for resting CBF (CBF_{rest}), finger tapping CBF (CBF_{FT}) and delta CBF in the primary motor cortex. CBF: cerebral blood flow, SD: standard deviation, wsCV: within subject coefficient of variation, ICC: intraclass correlation coefficient, CI: confidence interval.

Figure 2-I and II show the agreement between sessions and sequences for CBF_{rest} and absolute delta CBF respectively. For both CBF_{rest} and delta CBF, differences between sessions were somewhat larger for measurements performed with GE (fig. 2A-I and II) than with Philips (fig. 2B-I and II). The low intra-sequence reproducibility of delta CBF (fig. 2A-II, 3B-II) is illustrated by the variability relative to the mean effect being higher for delta CBF than for CBF_{rest} , as the mean effect of delta CBF is much smaller than that of CBF_{rest} (fig. 2A-I, 2B-I). Both CBF_{rest} and delta CBF show a comparable spread in differences within and between sequences. Figure 2C-I and II show the agreement between sequences for CBF_{rest} and delta CBF respectively, and illustrate that although the spread in differences is higher for CBF_{rest} (2C-I), the variability relative to the mean effect is twice as large for delta CBF (fig. 2C-II), as the mean effect is small.

Discussion

Using pCASL product sequences as supplied by two MR vendors, we found that sensitivity to detect primary motor cortex activation was sufficient and comparable for both sequences. Secondly, we found intra- and inter-sequence reproducibility of resting CBF in the motor cortex to be reasonably good, as was reproducibility of CBF during finger tapping. More important in the context of fASL however, we found absolute CBF changes to be only moderately reproducible, both within and between sequences, despite a consistent task-induced CBF increase within sessions at the group level.

This study adopted a pragmatic and clinically applicable approach in employing pCASL product sequences as supplied by the vendors. Parameters were adjusted to match each other as much as possible, but within the constraints of the provided sequence. This reflects the de facto situation of commercially supplied sequences in which parameters can only be adjusted to a certain extent. As CBF measured with ASL is claimed to be and promoted as a quantitative measure, one would assume that measurements are independent of sequence parameters. Here we show to what extent standard implementation of the sequences gives rise to substantial differences and thus limited reproducibility for functional ASL.

The consistent increase in CBF in the motor cortex during finger tapping is in line with previous cross-sectional fASL studies employing finger tapping paradigms^{5, 7, 32, 33}. Our results replicate these findings between sessions for both sequences. Although we found the extent and spatial patterns of activation to differ between sequences, they both detected activation in the primary motor cortex as a result of finger tapping, and formal comparison of activation patterns between sequences demonstrated only minor difference in motor areas. This supports the notion that on the group level, fASL is sufficiently sensitive to detect activation in the primary motor cortex, and that differences in sensitivity between pCASL product sequences are acceptable.

We found reproducibility of resting CBF in the motor cortex to be reasonably good within and good between pCASL sequences. Our intra-sequence results are in line with previous whole-brain resting CBF studies that have shown reasonable to good reproducibility within and between sessions on the same scanner,²³ as well as between scanners of the same vendor^{16, 24}. We recently compared resting gray matter CBF between product sequences of two different vendors and also found it to be well reproducible on the global level²⁵. The current study focused on regional resting gray matter CBF and showed that, when compared to global CBF, reproducibility was slightly lower. Previous studies found that smaller regions

are subject to higher variability and thus may yield lower reproducibility estimates^{11, 23}. In addition, regional reproducibility has been found to be lower for CBF measured at an interval of 2-4 weeks than for measurements within one day, implying that temporal physiological differences dominate between-weeks reproducibility^{23, 34}. Other sources of physiological variation may also be present, such as the one participant with CBF values that were consistently higher than the group mean.

Apart from temporal dynamics in physiology, regional variability could also be affected by the difference in effective post-labeling delay (PLD) between pCASL sequences. Although the same initial PLD (1 525 ms) was applied for both sequences in the current study, the 2D multi-slice acquisition employed by Philips allows labeled blood more time to reach superior slices, including regions with longer arrival times, than does the single time-point 3D acquisition employed by GE. This difference in effective PLD between sequences may have contributed to decreased reproducibility between their respective measurements. Moreover, the level of reproducibility of different regions seems to vary with PLD,¹⁶ with a PLD of 2 500 ms yielding better reproducibility than a PLD of 1 500 ms when using a 3D single time-point sequence. Therefore, effective PLD differences may have affected our results, as the precentral gyrus is located at the superior aspect of the brain, and therefore exhibits longer transit delays. This may have led to an underestimation of CBF values due to incomplete inflow of label, and to higher variability due to difference in arterial arrival times.

Differences between sequences may not only affect resting CBF measures, but also those of motor activation. Studies that compared fASL data obtained with 2D and 3D sequences found that activated clusters are generally larger when using 3D sequences, while 2D sequences yield larger effect sizes in terms of relative CBF changes^{35, 36}. Our results on the other hand showed larger activated clusters with the 2D sequence, and larger relative CBF changes with the 3D sequence. The larger effective PLD of Philips may have allowed more labeled blood to reach the primary motor cortex during finger tapping than GE, yielding larger activation clusters. In addition, the 3D sequence is more susceptible to spatial blurring, which obscures the gray matter to white matter contrast,³⁵ and may attenuate signal from the gray matter. The larger relative signal change measured with GE on the other hand may be explained by decreasing arterial transit time (ATT) as a result of finger tapping³⁷. Shorter ATT after finger tapping may have caused the relative signal change as measured by GE to be higher because of its shorter effective PLD, particularly in the superior regions.

The reproducibility of delta CBF, i.e. the CBF difference observed between finger tapping and rest, is less straightforward to interpret. Despite the smaller inter-session variation of delta CBF differences (as

indicated by smaller standard deviations of differences) when compared to that of resting CBF and finger tapping CBF, wsCVs are extremely high because of the modest mean effect size of delta CBF. ICCs indicated poor intra-sequence reproducibility as well. Previous fASL studies reported wsCVs of 10-11%,^{38, 39} and ICCs up to 0.74,⁴⁰ between sessions that were a week apart. However, these studies assessed the reproducibility of relative CBF changes, instead of absolute CBF changes. It has been suggested that relative CBF changes are more accurate and robust than absolute CBF changes, as they may reduce potential effects of basal perfusion variations on measures of neuronal activation⁴⁰. Relative CBF changes may therefore generate higher ICCs than absolute CBF changes. Nevertheless, as absolute quantification is a specific advantage of fASL, it seems more appropriate to investigate the reproducibility of absolute CBF changes.

Slight variation in signal change as a result of finger tapping has been observed, but shown to be similar between sessions that took place on the same day or on different days³⁹. Raoult *et al.*⁴⁰ found similar levels of variation using a finger flexion-extension paradigm. Moreover, they found task-induced CBF to be higher, albeit not significantly, with shorter sequence lengths, and concluded that a sequence duration of 4 minutes – i.e. a motor paradigm with 4 blocks of 30s on/off activation – is optimal for clinical practice³⁸. Longer sequence durations are considered to induce habituation and thus decreased activation. Our paradigm consisted of 2 minute blocks of on/off activation because of the limited temporal resolution of the GE sequence. These relatively long blocks thus may have attenuated activation, and thus the effect of finger tapping as compared to other studies, which may have reduced reproducibility.

On the other hand, one of the major reasons to use ASL for functional imaging is its suitability for low frequency designs, as it is much less sensitive to drift effects over time than BOLD fMRI⁴¹. Wang *et al.*⁵ even demonstrated that fASL shows constant sensitivity across different task frequencies corresponding to blocks lengths ranging from 0.5 – 5 minutes, with ASL outperforming BOLD contrast at a block length of 4 minutes. Some higher cognitive functions, such as sustained attention,¹ depend on an experimental design with even longer blocks to detect slow, low-frequency signal changes of interest, for which fASL is particularly well suited. Despite ASL's appropriateness for such cognitive paradigms, we purposely chose a simple behavioral paradigm known to elicit robust and consistent regional activation, before moving on to more complex processes and paradigms. We find that even this simple motor activation paradigm gives rise to substantial variability, which warrants caution with respect to more complex and less robust designs.

To our knowledge, no studies exist on the reproducibility of task-induced CBF changes using pCASL product sequences from two different vendors. In the current study, we found reproducibility of task-induced CBF to be comparable within and between sequences, both in terms of wsCV and ICC. Nevertheless, the findings indicate that absolute CBF changes in the motor cortex still vary considerably, and this variation needs to be taken into account when comparing regional quantitative CBF changes, particularly between sequences. Therefore, absolute fASL data should not be simply pooled between vendors, i.e. between product sequences.

This study has some limitations. First, we did not collect information on motor behavior. Although variations in frequency were avoided by externally pacing the finger tapping, we may have missed individual variations in tapping, which may have added to the variability. Next, as time of acquisition differed between sequences, with GE data collected earlier on the day, diurnal fluctuations in CBF may have added to variability between sequences. This potentially affected reproducibility of resting CBF more than that of delta CBF, as the latter is based on a subtractive measure. Still, inter-sequence reproducibility of resting CBF was found to be reasonably good. Furthermore, subsequent analysis of the Philips data was performed in a similar manner to maximize comparability with the GE data, i.e. by averaging over rest and activation periods, whereas one would normally choose to exploit the higher temporal resolution in a more formal manner within the design matrix. Finally, due to practical constraints we studied the product sequences of only two out of the three major vendors on the market. Although assessment of variability between the three vendors would have been more comprehensive, the current study was conducted as a proof-of principle, and demonstrated as such that substantial variability is already evident when product sequences of two vendors are compared. Future work should be directed at optimizing ASL sequences for functional imaging, and at assessing sensitivity and reproducibility of fASL in single-subject designs, as longitudinal studies and clinical application of fASL will eventually need to be aimed at repeated measurements within individuals.

In conclusion, in a voxel-wise whole-brain analysis, fASL shows sufficient sensitivity to detect regional CBF changes on a group level, both within and between pCASL product sequences of two different vendors. The between sequence reproducibility of fASL is comparable with within sequence reproducibility, although inter-sequence differences in readout should be taken into account. Although reproducibility of regional resting CBF is affected by differences in sequence implementation, particularly in the readout, resting CBF in the motor cortex may provide a reasonably consistent baseline to compare task-induced CBF to. The relatively low reproducibility of task-induced CBF changes in the primary motor cortex, however, should be taken into consideration when comparing fASL data between

sessions and particularly between pCASL product sequences as implemented by different vendors. Its interpretation should be performed with caution in repeated measurements and multicenter designs, as current vendor-specific implementations do not allow for simple pooling of functional ASL data.

Reference list

1. Demeter E, Hernandez-Garcia L, Sarter M, Lustig C. Challenges to attention: a continuous arterial spin labeling (ASL) study of the effects of distraction on sustained attention. *Neuroimage* 2011; **54**: 1518- 1529.
2. Fernandez-Seara MA, Wang J, Wang Z, Korczykowski M, Guenther M, Feinberg DA, et al. Imaging mesial temporal lobe activation during scene encoding: comparison of fMRI using BOLD and arterial spin labeling. *Hum Brain Mapp* 2007; **28**: 1391-1400.
3. Kemeny S, Ye FQ, Birn R, Braun AR. Comparison of continuous overt speech fMRI using BOLD and arterial spin labeling. *Hum Brain Mapp* 2005; **24**: 173-183.
4. Cavusoglu M, Bartels A, Yesilyurt B, Uludag K. Retinotopic maps and hemodynamic delays in the human visual cortex measured using arterial spin labeling. *Neuroimage* 2012; **59**: 4044-4054.
5. Wang J, Aguirre GK, Kimberg DY, Roc AC, Li L, Detre JA. Arterial spin labeling perfusion fMRI with very low task frequency. *Magn Reson Med* 2003; **49**: 796-802.
6. Gaxiola-Valdez I, Goodyear BG. Origins of intersubject variability of blood oxygenation level dependent and arterial spin labeling fMRI: implications for quantification of brain activity. *Magn Reson Imaging* 2012; **30**: 1394-1400.
7. Pimentel MA, Vilela P, Sousa I, Figueiredo P. Localization of the hand motor area by arterial spin labeling and blood oxygen level-dependent functional magnetic resonance imaging. *Hum Brain Mapp* 2013; **34**: 96-108.
8. Ogawa S, Menon RS, Tank DW, Kim SG, Merkle H, Ellermann JM, et al. Functional brain mapping by blood oxygenation level-dependent contrast magnetic resonance imaging. A comparison of signal characteristics with a biophysical model. *Biophys J* 1993; **64**: 803-812.
9. Obata T, Liu TT, Miller KL, Luh WM, Wong EC, Frank LR, et al. Discrepancies between BOLD and flow dynamics in primary and supplementary motor areas: application of the balloon model to the interpretation of BOLD transients. *Neuroimage* 2004; **21**: 144-153.
10. Alsop DC, Detre JA, Golay X, Gunther M, Hendrikse J, Hernandez-Garcia L, et al. Recommended implementation of arterial spin-labeled perfusion MRI for clinical applications: A consensus of the ISMRM perfusion study group and the European consortium for ASL in dementia. *Magn Reson Med* 2014; doi: 10.1002/mrm.25197.
11. Wang Y, Saykin AJ, Pfeuffer J, Lin C, Mosier KM, Shen L, et al. Regional reproducibility of pulsed arterial spin labeling perfusion imaging at 3T. *Neuroimage* 2011; **54**: 1188-1195.
12. Parkes LM, Rashid W, Chard DT, Tofts PS. Normal cerebral perfusion measurements using arterial spin labeling: reproducibility, stability, and age and gender effects. *Magn Reson Med* 2004; **51**: 736-743.
13. Hermes M, Hagemann D, Britz P, Lieser S, Rock J, Naumann E, et al. Reproducibility of continuous arterial spin labeling perfusion MRI after 7 weeks. *MAGMA* 2007; **20**: 103-115.
14. Pfefferbaum A, Chanraud S, Pitel AL, Shankaranarayanan A, Alsop DC, Rohlfing T, et al. Volumetric cerebral perfusion imaging in healthy adults: regional distribution, laterality, and repeatability of pulsed continuous arterial spin labeling (PCASL). *Psychiatry Res* 2010; **182**: 266-73.
15. Xu G, Rowley HA, Wu G, Alsop DC, Shankaranarayanan A, Dowling M, et al. Reliability and precision of pseudo-continuous arterial spin labeling perfusion MRI on 3.0 T and comparison with 15O-water PET in elderly subjects at risk for Alzheimer's disease. *NMR Biomed* 2010; **23**: 286-293.

16. Wu B, Lou X, Wu X, Ma L. Intra- and interscanner reliability and reproducibility of 3D whole-brain pseudo-continuous arterial spin-labeling MR perfusion at 3T. *J Magn Reson Imaging* 2014; **39**: 402-409.
17. Yen YF, Field AS, Martin EM, Ari N, Burdette JH, Moody DM, et al. Test-retest reproducibility of quantitative CBF measurements using FAIR perfusion MRI and acetazolamide challenge. *Magn Reson Med* 2002; **47**: 921-928.
18. Jahng GH, Song E, Zhu XP, Matson GB, Weiner MW, Schuff N. Human brain: reliability and reproducibility of pulsed arterial spin-labeling perfusion MR imaging. *Radiology* 2005; **234**: 909-916.
19. Petersen ET, Mouridsen K, Golay X, all named co-authors of the QUASAR test-retest study. The QUASAR reproducibility study, Part II: Results from a multi-center Arterial Spin Labeling test-retest study. *Neuroimage* 2010; **49**: 104-113.
20. Floyd TF, Ratcliffe SJ, Wang J, Resch B, Detre JA. Precision of the CASL-perfusion MRI technique for the measurement of cerebral blood flow in whole brain and vascular territories. *J Magn Reson Imaging* 2003; **18**: 649-655.
21. Gevers S, Majoie CB, van den Tweel XW, Lavini C, Nederveen AJ. Acquisition time and reproducibility of continuous arterial spin-labeling perfusion imaging at 3T. *AJNR Am J Neuroradiol* 2009; **30**: 968-971.
22. Wu WC, Jiang SF, Yang SC, Lien SH. Pseudocontinuous arterial spin labeling perfusion magnetic resonance imaging--a normative study of reproducibility in the human brain. *Neuroimage* 2011; **56**: 1244-1250.
23. Chen Y, Wang DJ, Detre JA. Test-retest reliability of arterial spin labeling with common labeling strategies. *J Magn Reson Imaging* 2011; **33**: 940-949.
24. Gevers S, van Osch MJ, Bokkers RP, Kies DA, Teeuwisse WM, Majoie CB, et al. Intra- and multicenter reproducibility of pulsed, continuous and pseudo-continuous arterial spin labeling methods for measuring cerebral perfusion. *J Cereb Blood Flow Metab* 2011; **31**: 1706-1715.
25. Mutsaerts HJ, Steketee RME, Heijtel DF, Kuijter JP, van Osch MJ, Majoie CB, et al. Inter-vendor reproducibility of pseudo-continuous arterial spin labeling at 3 tesla. *PLoS One* 2014; **9**: e104108.
26. Bron EE, Steketee RME, Houston GC, Oliver RA, Achterberg HC, Loog M, et al. Diagnostic classification of arterial spin labeling and structural MRI in presenile early stage dementia. *Hum Brain Mapp* 2014; **35**: 4916-4931.
27. Ashburner J, Friston KJ. Unified segmentation. *Neuroimage* 2005; **26**: 839-851.
28. Klein S, Staring M, Murphy K, Viergever MA, Pluim JP. Elastix: a Toolbox for Intensity-Based Medical Image Registration. *IEEE Trans Med Imaging* 2010; **29**: 196-205.
29. Hammers A, Allom R, Koeppe MJ, Free SL, Myers R, Lemieux L, et al. Three-dimensional maximum probability atlas of the human brain, with particular reference to the temporal lobe. *Hum Brain Mapp* 2003; **19**: 224-247.
30. Gousias IS, Rueckert D, Heckemann RA, Dyet LE, Boardman JP, Edwards AD, et al. Automatic segmentation of brain MRIs of 2-year-olds into 83 regions of interest. *Neuroimage* 2008; **40**: 672-684.
31. Shrout PE, Fleiss JL. Intraclass correlations: uses in assessing rater reliability. *Psychol Bull* 1979; **86**: 420-428.
32. Mildner T, Trampel R, Moller HE, Schafer A, Wiggins CJ, Norris DG. Functional perfusion imaging using continuous arterial spin labeling with separate labeling and imaging coils at 3 T. *Magn Reson Med* 2003; **49**: 791-795.
33. Ye FQ, Yang Y, Duyn J, Mattay VS, Frank JA, Weinberger DR, et al. Quantitation of regional cerebral blood flow increases during motor activation: A multislice, steady-state, arterial spin tagging study. *Magn Reson Med* 1999; **42**: 404-407.
34. Klomp A, Caan MW, Denys D, Nederveen AJ, Reneman L. Feasibility of ASL-based pHMRI with a single dose of oral citalopram for repeated assessment of serotonin function. *Neuroimage* 2012; **63**: 1695-1700.

35. Vidorreta M, Wang Z, Rodriguez I, Pastor MA, Detre JA, Fernandez-Seara MA. Comparison of 2D and 3D single-shot ASL perfusion fMRI sequences. *Neuroimage* 2012; **66C**: 662-671.
36. Hu Y, Glover GH. Three-dimensional spiral technique for high-resolution functional MRI. *Magn Reson Med* 2007; **58**: 947-951.
37. Qiu M, Paul Maguire R, Arora J, Planeta-Wilson B, Weinzimmer D, Wang J, et al. Arterial transit time effects in pulsed arterial spin labeling CBF mapping: insight from a PET and MR study in normal human subjects. *Magn Reson Med* 2010; **63**: 374-384.
38. Raoult H, Ferre JC, Petr J, Bannier E, Stamm A, Barillot C, et al. Functional arterial spin labeling: Optimal sequence duration for motor activation mapping in clinical practice. *J Magn Reson Imaging* 2012; **36**: 1435-1444.
39. Tjandra T, Brooks JC, Figueiredo P, Wise R, Matthews PM, Tracey I. Quantitative assessment of the reproducibility of functional activation measured with BOLD and MR perfusion imaging: implications for clinical trial design. *Neuroimage* 2005; **27**: 393-401.
40. Raoult H, Petr J, Bannier E, Stamm A, Gauvrit JY, Barillot C, et al. Arterial spin labeling for motor activation mapping at 3T with a 32-channel coil: reproducibility and spatial accuracy in comparison with BOLD fMRI. *Neuroimage* 2011; **58**: 157-167.
41. Aguirre GK, Detre JA, Zarahn E, Alsop DC. Experimental design and the relative sensitivity of BOLD and perfusion fMRI. *Neuroimage* 2002; **15**: 488-500.
42. St Lawrence KS, Wang J. Effects of the apparent transverse relaxation time on cerebral blood flow measurements obtained by arterial spin labeling. *Magn Reson Med* 2005; **53**: 425-433.
43. Heijtel DF, Mutsaerts HJ, Bakker E, Schober P, Stevens MF, Petersen ET, et al. Accuracy and precision of pseudo-continuous arterial spin labeling perfusion during baseline and hypercapnia: A head-to-head comparison with O HO positron emission tomography. *Neuroimage* 2014; **92C**: 182-192.
44. Lu H, Clingman C, Golay X, van Zijl PC. Determining the longitudinal relaxation time (T1) of blood at 3.0 Tesla. *Magn Reson Med* 2004; **52**: 679-682.
45. Aslan S, Xu F, Wang PL, Uh J, Yezhuvath US, van Osch M, et al. Estimation of labeling efficiency in pseudocontinuous arterial spin labeling. *Magn Reson Med* 2010; **63**: 765-771.
46. Garcia DM, Duhamel G, Alsop DC. Efficiency of inversion pulses for background suppressed arterial spin labeling. *Magn Reson Med* 2005; **54**: 366-372.

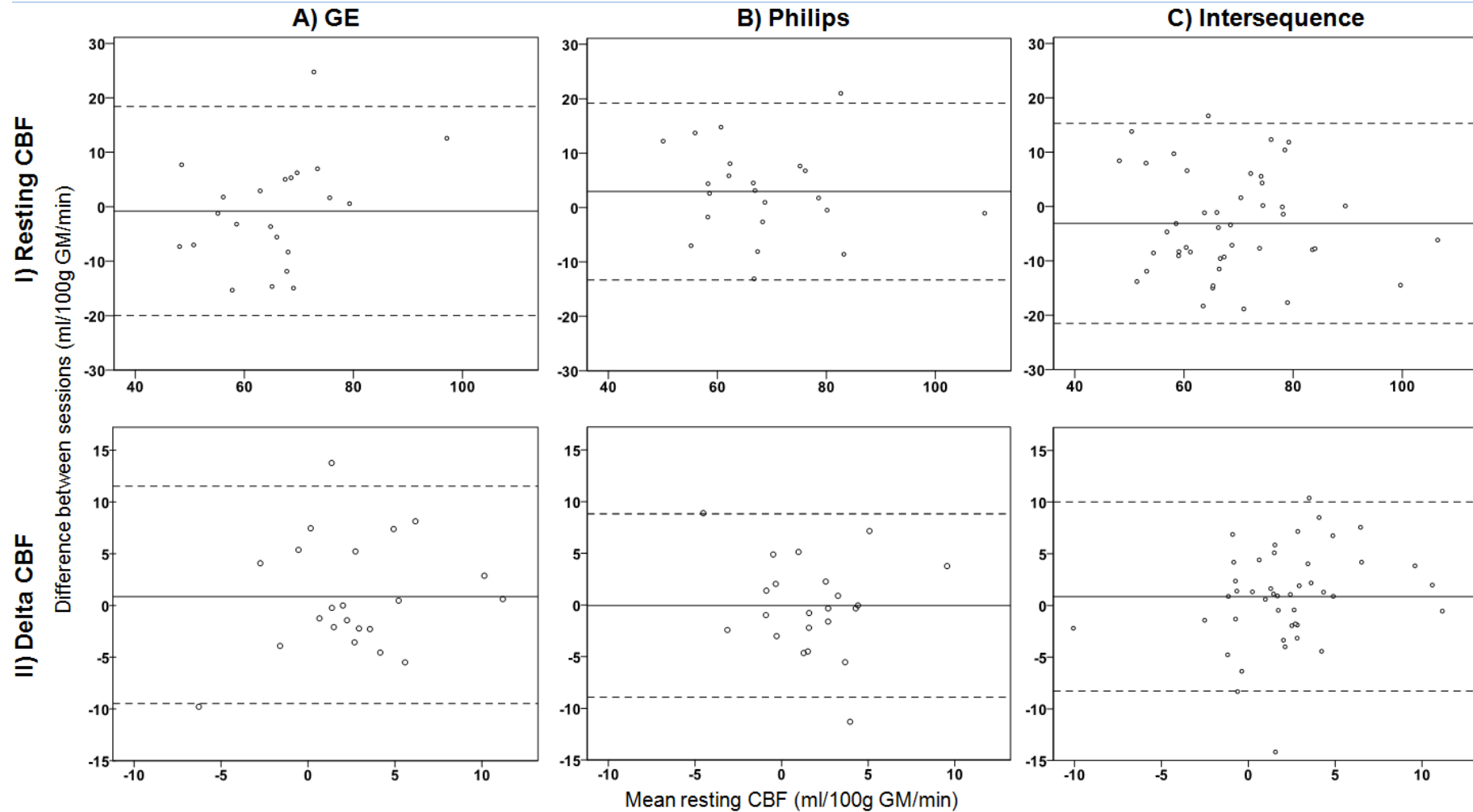


Figure 2. Agreement within and between pCASL sequences for resting CBF and delta CBF. Bland Altman plots of intra-sequencer (A, B) and inter-sequencer (C) agreement for resting CBF (I) and delta CBF (II) in the primary motor cortex. The solid line indicates the mean difference between sessions, dotted lines the 95% limits of agreement.

5

Multi-vendor reliability of arterial spin labeling perfusion MRI using a near-identical sequence: implications for multi-center studies

HJMM Mutsaerts, MJP van Osch

FO Zelaya, DJJ Wang

W Nordhøy, Y Wang

S Wastling, MA Fernandez-Seara

ET Petersen, FB Pizzini

S Fallatah, J Hendrikse

O Geier, M Günther

X Golay, AJ Nederveen

A Bjørnerud, IR Groote

In submission

Abstract

Introduction A main obstacle that impedes standardized clinical and research applications of arterial spin labeling (ASL), is the substantial differences between the commercial implementations of ASL from major MRI vendors. In this study, we compare a single identical 2D gradient-echo EPI pseudo-continuous ASL (PCASL) sequence implemented on 3T scanners from three vendors (General Electric Healthcare, Philips Healthcare and Siemens Healthcare) within the same center and with the same subjects.

Material and Methods Fourteen healthy volunteers (50% male, age 26.4 ± 4.7 yrs) were scanned twice on each scanner in an interleaved manner within three hours. Because of differences in gradient and coil specifications, two separate studies were performed with slightly different sequence parameters, with one scanner used across both studies for comparison. Reproducibility was evaluated by means of quantitative cerebral blood flow (CBF) agreement and inter-session variation, both on a region-of-interest (ROI) and voxel level. In addition, a qualitative similarity comparison of the CBF maps was performed by three experienced neuro-radiologists.

Results There were no CBF differences between vendors in study 1 ($p > 0.1$), but there were CBF differences of 2-19% between vendors in study 2 ($p < 0.01$ in most ROIs) and 10-22% difference in CBF values obtained with the same vendor between studies ($p < 0.01$ in most ROIs). The inter-vendor inter-session variation was not significantly larger than the intra-vendor variation in all ($p > 0.1$) but one of the ROIs ($p < 0.01$).

Conclusion This study demonstrates the possibility to acquire comparable cerebral CBF maps on scanners of different vendors. Small differences in sequence parameters can have a larger effect on the reproducibility of ASL than hardware or software differences between vendors. These results suggest that researchers should strive to employ identical labeling and readout strategies in multi-center ASL studies.

Introduction

Through a number of methodological advances, arterial spin labeling (ASL) perfusion MRI has reached a level that allows its application in multiple clinical and research applications for the visualization and quantification of cerebral blood flow (CBF) ^{1, 2}. Since ASL is non-invasive and offers absolute CBF quantification, it is an attractive tool compared to alternative perfusion modalities ^{3, 4}. Furthermore, quantitative ASL CBF maps are reproducible and comparable with perfusion measurements from the "gold standard" H_2O^{15} -PET ⁵⁻⁷. Implementations of ASL are commercially available on all major MRI systems and the number of clinical applications is continuously growing. Measurements of regional CBF promise clinical value in a variety of common neurological disorders, such as cerebrovascular disease, epilepsy, neurodegeneration and brain tumors, and ASL is recognized as a particularly valuable research tool for cognitive and pharmacological neuroscience ^{8, 9}.

One obstacle that impedes standardized clinical and research applications of ASL, is the substantial differences in the commercial implementations of ASL from the major MRI vendors ¹⁰. A variety of possible labeling and readout strategies exists, and each vendor has implemented a different combination of labeling and readout strategies for their commercial ASL release ¹⁰. General Electric (GE) Healthcare offers pseudo-continuous ASL (PCASL) with a segmented 3D spiral fast spin-echo (FSE) readout, Philips Healthcare has PCASL paired with a single-shot 2D echo-planar imaging (EPI) readout and Siemens Healthcare provides pulsed ASL (PASL) combined with a segmented 3D gradient and spin-echo (GRASE) readout ¹¹⁻¹³.

These labeling and readout differences between product sequences produce qualitatively different perfusion-weighted images, which can be visually appreciated on a single-subject level as shown in Figure 1a ^{14, 15}. On a group level, it is currently not possible to compare CBF-values from a single region of interest (ROI) in a multi-center study, mainly because of differences in readout between sequences from different vendors ^{16, 17}. Global CBF-values, however, show quantitative agreement between vendors ¹⁶. Furthermore, the inter-vendor global CBF inter-session variation is comparable to the intra-vendor global CBF variation ^{15, 16}. These observations support the possibility of future multi-center ASL research, if all vendors could implement an identical ASL sequence.

The current study aims to assess multi-vendor ASL CBF variations using a near-identical sequence across vendors, with the same labeling and readout approach. PCASL was selected as a labeling strategy, because of its wide compatibility with all platforms and superior labeling efficiency for single time-point

CBF measurements^{10, 15, 18}. A multi-slice single-shot 2D EPI readout was selected because of its availability on all systems and as it has been used in the majority of previous ASL studies¹⁰. Because of differences in gradient and RF coil specifications between two vendor systems available for our study, two 2D echo-planar imaging (EPI) PCASL sequences were used with slightly different labeling and readout parameters. These will be referred to as study 1 and 2. For one vendor system, both variants of our sequence could be implemented, enabling an additional intra-vendor comparison of these slightly different sequences.

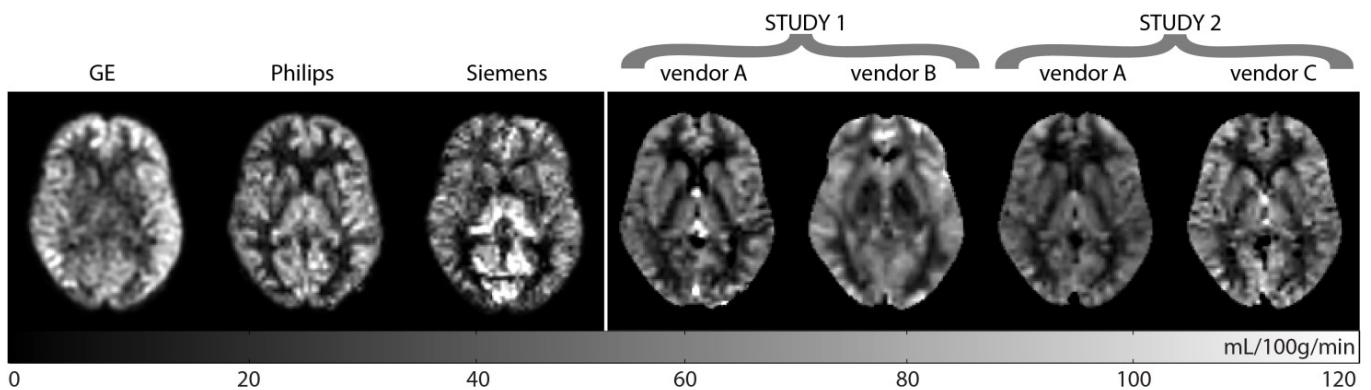


Figure 1. a) Perfusion-weighted maps from a single subject scanned with product sequences from GE (PCASL with a 3D spiral FSE readout), Philips (PCASL with a 2D EPI readout) and Siemens (PASL with a 3D GRASE readout). Sequence parameters included PLD=1525 ms, 4 time points, true axial (GE), PLD=1525 ms (Philips) and TI=2300 ms, TI1=80 ms, 4 time points (Siemens). b) Perfusion-weighted maps from a single representative subject scanned with the sequence used in the current study (parameters shown in Table 1 and 2). All perfusion weighted maps were scaled to have a mean gray matter cerebral blood flow of 60 mL/100g/min, linearly registered, re-sliced and skull-stripped.

Labeling approach	Balanced waveform PCASL
Labeling pulse shape	Hanning
Mean labeling gradient	0.6 mT/m
Max labeling gradient	6 mT/m
Labeling flip angle	25°
Labeling duration	1771 ms
Initial post-label delay	1800 ms
Labeling position	fixed, 9 cm below ACPC
Readout approach	Single shot EPI
Slices	20
Slice thickness	6 mm
Matrix size	64x64
Field of view	224x224 mm
Fat suppression	SPIR
Parallel imaging	Off
B1-filtering	Off
Partial Fourier	Off
Background suppression	Off
Vascular suppression	Off
Label-control pairs	70

Table 1. Identical labeling and readout parameters. ACPC = anterior-posterior commissure; EPI = echo-planar imaging; PCASL = pseudo-continuous arterial spin labeling; SPIR = spectral pre-saturation by inversion recovery

	Study 1		Study 2	
	Vendor A	Vendor B	Vendor A	Vendor C
Inter-pulse time	1.24 ms	1.24 ms	1.15 ms	1.15 ms
Shimming labeling plane	Yes	No	Yes	Yes
TE	28 ms	28 ms	21 ms	21 ms
TR	4800 ms	4800 ms	4700 ms	4700 ms
Slice readout time	60.9 ms	61.5 ms	50.2 ms	52 ms
Mean effective PLD	2410 ms	2420 ms	2300 ms	2320 ms
Total scan duration	11:12 min	11:12 min	10:58 min	10:58 min

Table 2. Different labeling and readout parameters. PLD = post-label delay; TE = echo time; TR = readout time

Materials and Methods

MRI scanners

Three 3T MRI scanners were used in this single-center multi-vendor comparison: GE Signa HDxt (2006, 60 cm bore opening, General Electric Healthcare, Milwaukee, WI, US), Philips Achieva (2007, 60 cm bore opening, Philips Healthcare, Best, the Netherlands) and Siemens Skyra (2011, 70 cm bore opening, Siemens Healthcare, Erlangen, Germany). None of the vendors were involved in designing or conducting this study, none had access to the data, and none were involved in data analysis or preparation of this manuscript. Because the main purpose of the study was to compare the inter- and intra-vendor reproducibility, without addressing the performance of each vendor system explicitly, vendor and coil names were anonymized by pseudo-randomly reordering the vendor names into vendor A, B and C. Vendor A was included in both studies because its gradient and RF coil specifications allowed sequence implementation identical to both vendor B and C. The scanners of vendor A and B were equipped with 8-channel head coils, whereas the scanner of vendor C was equipped with a 20-channel head-neck coil. Vendor A and C were separated by a five-minute walk, whereas vendor B was located at 20 minutes traveling distance by public transport from the location of the two other scanners.

Study design

Fourteen healthy volunteers (50% male, mean age 26.4 ± 4.7 (SD) years) were included, of which 11 (5 men, mean age 25.2 ± 4.5 years) were included in study 1 and all 14 subjects were included in study 2. Both the local regional ethics committee and the local University Hospital internal ethical review board approved the study and all subjects provided written informed consent. In addition to standard MRI exclusion criteria, subjects with history of brain or psychiatric disease or use of medication - except for oral contraceptives - were excluded. To minimize physiological perfusion fluctuation, physical exercise and consumption of alcohol or recreational drugs was prohibited for 24 hours prior to scanning, except for caffeine or nicotine, which were restricted for 6 hours before the scanning sessions¹⁹. In both studies, each participant was scanned twice on two different scanners (i.e. four MRI examinations per participant per study) within three hours, to limit the effect of physiological perfusion fluctuations (Figure 2). Order effects were avoided by randomly starting with either vendor A or B (study 1) or with either vendor A or C (study 2). Foam padding inside the head coil was used to restrict head motion during scanning. Subjects were awake and had their eyes closed during all ASL scans. In all sessions, PCASL acquisitions were performed 10 minutes after the positioning of the subject in the scanner to allow perfusion to stabilize.

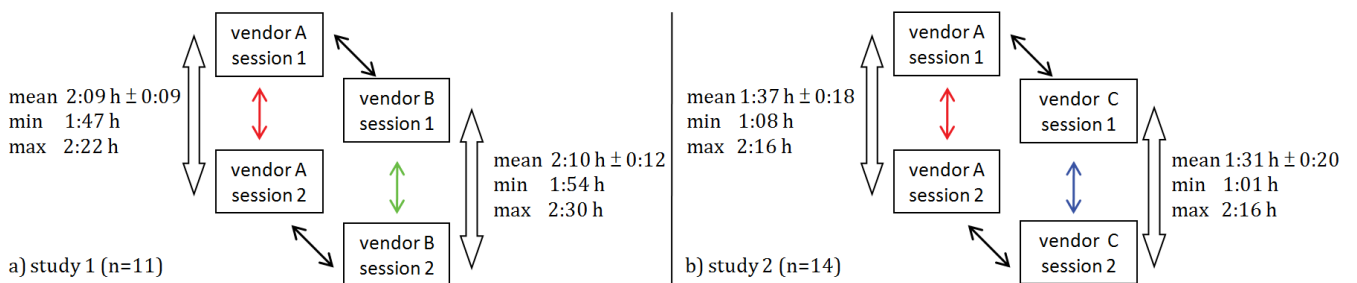


Figure 2. Study design and inter-session time differences between vendors of both studies (large transparent arrows). The small filled arrows correspond to the comparisons performed in this study: intra-vendor vendor A (red), intra-vendor vendor B (green), intra-vendor vendor C (blue), inter-vendor comparison (black). Note that the comparison between studies for vendor A is not indicated by an arrow.

Acquisition

Each scan session included a balanced PCASL sequence with a single-shot gradient-echo EPI readout and a 1 mm isotropic 3D T1-weighted structural scan for segmentation and registration purposes. Detailed similarities and differences between the PCASL protocols are summarized in Tables 1 and 2. The field-of-view was positioned parallel to the anterior-posterior commissure (ACPC) line. Due to restrictions imposed by two of the MR systems the labeling plane was fixed parallel to the stack of imaging slices.

Post-processing: quantification

Matlab 7.12.0 (MathWorks, MA, USA) and Statistical Parametric Mapping 8 (SPM8, Wellcome Trust Center for Neuroimaging, University College London, UK) were used for post-processing and statistical analyses. Motion parameters were estimated and did not differ between vendors ($p > 0.1$ for both studies, paired t-test). To avoid confounding effects from motion correction due to possible signal-to-noise ratio (SNR) differences between vendors or coils, no motion correction was applied. The first five control and label pairs were discarded to avoid any non-steady state effects in the MRI signal. The remaining control (M_{control}) and label (M_{label}) images were pair-wise subtracted and averaged. The average control image was used to derive M_0 , by assuming a fixed single T1 of tissue (equal to $T1_{\text{GM}}$ described below). These perfusion-weighted images were quantified into CBF maps using a single compartment model¹⁰:

$$CBF [mL/100g/min] = \frac{6000 \lambda (M_{\text{control}} - M_{\text{label}}) e^{PLD/T_{1a}} (1 - e^{-\frac{TR}{T1_{GM}}})}{2 \alpha T_{1a} M_{\text{control}} (1 - e^{-\frac{\tau}{T1a}})} \quad [1]$$

where λ is the brain-blood partition coefficient (0.9 mL/g), PLD is the post-label delay of each slice (Table 2); T_{1a} is the longitudinal relaxation time of arterial blood (1650 ms), α is the labeling efficiency (85%) and τ is the label duration (Table 2)^{11, 20, 21}. $1 - e^{(-TR/T1_{GM})}$ corrects for the incomplete signal recovery of the control images; TR is the repetition time (Table 2) and $T1_{\text{GM}}$ is the longitudinal relaxation time of GM (1240 ms). The same quantification parameters were used for GM and white matter (WM).

Post-processing: spatial normalization

A single 3D T1-weighted anatomical scan for each subject ($n=14$) was segmented into GM and WM tissue probability maps. To avoid registration effects from differences in the T1-weighted reference images, the T1-weighted images from a single vendor (vendor A) were used. All CBF maps were

transformed into anatomical space by a rigid-body registration of the average control image to the skull-stripped T1-weighted scan. To spatially normalize both anatomical differences between subjects and residual EPI geometric distortion differences between vendors, a three-stage normalization strategy was applied, based on DARTEL (Diffeomorphic Anatomical Registration analysis using Exponentiated Lie algebra) ²². First, a T1-based DARTEL template was created using the GM and WM probability maps from the T1-weighted scans. The resulting DARTEL flow fields were applied to the average control images of all vendors, removing anatomical differences between subjects. Afterwards, the normalized mean EPI control images were segmented into GM and WM probability maps from which vendor-specific EPI-based DARTEL templates were created. The resulting flow fields were applied to the mean control images, removing residual geometric differences between subjects ²³. Finally, the vendor-specific EPI-based DARTEL templates were warped to the T1-based DARTEL template, removing geometric distortion differences between vendors. All transformations were applied to the corresponding CBF maps.

Data analysis

Reproducibility was evaluated by means of quantitative CBF agreement and inter-session variation, testing whether the mean CBF is equal for different vendors and whether the inter-vendor inter-session variation is equal to the intra-vendor variation. These hypotheses were tested quantitatively on both a region of interest (ROI) and on a voxel level. In addition, a qualitative similarity comparison of the major features of the CBF maps was performed by three neuro-radiologists.

All intra-vendor reproducibility analyses were based on a comparison of session 1 with session 2 within each vendor ($n=11$ and $n=14$ for study 1 and 2 respectively, colored arrows in Figure 2). All inter-vendor reproducibility analyses were based on pooled comparisons of both the first sessions between vendors and the second sessions between vendors ($n=22$ and $n=28$ for study 1 and 2 respectively, black arrows in Figure 2). To compare both studies, the results from vendor A will be used because of its participation in both studies (first 11 subjects only). All reproducibility analyses were based on the mean CBF of the compared sessions and on the standard deviation of the paired inter-session CBF difference ($SD\Delta CBF$). The within-subject coefficient of variation ($wsCV$) – a normalized parameter of inter-session variation – was defined as the ratio of $SD\Delta CBF$ to the mean CBF of both compared sessions ²⁴:

$$wsCV = 100\% \frac{SD\Delta CBF}{mean\ CBF} \quad [2]$$

Data analysis: ROI definition

Subject-specific total cerebral GM and deep cerebral WM masks were obtained by thresholding GM and WM probability maps at 80% and 99% tissue probabilities respectively. WM masks were threefold eroded to avoid GM contamination²⁵. ROIs of anterior, middle and posterior flow territories (supplied by the anterior, middle and posterior cerebral artery respectively) were created from standard vascular territory templates²⁶ and ROIs associated with age-related dementia (anterior and posterior cingulate, precuneus) were created from the Wake Forest University Pick-atlas (<http://fmri.wfubmc.edu/cms/software>). All standard ROIs were masked with the subject-specific GM masks. Since almost all distributions deviated from normal - according to the Shapiro-Wilk test - the median was used to summarize CBF within a ROI.

Data analysis: voxel-based comparison

To assess reproducibility differences spatially, CBF- and wsCV-values were computed for each voxel. In order to visualize how much larger or smaller the inter-vendor $SD\Delta CBF$ was than the intra-vendor $SD\Delta CBF$, a voxel-wise variation ratio map was created according to the following equation²⁷:

$$100\% \frac{SD\Delta CBF_{inter-vendor}}{SD\Delta CBF_{intra-vendor}} \quad [3]$$

This map was created for each study, including the two inter- and the two intra-vendor inter-session comparisons (black and colored arrows respectively in Figure 2). If the inter-vendor covariance is equal to the intra-vendor covariance, we expect a mean variation ratio of 100%. Individual GM CBF histograms (80 bins, range -10–110 mL/100g/min) were averaged to generate a group-level histogram. GM wsCV (80 bins, range 0–100%) and ratio (80 bins, range 20–180%) histograms were generated.

Both on an ROI and on a voxel level, mean CBF differences between vendors were tested for significance using a paired two-tailed Student's t-test. The Levene's test was used to test whether the inter-vendor inter-session $SD\Delta CBF$ was significantly different from the intra-vendor inter-session $SD\Delta CBF$.

Data analysis: qualitative similarity index

In order to compare the inter- and intra-vendor reliability qualitatively, inter- and intra-vendor head-to-head CBF maps were rated for their similarity by three neuroradiologists (FBP, SF and JH) with at least five years of experience with ASL. The following comparisons were included: intra-vendor comparisons (colored arrows Figure 2) for vendor A and B ($n=2*11$) and vendor A and C ($n=2*14$) as well as inter-vendor comparisons (black arrows Figure 2) for vendor A vs. B sessions 1 and 2 ($n=2*11$) and vendor A vs. C sessions 1 and 2 ($n=2*14$), adding up to 100 comparisons in total. The 100 comparisons were pseudo-randomized and only the skull-stripped, spatially normalized cerebrum was included, to avoid any recognizable vendor-specific geometric distortion or susceptibility artifacts. The spatially normalized CBF maps were divided into 20 slices and rescaled slice-wise, such that the mean GM CBF of each slice was equal for the compared sessions. All comparisons were converted into color-scaled DICOM images containing the two compared sessions per image, horizontally side by side.

After giving a first general impression for the total GM, the raters provided an ordinal score from 1 to 5 for the anterior, middle and posterior flow territories and for the deep GM consecutively, based on similarity of morphology and intensity. Similarity scores were defined as 1) poor, 2) fair, 3) moderate, 4) good and 5) excellent. Krippendorff's alpha was used to quantify the inter-rater agreement. The mean rating of all three neuroradiologists was used for analysis. Intra- and inter-vendor similarity scale histograms (5 bins, range 1–5) were generated for the abovementioned ROIs. A two-sample t-test was used to test whether the inter-vendor similarity was lower than the intra-vendor similarity. Significance was thresholded at $p=0.05$ in all analyses.

Results

Session timing

The intra-vendor inter-session time intervals did not differ between vendors in study 1 ($p=0.6$, paired t-test) or study 2 ($p=0.3$), but were 31 min longer for vendor A study 1 than for vendor A study 2 ($p<0.01$, Figure 2). The ASL scans of study 1 ($18\text{h}50 \pm 2\text{h}00$) were performed 2h20 later on each day ($p<0.01$) than those of study 2 ($16\text{h}30 \pm 3\text{h}20$). Study 1 was performed 2.7 weeks after study 2 ($p<0.01$).

Region-based comparison

Both the ROI-based median CBF-values (Table 3) and paired inter-session differences (summarized by wsCV in Table 4) were normally distributed. For all ROIs the mean CBF did not differ significantly between vendor A and B in study 1 ($p>0.1$). The mean regional CBF of vendor A was 2-19% higher ($p<0.01$ in most ROIs) than the mean regional CBF of vendor C in study 2, with the largest differences in the posterior flow territory and in the posterior cingulate gyrus. In addition, CBF values of vendor A in study 1 were 10-22% lower ($p<0.01$ in most ROIs) than those of the same vendor in study 2. Except for the posterior cingulate cortex in study 1 ($p<0.01$), there were no differences between the intra- and inter-vendor $\text{SD}\Delta\text{CBF}$ of study 1 ($p>0.1$) or of 2 ($p>0.2$). However, the $\text{SD}\Delta\text{CBF}$ of vendor A was 1.5-2 times as large for the sequence in study 1 as compared to the sequence in study 2, which was significant for the anterior ($p=0.04$) and posterior flow territory ($p=0.04$) and precuneus ($p=0.03$).

Voxel-based comparison

The CBF maps of a single representative subject show that visually the cortical and subcortical GM-WM differentiation was more comparable between vendors with the near-identical sequences (Figure 1b) than with product sequences (Figure 1a). The group mean CBF maps (Figure 3) of vendor A and B (study 1) appeared very similar visually, with slight differences in the inferior part of the cerebellum and in the orbito-frontal lobe. This was also reflected by the similarly appearing histograms. However, the mean CBF maps of vendor A and C (study 2) showed significant intensity differences, most notably in the posterior flow territory and in the cerebellum. The histograms of vendors A and C have an identical appearance, except for a shift of the peak location for vendor A to higher CBF as compared to vendor C. Interestingly, the largest difference was observed when the results of the same vendor (A) were compared between the sequences of study 1 and 2 (Figure 5a). The mean CBF and CBF distributions on histograms were lower and wider in study 1 compared to study 2 and for most voxels on the parametric maps the CBF-values were larger for study 2 than for study 1.

In both studies, the wsCV maps and histograms (Figure 4) appeared similar between vendors, with only slightly larger variation for vendor A compared to vendor B (study 1) throughout the brain and for vendor C compared to vendor A (study 2) in the posterior flow territory. Areas of largest variation were the deep GM, posterior flow territory (including the cerebellum) and the orbito-frontal cortex. The inter-vendor wsCV maps showed the same spatial distribution as the intra-vendor maps, but the overall wsCV was somewhat higher. Likewise, the inter- and intra-vendor wsCV histograms appeared similar, but the inter-vendor wsCV distribution was shifted towards higher values. Interestingly, the wsCV histograms of vendor A in study 1 were higher and wider than the histograms of the same vendor in study 2. The values on the wsCV maps of vendor A study 2 visually appeared lower and more homogeneous compared to vendor A study 1, which was shown to be significant in the majority of the voxels (Figure 5b).

The inter- to intra-vendor variation ratio (Figure 6) was heterogeneously distributed and ranged from 75 - 125 % in the majority of voxels. Based on the histograms, the mean ratio was slightly higher than 100% and the distribution was approximately Gaussian, with slightly more voxels having a higher inter- than intra-vendor $SD\Delta CBF$. There were a few voxels with significantly higher inter- than intra-vendor $SD\Delta CBF$, which were mainly situated in the posterior flow territory for vendor A vs. B and spread throughout the brain for vendor A vs. C.

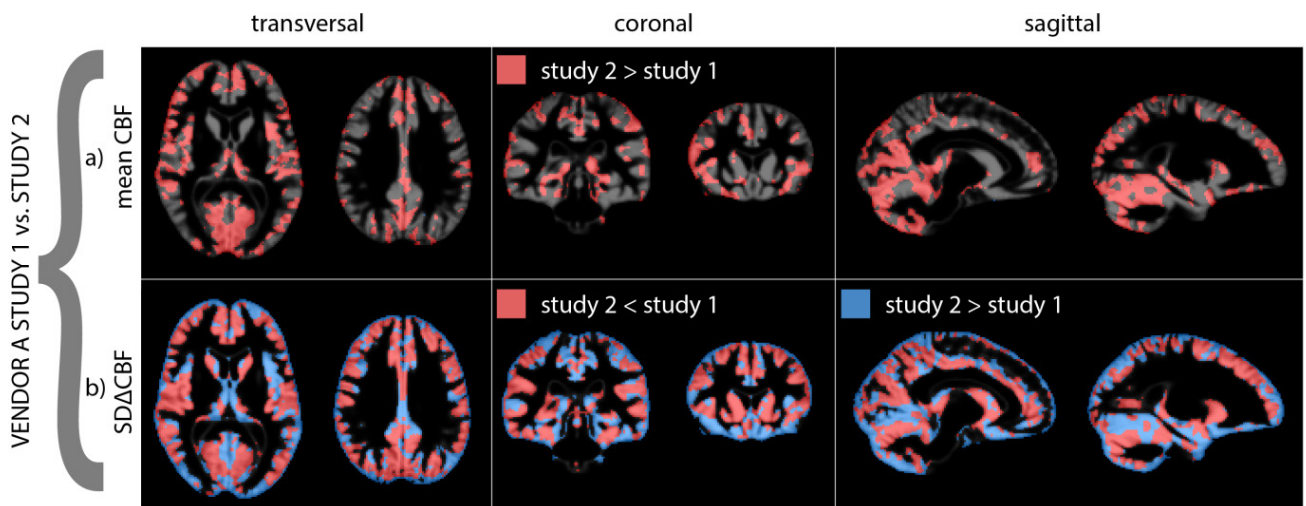


Figure 5. Binary parametric maps projected on mean gray matter (GM) probability maps: a) voxel-wise significant CBF differences between study 1 and 2 ($p < 0.05$). There were no voxels for which the mean CBF of study 1 was significantly larger than the mean CBF of study 2. b) voxel-wise significant differences in standard deviation of the paired inter-session CBF difference ($SD\Delta CBF$) ($p < 0.05$).

Similarity scale

The inter-rater agreement of the visual similarity scale was moderate (Krippendorff's $\alpha=0.44-0.57$) in most ROIs, but only fair in the deep GM ($\alpha=0.28$). There was no substantial inter-rater agreement difference between the intra-vendor (Krippendorff's $\alpha=0.27-0.48$) and inter-vendor ($\alpha=0.26-0.62$) comparisons.

For both the intra- and inter-vendor similarity, the average rate ranged from fair to good, and was 'moderate' in most ROIs (Figure 7). In study 1, the inter-vendor similarity (2.7 ± 0.2) was on average $10.8 \pm 2.3\%$ lower than the intra-vendor similarity (3.0 ± 0.2). In study 2, the inter-vendor similarity (3.4 ± 0.3) was on average $8.8 \pm 4.8\%$ lower than the intra-vendor similarity (3.8 ± 0.2), which was significant for the total GM, posterior flow territory and deep GM. Whereas the similarity scale histograms of the total GM, anterior and middle flow territories had similar means, the deep GM histogram was somewhat lower and the posterior flow territory histograms had the lowest mean. All histograms of study 2 had a smaller distribution and higher mean than the histograms of study 1 ($p < 0.01$).

Discussion

Using near-identical PCASL sequences, we were able to acquire similar CBF images on 3T systems from the three major MRI vendors. The main results of this study are threefold. First, there were no significant CBF differences between vendors within study 1, but there was a significant difference between vendors within study 2 as well as a significant difference in CBF obtained with the sequence of study 1 versus the sequence of study 2 within the same vendor. Second, the inter-vendor inter-session variation was larger than the intra-vendor variation, although this did not reach significance in most ROIs or voxels. Finally, for the qualitative expert ratings, the inter-vendor similarity was 9-11% lower than the intra-vendor similarity, but the inter-vendor similarity was still 'moderate'. These results indicate that it may be possible to pool multi-vendor ASL results obtained with near-identical sequences, but also that minor residual sequence differences can have a large effect on the reliability of ASL.

The general appearance of the CBF and wsCV-maps obtained from the current work is in agreement with what can be expected from PCASL with a 2D gradient-echo EPI readout: excellent GM-WM contrast, heterogeneously appearing GM CBF and wsCV with vascular CBF peaks and lower CBF and higher wsCV in regions sensitive to susceptibility induced artifacts such as the orbito-frontal and inferior temporal cortices^{16, 28}. The visual similarity of these CBF- and wsCV-maps is substantially higher than

that shown in previous multi-vendor ASL comparisons, in particular one in which a different readout (2D EPI vs. 3D spiral) was employed¹⁶. The largest difference between vendors in that study was the difference in spatial blurring between the readouts and reconstruction as used by both vendors, which was reflected in the GM-WM CBF contrast. Whereas the GM-WM CBF ratio differed by a factor 2 between 2D and 3D readouts, this ratio was very consistent in the present results, ranging from 3.5 - 3.9 for all vendors^{14, 16, 17}. This indicates that if a similar readout and reconstruction is used, ASL results are comparable between vendors, despite residual hardware differences such as differences in gradient or coil specifications. Since differences in spatial correlation can seriously affect the ability of ASL to detect regional CBF differences, these results provide a strong argument for the importance of using the same ASL readout in multi-center studies.

To our surprise the mean and inter-session variation of CBF differed more for the same vendor across the two studies than between different vendors within the same study, both in the quantitative and qualitative analysis. These results strongly suggest that even minor sequence changes can result in a significant effect on the mean and inter-session variation of CBF. Moreover, this indicates that small differences in sequence parameters have a larger effect on the reproducibility of ASL than hardware or software differences between vendors, even when the same labeling and readout strategies are used. Future multi-center perfusion studies should therefore not only focus on keeping ASL sequence parameters as equal as possible between centers, but also within a center (i.e. no software updates or upgrades resulting in small sequence changes).

One possible explanation for the mean CBF difference between studies could be the different slice readout times, leading to a mean effective PLD that is 100 ms longer for study 1 than for study 2. A longer PLD leads to more T1 decay, lower SNR and proportionally more spins in the tissue compartment than blood compartment - hence proportionally more faster decay with the T1 of tissue. This results in a relative underestimation of CBF for study 1 compared to study 2. These PLD effects lead to an arrival time dependent relative CBF underestimation for study 1 compared to study 2, which is in agreement with our results. Furthermore, the larger T2* decay with longer TE in study 1 reduces SNR for both the ΔM and M_0 (control) image which can partly explain its larger variation compared to study 2, both in the wsCV-maps as well as in the qualitative similarity rating. Another effect of the differences in effective PLD is a different macro-vascular weighting between study 1 and study 2. The shorter effective PLD in study 2 compared to study 1 may have provided more macro-vascular weighting, which may overestimate CBF. Despite the variation differences between the studies, the inter- to intra-vendor inter-session variation ratio was very similar. The histogram showed only slightly more

voxels where inter-vendor inter-session variation was larger than intra-vendor variation in study 1 compared to study 2. Again, these voxels seemed to be mainly found in the posterior region and cerebellum. This suggests that the abovementioned additional sources of variability for study 1 – such as larger T2* decay and larger PLD for study 1 – have a relatively similar contribution to both the intra- and inter-vendor variability. Another difference between the sequences in both studies, was the inter-pulse time of the labeling RF train - a difference of approximately 150 μ s. This is expected to have affected the labeling efficiency, although we do not expect that this had a significant effect on the wsCV²⁹.

Whereas we observed very good agreement between the mean CBF values of vendor A and vendor B in study 1, there was a significant whole brain CBF difference between vendor A and vendor C in study 2. The most likely cause of the larger CBF difference in study 2 is the different receiver coils used by the two vendors in this study (8 versus 20 channels); contrary to study 1 where both vendors had identical 8-channel head coils. A post-hoc quality assurance analysis (head phantom scanned with an IEC 2D spin echo sequence, data not shown) showed that the SNR of the scanners of vendor B and C were 71% and 155% relative to vendor A^{30, 31}. However, the inter-session variation of vendor C was only lower than vendor A in the anterior orbito-frontal region and not in other areas of the brain. Perhaps, physiological variability already dominated most regions of the brain and additional SNR only helped in regions with lowest sensitivity, such as areas prone to susceptibility induced artifacts. Additional explanations could include differences in gradient specifications or shimming of the labeling plane. The fact that the CBF disagreement between vendors in study 2 was largest in the posterior flow territory could be attributed to the fact that vertebral arteries are more tortuous than carotid arteries, increasing the possibility for a less perpendicular intersection of the vertebral arteries by the labeling plane¹¹. This could also explain the higher wsCV and lower qualitative similarity rates in the posterior flow territory.

It should be acknowledged that the main strength of this study is at the same time also its main weakness. The study design was optimized for an optimal similarity of pulse sequences between vendors within the same study, and not for optimal ASL SNR across all three scanners. This included the disabling of imaging enhancement features such as background suppression, parallel acceleration, partial Fourier and geometric distortion filters. These features were disabled to narrow down possible origins of inter-vendor variability, to achieve a more valid basis for comparison. Although the SNR penalty by disabling the image enhancement features were counterbalanced by longer scanning as well as scanning healthy young volunteers, the results of the current study may deviate from normal clinical or research

practice. These enhancement features may reduce the intra-scanner variability because of increased SNR, but may increase the inter-vendor variability because they are implementations that may vary between vendors¹⁷. Therefore, it remains unknown to what extent these features can affect the multi-center reproducibility of ASL. Still, the sequence as validated in this study could serve as a benchmark to compare other, more optimal, sequences between scanners from different vendors.

Another limitation of the current study is the use of 2D sequences, whereas 3D sequences have recently been proposed as the recommended standard¹⁰. The practical reason for choosing a 2D readout was that the implementation and reconstruction of identical 3D sequences on all vendors was not deemed feasible at the initiation of this study. When similar implementations of 3D sequences would be available on all vendors, both the intra- and inter-vendor variability could be expected to be lower because of the relatively higher SNR of 3D readouts. Especially because of the optimal performance of background suppression for 3D readouts, which greatly improves the reproducibility of ASL^{10, 17}. However, it remains unclear whether spatial correlation and blurring differences are smaller or larger between different 3D readouts than between 2D and 3D readouts¹⁷.

Conclusion

Using near-identical ASL sequences, this multi-vendor study demonstrates the possibility to acquire comparable cerebral CBF maps on scanners from different vendors. Small differences in sequence parameters can have a larger effect on the reproducibility of ASL than hardware or software differences between vendors. These results stress the importance of using identical labeling and readout strategies when perfusion maps from multiple MRI scanners are pooled. Future efforts towards harmonization of pulse sequence approaches between vendors should pave the way for multi-center clinical perfusion studies.

Reference list

1. Detre JA, Rao H, Wang DJ, Chen YF, Wang Z. Applications of arterial spin labeled MRI in the brain. *J Magn Reson Imaging* 2012; **35(5)**:1026-1037.
2. Williams DS, Detre JA, Leigh JS, Koretsky AP. Magnetic resonance imaging of perfusion using spin inversion of arterial water. *Proc Natl Acad Sci U S A* 1992; **89(1)**:212-216.
3. Golay X, Hendrikse J, Lim TC. Perfusion imaging using arterial spin labeling. *Top Magn Reson Imaging* 2004; **15(1)**:10-27.
4. Hendrikse J, Petersen ET, Golay X. Vascular disorders: insights from arterial spin labeling. *Neuroimaging Clin N Am* 2012; **22(2)**:259-2xi.

5. Xu G, Rowley HA, Wu G, Alsop DC, Shankaranarayanan A, Dowling M, *et al.* Reliability and precision of pseudo-continuous arterial spin labeling perfusion MRI on 3.0 T and comparison with ¹⁵O-water PET in elderly subjects at risk for Alzheimer's disease. *NMR Biomed* 2010; **23(3)**:286-293.
6. Heijtel DF, Mutsaerts HJ, Bakker E, Schober P, Stevens MF, Petersen ET, *et al.* Accuracy and precision of pseudo-continuous arterial spin labeling perfusion during baseline and hypercapnia: a head-to-head comparison with (1)(5)O H(2)O positron emission tomography. *Neuroimage* 2014; **92**:182-192.
7. Petersen ET, Mouridsen K, Golay X. The QUASAR reproducibility study, Part II: Results from a multi-center Arterial Spin Labeling test-retest study. *Neuroimage* 2010; **49(1)**:104-113.
8. Deibler AR, Pollock JM, Kraft RA, Tan H, Burdette JH, Maldjian JA. Arterial spin-labeling in routine clinical practice, part 2: hypoperfusion patterns. *AJNR Am J Neuroradiol* 2008; **29(7)**:1235-1241.
9. Wang DJ, Chen Y, Fernandez-Seara MA, Detre JA. Potentials and challenges for arterial spin labeling in pharmacological magnetic resonance imaging. *J Pharmacol Exp Ther* 2011; **337(2)**:359-366.
10. Alsop DC, Detre JA, Golay X, Gunther M, Hendrikse J, Hernandez-Garcia L, *et al.* Recommended implementation of arterial spin-labeled perfusion MRI for clinical applications: A consensus of the ISMRM perfusion study group and the European consortium for ASL in dementia. *Magn Reson Med* 2014.
11. Aslan S, Xu F, Wang PL, Uh J, Yezhuvath US, van OM, *et al.* Estimation of labeling efficiency in pseudocontinuous arterial spin labeling. *Magn Reson Med* 2010; **63(3)**:765-771.
12. Gunther M, Oshio K, Feinberg DA. Single-shot 3D imaging techniques improve arterial spin labeling perfusion measurements. *Magn Reson Med* 2005; **54(2)**:491-498.
13. Ye FQ, Frank JA, Weinberger DR, McLaughlin AC. Noise reduction in 3D perfusion imaging by attenuating the static signal in arterial spin tagging (ASSIST). *Magn Reson Med* 2000; **44(1)**:92-100.
14. Kilroy E, Apostolova L, Liu C, Yan L, Ringman J, Wang DJ. Reliability of two-dimensional and three-dimensional pseudo-continuous arterial spin labeling perfusion MRI in elderly populations: Comparison with ¹⁵O-water positron emission tomography. *J Magn Reson Imaging* 2013.
15. Chen Y, Wang DJ, Detre JA. Test-retest reliability of arterial spin labeling with common labeling strategies. *J Magn Reson Imaging* 2011; **33(4)**:940-949.
16. Mutsaerts HJ, Steketee RM, Heijtel DF, Kuijter JP, van Osch MJ, Majoie CB, *et al.* Inter-vendor reproducibility of pseudo-continuous arterial spin labeling at 3 tesla. *PLoS One* 2014; **9(8)**:e104108.
17. Vidorreta M, Wang Z, Rodriguez I, Pastor MA, Detre JA, Fernandez-Seara MA. Comparison of 2D and 3D single-shot ASL perfusion fMRI sequences. *Neuroimage* 2012; **66C**:662-671.
18. Dai W, Garcia D, de BC, Alsop DC. Continuous flow-driven inversion for arterial spin labeling using pulsed radio frequency and gradient fields. *Magn Reson Med* 2008; **60(6)**:1488-1497.
19. Golay X. How to do an ASL multicenter neuroimaging study. In: International Society of Magnetic Resonance in Medicine; 2009.
20. Lu H, Clingman C, Golay X, van Zijl PC. Determining the longitudinal relaxation time (T₁) of blood at 3.0 Tesla. *Magn Reson Med* 2004; **52(3)**:679-682.
21. Herscovitch P, Raichle ME. What is the correct value for the brain--blood partition coefficient for water? *J Cereb Blood Flow Metab* 1985; **5(1)**:65-69.
22. Ashburner J. A fast diffeomorphic image registration algorithm. *Neuroimage* 2007; **38(1)**:95-113.
23. Petr J, Ferre JC, Raoult H, Bannier E, Gauvrit JY, Barillot C. Template-based approach for detecting motor task activation-related hyperperfusion in pulsed ASL data. *Hum Brain Mapp* 2014; **35(4)**:1179-1189.

24. Bland JM, Altman DG. Measuring agreement in method comparison studies. *Stat Methods Med Res* 1999; **8(2)**:135-160.
25. Mutsaerts HJ, Richard E, Heijtel DF, van Osch MJ, Majoie CB, Nederveen AJ. Gray matter contamination in arterial spin labeling white matter perfusion measurements in patients with dementia. *Neuroimage Clin* 2013; **4**:139-144.
26. Tatu L, Moulin T, Bogousslavsky J, Duvernoy H. Arterial territories of the human brain: cerebral hemispheres. *Neurology* 1998; **50(6)**:1699-1708.
27. Asllani I, Borogovac A, Wright C, Sacco R, Brown TR, Zarahn E. An investigation of statistical power for continuous arterial spin labeling imaging at 1.5 T. *Neuroimage* 2008; **39(3)**:1246-1256.
28. Gevers S, van Osch MJ, Bokkers RP, Kies DA, Teeuwisse WM, Majoie CB, *et al*. Intra- and multicenter reproducibility of pulsed, continuous and pseudo-continuous arterial spin labeling methods for measuring cerebral perfusion. *J Cereb Blood Flow Metab* 2011.
29. van der Meer JN, Heijtel DF, van HG, Plattel GJ, van Osch MJ, van Someren EJ, *et al*. Acoustic noise reduction in pseudo-continuous arterial spin labeling (pCASL). *MAGMA* 2014; **27(3)**:269-276.
30. Murphy BW, Carson PL, Ellis JH, Zhang YT, Hyde RJ, Chenevert TL. Signal-to-noise measures for magnetic resonance imagers. *Magn Reson Imaging* 1993; **11(3)**:425-428.
31. International Electrotechnical Commission (IEC). Magnetic resonance equipment for medical imaging - Part 1: Determination of essential image quality parameters. In: 2014.

	STUDY 1			STUDY 2			STUDY 1 VS. 2
	vendor A	vendor B	% Δ CBF	vendor A	vendor C	% Δ CBF	% Δ CBF vendor A
Whole brain regions							
Total gray matter	48.9 (9.8)	49.6 (14.4)	1.4	57.1 (7.6)	53.8 (6.7)	†6.0	15.5†
Total white matter	14.3 (3.1)	13.0 (3.7)	10.1	15.9 (3.3)	15.1 (2.9)	4.8	10.2
GM-WM ratio	3.5 (0.7)	3.9 (1.0)	11.8	3.7 (0.6)	3.7 (0.8)	0.9	5.7
Flow territories							
Anterior	50.3 (10.2)	50.2 (14.9)	0.2	58.6 (8.2)	54.8 (7.5)	†6.6	15.2†
Middle	49.8 (9.6)	51.5 (14.3)	3.5	58.0 (7.8)	55.9 (6.5)	3.7	15.4†
Posterior	44.5 (12.2)	42.7 (15.6)	4.2	52.8 (8.2)	44.7 (8.4)	†16.7	17.0†
Dementia regions							
Anterior cingulate cortex	48.9 (12.7)	52.0 (15.4)	6.3	57.5 (8.3)	56.6 (7.7)	1.6	16.2*
Posterior cingulate cortex	46.8 (14.7)	44.4 (19.3)	5.3	58.4 (11.5)	48.0 (12.4)	†19.4	22.0†
Precuneus	51.6 (12.6)	49.0 (17.0)	5.2	59.7 (9.6)	52.1 (9.3)	†13.7	14.6*

Table 3. Cerebral blood flow (CBF) (SD), shown in mL/100g/min. % Δ CBF represents the percentual CBF difference between vendors - except for the GM-WM CBF ratio, where it represents the percentual CBF ratio difference - within study 1 or 2, and between studies for the same vendor (vendor A) in the last column. CI = confidence interval. * $p < 0.05$, † $p < 0.001$.

	STUDY 1				STUDY 2				STUDY 1
	vendor A	vendor B	inter- vendor	ratio	vendor A	vendor C	inter- vendor	ratio	ratio vs. 2 vendor A
Total gray matter	15.9 (7.6)	15.4 (10.4)	20.5 (6.4)	1.3	9.1 (4.9)	8.2 (4.3)	11.3 (3.4)	1.3	1.8
Flow territories									
Anterior	18.4 (8.3)	14.6 (10.6)	21.9 (6.7)	1.3	10.2 (5.4)	9.9 (4.9)	11.6 (3.6)	1.2	1.8*
Middle	13.8 (7.3)	15.3 (10.4)	18.5 (6.2)	1.3	8.1 (4.9)	8.1 (4.2)	11.2 (3.3)	1.4	1.7
Posterior	23.4 (9.7)	22.3 (11.5)	32.4 (7.7)	1.4	13.1 (5.5)	16.6 (5.8)	17.3 (4.3)	1.2	1.8*
Dementia regions									
Anterior cingulate cortex	24.1 (10.4)	11.4 (10.7)	25.5 (7.5)	1.4	12.1 (5.6)	10.3 (5.1)	11.9 (3.6)	1.1	2.0
Posterior cingulate cortex	32 (12.4)	19.7 (13.7)	46.1 (10.2)	†1.8	21.2 (8.5)	30.8 (9.5)	22 (6.0)	0.8	1.5
Precuneus	23.9 (10.5)	17.7 (12.2)	29.4 (8.2)	1.4	12.4 (6.4)	17.9 (6.7)	14.4 (4.6)	1.0	1.9*

Table 4. Inter-session within-subject coefficient of variation (wsCV) (confidence intervals), shown in percentages (%). Ratio represents the inter- / intra-vendor SD Δ CBF-ratio. The study 1/study 2 SD Δ CBF-ratio for vendor A is shown in the last column. CI = confidence interval. * $p < 0.05$, † $p < 0.001$

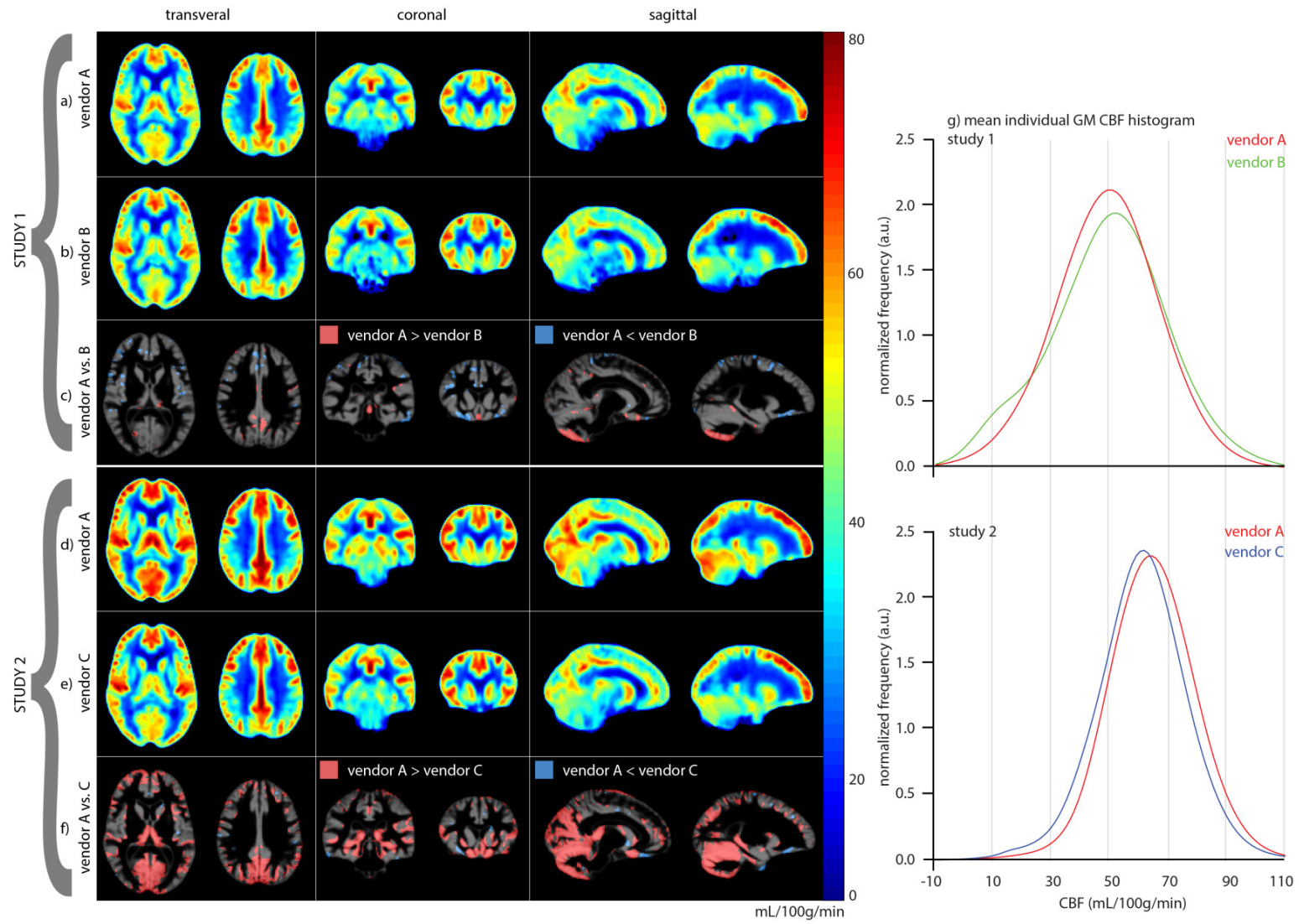


Figure 3. a-b,d-e) mean cerebral blood flow (CBF) maps; c,f) voxel-wise significant CBF differences between vendors visualized by binary parametric maps projected on the mean gray matter (GM) probability maps ($p < 0.05$ unc.); g) GM CBF histograms.

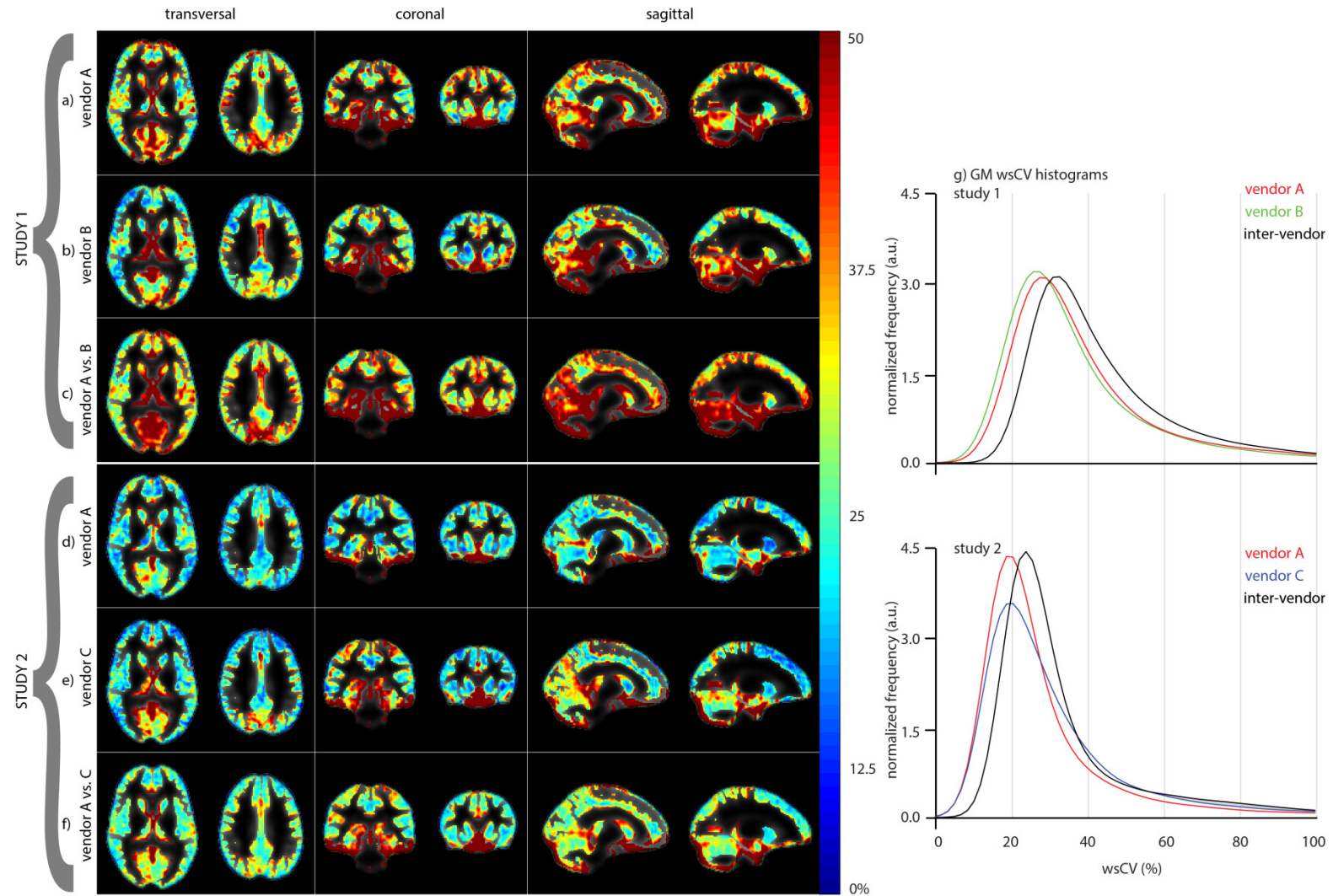


Figure 4. within-subject coefficient of variability (wsCV)-maps of study 1 (a-c) and study 2 (d-f) projected on mean gray matter (GM) probability maps; g) GM wsCV histograms

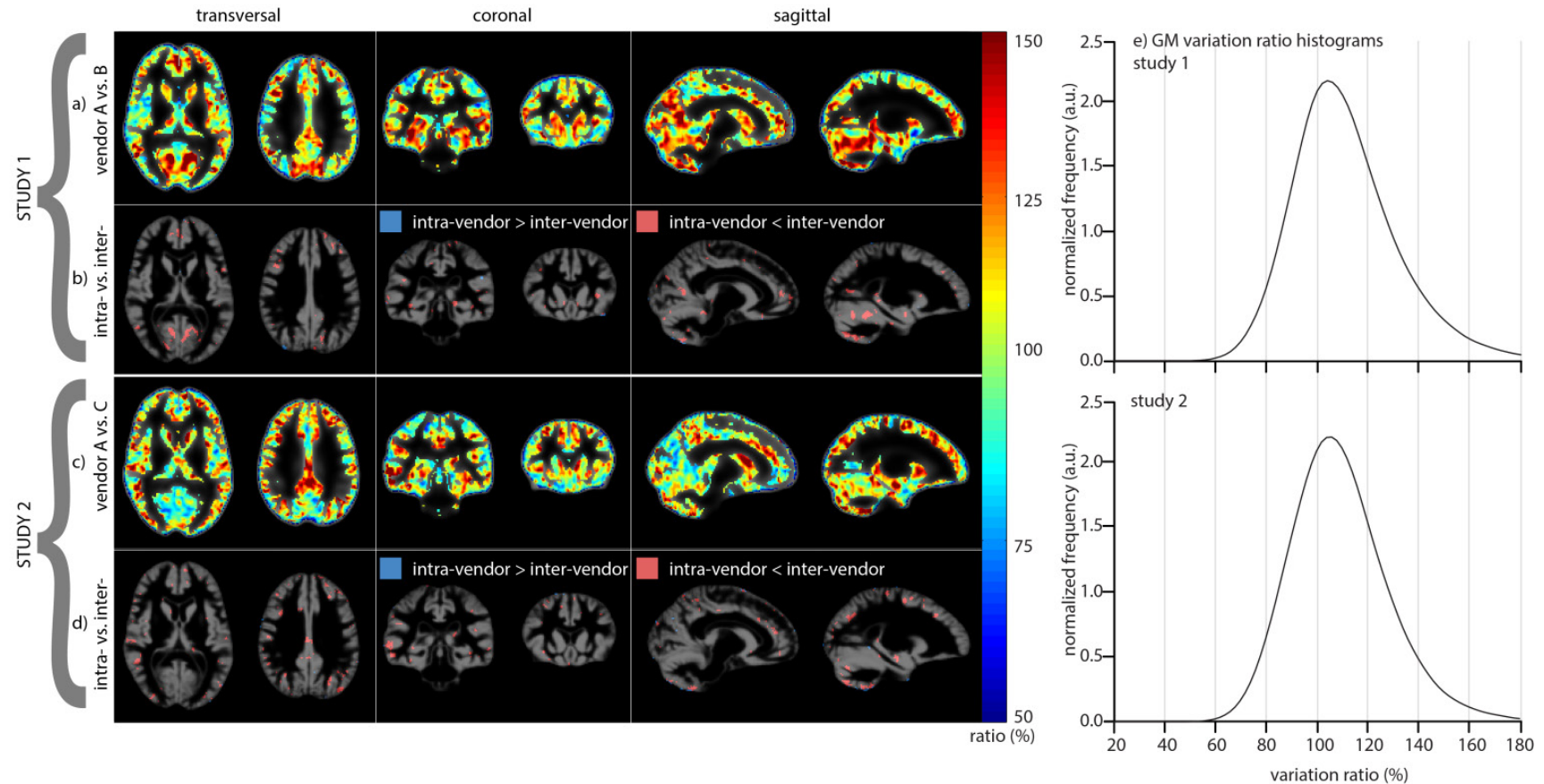


Figure 6. Variation ratio. a,c) ratio of inter- over intra-vendor standard deviation of paired inter-session differences ($SD\Delta CBF$) and b,d) binary maps projected on mean gray matter (GM) probability maps, indicating for which voxels the variation ratio is significantly different from 100%. e) gray matter variation ratio histograms.

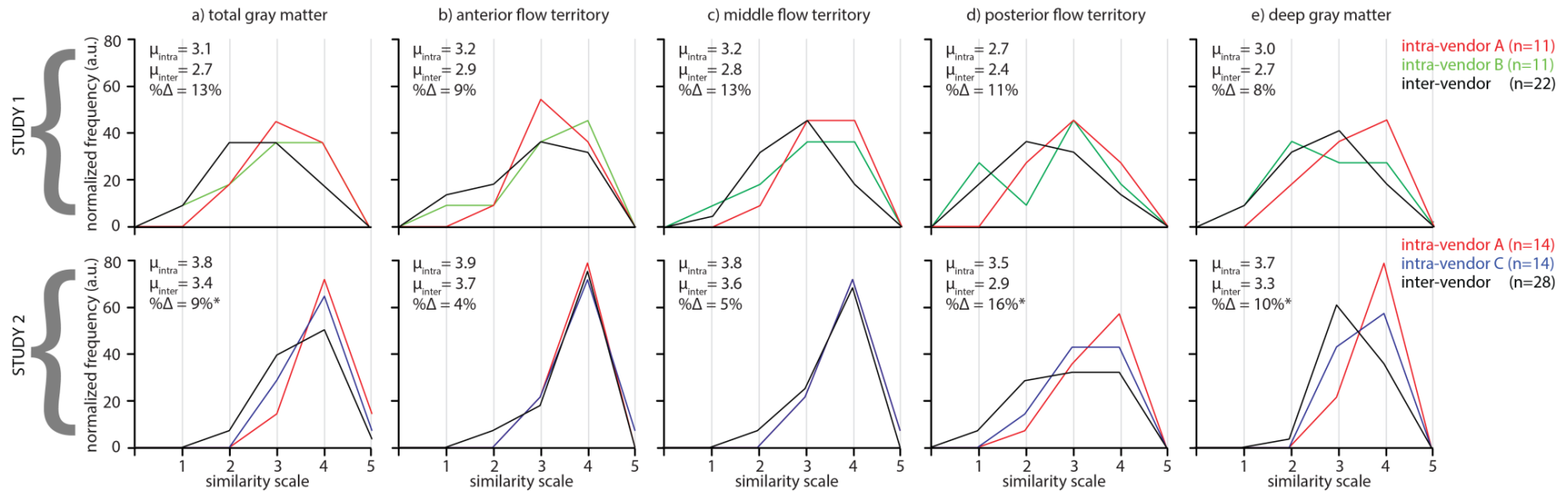


Figure 7. Qualitative similarity scale histograms, 5 indicating excellent similarity and 1 indicating poor similarity. These histograms enable the comparison of visual similarity between two sessions on different vendors (black lines) with visual similarity between two sessions on the same vendor (colored lines). μ = mean score for intra- or inter-vendor comparison. $\% \Delta$ = percentual difference between inter-vendor and mean intra-vendor similarity (* $p < 0.05$).

Part II

Clinical applicability of ASL

6

Gray matter contamination in arterial spin labeling white matter perfusion measurements in patients with dementia

HJMM Mutsaerts

E Richard

DFR Heijtel

MJP van Osch

CBLM Majoie

AJ Nederveen

NeuroImage: Clinical 2013;4:139-44

Abstract

Introduction White matter (WM) perfusion measurements with arterial spin labeling can be severely contaminated by gray matter (GM) perfusion signal, especially in the elderly. The current study investigates the spatial extent of GM contamination by comparing perfusion signal measured in the WM with signal measured outside the brain.

Material and Methods Four minute 3T pseudo-continuous arterial spin labeling scans were performed in 41 elderly subjects with cognitive impairment. Outward and inward geodesic distance maps were created, based on dilations and erosions of GM and WM masks. For all outward and inward geodesic distances, the mean CBF was calculated and compared.

Results GM contamination was mainly found in the first 3 subcortical WM voxels and had only minor influence on the deep WM signal (distances 4 to 7 voxels). Perfusion signal in the WM was significantly higher than perfusion signal outside the brain, indicating the presence of WM signal.

Conclusion These findings indicate that WM perfusion signal can be measured unaffected by GM contamination in elderly patients with cognitive impairment. GM contamination can be avoided by the erosion of WM masks, removing subcortical WM voxels from the analysis. These results should be taken into account when exploring the use of WM perfusion as micro-vascular biomarker.

Introduction

White matter (WM) perfusion measured with arterial spin labeling (ASL) is a potential *in vivo* micro-vascular parameter to investigate the interplay between normal aging and degenerative and vascular pathology, such as small vessel disease^{1,2}. Data on WM perfusion are relatively scarce, because ASL has long been considered unsuitable to measure stable WM cerebral blood flow (CBF)³. Although recent technical advances have enabled these measurements, still a relatively long scan time (10-20 min) is required to capture single voxel WM CBF⁴.

Due to the often limited available scan time, clinical investigators either ignore WM perfusion or use it as a reference value⁵. Fortunately, voxel-wise comparison of WM perfusion is not always required. It may suffice to average the signal from all WM voxels to provide a single value for the hemodynamic status of the total WM region of interest (ROI). Perfusion signal from such a ROI has recently been shown to be reproducible in elderly patients with dementia².

However, contamination of GM signal into WM voxels may seriously affect WM perfusion measurements, because the contrast between GM and WM CBF is large⁶. Furthermore, changes and correlations are mainly found in GM CBF, while the WM CBF often remains relatively stable^{5,7}. Therefore, even a fraction of GM contamination may distort WM CBF measurements and its possible clinical correlations.

Main sources of GM contamination are the point spread function (PSF) of the ASL imaging readout module and partial volume (PV) voxels^{3,8}. Both have a large effect in ASL due to its low imaging resolution, which is required to compensate for its low signal-to-noise ratio (SNR). Currently, PV voxels are excluded based on the segmentation of a high resolution anatomical scan^{1,2,9}. However, simulations indicate that WM voxels without PV may still experience GM contamination due to the PSF⁶.

Therefore, to correctly interpret perfusion signal averaged from a WM ROI, it is essential to investigate the spatial extent of GM contamination. Can perfusion signal originating from the WM be distinguished from signal blurred from the GM? With this knowledge a WM ROI could be constructed that experiences minimal GM contamination without excluding too many WM voxels. Constructing a WM ROI may be especially challenging in the elderly, because of the decreased T1 and ASL GM-WM contrast and WMH associated with aging^{1,2,10}. The current study investigates the spatial extent of GM contamination in elderly patients with dementia.

Material and methods

Subject recruitment

41 patients (19 men/22 women, mean age 74.9 ± 9.7 (SD) years) presenting to an outpatient memory clinic were included in this study. Main inclusion criteria were age higher than 18 years and score on the mini-mental state examination equal to or higher than 20. Main exclusion criteria were history of transient ischemic attack or stroke in the last two years or with cognitive decline within three months after the event, major depressive disorder, psychosis or schizophrenia, alcohol abuse, brain tumor, and epilepsy. All patients provided written informed consent and the study was approved by the VU University Medical Center and Academic Medical Center ethical review boards. Of the 41 enrolled participants, 18 fulfilled criteria for mild cognitive impairment and 23 fulfilled criteria for probable Alzheimer's Disease or mixed dementia ¹¹.

MRI protocol

All imaging was performed on a 3.0 T Intera with a SENSE-8-channel head coil and body coil transmission (Philips Healthcare, Best, The Netherlands). To restrict motion the subjects' head was stabilized with foamed material inside the head coils. An isotropic 1 mm 3D T1 weighted scan and 2D FLAIR scan with 3 mm slice thickness were collected using a routine clinical protocol. Added to this protocol was a gradient echo single shot echo-planar imaging pseudo-continuous ASL sequence with the following imaging parameters: resolution, $3 \times 3 \times 7$ mm³; FOV, 240×240 mm²; 17 continuous axial slices; TE/TR, 14/4000 ms; flip angle, 90 degrees; SENSE, 2.5; labeling duration, 1650 ms; post-labeling delay, 1525 ms. Slices were acquired in sequential ascending order. 30 label and control pairs were acquired, resulting in a total scan time of 4 min. Background suppression was implemented with two inversion pulses 1680 and 2830 ms after a pre-labeling saturation pulse. The labeling plane was positioned parallel and 9 cm caudal to the center of the imaging volume ¹². For descriptive purposes of the presence of small vessel disease, the Fazekas WM hyperintensity severity scale and four-point global cortical atrophy score were assessed by a trained rater, blinded to the clinical information ^{13,14}.

ASL post-processing

Matlab 7.12.0 (The MathWorks, Inc., Natick, MA USA) and the SPM8 toolbox (Statistical Parametric Mapping, Wellcome Trust Centre for Neuroimaging, London, UK) were used for offline data processing with custom-built software. The label and control pairs were pair-wise subtracted after 3D realignment and subsequently averaged to generate perfusion weighted maps. These maps were converted to CBF

based on a single compartment model, which assumes that the label remains in the vascular compartment¹⁵:

$$\text{CBF} = \frac{6000 \lambda \Delta M e^{(\text{TE}/T_{2a}^*)}}{M_{0a} 2 \alpha \alpha_{inv} T_{1a} [e^{-w/T_{1a}} - e^{-(w+\tau)/T_{1a}}]} \text{ [mL/100g/min]}$$

where λ is the brain-blood water partition coefficient (0.9 mL/g)¹⁶, ΔM is the average difference between control and label for all 30 dynamics, TE is the echo time (14 ms), T_{2a}^* is the transverse relaxation time of arterial blood (50 ms)¹⁷, M_{0a} is the equilibrium magnetization of arterial blood, of which an average scanner value was calculated ($4.12 \cdot 10^6$) according to previously described methods¹⁸, α is the assumed pseudo-continuous ASL labeling efficiency (0.85)¹², α_{inv} is the correction for label loss due to background suppression pulses (0.83)¹⁹, T_{1a} is the T_1 relaxation time of arterial blood (1.650 s)²⁰, w is the post-labeling delay (1.525 s), τ is the labeling duration (1.650 s). Post-labeling delay differences between slices due to the 2D readout were accounted for. No distinction was made between the quantification of GM and WM voxels. GM and WM probability maps were segmented from the 3D T1 weighted scan and transformed into ASL space by rigid registration of the GM probability map to the perfusion map. Default SPM8 settings were used for segmentation and registration except for the distance between sampling points, which was decreased to 1 mm for increased precision. All CBF maps were scaled such that the mean GM CBF (tissue probabilities > 90%) of each patient matched the population mean (36.8 mL/100 g/min) for the slice used in the distance analysis. Negative values were not excluded. All data analyses were performed in native ASL space to avoid GM contamination due to interpolation.

Distance analysis

Two distance maps were constructed to compare the extent of inward and outward GM contamination. This method enables the comparison between perfusion signal measured in the WM to signal measured outside the brain. Outside the brain, where air or tissue types such as cerebrospinal fluid (CSF), meninges, bone and skin are located, no perfusion signal is expected except from outward GM contamination. This analysis was carried out in 2D and restricted to a single transversal slice (Figure 1) located 2 slices (14 mm) superior to the basal ganglia. This slice contains a relatively large area of WM, has no central GM and does not experience much distortion or signal dropout as frequently observed anterior in echo-planar imaging. The procedures of the distance analysis are stepwise listed here, and visualized in Figure 1.

- 1) The WM probability map (a) was converted into a WM mask (b), including tissue probabilities $> 10\%$. This low probability threshold avoids the exclusion of WM hyperintensity voxels, which are frequently misclassified as GM voxels. Subsequently, the GM probability map (A) was converted into a GM mask (B), including tissue probabilities $> 90\%$, which is complementary to the WM mask at the GM/WM boundary.
- 2) Any remaining regions inside the WM or GM masks (such as CSF) were masked as well (c and C), such that erosions or dilations affected the outer borders of the masks only.
- 3) Erosions were applied to the WM mask (d) and dilations to the GM mask (D), using a cross structural element with radius 1.
- 4) Inward (e) and outward (E) city-block geodesic distance maps were created by labeling each voxel for number of erosions required to remove this voxel from the WM mask (e) or for the number of dilations required to add this voxel to the GM mask (E).

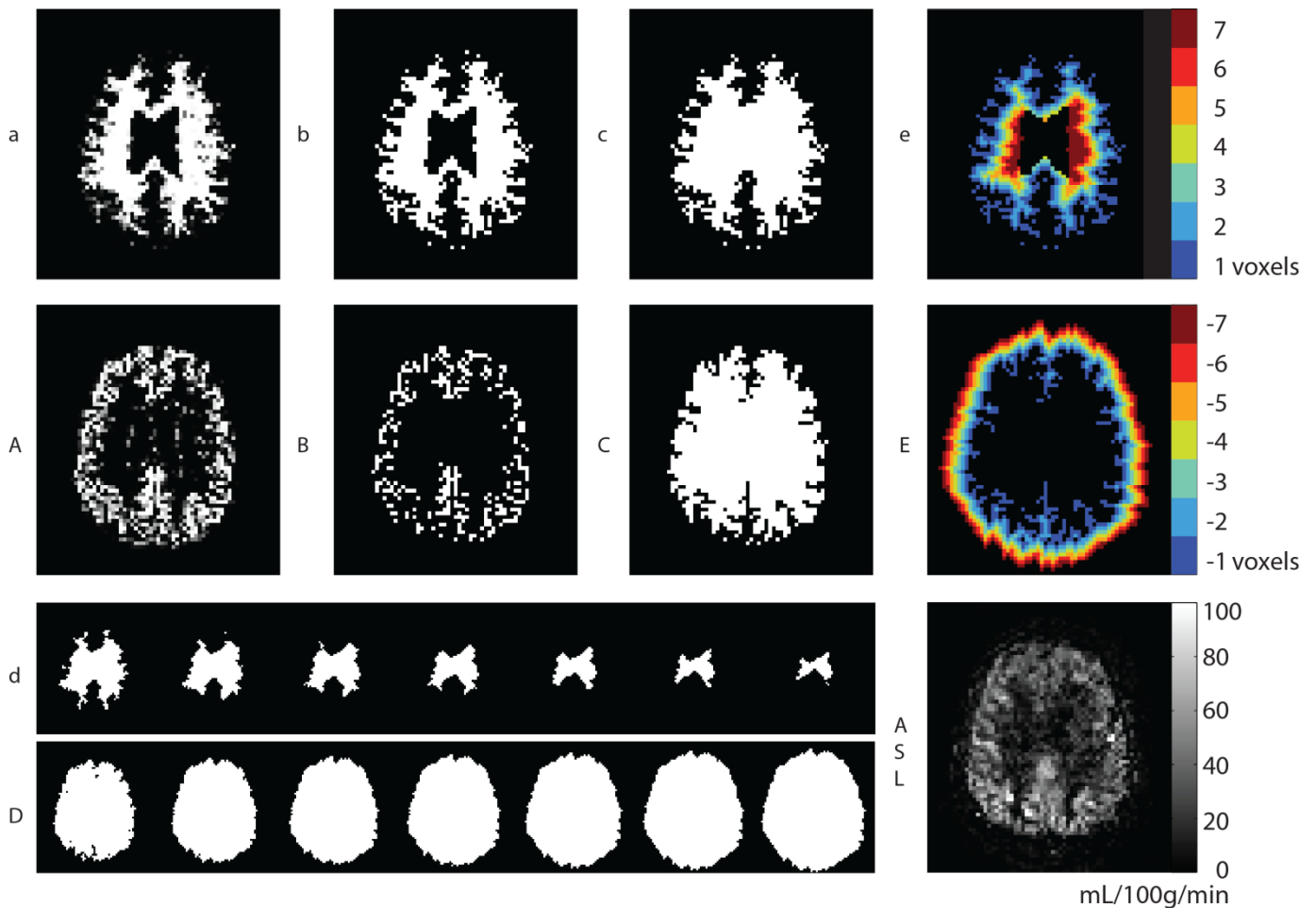


Figure 1. Single slice distance analysis pipeline visualized for a single patient: tissue probability maps (a, A) converted into masks (b, B), gaps filled (c, C), erosion and dilation (d, D) and the resulting city-block geodesic maps (e, E). Lower and upper case represent WM and GM respectively. In the right lower corner the ASL slice is shown for reference.

Consequently, the resulting distance maps show for each WM voxel its shortest distance (in voxels) to the outer border of the WM mask (Figure 1e) and for each voxel outside the brain its shortest distance to the outer border of the GM mask (Figure 1E). Since the in-plane voxel size is 3x3 mm, a distance of 1 voxel presents a distance of 3 mm. All voxels with the same distance were projected on the CBF maps, to compute the mean CBF and voxel count for each distance.

Partial volume analysis

To investigate the influence of PV voxels, the same WM tissue probability map as used for the distance analysis was converted to multiple binary masks with WM tissue probabilities ranging from 80% to 100% with a bin size of 1% (e.g. 80-81%, 81-82%, etc.). This range was selected, as it encloses probability thresholds that have been previously selected in WM research^{1,2,4}. These WM masks were projected on the ASL data and their mean WM CBF, GM-WM CBF ratio and voxel count were calculated. For both the distance and PV analysis, the individual mean GM CBF (tissue probabilities > 90%) was defined as GM CBF. This GM CBF was also used to calculate the GM-WM ratio for the inward distances 1 to 7 voxels.

Results

Patient characteristics are summarized in Table 1. The mean GM CBF was 36.8 ± 8.5 mL/100 g/min. Outward GM contamination was mainly observed in the first three voxels (distances -1 to -3 voxels), whereas distances -4 to -7 voxels showed very low signal (Figure 2a). The inward decrease of WM signal was smaller than the outward signal decrease ($p < 0.001$ with paired sample Student's t-test, indicated with asterisks in Table 2 and Figure 2a). In the PV analysis, the WM CBF and GM-WM ratio seemed to show decreasing GM contamination with increasing tissue probabilities (Figure 2a).

A comparison of the left and right graphs of Figure 2a-b shows the relation of GM contamination with the inclusion of voxels containing 80 - 100 % WM PV. Mean CBF and GM-WM CBF ratio of tissue probabilities 80 to 99% can be compared with distances 1 to 3 voxels ($p = 0.728$ independent sample t-test). The WM CBF and GM-WM CBF ratio at 100% WM tissue probability (i.e. WM voxels without PV) can be compared with distance 4 voxels ($p = 0.810$). At higher inward distances (5-7) the mean CBF decreased further and reached lower values than with the exclusion of all PV voxels (tissue probability 100%) ($p < 0.001$). Similarly, at these higher distances the GM-WM CBF ratio reached higher values than with the exclusion of all voxels containing < 100 % WM PV. Figure 3 shows the difference between a WM mask without these voxels (tissue probability = 100% without erosions) and a WM mask with these

voxels (tissue probabilities > 10%) but with three erosions applied. It illustrates that the exclusion of voxels containing < 100% WM PV did not remove all subcortical WM voxels whereas it did remove voxels within the deep WM.

Age (years)	74.9 (9.7)
Gender (male/female)	19/ 22
Mini-mental state examination	24.9 (2.9)
Geriatric depression scale	2.6 (2.1)
Fazekas	
0	4%
1	44%
2	15%
3	37%
Global cortical atrophy	
1	19%
2	59%
3	22%

Table 1. Clinical and radiological characteristics (n=41). Of continuous variables the mean is shown. Standard deviations are shown in parentheses. Findings of categorical variables are presented in percentages. Mini-mental state examination ranges from 0 to 30 (higher score equates with better cognitive function) and the geriatric depression scale ranges from 0 to 15 (higher score equates with more symptoms of depression).

Distance (voxels)	CBF (mL/100g/min)	Distance (voxels)	CBF (mL/100g/min)	GM-WM ratio
-1	35.7 ± 7.4	+1	27.3 ± 5.8 *	1.4 ± 0.3
-2	15.2 ± 9.3	+2	19.4 ± 6.4 *	2.0 ± 0.7
-3	6.0 ± 4.3	+3	17.7 ± 7.0 *	2.3 ± 1.0
-4	4.5 ± 4.1	+4	14.2 ± 6.2 *	4.1 ± 2.8
-5	3.7 ± 3.9	+5	11.5 ± 6.7 *	4.1 ± 2.2
-6	2.1 ± 2.6	+6	9.3 ± 6.8 *	5.0 ± 3.4
-7	1.2 ± 1.7	+7	8.4 ± 6.3 *	4.9 ± 3.0

Table 2. Outward and inward GM contamination (n=41). Mean ± standard deviation of CBF are shown for distances -1 to -7, representing outward GM contamination (left columns) and for distances 1 to 7, representing inward GM contamination (right columns). The GM-WM ratio for the inward distances are shown as well. Significant differences ($p < 0.001$) between negative and positive distances are indicated by an asterisk (*).

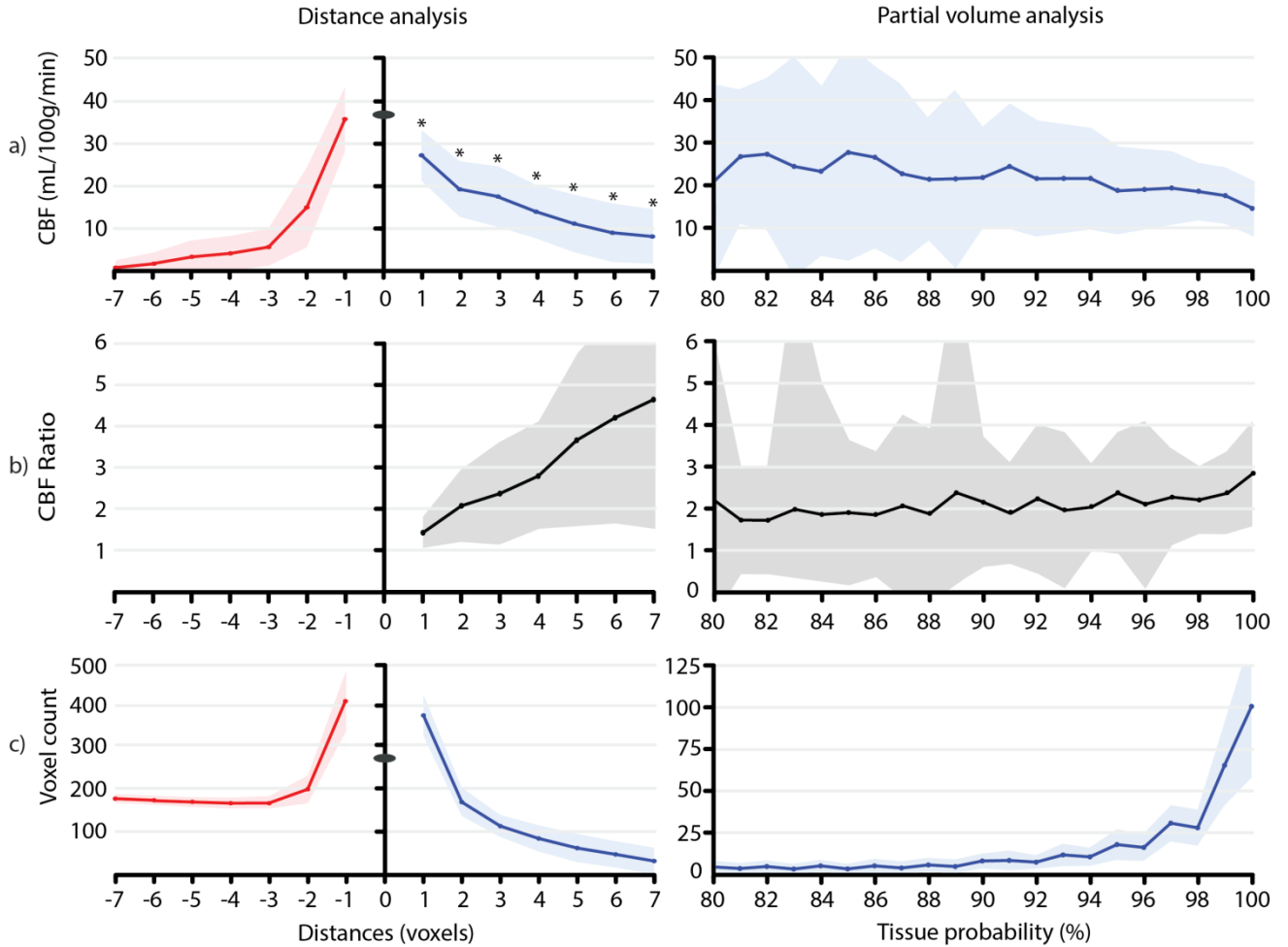


Figure 2. a-c shows single slice distance analysis (left column) and partial volume analysis (right column). a) mean CBF; b) mean GM-WM CBF ratio; c) mean number of voxels. The distance numbers on the left x-axis correspond with distances in Figure 1. Distances -1 to -7 represent GM mask dilation steps, distances 1 to 7 represent WM mask erosion steps. Distance 0 represents the mean GM CBF (tissue probabilities > 90%). The numbers on the right x-axis represent bins of the WM tissue probabilities (bin size 1%). Lines and planes represent mean values and \pm 95% CI respectively. Significant differences ($p < 0.001$) between negative and positive distances are indicated by an asterisk (*).

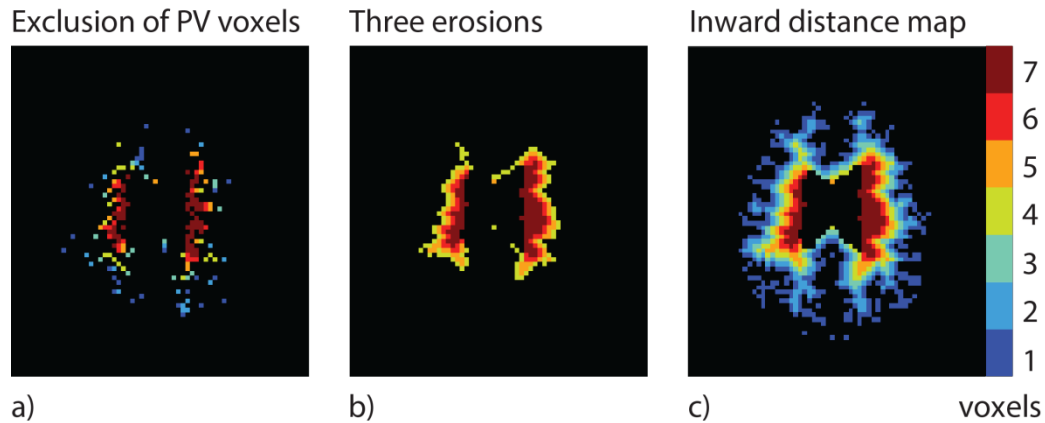


Figure 3. a-c visualizes the difference between two masks obtained by either a) the exclusion of partial volume (PV) voxels by thresholding the WM mask at a tissue probability of 100% or b) the application of three erosions on a large WM mask (tissue probabilities $> 10\%$). The same WM distance map color scale (Figure 1c, reprinted here for reference (c)) is applied here to visualize the position of the voxels included in both masks.

Discussion

The findings of this study are threefold. Firstly, the outward GM contamination suggests that GM contamination mainly affects the first three subcortical WM voxels and has only minor influence on deep WM signal, beyond three voxels distance from the GM. Secondly, the significant asymmetry between the inward and outward signal indicates that the detected signal within the WM voxels reflects WM perfusion signal. Finally, Figure 3 indicates that GM contamination is not restricted to voxels that contain more than 0% GM PV. These results provide insight in the distinction of PSF from the effect of PV voxels, and show that, within a WM ROI, WM signal can be separated from the contamination of GM signal.

Using probabilistic tissue segmentation, generally two different methods can be applied to avoid GM contamination^{2,4}. The tissue probability threshold can be set high to exclude all voxels containing less than 100% WM PV. Alternatively, it can be set relatively low (e.g. only excluding $< 10\%$ WM PV) in combination with a number of erosions applied on the outside of the mask. Here, we have compared the two methods. With an increase in excluded voxels that contain GM or CSF PV, we observed decreasing GM contamination, a trend that is in agreement with previous findings⁴. As the WM CBF and GM-WM CBF ratio at 100% tissue probability (i.e. only voxels containing 100% WM PV) were comparable to CBF and GM-WM CBF ratio at a distance of 4 voxels, it appears that it would suffice to exclude all voxels containing less than 100% WM PV. However, Figure 3a shows that 100% WM voxels also

resided within the subcortical WM, where GM contamination was observed. In addition, the segmentation algorithm removed voxels within the deep WM, where no GM contamination was observed. The removal of deep WM voxels is probably the result of segmentation errors due to WM hyperintensities or CSF PV voxels²¹. Although CSF contamination decreases the measured WM CBF, this effect includes only noise and does not bias clinical correlations -- as is the case for GM contamination. Therefore, we conclude that the application of erosion on the outer boundary of a WM mask is a more effective way to avoid GM contamination compared to the exclusion of voxels containing less than 100% WM PV.

The GM-WM ratio has been frequently used to compare perfusion results independent from global quantification differences. Nevertheless, discrepancies exist between literature values of this ratio, even within modalities. Where some authors have reported ratios between 2 and 3, others reported ratios between 4 and 6^{6, 22, 23}. Whereas studies with the highest values were focused on deep WM or used methods that were less sensitive to GM contamination, studies with lower values seem to have employed a larger ROI or lower imaging resolution^{3, 6}. Our ratios in the deep WM (distances 4-7 voxels) are within the range of the first whereas our ratios in subcortical WM (distances 1-3 voxels) are more comparable to the latter. In addition, the ratios in subcortical WM are comparable to those obtained in the PV analysis (80-99%). This adds to the point that the exclusion of voxels containing less than 100% WM PV may not suffice to avoid GM contamination.

Our ratios in deep WM, on the other hand, are still slightly lower than previously reported values. This may be attributable to aging or WMH^{1, 10}. Alternatively, these ratios may depend on quantification differences between GM and WM CBF, such as the T_1 relaxation time of tissue, blood-brain partition coefficient or tissue arrival times. In the current study, we aimed to visualize the distance analysis in CBF units without influencing our results by differences in CBF quantification. Therefore, an identical model was applied for the quantification of GM and WM CBF and the label was assumed to remain in the vascular compartment²⁴. This assumption may especially be valid in the elderly, because of their prolonged transit times¹⁰. Moreover, such a simple model eliminates PV effects introduced by quantification based on T1 segmentation, due to the possibility of registration mismatches. Alternatively, tissue probability maps can be acquired using the same ASL readout module, which enables separate GM- and WM-quantification that is not affected by registration mismatches⁸. In the current study, these mismatches may be increased by echo-planar imaging distortions in regions that are close to air-tissue transitions, which are predominantly GM areas²⁵. This highlights the importance of proper registration between the T1 and the ASL scan.

It should be acknowledged that the design of the current analysis is based on segmentations of an anatomical 3D T1 scan, and assumes homogeneous perfusion values across all voxels with the same distance from the GM-WM boundary. This assumption is required to average multiple voxels for sufficient SNR. Whether or not perfusion is homogeneous across WM is currently unknown. On the other hand, it is well known that transit times differ within the WM⁶. This heterogeneity has probably contributed to the continuing CBF decrease from distances 4 to 7 voxels, where no GM contamination is expected (as shown in Table 2 and Figure 2a). Alternatively, this may be caused by CBF decreasing lesions, such as WM hyperintensities, or CSF contamination¹. Outside the brain, the measured signal may not entirely be dependent upon the PSF. Factors that may have contributed to the signal found outside the GM include extra-cranial vessels, perfusion of the skin and motion artifacts.

The heterogeneity of acquisition details that determine the PSF, such as the ASL readout resolution, readout time or T2* blurring, may limit the extrapolation of the present results to other studies. One previous study simulated the effect of PSF in a single large central WM voxel on multiple spatial resolutions, assuming a GM and WM CBF of 80 and 0 mL/100g/min, respectively. Whereas on a low isotropic resolution such as 12.5 mm a contamination of 10 mL/100g/min could be measured in the central WM, on an isotropic resolution of 3.1 mm (which is in-plane comparable to our acquisition) only 0.08 mL/100g/min GM contamination was left⁶. This simulation is in line with the present results, which demonstrate that perfusion measured in deep WM contains only minor GM contamination. Furthermore, the PSF differs between 2D and 3D readouts.

The current distance analysis was restricted to a single slice to compare the 2D in-plane PSF versus the effect of PV voxels. This is a valid comparison for 2D readout modules, since they have no PSF in the through-plane direction -- except for crosstalk from slice profile, which is negligible in slices as thick as 7 mm. Although 3D readouts exhibit increased SNR and improved background suppression allowing for higher spatial resolution, they experience increased GM contamination due to their wider 3D PSF -- especially in the through-plane direction²⁶. Even though methods exist that numerically correct this GM-WM contamination, a 2D readout module can be preferred when uncontaminated WM CBF measurements are more important than spatial or temporal SNR^{26,27}.

To summarize, these data illustrate that, using pseudo-continuous ASL, WM perfusion signal can be distinguished from GM contamination within clinically feasible scan time in patients with cognitive impairment. Because of the PSF, GM contamination is not restricted to PV voxels and it seems

necessary to apply erosion to remove subcortical WM voxels. It is expected that this method would only work in some slices, as for the majority of slices too few or no WM voxels will be left after 3 erosions. Whether this is sufficient for clinical studies should be clarified in further research. These results should be taken into account when exploring the use of WM perfusion as micro-vascular biomarker.

Reference list

1. Brickman AM, Zahra A, Muraskin J, Steffener J, Holland CM, Habeck C, *et al.* Reduction in cerebral blood flow in areas appearing as white matter hyperintensities on magnetic resonance imaging. *Psychiatry Res* 2009; 172(2):117-120.
2. Zhang Q, Stafford RB, Wang Z, Arnold SE, Wolk DA, Detre JA. Microvascular Perfusion Based on Arterial Spin Labeled Perfusion MRI as a Measure of Vascular Risk in Alzheimer's Disease. *J Alzheimers Dis* 2012; 32(3):677-687.
3. van Gelderen P, de Zwart JA, Duyn JH. Pitfalls of MRI measurement of white matter perfusion based on arterial spin labeling. *Magn Reson Med* 2008; 59(4):788-795.
4. van Osch MJ, Teeuwisse WM, van Walderveen MA, Hendrikse J, Kies DA, van Buchem MA. Can arterial spin labeling detect white matter perfusion signal? *Magn Reson Med* 2009; 62(1):165-173.
5. Firbank MJ, He J, Blamire AM, Singh B, Danson P, Kalaria RN, *et al.* Cerebral blood flow by arterial spin labeling in poststroke dementia. *Neurology* 2011; 76(17):1478-1484.
6. Pohmann R. Accurate, localized quantification of white matter perfusion with single-voxel ASL. *Magn Reson Med* 2010; 64(4):1109-1113.
7. Parkes LM, Rashid W, Chard DT, Tofts PS. Normal cerebral perfusion measurements using arterial spin labeling: reproducibility, stability, and age and gender effects. *Magn Reson Med* 2004; 51(4):736-743.
8. Petr J, Schramm G, Hofheinz F, Langner J, van den Hoff J. Partial volume correction in arterial spin labeling using a Look-Locker sequence. *Magn Reson Med* 2012; 70(6):1535-1543.
9. Bastos-Leite AJ, Kuijter JP, Rombouts SA, Sanz-Arigita E, van Straaten EC, Gouw AA, *et al.* Cerebral blood flow by using pulsed arterial spin-labeling in elderly subjects with white matter hyperintensities. *AJNR Am J Neuroradiol* 2008; 29(7):1296-1301.
10. Liu Y, Zhu X, Feinberg D, Guenther M, Gregori J, Weiner MW, *et al.* Arterial spin labeling MRI study of age and gender effects on brain perfusion hemodynamics. *Magn Reson Med* 2012; 68(3):912-922.
11. Winblad B, Palmer K, Kivipelto M, Jelic V, Fratiglioni L, Wahlund LO, *et al.* Mild cognitive impairment--beyond controversies, towards a consensus: report of the International Working Group on Mild Cognitive Impairment. *J Intern Med* 2004; 256(3):240-246.
12. Aslan S, Xu F, Wang PL, Uh J, Yezhuvath US, van OM, *et al.* Estimation of labeling efficiency in pseudocontinuous arterial spin labeling. *Magn Reson Med* 2010; 63(3):765-771.
13. Fazekas F, Chawluk JB, Alavi A, Hurtig HI, Zimmerman RA. MR signal abnormalities at 1.5 T in Alzheimer's dementia and normal aging. *AJR Am J Roentgenol* 1987; 149(2):351-356.
14. Pasquier F, Leys D, Weerts JG, Mounier-Vehier F, Barkhof F, Scheltens P. Inter- and intraobserver reproducibility of cerebral atrophy assessment on MRI scans with hemispheric infarcts. *Eur Neurol* 1996; 36(5):268-272.

15. Wang J, Alsop DC, Li L, Listerud J, Gonzalez-At JB, Schnall MD, *et al.* Comparison of quantitative perfusion imaging using arterial spin labeling at 1.5 and 4.0 Tesla. *Magn Reson Med* 2002; 48(2):242-254.
16. Herscovitch P, Raichle ME. What is the correct value for the brain--blood partition coefficient for water? *J Cereb Blood Flow Metab* 1985; 5(1):65-69.
17. St Lawrence KS, Wang J. Effects of the apparent transverse relaxation time on cerebral blood flow measurements obtained by arterial spin labeling. *Magn Reson Med* 2005; 53(2):425-433.
18. Chalela JA, Alsop DC, Gonzalez-Atavales JB, Maldjian JA, Kasner SE, Detre JA. Magnetic resonance perfusion imaging in acute ischemic stroke using continuous arterial spin labeling. *Stroke* 2000; 31(3):680-687.
19. Garcia DM, Duhamel G, Alsop DC. Efficiency of inversion pulses for background suppressed arterial spin labeling. *Magn Reson Med* 2005; 54(2):366-372.
20. Zhang X, Petersen ET, Ghariq E, De Vis JB, Webb AG, Teeuwisse WM, *et al.* In vivo blood T(1) measurements at 1.5 T, 3 T, and 7 T. *Magn Reson Med* 2012; 70(4):1082-1086.
21. Chen JJ, Rosas HD, Salat DH. Age-associated reductions in cerebral blood flow are independent from regional atrophy. *Neuroimage* 2011; 55(2):468-478.
22. Rempp KA, Brix G, Wenz F, Becker CR, Guckel F, Lorenz WJ. Quantification of regional cerebral blood flow and volume with dynamic susceptibility contrast-enhanced MR imaging. *Radiology* 1994; 193(3):637-641.
23. Xu G, Rowley HA, Wu G, Alsop DC, Shankaranarayanan A, Dowling M, *et al.* Reliability and precision of pseudo-continuous arterial spin labeling perfusion MRI on 3.0 T and comparison with ¹⁵O-water PET in elderly subjects at risk for Alzheimer's disease. *NMR Biomed* 2010; 23(3):286-293.
24. Parkes LM. Quantification of cerebral perfusion using arterial spin labeling: two-compartment models. *J Magn Reson Imaging* 2005; 22(6):732-736.
25. Deichmann R, Josephs O, Hutton C, Corfield DR, Turner R. Compensation of susceptibility-induced BOLD sensitivity losses in echo-planar fMRI imaging. *Neuroimage* 2002; 15(1):120-135.
26. Vidorreta M, Wang Z, Rodriguez I, Pastor MA, Detre JA, Fernandez-Seara MA. Comparison of 2D and 3D single-shot ASL perfusion fMRI sequences. *Neuroimage* 2012; 66C:662-671.
27. Asllani I, Borogovac A, Brown TR. Regression algorithm correcting for partial volume effects in arterial spin labeling MRI. *Magn Reson Med* 2008; 60(6):1362-1371.

7

Cerebral perfusion measurements in the elderly using arterial spin labeling

HJMM Mutsaerts

JW van Dalen

DFR Heijtel

PFC Groot

CBLM Majoie

E Richard

AJ Nederveen

In submission

Abstract

Purpose The current study assesses the feasibility and value of crushed cerebral blood flow ($CBF_{crushed}$) and transit time (TT) estimations for large clinical imaging studies in the elderly.

Material and Methods Two pseudo-continuous arterial spin labeling (ASL) scans with ($CBF_{crushed}$) and without flow crushers ($CBF_{non-crushed}$) were performed in 186 elderly with hypertension, from which CBF and TT maps were calculated. Standard flow territory maps were subdivided into proximal, intermediate and distal flow territories, based on the measured TT. The coefficient of variation (CV) and physiological correlations with age and gender were compared between the three perfusion parameters.

Results There was no difference in CV between $CBF_{crushed}$ and $CBF_{non-crushed}$ (15-24%, $p>0.4$) but the CV of TT (4-9%) was much smaller. The total gray matter correlations with age and gender were most significant with TT ($p=.016$ and $p<.001$ respectively), in between for $CBF_{crushed}$ ($p=.206$ and $p=.019$) and least significant for $CBF_{non-crushed}$ ($p=.236$ and $p=.100$).

Conclusion These data show the feasibility and added value of combined measurements of both crushed CBF and TT for group analyses in the elderly. The obtained flow territories provide knowledge on normal vascular anatomy and can be used in future studies to investigate regional vascular effects.

Introduction

Perfusion as measured with arterial spin labeling (ASL) is a promising *in vivo* hemodynamic parameter to investigate the interplay between normal aging and neurodegenerative and cerebrovascular pathology^{1,2}. Parallel to the optimization of conventional ASL-based cerebral blood flow (CBF) measurements for clinical applications, advanced ASL methods have been developed that enable the acquisition of multiple perfusion parameters simultaneously³⁻⁵.

One example is the acquisition of both CBF and the micro-vascular transit time (TT) by the flow-encoding arterial spin tagging (FEAST) method. FEAST is based upon the subdivision of an imaging voxel into macro- and micro-vascular compartments based on differences in blood flow velocity⁶. By performing ASL with and without the application of a vascular crusher, FEAST separately acquires CBF of the micro-vascular compartment (CBF_{crushed}) and CBF of the macro- and micro-vascular compartments together ($CBF_{\text{non-crushed}}$) (Figure 1). The ratio of the perfusion signal of $CBF_{\text{non-crushed}}$ over CBF_{crushed} is then proportional to the TT, which is defined as the time it takes for the labeled blood to travel from the labeling plane to the micro-vascular compartment of the imaging voxel.

Several advantages exist for the application of a vascular crusher and the estimation of TT using FEAST. CBF_{crushed} may be preferable to $CBF_{\text{non-crushed}}$, since micro-vascular CBF changes are generally assumed to reflect (patho-)physiological changes in neuronal activity and energy demand whereas macro-vascular CBF is believed to be dominated by cardiovascular fluctuation⁷. TT has been shown to be able to provide additional diagnostic value to CBF measurements, especially in cerebrovascular pathology^{8,9}. However, these possible advantages may come at the cost of a decrease of reliability. Considering the often limited available scanning time, vascular crushing reduces the available SNR for the CBF measurement⁶. Therefore, it has been recently agreed upon that crushing is currently not recommended in the individual subject¹⁰. However, for group analyses, the feasibility and utility of crushed CBF or TT is still under debate.

The primary purpose of this study was to assess the feasibility and value of the combined measurement of CBF_{crushed} and TT for large clinical imaging studies in the elderly. To investigate the spatial distribution of these parameters, we used the estimated TTs to divide standard flow territory maps into proximal, intermediate and distal flow territories. We study the reliability of these perfusion parameters in terms of their population variation and physiological correlations with age and gender.

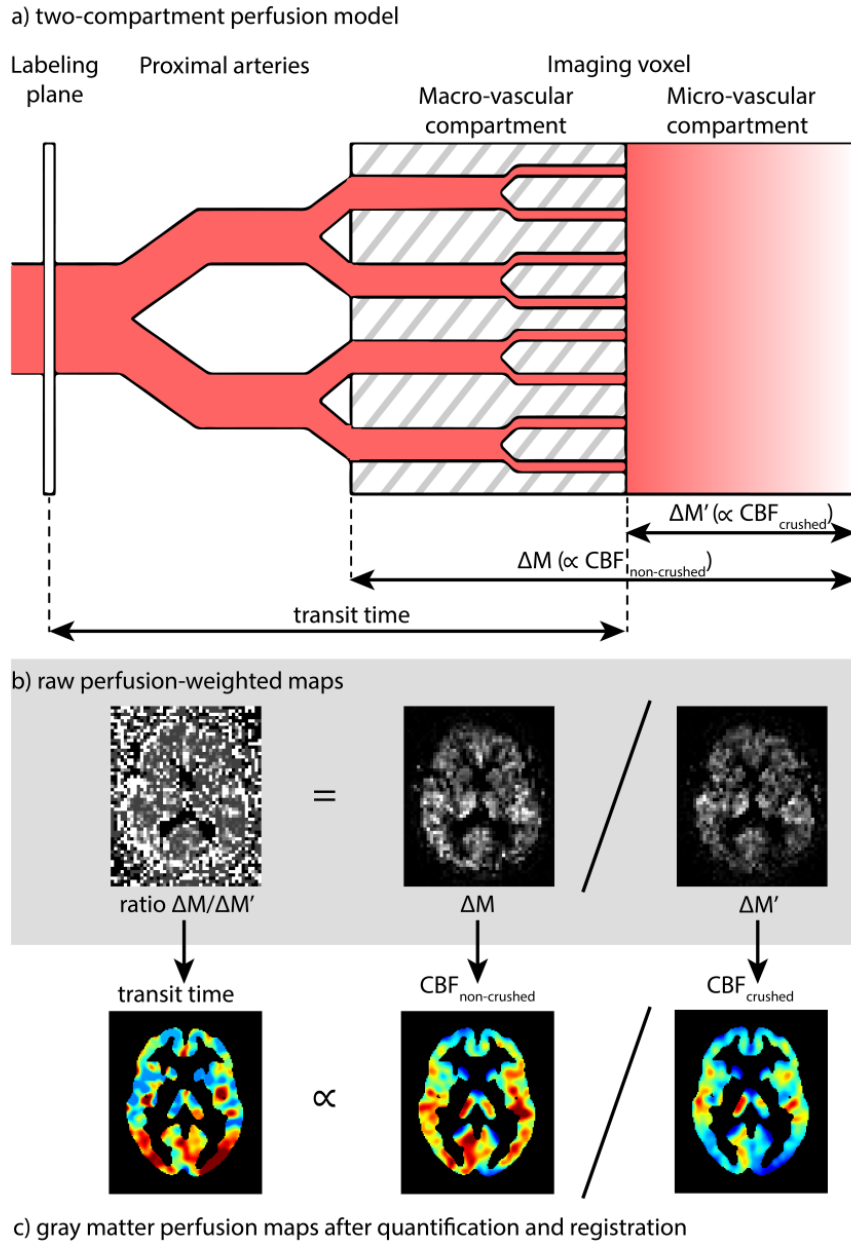


Figure 1. a) Schematic overview of the two-compartment perfusion model explains the FEAST technique, adapted from Wang *et al.*⁶ b) shows raw perfusion-weighted maps and c) perfusion maps after post-processing for a representative subject. Note that the signal intensity is lower after crushing ($\Delta M'$) than before (ΔM) and that crushed CBF ($CBF_{crushed}$) is weighted toward the micro-vascular CBF whereas non-crushed CBF ($CBF_{non-crushed}$) is weighted toward both micro- and macro-vascular CBF. $\propto =$ proportional to

Materials and methods

Subjects

195 community-dwelling elderly (46% male, mean age 77 years, range 72-80 years) with hypertension (systolic blood pressure higher than 140 mmHg) participating in the Pre-DIVA study were eligible for inclusion¹¹. Exclusion criteria were dementia and disorders or circumstances expected to interfere with successful follow-up. Nine subjects were excluded from analysis because of severe labeling or motion artifacts.

Ethics statement

All patients provided written informed consent and the study was approved by the institutional review board of the Academic Medical Center, Amsterdam.

Imaging protocol

All imaging was performed on a 3T system (Intera, Philips Healthcare, Best, The Netherlands) equipped with an 8-channel head coil. Foam padding was used to restrict head motion. A slightly adapted version of the original FEAST acquisition, which enables the simultaneous acquisition and quantification of CBF_{crushed} , $CBF_{\text{non-crushed}}$ and TT within clinical scanning time, was added to a routine clinical dementia protocol. Two ASL scans were performed with (CBF_{crushed}) and without ($CBF_{\text{non-crushed}}$) flow-crushing gradients in three directions (velocity encoding 50 mm/s). Identical imaging parameters of the two consecutive gradient-echo single-shot EPI pseudo-continuous ASL (pCASL) sequences were: matrix = 64x64, FOV = 240 x 240 mm, 17 axial slices, slice thickness 7 mm, no gap, echo time/repetition time = 17/4000 ms, flip angle = 90 degrees, SENSE = 2.5, initial post-label delay (PLD) = 1525 ms; slice readout time = 34.9 ms; resulting PLD range for 17 slices = 1525-2080 ms, labeling duration = 1650 ms and two background suppression pulses at 1710 and 2860 ms after a pre-labeling saturation pulse. 20 label-control pairs were acquired – resulting in a duration of 2:40 minutes for each scan. The labeling plane was positioned parallel and 8.3 cm inferior to the center of the imaging volume¹². An isotropic 1 mm³ 3D T1-weighted scan was included in the imaging protocol for segmentation and registration purposes.

Quantification

The raw EPI control and label images were 3D motion corrected using SPM8 (Statistical Parametric Mapping, Wellcome Trust Centre for Neuroimaging, London, UK). After pair-wise subtraction, these

raw maps were converted to CBF with a single compartment model, assuming that the label decays with the T1 of blood ^{10, 13}:

$$CBF[mL/100g/min] = \frac{\Delta M e^{TE/T_{2a}^*}}{\rho M_{0a} 2\alpha\alpha_{inv} T_{1a} (e^{-\delta/T_{1a}} - e^{(-\omega-\tau)/T_{1a}})} \quad [1]$$

where ρ is the density of brain tissue (1.05 g/mL) ¹⁴, ΔM is the difference between control and label intensities, TE is the echo time (17 ms), T_{2a}^* is the transverse relaxation time of arterial blood (50 ms) ¹⁵, M_{0a} is the equilibrium magnetization of arterial blood, for which an average scanner value was used ¹⁶, calculated according to previously described methods ¹⁷, α is the labeling efficiency (0.85) ¹², α_{inv} is the correction for label loss due to background suppression pulses (0.83) ¹⁸, T_{1a} is the T₁ relaxation time of arterial blood (1650 ms) ¹⁹, $\omega = 1525 \text{ ms} + 34.9 \text{ ms/slice}$, τ is the labeling duration (1650 ms) and δ is the measured TT (averaged per subject for each flow territory, as described below) for CBF_{crushed}, which is replaced by the PLD for CBF_{non-crushed}.

TT was calculated based on the following two FEAST equations ⁶:

$$\Delta M = A (e^{-w/T_{1a}} - e^{(-w-\tau)/T_{1a}}) \quad [2]$$

$$\Delta M' = A (e^{-\delta/T_{1a}} - e^{(-w-\tau)/T_{1a}}) \quad [3]$$

where A is a constant and ΔM and $\Delta M'$ represent the scans acquired without and with vascular crushing, respectively (Figure 1).

Registration

The 3D T1-weighted anatomical scans were segmented using SPM8 into gray matter tissue probability maps, on which the CBF and TT maps were rigid-body registered. The tissue probability maps were spatially normalized using the Diffeomorphic Anatomical Registration analysis using Exponentiated Lie algebra (DARTEL) algorithm and the resulting normalization fields were applied to the CBF and TT maps ²⁰.

Flow territories

The total cerebral gray matter was defined as tissue probabilities >70%. Standard flow territory templates (left and right combined) were used to investigate vascular territories supplied by the bilateral

anterior, middle and posterior cerebral arteries (referred to as ACA, MCA and PCA respectively) ²¹. Within each flow territory the TTs were ranked in tertiles, resulting in three proximal, three intermediate and three distal flow territories.

Statistics

Prior to all analyses, the distributions of investigated values were tested for normality using the Shapiro-Wilk test. Because most distributions of perfusion parameters deviated from normal, distributions were summarized by the median and mean absolute deviation (instead of mean and standard deviation). To compare variation between the perfusion parameters, the coefficient of variation (CV) was used, calculated as mean absolute deviation divided by the median. To test whether respectively the median or CV differed between $CBF_{crushed}$ and $CBF_{non-crushed}$, the sign test and Brown-Forsythe test were used (comparable to Student's t-test and Levene's test but more robust in distributions that deviate from normality). To provide insight in the distribution of CBF and TT values in the ACA, MCA and PCA, median group-level histograms were generated from the histograms of individual maps (100 bins, smoothed with 2 bins full-width-half-maximum). To investigate physiological correlations, robust linear regression analyses were performed to model cross-sectional correlations between the predictors age or gender and the dependent variables $CBF_{non-crushed}$, $CBF_{crushed}$ or TT, adjusted for total brain volume (defined as the combined volume of gray and white matter segmentations).

Results

Flow territories

The TT-based flow territories showed an almost entirely continuous sequence from anterior-inferior to posterior-superior (ACA), inferior to superior (MCA) and anterior-inferior to posterior-superior (PCA) (Figure 2).

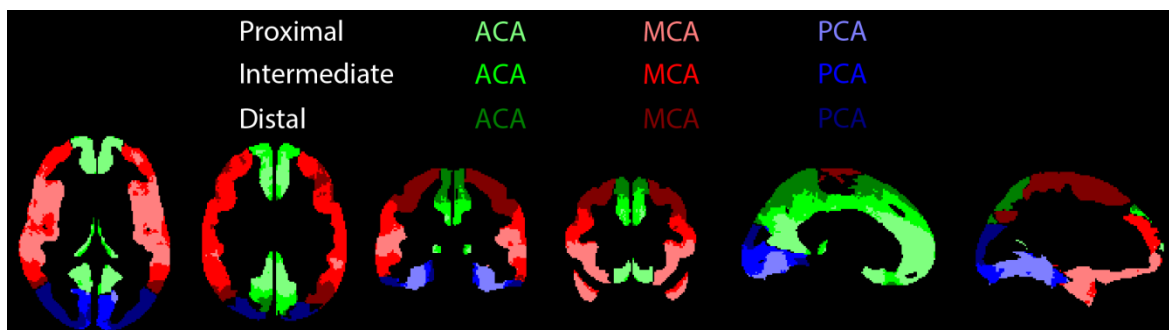


Figure 2. Flow territories. ACA (green), MCA (red) and PCA (blue) refer to the standard flow territories perfused by the bilateral anterior, middle and posterior cerebral arteries respectively, whereas the

shadings represent their subdivision into proximal, intermediate and distal flow territories, based on transit times.

Comparison perfusion parameters

Figure 3 shows the median and CV maps of the perfusion parameters. The perfusion patterns in the median $\text{CBF}_{\text{crushed}}$ and $\text{CBF}_{\text{non-crushed}}$ maps had a similar appearance. Whereas the median $\text{CBF}_{\text{crushed}}$ differed in nearly all flow territories from the median $\text{CBF}_{\text{non-crushed}}$, there was no CV difference between $\text{CBF}_{\text{crushed}}$ and $\text{CBF}_{\text{non-crushed}}$ ($p > 0.4$ all flow territories), both ranging from 15% to 20% (Table 1). The CV of TT was much smaller than the CV of $\text{CBF}_{\text{crushed}}$ or $\text{CBF}_{\text{non-crushed}}$, ranging from 4% to 9%. For all perfusion parameters, CV increased from proximal to distal flow territories (Table 1). All perfusion histograms appeared to approximate a normal distribution, except for the TT histogram in the PCA (Figure 3h).

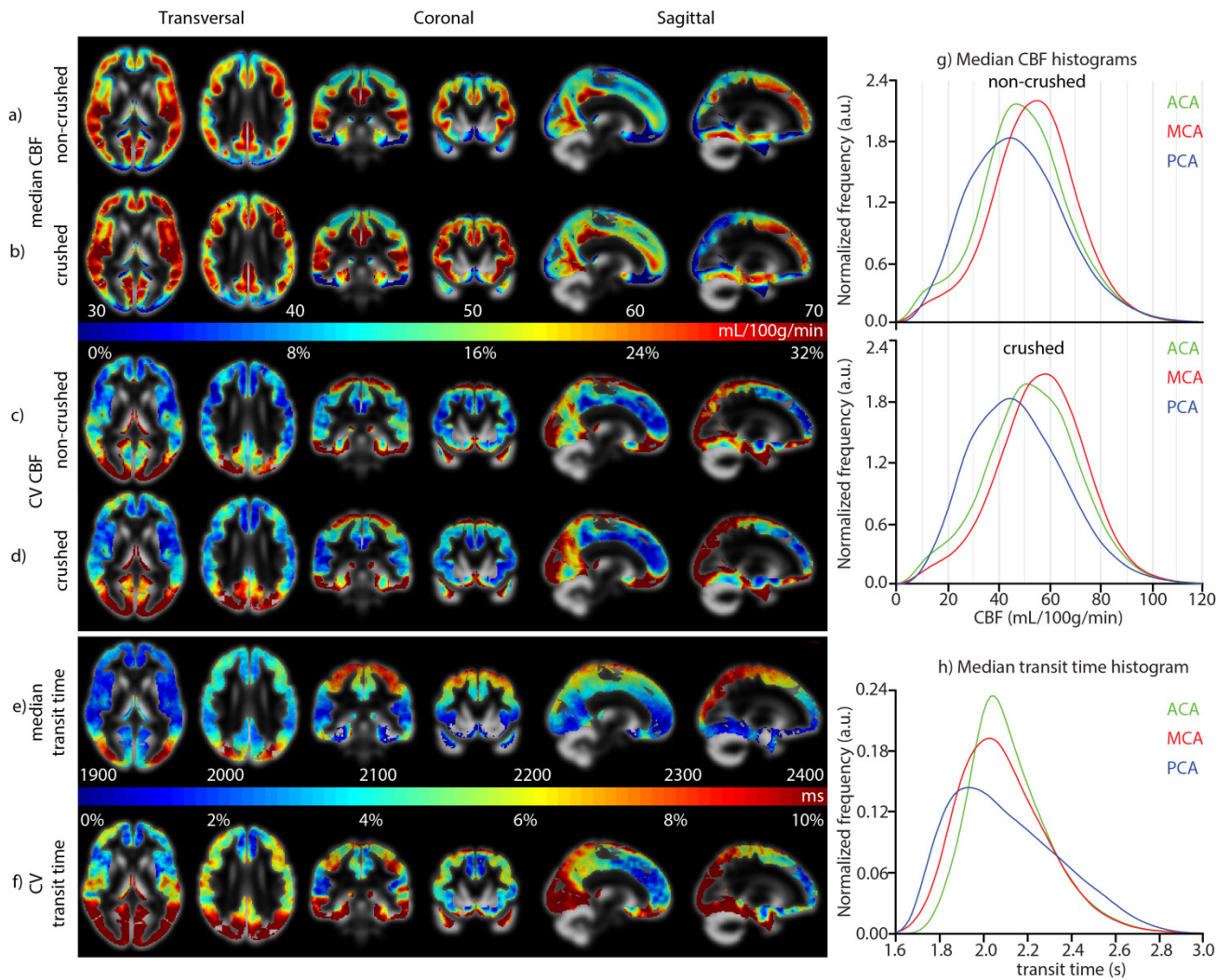


Figure 3. a-b) median and c-d) coefficient of variation (CV) maps of non-crushed CBF and crushed CBF, e) median and f) CV maps of transit time (TT). g,h) median histograms of (non-)crushed CBF and

TT maps for the three vascular territories. ACA, MCA and PCA refer to the vascular territories perfused by the anterior, middle and posterior cerebral arteries respectively, corresponding to Figure 2.

	CBF _{non-crushed} (CV) [mL/100g/min]	CBF _{crushed} (CV) [mL/100g/min]	Difference median · CV	TT (CV) [ms]
ACA proximal	48.4 ± 8.5 (17%)	52.8 ± 9.1 (17%)	Y · N	1990 ± 90 (4%)
intermediate	53.8 ± 9.0 (17%)	58.0 ± 9.1 (16%)	Y · N	2070 ± 100 (5%)
distal	46.8 ± 9.0 (19%)	49.6 ± 9.4 (19%)	Y · N	2210 ± 130 (6%)
MCA proximal	53.5 ± 8.8 (17%)	57.8 ± 8.7 (15%)	Y · N	1930 ± 80 (4%)
intermediate	54.8 ± 9.3 (17%)	58.5 ± 9.4 (16%)	Y · N	2040 ± 110 (5%)
distal	53.9 ± 9.7 (18%)	55.7 ± 10.0 (18%)	Y · N	2210 ± 140 (6%)
PCA proximal	45.2 ± 8.5 (19%)	46.8 ± 8.9 (19%)	Y · N	1930 ± 140 (7%)
intermediate	45.9 ± 10.1 (22%)	46.7 ± 10.4 (22%)	Y · N	2030 ± 170 (9%)
distal	46.8 ± 10.9 (23%)	46.3 ± 10.9 (24%)	N · N	2290 ± 200 (9%)
Total gray matter	51.4 ± 8.6 (17%)	54.6 ± 8.9 (16%)	Y · N	2080 ± 110 (5%)

Table 1. Distributions of perfusion parameters (n=186). Shown are the median ± mean absolute deviation from median (with the coefficient of variation (CV) between parentheses) of CBF and transit time (TT). ACA, MCA and PCA refer to the flow territories perfused by the anterior, middle and posterior cerebral arteries respectively, corresponding to Figure 2. Difference (4th column) shows whether the median or CV differed (Y) or not (N) ($p < 0.01$) between CBF_{crushed} and CBF_{non-crushed}.

Physiological correlations

In all vascular territories, CBF_{crushed} and CBF_{non-crushed} decreased and the TT increased with age, although the changes with age were significant in some flow territories only (Table 2). In almost all flow territories, men had lower CBF and longer TTs compared to women. Generally, correlations were strongest with TT and slightly stronger with CBF_{crushed} than with CBF_{non-crushed}. The regression coefficients roughly suggested that both aging 10 years and being male decreases total gray matter CBF with 8% and increases total gray matter TT with 5%. For all perfusion parameters, correlation coefficients and p -values increased and decreased respectively from proximal to distal flow territories.

	CBF _{non-crushed}	CBF _{crushed}	TT
Age	[mL/100g/min/decade]	[mL/100g/min/decade]	[ms/decade]
ACA proximal	- 3.08 .. $p=.334$	- 4.11 .. $p=.226$	70 .. $p=.033$
intermediate	- 3.43 .. $p=.316$	- 2.92 .. $p=.389$	80 .. $p=.015$
distal	- 5.21 .. $p=.138$	- 5.89 .. $p=.112$	110 .. $p=.013$
MCA proximal	- 2.93 .. $p=.392$	- 2.36 .. $p=.484$	50 .. $p=.082$
intermediate	- 2.42 .. $p=.501$	- 2.63 .. $p=.466$	70 .. $p=.088$
distal	- 4.65 .. $p=.219$	- 5.31 .. $p=.172$	110 .. $p=.036$
PCA proximal	- 6.32 .. $p=.052$	- 6.74 .. $p=.042$	130 .. $p=.008†$
intermediate	-10.07 .. $p=.008†$	-10.68 .. $p=.006†$	180 .. $p=.006†$
distal	- 9.58 .. $p=.025$	- 8.81 .. $p=.038$	170 .. $p=.020$
Total gray matter	- 3.96 .. $p=.236$	- 4.31 .. $p=.206$	100 .. $p=.016$
Gender	[mL/100g/min M>F]	[mL/100g/min M>F]	[ms M>F]
ACA proximal	- 3.00 .. $p=.102$	- 4.93 .. $p=.011$	50 .. $p=.003†$
intermediate	- 4.67 .. $p=.017$	- 5.56 .. $p=.004†$	90 .. $p<.001†$
distal	- 4.20 .. $p=.036$	- 5.12 .. $p=.014$	130 .. $p<.001†$
MCA proximal	0.29 .. $p=.881$	- 1.45 .. $p=.451$	50 .. $p=.010†$
intermediate	- 1.82 .. $p=.379$	- 3.90 .. $p=.061$	100 .. $p<.001†$
distal	- 3.93 .. $p=.068$	- 5.69 .. $p=.010†$	170 .. $p<.001†$
PCA proximal	- 3.43 .. $p=.068$	- 4.90 .. $p=.010†$	100 .. $p<.001†$
intermediate	- 5.99 .. $p=.006†$	- 7.64 .. $p=.001†$	160 .. $p<.001†$
distal	- 8.52 .. $p<.001†$	- 9.40 .. $p<.001†$	250 .. $p<.001†$
Total gray matter	- 3.15 .. $p=.100$	- 4.57 .. $p=.019$	110 .. $p<.001†$

Table 2. Regression coefficients for age and gender (n=186). For each ROI, estimated cross-sectional regression coefficients and p -values are shown. † $p<0.01$. ACA, MCA and PCA refer to the flow territories perfused by the anterior, middle and posterior cerebral arteries respectively, corresponding to Figure 2.

Discussion

The results of this study prove the feasibility of ASL-based CBF_{crushed} and FEAST-based TT measurements within acceptable scanning time in an elderly population. These perfusion parameters showed stronger correlations with age and gender compared to conventional CBF measurements, demonstrating the potential value of CBF_{crushed} and TT for group analyses. The observation that the variation of perfusion parameters within flow territories was comparable with the variation of the total gray matter, suggests that the reliability of crushing and FEAST within flow territories is sufficient on a

group level, and no further spatial averaging is required. For large clinical imaging studies in the elderly, therefore, there appears to be potential to study more perfusion parameters than CBF alone.

The TT maps comply with the trajectory of the cerebral vessels, with shortest TTs where the vessels enter the cerebrum and longest at the superior-posterior watershed area²². The resulting TT-based flow territories can be used as ROIs in future studies if hypothesized perfusion effects are restricted to certain flow territories only, or if spatial averaging is required when an anatomical structure is too small considering ASL limitations in terms of SNR or spatial smoothing¹⁰. Potential applications include the investigation of a vascular component to degeneration of the dementia-related regions precuneus and hippocampus, which are supplied by the distal ACA and PCA^{23, 24}. The fact that distal flow territories demonstrated the largest variation and strongest correlations, could be due to the fact that these regions are most vulnerable to inadequacy of arterial supply due to cerebrovascular pathology²⁵. In addition, whole-brain vascular effects across the population can be envisioned to accumulate in the distal flow territories. This suggests that perfusion measurements in distal flow territories have the highest statistical power to detect vascular effects, even if these effects are expected to be distributed across the total brain.

The observed correlations of the perfusion parameters with age lie within the range of previously reported values, whereas the differences with gender were relatively small compared to previous values²⁶⁻²⁹. These correlation differences with previous studies may result from our specific population of high age and hypertension, in which large and small vessel disease is expected to be highly prevalent^{30, 31}.

The observation that the population variation of TT was much smaller than the variation of CBF could originate from the fact that the physiological perfusion fluctuations affect CBF more than TT. Methodologically, the measured physiological variation can be expected to be similar for $\Delta M'$ ($\text{CBF}_{\text{crushed}}$) and ΔM ($\text{CBF}_{\text{non-crushed}}$), and will thus not propagate into the FEAST-based TT measurement, which is derived from the ratio of the two perfusion scans (Figure 1). The smaller extent of random variation of TT could explain its stronger correlations with age and gender, indicating that TT measured by FEAST can be a more sensitive parameter for physiological correlations in the elderly than CBF.

Our study includes the following limitations. The main drawback for the quantification of TT using the FEAST method, is that the dichotomization of macro- and micro-vascular compartments is based on a single pre-defined velocity cutoff (Figure 1). We have employed a conservative velocity cutoff of 50 mm/s, which is required to retain sufficient SNR in the ASL readout of the $\text{CBF}_{\text{crushed}}$ measurement

(Figure 1)¹⁰. The drawback of this high velocity cutoff is that $\text{CBF}_{\text{crushed}}$ is more similar to $\text{CBF}_{\text{non-crushed}}$, which is illustrated by the fact that the median images of both CBF parameters have a similar visual appearance. Consequentially, the micro-vascular compartment is defined more proximal, resulting in T^* -values that are more weighted towards the macro-vascular T^* than would be the case with lower velocity cutoffs as implemented in the original FEAST method. Although it has been shown in young healthy volunteers that this penalty is not severe, it is advisable to perform multi- T^* measurements in a small subset of subjects, for calibration of FEAST-based T^* in the elderly^{6,32}.

Another drawback of the FEAST method, is that its T^* estimates depend on the selected PLD. A too long PLD will overestimate the T^* , since the FEAST method cannot measure T^* s that are shorter than the PLD⁶. On the other hand, a too short PLD leads to measurement errors if the labeled blood has not yet arrived in the imaging voxel at the time of imaging, which may lead to severe underestimation³². To satisfy PLD criteria for both CBF and T^* measurements, we applied a PLD that is a trade-off between conventional CBF measurements and FEAST-based T^* measurements. The penalty of this PLD trade-off seems small for the ACA and MCA, since their T^* distributions appear close to normal. For the PCA, however, the distribution of T^* values was more skewed to the left. This can be expected to result mainly from a too short PLD, considering the fact that T^* are known to be longest in this region³². Therefore, the reliability of FEAST-based T^* measurements in the elderly is limited for the PCA.

In conclusion, we have shown the feasibility and value of combined measurements of CBF and FEAST-based T^* for large imaging studies in the elderly. The obtained flow territories can be used in future studies to identify regional vascular effects. On a group level, crushing can improve correlations with physiological parameters such as age and gender. The high physiological correlations of T^* suggest that this perfusion parameter can be more relevant than conventional CBF measurements. However, the PLD should be carefully selected and one should account for the possible under- and overestimation of T^* . These data encourage future clinical imaging studies in the elderly to investigate multiple MRI perfusion parameters, instead of focusing at CBF only.

Reference list

1. Detre JA, Rao H, Wang DJ, Chen YF, Wang Z. Applications of arterial spin labeled MRI in the brain. *J Magn Reson Imaging* 2012; **35(5)**:1026-1037.
2. de la Torre JC. Cerebral hemodynamics and vascular risk factors: setting the stage for Alzheimer's disease. *J Alzheimers Dis* 2012; **32(3)**:553-567.
3. Dai W, Shankaranarayanan A, Alsop DC. Volumetric measurement of perfusion and arterial transit delay using hadamard encoded continuous arterial spin labeling. *Magn Reson Med* 2013; **69(4)**:1014-1022.
4. Petersen ET, Mouridsen K, Golay X. The QUASAR reproducibility study, Part II: Results from a multi-center Arterial Spin Labeling test-retest study. *Neuroimage* 2010; **49(1)**:104-113.
5. Mildner T, Muller K, Hetzer S, Trampel R, Driesel W, Moller HE. Mapping of arterial transit time by intravascular signal selection. *NMR Biomed* 2014; **27(5)**:594-609.
6. Wang J, Alsop DC, Song HK, Maldjian JA, Tang K, Salvucci AE, et al. Arterial transit time imaging with flow encoding arterial spin tagging (FEAST). *Magn Reson Med* 2003; **50(3)**:599-607.
7. Sadaghiani S, Hesselmann G, Friston KJ, Kleinschmidt A. The relation of ongoing brain activity, evoked neural responses, and cognition. *Front Syst Neurosci* 2010; **4**:20.
8. MacIntosh BJ, Graham SJ. Magnetic resonance imaging to visualize stroke and characterize stroke recovery: a review. *Front Neurol* 2013; **4**:60.
9. Donahue J, Sumer S, Wintermark M. Assessment of collateral flow in patients with cerebrovascular disorders. *J Neuroradiol* 2013.
10. Alsop DC, Detre JA, Golay X, Gunther M, Hendrikse J, Hernandez-Garcia L, et al. Recommended implementation of arterial spin-labeled perfusion MRI for clinical applications: A consensus of the ISMRM perfusion study group and the European consortium for ASL in dementia. *Magn Reson Med* 2014.
11. Richard E, Van den Heuvel E, Moll van Charante EP, Achthoven L, Vermeulen M, Bindels PJ, et al. Prevention of dementia by intensive vascular care (PreDIVA): a cluster-randomized trial in progress. *Alzheimer Dis Assoc Disord* 2009; **23(3)**:198-204.
12. Aslan S, Xu F, Wang PL, Uh J, Yezhuvath US, van OM, et al. Estimation of labeling efficiency in pseudocontinuous arterial spin labeling. *Magn Reson Med* 2010; **63(3)**:765-771.
13. Wang J, Alsop DC, Li L, Listerud J, Gonzalez-At JB, Schnall MD, et al. Comparison of quantitative perfusion imaging using arterial spin labeling at 1.5 and 4.0 Tesla. *Magn Reson Med* 2002; **48(2)**:242-254.
14. Herscovitch P, Raichle ME. What is the correct value for the brain--blood partition coefficient for water? *J Cereb Blood Flow Metab* 1985; **5(1)**:65-69.
15. St Lawrence KS, Wang J. Effects of the apparent transverse relaxation time on cerebral blood flow measurements obtained by arterial spin labeling. *Magn Reson Med* 2005; **53(2)**:425-433.
16. Heijtel DF, Mutsaerts HJ, Bakker E, Schober P, Stevens MF, Petersen ET, et al. Accuracy and precision of pseudo-continuous arterial spin labeling perfusion during baseline and hypercapnia: a head-to-head comparison with (1)(5)O H(2)O positron emission tomography. *Neuroimage* 2014; **92**:182-192.
17. Chalela JA, Alsop DC, Gonzalez-Atavales JB, Maldjian JA, Kasner SE, Detre JA. Magnetic resonance perfusion imaging in acute ischemic stroke using continuous arterial spin labeling. *Stroke* 2000; **31(3)**:680-687.
18. Garcia DM, Duhamel G, Alsop DC. Efficiency of inversion pulses for background suppressed arterial spin labeling. *Magn Reson Med* 2005; **54(2)**:366-372.
19. Zhang X, Petersen ET, Ghariq E, De Vis JB, Webb AG, Teeuwisse WM, et al. In vivo blood T(1) measurements at 1.5 T, 3 T, and 7 T. *Magn Reson Med* 2012; **70(4)**:1082-1086.
20. Ashburner J. A fast diffeomorphic image registration algorithm. *Neuroimage* 2007; **38(1)**:95-113.

21. Tatu L, Moulin T, Bogousslavsky J, Duvernoy H. Arterial territories of the human brain: cerebral hemispheres. *Neurology* 1998; **50(6)**:1699-1708.
22. Nowinski WL, Chua BC, Marchenko Y, Puspitsari F, Volkau I, Knopp MV. Three-dimensional reference and stereotactic atlas of human cerebrovasculature from 7Tesla. *Neuroimage* 2011; **55(3)**:986-998.
23. Szabo K, Forster A, Jager T, Kern R, Griebel M, Hennerici MG, *et al.* Hippocampal lesion patterns in acute posterior cerebral artery stroke: clinical and MRI findings. *Stroke* 2009; **40(6)**:2042-2045.
24. Cavanna AE, Trimble MR. The precuneus: a review of its functional anatomy and behavioural correlates. *Brain* 2006; **129(Pt 3)**:564-583.
25. Hendrikse J, Petersen ET, van Laar PJ, Golay X. Cerebral border zones between distal end branches of intracranial arteries: MR imaging. *Radiology* 2008; **246(2)**:572-580.
26. Chen JJ, Rosas HD, Salat DH. Age-associated reductions in cerebral blood flow are independent from regional atrophy. *Neuroimage* 2011; **55(2)**:468-478.
27. Liu Y, Zhu X, Feinberg D, Guenther M, Gregori J, Weiner MW, *et al.* Arterial spin labeling MRI study of age and gender effects on brain perfusion hemodynamics. *Magn Reson Med* 2012; **68(3)**:912-922.
28. Parkes LM, Rashid W, Chard DT, Tofts PS. Normal cerebral perfusion measurements using arterial spin labeling: reproducibility, stability, and age and gender effects. *Magn Reson Med* 2004; **51(4)**:736-743.
29. Shin W, Horowitz S, Ragin A, Chen Y, Walker M, Carroll TJ. Quantitative cerebral perfusion using dynamic susceptibility contrast MRI: evaluation of reproducibility and age- and gender-dependence with fully automatic image postprocessing algorithm. *Magn Reson Med* 2007; **58(6)**:1232-1241.
30. de Leeuw FE, de Groot JC, Bots ML, Witteman JC, Oudkerk M, Hofman A, *et al.* Carotid atherosclerosis and cerebral white matter lesions in a population based magnetic resonance imaging study. *J Neurol* 2000; **247(4)**:291-296.
31. Brown WR, Thore CR. Review: cerebral microvascular pathology in ageing and neurodegeneration. *Neuropathol Appl Neurobiol* 2011; **37(1)**:56-74.
32. Chen Y, Wang DJ, Detre JA. Comparison of arterial transit times estimated using arterial spin labeling. *MAGMA* 2012; **25(2)**:135-144.

8

Cerebral perfusion and white matter hyperintensities

JW van Dalen
HJMM Mutsaerts
AJ Nederveen
H Vrenken
M Steenwijk
MWA Caan
CBLM Majoie
WA van Gool
E Richard

In submission

Abstract

Objective To assess whether white matter hyperintensities (WMH) of presumed vascular origin in elderly with hypertension are associated with reduced perfusion, not only in the WMH, but also in the surrounding normal appearing white matter (NAWM) and grey matter (GM).

Methods We studied 185 participants of the Prevention of Dementia by Intensive Vascular care (preDIVA) trial, with systolic hypertension, aged between 72 and 80 years old. WMH volume and cerebral blood flow (CBF) were derived from 3D FLAIR and Arterial Spin Labelling (ASL) MRI respectively. We compared WMH CBF, NAWM CBF and GM CBF across quartiles of WMH volume. In addition, we assessed the continuous relation between these CBF estimates and WMH volume using linear regression analyses.

Results From the lowest two quartiles of WMH volume upward, with each quartile increase in WMH volume the mean WMH CBF markedly declined. There was a negative association between increasing WMH volume and WMH CBF (beta: -0.248 , $p=0.001$). There was no difference in NAWM or GM CBF across quartiles of WMH volume nor was there a relation between WMH volume and NAWM CBF (beta: -0.065 , $p=0.643$) or GM CBF (beta: -0.035 , $p=0.382$). Results remained largely unchanged after adjusting for confounders.

Interpretation WMH in community-dwelling elderly with hypertension is associated with lower perfusion in the WMH not present in the surrounding NAWM and GM. This suggests that WMH in old age hypertension relate to local microvascular alterations rather than a more general perfusion deficit. These findings help elucidate the pathophysiology of WMH in elderly and may help developing prevention and treatment strategies.

Introduction

White matter hyperintensities of presumed vascular origin (WMH) are a common finding on brain magnetic resonance imaging (MRI) in older individuals. Estimations of WMH prevalence range from 11% to over 90% of adults, depending on age and WMH severity¹. Clinically, WMH are associated with cognitive decline, neuropsychiatric symptoms, loss of functional independence and increased mortality^{2,3}. Old age and hypertension are the strongest risk factors for WMH, especially for the confluent subtype^{1,4}.

The pathophysiology of WMH has not yet been fully elucidated. They often appear together with other signs of cerebral small vessel disease (SVD), an umbrella term for radiological anomalies often found on neuroimaging of asymptomatic elderly^{4,5}. Histologically, confluent WMH appear as a continuum of increasing tissue damage resembling chronic low-grade ischemia^{1,5}. Thus, WMH may result from chronic low-grade white matter (WM) hypoperfusion^{1,5,6}. In agreement with this hypothesis, cerebral blood flow (CBF) within WMH is lower compared to normal appearing WM (NAWM)⁷⁻¹⁴.

Whether the lower perfusion within WMH is related to a more general perfusion deficit which also involves the surrounding NAWM and GM is unclear. Some findings suggest that WMH may be related to lower whole brain or grey matter (GM) perfusion^{7,11,15}, and WMH have been associated with reduced blood flow velocity in the large intra-cranial arteries, outside of the WM¹⁶⁻¹⁸. On a broader level, the association between WMH and chronic cardiac disease, also hints at a relation with general perfusion deficits¹⁹. WMH primarily originate in areas which are physiologically poorly perfused, explaining how a slight, general perfusion deficit could provoke chronic low-grade ischemia in specifically those regions associated with WMH^{20,21}. While these findings seem to suggest that WMH are related to a perfusion deficit extending beyond the WMH, current evidence remains circumstantial.

In this study, we address the hypothesis that WMH are not only associated with reduced perfusion within the WMH, but also with more widespread perfusion deficits in the surrounding NAWM and the GM. We tested this hypothesis using non-invasive arterial spin labelling MRI in a large cohort of community dwelling elderly with hypertension.

Methods

Participants were derived from the Prevention of Dementia by Intensive Vascular care trial (preDIVA). This is an ongoing randomised controlled trial in non-demented community-dwelling older people to study the efficacy of a nurse-led intervention aimed at vascular risk factor modification to prevent dementia²². In the preDIVA-MRI (Prediva-M) sub-study, 195 participants with systolic hypertension (>140 mmHg) and without dementia, underwent brain MRI. Clinical data from preDIVA assessment prior to MRI included medical history and vascular risk factors (systolic and diastolic blood pressure, smoking status (current, former, never), diabetes mellitus (DM) and body mass index (BMI)). The preDIVA-M sub-study was approved by the Academic Medical Centre medical ethical review board. All subjects provided written informed consent prior to MRI.

MRI acquisition

All imaging was performed on a 3T Intera with a SENSE-8-channel head coil and body coil transmission (Philips Healthcare, Best, the Netherlands). Foam padding was used to restrict head motion. An isotropic 1 mm³ 3D T1-weighted and an isotropic 1 mm³ 3D FLAIR scan were collected using a routine clinical protocol. Two ASL scans were obtained: one with flow-crushing diffusion gradients in three directions (CBF crushed, b-value = 0.6 s/mm², velocity encoding 50 mm/s) and one without (CBF non-crushed, b-value = 0 s/mm²). Identical imaging parameters of the two consecutive gradient echo single shot echo planar imaging pseudocontinuous ASL (pCASL) sequences were: matrix: 64x64, FOV: 240x240 mm, 17 axial slices, no gap, echo time/repetition time: 17/4000 ms, flip angle: 90 degrees, SENSE: 2.5, post-label delay: 1525-2120 ms, labelling duration: 1650 ms. For each scan, 20 dynamics were acquired, resulting in a total scan duration of 2x180=360 seconds. Background suppression was implemented with two inversion pulses respectively 1680 and 2830 ms after a pre-labelling saturation pulse. The labelling plane was positioned parallel to the imaging volume, 9 cm inferior to the centre of the imaging volume²³.

Image processing

An overview of image processing is provided in Figure 1. WMH segmentation was performed using a k nearest neighbor algorithm with tissue type priors²⁴. In total, 194 scans were automatically segmented.

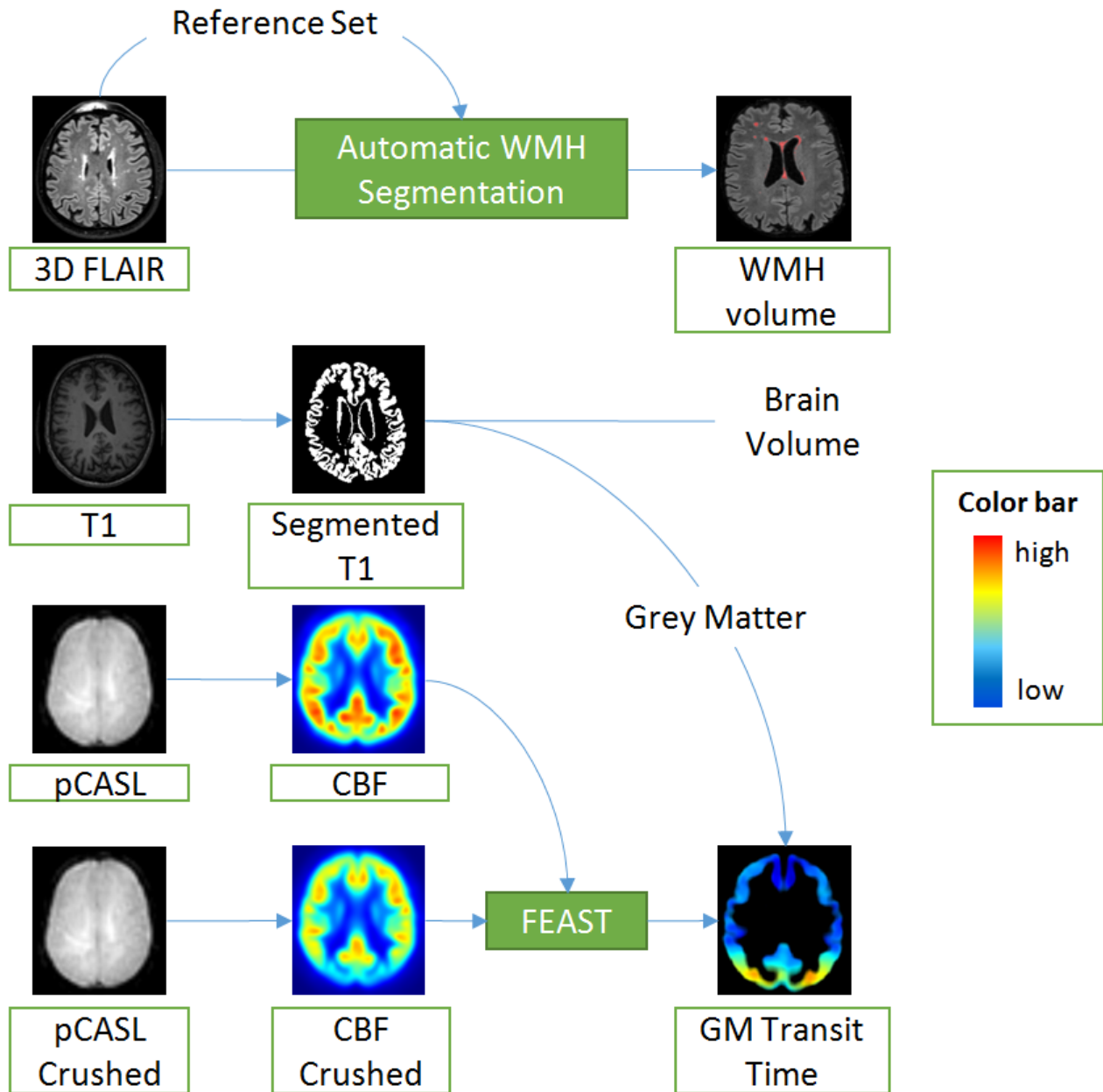


Figure 1. Scan processing. WMH: white matter hyperintensity, pCASL: pseudo-continuous arterial spin labeling, Reference Set: set of 20 scans with manually segmented WMH, FEAST = Flow Encoded Arterial Spin Tagging transit time calculation equation, GM = grey matter, CBF = cerebral blood flow

MRI data was processed using the SPM 8 toolbox (Wellcome Trust Center for Neuroimaging, University College London, UK) and custom scripts in Matlab 7.12.0 (MathWorks, MA, USA). T1-weighted images were segmented into GM and WM probability maps. After motion correction, 2x20 pairs of pCASL labelled and control images were pair-wise subtracted and subsequently averaged to generate perfusion-weighted maps. These perfusion weighted maps were converted to mL/100g/min using a single compartment model^{25,26}, described in more detail in the supplement. No distinction was made between

the quantification of GM and WM voxels. After quantification, the CBF crushed maps were registered to the CBF non-crushed maps. For the main analyses, CBF was derived from the crushed CBF maps.

Outcome measures

WMH volume was calculated from the automatic segmentation maps and logarithmically transformed to approach a normal distribution. CBF estimates were calculated for the segmented GM, the WM, the WMH and the normal appearing white matter (NAWM), which was operationalized as the WM outside of the WMH. To assess atrophy as a potential confounder, the brain parenchymal fraction (BPF) was calculated as the ratio (GM+WM volume)/(intra cranial volume). As another potential confounder, transit time (TT), representing the mean transit time from the cervical arteries, at the plane where the blood was labelled, to the GM tissue arterioles (Figure 4), was calculated from crushed and CBF non-crushed values per subject using the Flow Encoding Arterial Spin Tagging (FEAST)-equation ²⁵. Computations were performed using Matlab 7.12.0 (MathWorks, MA, USA), SPM8 (Wellcome Trust Center for Neuroimaging, University College London, UK), the FMRIB Software Library v5.0 ²⁷ and IBM SPSS statistics version 20 and 21 (Armonk, NY: IBM Corp).

Statistical Analysis

Two- tailed paired samples t-tests were used to compare GM CBF to WM CBF, and NAWM CBF to WMH CBF. Differences in mean CBF between quartiles of WMH volume were compared using one-way analyses of variance followed by Turkey post hoc testing.

The relation between WMH volume and CBF in the WMH, NAWM, and GM was assessed in separate linear regression analyses. In model 1, these analyses were adjusted for total brain volume. In model 2, analyses were additionally adjusted for potential confounders. Age, gender, BPF, TT, smoking status (current, former, never), a history of stroke (including TIA), a history of other cardiovascular disease (peripheral arterial disease, angina pectoris, myocardial infarction), diabetes mellitus (DM), antihypertensive drug use, systolic blood pressure, and diastolic blood pressure were considered as potential confounders, as they could potentially affect both CBF and WMH volumes ^{1,4,5,28,29}. Separate linear regression analyses were performed for each of these variables. Any variable associated with WMH volume adjusted for total brain volume with a p-value ≤ 0.1 was included as potential confounder in model 2.

Finally, two sensitivity analyses were performed. Firstly, since it is plausible that WMH, NAWM and GM CBF estimates only decrease from a certain minimum threshold of WMH volume ³⁰, the

abovementioned analyses were repeated with exclusion of the participants in the lowest quartile of WMH volume. Secondly, to assess the influence of excluding participants with CBF values differing ≥ 3 standard deviations from the mean, we repeated the analyses without excluding these participants. For the sensitivity analyses, the outcomes of the adjusted model (model 2) are shown in the results section.

Results

Participant characteristics are listed in Table 1. Data of 10 participants were discarded due to processing errors in CBF (9) or WMH (1) assessment. Another 4 participants were excluded from the main analyses due to CBF estimates differing >3 standard deviations from the mean. Excluded participants did not significantly differ from the included participants regarding demographics and structural MRI parameters (Table 2). The median WMH volume was 6.5 mL (IQR 3.6–11.2, range: 0.2–52.1 mL.) The mean population CBF in the GM, WM, NAWM and WMH is depicted in Figure 2. The mean GM CBF was significantly higher than the WM CBF (43.8 vs. 21.9 mL/100g/min, $p < 0.001$), and the mean NAWM CBF was significantly higher than the mean WMH CBF (22.5 vs. 10.6 mL/100g/min, $p < 0.001$).

Characteristic (n=185)	
Age	77 (3)
Female, n (%)	100 (55)
MMSE	29 (28-30)*
BMI	25.6 (24-28)*
Diabetes Mellitus, n (%)	19 (10)
Smoking status	
- never, n (%)	84 (45)
- former, n (%)	87 (47)
- current, n (%)	14 (8)
RR systolic	148 (139-166)*
RR diastolic	80 (74-89)*
Brain parenchymal fraction	.60 (.048)
WMH volume cm ³	6.5 (3.6-11.2)*

Table 1. General characteristics. Reported are means and standard deviations unless marked otherwise, n (%): number and percentage, *: median and IQR, MMSE = mini mental state examination, BMI = body mass index, RR = blood pressure, brain parenchymal fraction = (total cerebral volume) / total intra cranial volume, WMH = white matter hyperintensity

	Included (n=181)	Not Included (n=14)
Age	77 (2)	76 (3)
Female, n (%)	96 (53)	8 (57)
MMSE, m (IQR)	29 (28-30)	29 (29-30)
BMI, m (IQR)	26.3 (24.0-27.9)	25.9 (23.2-28.6)
History of stroke or TIA, n%	19 (11)	2 (15)
History of CVD, n%	41 (23)	3 (23)
Diabetes Mellitus, n (%)	20 (11)	0 (0)
Smoking status		
- never, n (%)	82 (45)	8 (57)
- former, n (%)	88 (49)	5 (36)
- current, n (%)	11 (6)	1 (7)
Antihypertensive drug use, n %	108 (60)	7 (50)
RR systolic, m (IQR)	148 (138-165)	144 (122-171)
RR diastolic, m (IQR)	81 (74-90)	82 (76-86)
Brain parenchymal fraction	.61 (.02)	.61 (.02)
WMH volume cm ³ , m (IQR)	6.5 (3.6-11.2)	6,9 (2.5-12.8)

Table 2. Differences in general characteristics between included and not included participants. Means and standard deviations unless noted otherwise, n (%) = number (percentage of total), m (IQR) = median (inter quartile range), MMSE = mini mental state examination, BMI = body mass index, CVD = cardiovascular disease (peripheral arterial disease, angina pectoris, myocardial infarction), RR = blood pressure, WMH = white matter hyperintensity. Values did not differ significantly between groups.

	Quartiles of white matter hyperintensity volume			
	Low (≤ 3.58 mL)	Mild (3.59-6.50 mL)	Moderate (6.51-11.56 mL)	High (11.57 < mL)
CBF in WMH	17.9 (6.0)	17.6 (6.3)	15.9 (5.8)	15.0 (5.5)
CBF in NAWM	32.0 (6.8)	32.1 (7.7)	31.0 (8.2)	32.1 (8.9)
CBF in GM	50.6 (11.3)	53.5 (9.8)	51.2 (12.4)	50.3 (10.6)

Table 3. Cerebral blood flow in subgroups based on quartiles of WMH volume. CBF = cerebral blood flow, GM = grey matter, NAWM = normal appearing white matter, WMH = white matter hyperintensity.

Predictor	Model 1			Model 2		
	St. beta	<i>p</i>	R ²	St. beta	<i>p</i>	R ²
CBF in WMH	-.248	.001	0.06	-.201	.029	0.06
CBF in NAWM	-.035	.643	0.00	.175	.098	0.05
CBF in GM	-.065	.382	0.00	.175	.133	0.05

Table 4. Association between white matter hyperintensity volume and cerebral perfusion. St. beta: standardized beta, R²: adjusted R² representing the proportion of variation in white matter hyperintensity volume explained by all variables in the model correcting for the number of variables, all analyses were adjusted for total brain volume, model 2: additionally corrected for age, antihypertensive drug use, brain parenchymal fraction and transit time. CBF = cerebral blood flow in mL/100g/min, WMH = white matter hyperintensities, NAWM = normal appearing white matter, GM = grey matter

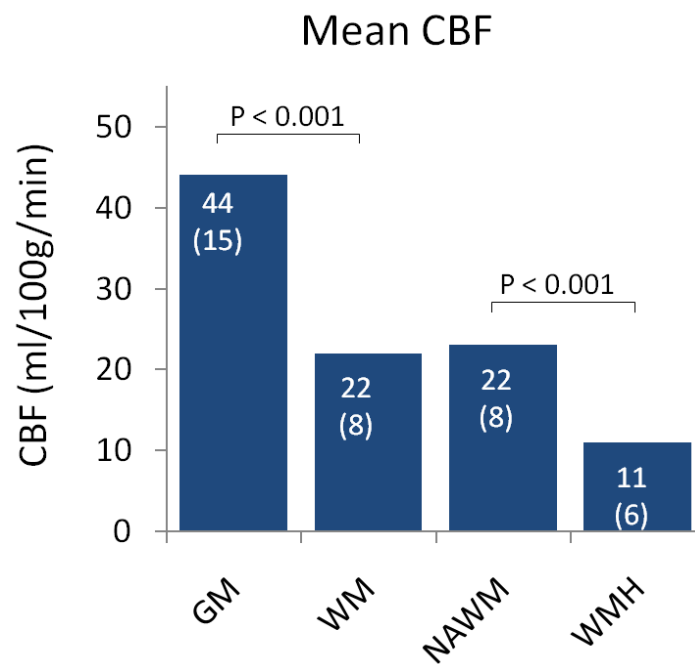


Figure 2. Cerebral blood flow (CBF) in the grey matter (GM), white matter (WM), normal appearing white matter unaffected by WMH (NAWM) and white matter hyperintensities (WMH). Denoted are means (SD) and p-values of paired sample T-tests.

Mean WMH, NAWM and GM CBF values per quartile of WMH volume are depicted in Figure 3 and Table 3. WMH load in the lowest quartile was ≤ 3.58 mL (low WMH), in the second quartile 3.59-6.40

mL (mild WMH), in the third quartile 6.41-11.18 mL (moderate WMH), and in the highest quartile ≥ 11.18 mL (high WMH). From the lower two quartiles upward, the mean WMH CBF per quartile declined with increasing WMH volume (Figure 3, Table 3). The mean NAWM and GM CBF did not show any clear relation with WMH volume (Figure 3, Table 3). One-way analysis of variance showed a significant difference between quartiles of WMH volume in WMH CBF ($F(3,177)$, $p=0.002$) but not in NAWM CBF ($F(3,177)$, $p=0.244$) or GM CBF ($F(3,177)$, $p=0.059$). Turkey post-hoc testing revealed that CBF in the quartile with the highest WMH load was significantly lower compared to the quartiles with the lowest (mean difference (MD): -4.2 mL/100g/min, $p=0.007$) and the second lowest (MD: -4.41 mL/100g/min, $p=0.007$) WMH load.

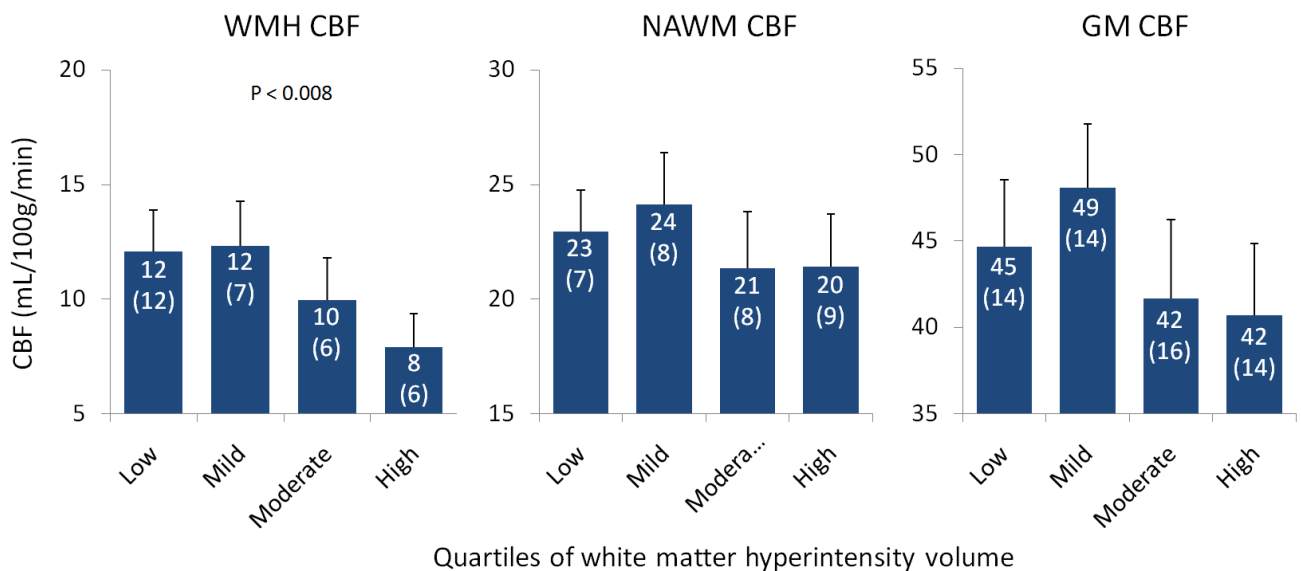


Figure 3. Cerebral blood flow per quartile of WMH load. Cerebral blood flow (CBF) in the grey matter (GM), normal appearing white matter unaffected by WMH (NAWM) and white matter hyperintensities (WMH) in subgroups based on quartiles of WMH volume. Denoted are means (SD) and significant p-values of one-way analysis of variance.

Results of the linear regression analyses are listed in Table 4. In model 1, adjusted for total brain volume, a higher WMH volume was associated with a lower CBF in the WMH (beta -0.248 , $p=0.001$). No association was found between WMH volume and CBF in the NAWM (beta -0.035 , $p=0.643$) or the GM (beta: -0.07 , $p=0.382$).

Age (beta .130, $p=0.09$), BPF (beta: -.13, $p<0.10$), GM TT (beta: .15, $p=.05$) and antihypertensive use (beta .138, $p=0.07$) were univariately associated with WMH volume and were included as covariates in model 2. There was no relation between WMH and female gender (beta: .07, $p=.474$) systolic blood pressure (beta: -.04, $p=0.63$), diastolic blood pressure (beta: .01, $p=0.88$), smoking status (current vs. never: beta: -0.06, $p=0.45$, former vs. never: beta: -.08, $p=0.29$), history of stroke (beta: 0.10, $p=0.23$), history of other cardiovascular disease (beta: -.06, $p=0.41$), diabetes mellitus (beta: .01, $p=0.89$) or body mass index (beta: -.10, $p=0.19$).

In model 2, adjusted for total brain volume, age, antihypertensive drug use, BPF and TT, WMH volume remained significantly inversely associated with WMH CBF (beta: -.201, $p=0.029$). The relation between WMH volume and GM or NAWM CBF was not significant (Table 4). There were no interactions between the individual covariates and the CBF estimates in their relation with WMH volume. Sensitivity analyses excluding participants in the lowest quartile of WMH volume ($n=132$) gave similar results for the relation between WMH volume and WMH CBF (beta: -.253, $p=0.02$), NAWM CBF (beta: .05, $p=0.69$) and GM CBF (beta: -.02, $p=0.74$). Sensitivity analyses including participants with mean CBF values deviating >3 standard deviations from the mean somewhat inflated the results for the relation between WMH volume and WMH CBF (beta: -.34, $p=0.00$), and gave similar results for the NAWM CBF (beta: .18, $p=0.09$) and GM CBF (beta: .18, $p=0.11$).

Discussion

In a cohort of community dwelling elderly with hypertension, we found that CBF within WMH is lower than CBF in NAWM and that WMH CBF decreases with increasing WMH volume. Contrary to our hypothesis, we did not find any indications that CBF in the surrounding NAWM or GM is also lower in patients with WMH. These results suggest that WMH in elderly with hypertension are not caused by a general cerebral perfusion problem. As a serendipitous finding, higher GM TT was associated with higher WMH volume.

A declining CBF within WMH with increasing WMH volume has been reported previously¹³. Partial volume effects may also play a role. Since ASL voxels are relatively large, each voxel will contain both WMH and NAWM. As WMH get larger, less NAWM is erroneously included. This way, the WMH CBF estimate in patients with WMH large enough to encompass entire ASL voxels approximate the WMH CBF more accurately, resulting in a lower CBF estimate with increasing WMH volume. The absence of a relation between WMH volume and NAWM or GM CBF is somewhat surprising since results of other

studies have hinted at such a relation^{7,11,15}. Conceivably, GM and NAWM CBF only diminish with increasing WMH volume from a certain threshold of WMH volume³⁰. However, sensitivity analyses evaluating this possibility did not alter our findings. Differences between study populations may play a role. Studies linking WMH to lower overall cerebral or GM perfusion were performed in mixed populations, including patients with mild cognitive impairment (MCI) and Alzheimer's disease (AD)^{7,11,15}. MCI and AD are associated with alterations in CBF³¹. WMH formation in these conditions may be incited by decreased perfusion in WM susceptible to developing WMH¹⁴. Recent reports that a negative correlation between GM CBF and WMH does exist in patients with AD but not in memory clinic patients without MCI or dementia support this explanation¹⁵.

Our results suggest that hypoperfusion in WMH in elderly with hypertension is predominantly related to local hypoperfusion rather than to a global perfusion deficit. Hypoperfusion within WMH may be a direct consequence of local extensive tissue damage and obliteration of capillaries³². The capillary obliteration in WMH may contribute to a maintained perfusion in the NAWM, explaining why NAWM perfusion is left unaltered. However, the location of WMH primarily in regions where perfusion is physiologically low does suggest that hypoperfusion plays a role in WMH conception^{20,21}. The microvascular alterations associated with aging and hypertension, which include narrowing of the lumen and stiffening of the arteriolar vessel walls, may cause increased arteriolar resistance, reducing perfusion pressure^{5,6}. This could incite low grade hypoperfusion distally in the WM, where perfusion pressure is the lowest, evoking the chronic hypoxic tissue damage and capillary obliteration associated with WMH (Figure 4)^{5,6,33}. In patients with diseases that are associated with cerebral perfusion deficits, for example heart failure or Alzheimer's disease, WMH could originate via the same mechanism of reduced perfusion pressure. Microvascular alterations associated with hypertension could still exacerbate WMH formation in these patients. Correspondingly, hypertension has been associated with WMH in both heart failure and Alzheimer's disease^{14,19,34}.

Serendipitously, we found that higher GM TT is associated with higher WMH volume. Thus GM perfusion does appear to be altered in patients with WMH. Interpretation of this finding is not straightforward. TT depends on the length of the blood flow trajectory from the cervical arteries to the cerebral capillaries and on the blood flow velocity along this trajectory²⁹. WMH have been associated with reduced blood flow velocity in the large intra-cranial arteries, of which longer TT could be a proxy¹⁶⁻¹⁸. This velocity reduction could be caused by increased resistance in the large intracranial arteries due to atherosclerosis, or in the arterioles due to arteriolosclerosis, which are both associated with WMH and other SVD^{6,31,35}. The association between antihypertensive medication use and a higher WMH volume

may be due to antihypertensive use being associated with more chronic and severe hypertension. Alternatively, the use of antihypertensive drugs may lead to hypoperfusion, aggravating WMH, although recent study findings make that possibility unlikely^{36,37}.

This study has some limitations. We cannot exclude that WMH are associated with slight perfusion deficits in the NAWM and GM. The physiological variability of CBF may be too great to reveal such small perfusion differences between subjects. TT may be less subject to this variability and higher TT could reflect slight reductions in GM perfusion. If so, these slight reductions could contribute to WMH development. As another limitation, it is unsure whether the signal to noise ratio of WM perfusion using ASL is sufficient to accurately estimate WM CBF within our short scanning time^{38,39}. However, although current ASL techniques may be unable to measure WM CBF with high accuracy on a voxel-level, on a region of interest level it has been shown that WM CBF can be measured within a scanning time of 5 minutes⁴⁰⁻⁴². Our measurements were precise enough to measure significant differences in CBF between the NAWM and WMH, and between the whole WM and the NAWM only. Moreover, the reliability of our findings is supported by the ratios between the GM, WM, NAWM and WMH CBF found in our study, which are similar to those reported in studies in which exogenous contrast agents were used^{9,13,14}.

To our knowledge, this study is the first to assess the relationship between GM and WM CBF and WMH volume in a large sample of community dwelling elderly with hypertension. Our results suggest that WMH formation in these patients is associated with hypoperfusion locally in the WMH, making it unlikely that WMH in this population are the result of a general perfusion deficit. Our results may contribute to the understanding of the pathophysiology of WMH in elderly without general perfusion deficits and help to develop prevention and treatment strategies for WMH and their clinical correlates.

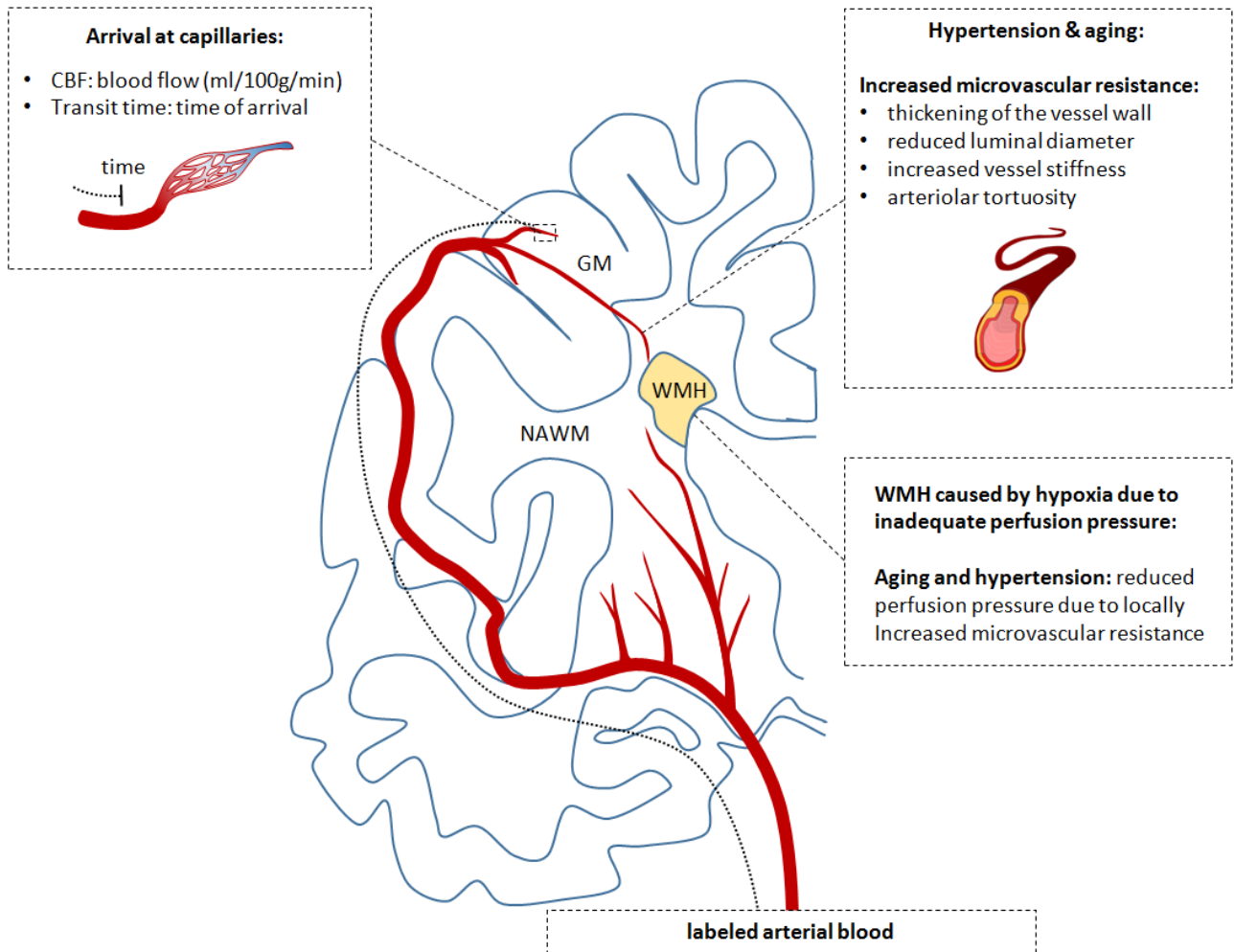


Figure 4. Perfusion parameters and CBF regions. CBF = cerebral blood flow, GM = grey matter, NAWM = normal appearing white matter, WMH = white matter hyperintensity, CBF was measured in the GM, NAWM and WMH, transit time was calculated in the GM only.

Reference list

- 1 Schmidt R, Schmidt H, Haybaeck J, Loitfelder M, Weis S, Cavalieri M *et al.* Heterogeneity in age-related white matter changes. *Acta Neuropathol* 2011; **122**: 171–185.
- 2 Debette S, Markus HS. The clinical importance of white matter hyperintensities on brain magnetic resonance imaging: systematic review and meta-analysis. *BMJ*. 2010; **341**: c3666–c3666.
- 3 Schmahmann JD, Smith EE, Eichler FS, Filley CM. Cerebral white matter: neuroanatomy, clinical neurology, and neurobehavioral correlates. *Ann N Y Acad Sci* 2008; **1142**: 266–309.
- 4 Moran C, Phan TG, Srikanth VK. Cerebral small vessel disease: a review of clinical, radiological, and histopathological phenotypes. *Int J Stroke* 2012; **7**: 36–46.
- 5 Pantoni L. Cerebral small vessel disease: from pathogenesis and clinical characteristics to therapeutic challenges. *Lancet Neurol* 2010; **9**: 689–701.

- 6 Brown WR, Thore CR. Review: cerebral microvascular pathology in ageing and neurodegeneration. *Neuropathol Appl Neurobiol* 2011; **37**: 56–74.
- 7 Bastos-Leite AJ, Kuijter JP, Rombouts SA, Sanz-Arigita E, van Straaten EC, Gouw AA *et al.* Cerebral blood flow by using pulsed arterial spin-labeling in elderly subjects with white matter hyperintensities. *AJNR Am J Neuroradiol* 2008; **29**: 1296–1301.
- 8 Markus HS, Lythgoe DJ, Ostegaard L, O'Sullivan M, Williams SC. Reduced cerebral blood flow in white matter in ischaemic leukoaraiosis demonstrated using quantitative exogenous contrast based perfusion MRI. *J Neurol Neurosurg Psychiatry* 2000; **69**: 48–53.
- 9 O'Sullivan M, Lythgoe DJ, Pereira AC, Summers PE, Jarosz JM, Williams SC *et al.* Patterns of cerebral blood flow reduction in patients with ischemic leukoaraiosis. *Neurology* 2002; **59**: 321–326.
- 10 Brickman AM, Zahra A, Muraskin J, Steffener J, Holland CM, Habeck C *et al.* Reduction in cerebral blood flow in areas appearing as white matter hyperintensities on magnetic resonance imaging. *Psychiatry Res* 2009; **172**: 117–120.
- 11 Zhang Q, Stafford RB, Wang Z, Arnold SE, Wolk DA, Detre JA. Microvascular perfusion based on arterial spin labeled perfusion MRI as a measure of vascular risk in Alzheimer's disease. *J Alzheimers Dis* 2012; **32**: 677–687.
- 12 Marstrand JR, Garde E, Rostrup E, Ring P, Rosenbaum S, Mortensen EL *et al.* Cerebral Perfusion and Cerebrovascular Reactivity Are Reduced in White Matter Hyperintensities. *Stroke* 2002; **33**: 972–976.
- 13 Sachdev P, Wem W, Shnier R, Brodaty H. Cerebral Blood Volume in T2-Weighted White Matter Hyperintensities Using Exogenous Contrast Based Perfusion MRI. *J Neuropsychiatr* 2004; **16**: 83–92.
- 14 Makedonov I, Black SE, Macintosh BJ. Cerebral small vessel disease in aging and Alzheimer's disease: a comparative study using MRI and SPECT. *Eur J Neurol* 2013; **20**: 243–250.
- 15 Benedictus MR, Binnewijzend MA, Kuijter JP, Steenwijk MD, Versteeg A, Vrenken H *et al.* Brain volume and white matter hyperintensities as determinants of cerebral blood flow in Alzheimer's disease. *Neurobiol Aging* 2014; **35**: 2665–2670.
- 16 Tzourio C, Lévy C, Dufouil C, Touboul PJ, Ducimetiere P, Alperovitch A. Low cerebral blood flow velocity and risk of white matter hyperintensities. *Ann Neurol* 2001; **49**: 411–414.
- 17 Novak V, Last D, Alsop DC, Abduljalil AM, Hu K, Lepicovsky L *et al.* Cerebral blood flow velocity and periventricular white matter hyperintensities in type 2 diabetes. *Diabetes Care* 2006; **29**: 1529–1534.
- 18 Heliopoulos I, Artemis D, Vadikolias K, Tripsianis G, Piperidou C, Tsivgoulis G. Association of Ultrasonographic Parameters with Subclinical White-Matter Hyperintensities in Hypertensive Patients. *Cardiovasc Psychiatry Neurol*. 2012; **2012**: 1–8.
- 19 Alosco ML, Brickman AM, Spitznagel MB, Griffith EY, Narkhede A, Raz N *et al.* Independent and interactive effects of blood pressure and cardiac function on brain volume and white matter hyperintensities in heart failure. *J Am Soc Hypertens* 2013; **7**: 336–343.
- 20 Holland CM, Smith EE, Csapo I, Gurol ME, Brylka DA, Killiany RJ *et al.* Spatial distribution of white-matter hyperintensities in Alzheimer disease, cerebral amyloid angiopathy, and healthy aging. *Stroke* 2008; **39**: 1127–1133.
- 21 Ten Dam VH, van den Heuvel DM, de Craen AJ, Bollen EL, Murray HM, Westendorp R *Get al.* Decline in total cerebral blood flow is linked with increase in periventricular but not deep white matter hyperintensities. *Radiology* 2007; **243**: 198–203.
- 22 Richard E, Van den Heuvel E, Moll van Charante EP, Achthoven L, Vermeulen M, Bindels PJ *et al.* Prevention of dementia by intensive vascular care (PreDIVA): a cluster-randomized trial in progress. *Alzheimer Dis Assoc Disord* 2009; **23**: 198–204.
- 23 Alsop DC, Dai W, Grossman M, Detre JA. Arterial spin labeling blood flow MRI: its role in the early characterization of Alzheimer's disease. *J Alzheimers Dis* 2010; **20**: 871–880.

- 24 Steenwijk MD, Pouwels PJ, Daams M, van Dalen JW, Caan MW a, Richard E *et al.* Accurate white matter lesion segmentation by k nearest neighbor classification with tissue type priors (kNN-TTPs). *NeuroImage Clin* 2013; **3**: 462–469.
- 25 Wang J, Alsop DC, Song HK, Maldjian JA, Tang K, Salvucci AE *et al.* Arterial transit time imaging with flow encoding arterial spin tagging (FEAST). *Magn Reson Med* 2003; **50**: 599–607.
- 26 Buxton RB, Frank LR, Wong EC, Siewert B, Warach S, Edelman RR. A general kinetic model for quantitative perfusion imaging with arterial spin labeling. *Magn Reson Med* 1998; **40**: 383–396.
- 27 Jenkinson M, Beckmann CF, Behrens TE, Woolrich MW, Smith SM. FSL. *Neuroimage*. 2012; **62**: 782–790.
- 28 Gouw AA, Seewann A, van der Flier WM, Barkhof F, Rozemuller AM, Scheltens P *et al.* Heterogeneity of small vessel disease: a systematic review of MRI and histopathology correlations. *J Neurol Neurosurg Psychiatry* 2011; **82**: 126–135.
- 29 Yang Y, Engelien W, Xu S, Gu H, Silbersweig DA, Stern E. Transit time, trailing time, and cerebral blood flow during brain activation: Measurement using multislice, pulsed spin-labeling perfusion imaging. *Magn Reson Med* 2000; **44**: 680–685.
- 30 Wen W, Sachdev P, Shnier R, Brodaty H. Effect of white matter hyperintensities on cortical cerebral blood volume using perfusion MRI. *Neuroimage* 2004; **21**: 1350–1356.
- 31 De la Torre JC. Cerebral hemodynamics and vascular risk factors: setting the stage for Alzheimer’s disease. *J Alzheimers Dis* 2012; **32**: 553–567.
- 32 Teodorczuk a, Firbank MJ, Pantoni L, Poggesi A, Erkinjuntti T, Wallin A *et al.* Relationship between baseline white-matter changes and development of late-life depressive symptoms: 3-year results from the LADIS study. *Psychol Med* 2010; **40**: 603–610.
- 33 Qureshi AI, Caplan LR. Intracranial atherosclerosis. *Lancet* 2014; **383**: 984–998
- 34 Benedictus MR, Goos JD, Binnewijzend MA, Muller M, Barkhof F, Scheltens P *et al.* Specific risk factors for microbleeds and white matter hyperintensities in Alzheimer’s disease. *Neurobiol Aging* 2013; **34**: 2488–2494.
- 35 MacIntosh BJ, Marquardt L, Schulz UG, Jezzard P, Rothwell PM. Hemodynamic Alterations in Vertebrobasilar Large Artery Disease Assessed by Arterial Spin-Labeling MR Imaging. *ANJR Am J Neuroradiol* 2012; **33**: 1939–1944.
- 36 Tryambake D, He J, Firbank MJ, O’Brien JT, Blamire AM, Ford GA. Intensive blood pressure lowering increases cerebral blood flow in older subjects with hypertension. *Hypertension* 2013; **61**: 1309–1315.
- 37 Muller M, van der Graaf Y, Visseren FL, Vlek AL, Mali WP, Geerlings MI. Blood pressure, cerebral blood flow, and brain volumes. The SMART-MR study. *J Hypertens* 2010; **28**: 1498–1505.
- 38 Van Gelderen P, de Zwart JA, Duyn JH. Pitfalls of MRI measurement of white matter perfusion based on arterial spin labeling. *Magn Reson Med* 2008; **59**: 788–795.
- 39 Petersen ET, Zimine I, Ho YC, Golay X. Non-invasive measurement of perfusion: a critical review of arterial spin labelling techniques. *Br J Radiol* 2006; **79**: 688–701.
- 40 Mutsaerts HJ, Richard E, Heijtel DF, van Osch MJ, Majoie CB, Nederveen AJ. Gray matter contamination in arterial spin labeling white matter perfusion measurements in patients with dementia. *NeuroImage Clin* 2013; **4**: 139–144.
- 41 Wu WC, Lin SC, Wang DJ, Chen KL, Li YD. Measurement of cerebral white matter perfusion using pseudocontinuous arterial spin labeling 3T magnetic resonance imaging--an experimental and theoretical investigation of feasibility. *PLoS One* 2013; **8**: e82679.
- 42 Van Osch MJP, Teeuwisse WM, Van Walderveen MA, Hendrikse J, Kies DA, Van Buchem MA. Can arterial spin labeling detect white matter perfusion signal? *Magn Reson Med* 2009; **62**: 165–173.

Supplement – Full description of ASL quantification

After 3D motion correction of the raw EPI control and label images using SPM8 (Statistical Parametric Mapping, Wellcome Trust Centre for Neuroimaging, London, UK), they were pair-wise subtracted and converted to CBF with a single compartment model, assuming that the label decays with the T1 of blood ^{1,2}:

$$CBF[mL/100g/min] = \frac{\Delta M e^{TE/T_{2a}^*}}{\rho M_{0a} 2\alpha\alpha_{inv} T_{1a} (e^{-\delta/T_{1a}} - e^{(-\omega-\tau)/T_{1a}})} \quad [1]$$

where ρ is the density of brain tissue (1.05 g/mL) ³, ΔM is the difference between control and label intensities, TE is the echo time (17 ms), T_{2a}^* is the transverse relaxation time of arterial blood (50 ms) ⁴, M_{0a} is the equilibrium magnetization of arterial blood, for which an average scanner value was calculated according to previously described methods ⁵, α is the labeling efficiency (0.85) ⁶, α_{inv} is the correction for label loss due to background suppression pulses (0.83) ⁷, T_{1a} is the T₁ relaxation time of arterial blood (1650 ms) ⁸, PLD = 1525 ms + 34.9 ms/slice, τ is the labeling duration (1650 ms) and δ is the PLD for CBF_{non-crushed} and the measured TT (averaged per subject for each ROI, as described in the ROI section below) for CBF_{crushed}.

TT was calculated based on the following two FEAST equations ⁹:

$$\Delta M = A (e^{-w/T_{1a}} - e^{(-w-\tau)/T_{1a}}) \quad [2]$$

$$\Delta M' = A (e^{-\delta/T_{1a}} - e^{(-w-\tau)/T_{1a}}) \quad [3]$$

where A is a constant and ΔM and $\Delta M'$ represent the scans acquired without and with vascular crushing, respectively.

Reference list

1. Alsop DC, Detre JA, Golay X, Gunther M, Hendrikse J, Hernandez-Garcia et al. Recommended implementation of arterial spin-labeled perfusion MRI for clinical applications: A consensus of the ISMRM perfusion study group and the European consortium for ASL in dementia. *Magn Reson Med*; e-pub ahead of print 8 April 2014; doi: 10.1002/mrm.25197.
2. Wang J, Alsop DC, Li L, Listerud J, Gonzalez-At JB, Schnall MD, et al. Comparison of quantitative perfusion imaging using arterial spin labeling at 1.5 and 4.0 Tesla. *Magn Reson Med* 2002; **48**:242-254.
3. Herscovitch P, Raichle ME. What is the correct value for the brain--blood partition coefficient for water? *J Cereb Blood Flow Metab* 1985; **5**:65-69.
4. St Lawrence KS, Wang J. Effects of the apparent transverse relaxation time on cerebral blood flow measurements obtained by arterial spin labeling. *Magn Reson Med* 2005; **53**:425-433.
5. Chalela JA, Alsop DC, Gonzalez-Atavales JB, Maldjian JA, Kasner SE, Detre JA. Magnetic resonance perfusion imaging in acute ischemic stroke using continuous arterial spin labeling. *Stroke* 2000; **31**:680-687.
6. Aslan S, Xu F, Wang PL, Uh J, Yezhuvath US, van Osch M et al. Estimation of labeling efficiency in pseudocontinuous arterial spin labeling. *Magn Reson Med* 2010; **63**:765-771.
7. Garcia DM, Duhamel G, Alsop DC. Efficiency of inversion pulses for background suppressed arterial spin labeling. *Magn Reson Med* 2005; **54**:366-372.
8. Zhang X, Petersen ET, Ghariq E, De Vis JB, Webb AG, Teeuwisse WM et al. In vivo blood T(1) measurements at 1.5 T, 3 T, and 7 T. *Magn Reson Med* 2012; **70**:1082-1086.
9. Wang J, Alsop DC, Song HK, Maldjian JA, Tang K, Salvucci AE et al. Arterial transit time imaging with flow encoding arterial spin tagging (FEAST). *Magn Reson Med* 2003; **50**:599-607.

9

Risk factor analysis of cerebral white matter hyperintensities in children with sickle cell disease

V van der Land
HJMM Mutsaerts
M Engelen
H Heijboer
M Roest
MJ Hollestelle
TW Kuijpers
PJ Nederkoorn
MH Cnossen
CBLM Majoie
AJ Nederveen
K Fijnvandraat

In submission

Abstract

Sickle cell disease (SCD) is complicated by silent cerebral infarcts, visible as white matter hyperintensities (WMHs) on magnetic resonance imaging (MRI). Both local vaso-occlusion, elicited by endothelial dysfunction and insufficiency of cerebral blood flow (CBF) are possibly involved in the etiology. We investigated the associations between markers of endothelial dysfunction, CBF and WMHs in 40 children with HbSS or HbS β^0 thalassemia with a mean age of 12.1 ± 2.6 years by quantifying WMH volume on 3.0 Tesla MRI. Boys demonstrated an increased risk for WMHs (odds ratio 4.5, 95% CI 1.2 - 17.4), unrelated to G6PD deficiency. In patients with WMHs, lower fetal hemoglobin (HbF) was associated with a larger WMH volume (regression coefficient -0.62, $R^2=0.25$, $p=0.04$). Lower ADAMTS13 levels were associated with lower CBF in the white matter (WM) (regression coefficient 0.07, R^2 0.15, $p=0.03$), suggesting that endothelial dysfunction could potentially hamper CBF. Our findings suggest that a high level of fetal hemoglobin may be protective for WMHs and that endothelial dysfunction may contribute to the development of WMHs by reducing CBF.

Introduction

Approximately 40% of children with a severe form of sickle cell disease (SCD) will be affected by silent cerebral infarction (SCIs) by the age of 14¹. SCIs are defined as an area of abnormal hyperintensity on magnetic resonance imaging (MRI) of the brain in a patient without a history or physical findings of a focal neurological deficit². Most SCIs are located in the white matter (WM) and visible as white matter hyperintensities (WMHs) on MRI. SCIs are associated with diminished neurocognitive functioning, potentially hampering social and academic achievement^{3,4}. Affected patients are at risk for progression of SCIs and overt stroke⁵. Studies on risk factors for SCIs are scarce and therapeutic options are still under investigation⁶.

Two possible disease mechanisms for the development of WMHs have been proposed. First, vaso-occlusion could occur in the blood vessels of the brain, leading to infarcts in the white matter. Vaso-occlusion occurs in the setting of endothelial and coagulation activation, increased expression of adhesion molecules and impaired vasodilatation due to a decreased bioavailability of nitric oxide⁷⁻⁹. These are well recognized phenomena even in young patients, leading to systemic vascular endothelial dysfunction. Intracerebral involvement is supported by the finding of diffuse thickening and sclerosis of intracerebral arterioles as described in one of the few autopsy studies in sickle cell disease¹⁰. Although in other disease conditions white matter or lacunar infarcts in the brain are associated with local small vessel pathology and are called 'cerebral small vessel disease', definite evidence for a vascular etiology of SCIs in sickle cell disease is lacking¹¹. Some evidence for the role of endothelial dysfunction in the etiology of WMHs was demonstrated in a small study which found lower concentrations of tissue plasminogen activator (t-PA) and ADAMTS13 in 9 SCD patients with SCIs compared to 38 patients without SCIs¹². The main risk factor for SCIs seems to be a low level of hemoglobin (Hb), as demonstrated in a multivariate analysis in a large (n=132), prospective study by Bernaudin *et al.*, as well as in the baseline results of the SITT (Silent Infarct Transfusion Trial) (n=814), and in a retrospective study (n=65) in very young children (mean age 3.7 ± 1.1 years)^{1,13,14}. These identified risk factors suggest that hematological factors such as the level of hemoglobin and perhaps endothelial and/or coagulation activation play a role in the etiology of SCIs.

A second, additional hypothesis for the development of SCIs is related to altered cerebral blood flow (CBF). Previous studies using an arterial spin labeling (ASL) technique on MRI have demonstrated an increased CBF in the gray matter (GM) of children with SCD compared to controls, probably as compensatory mechanism for the chronic anemia^{15,16}. Cerebral reactivity, i.e. vasodilatory capacity in

reaction to triggers such as hypercapnia, has been demonstrated to be significantly reduced in patients with SCD compared to controls¹⁷. This may lead to compromised CBF during episodes of increased metabolic demand such as fever or an acute drop in hemoglobin which could subsequently lead to cerebral ischemia. Indeed, acute SCIs have been identified by diffusion weighted imaging in children experiencing an acute decrease in hemoglobin¹⁸. The association between baseline CBF, i.e. during steady disease state, and the risk of SCIs is unclear. Patients with a high baseline CBF could be at risk for the development of SCIs due to insufficient reserve capacity of CBF. On the other hand, SCIs could potentially lead to a decrease in CBF in the white matter because blood flow to necrotic tissue is decreased and subsequently CBF would become lower in the white matter. Therefore, it is of particular interest to study CBF in GM and WM separately.

Probably both mechanisms – endothelial dysfunction leading to small vessel disease and insufficient CBF – are important factors in the etiology of SCIs in sickle cell disease. Additionally, besides being influenced directly by hemoglobin^{17,19} and hematocrit^{20,21} CBF could also be affected by endothelial and coagulation activation due to altered hemorheology and viscosity. The interaction between SCIs, endothelial dysfunction and CBF is described in the proposed hypothetical model in Figure 1. To help elucidate these interactions, our aim was to study the association between the presence and size of WMHs and parameters of endothelial and coagulation activation and CBF in GM and WM.

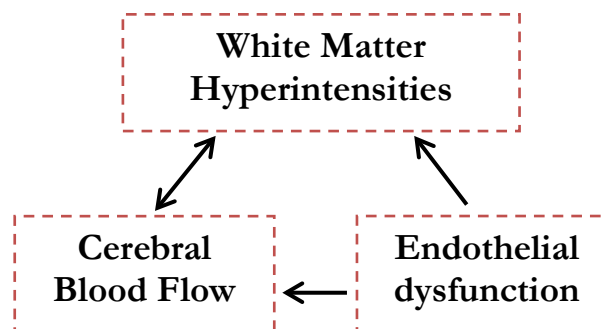


Figure 1. Proposed interaction between endothelial dysfunction, cerebral blood flow and white matter hyperintensities in sickle cell disease

SCI is a term used to describe the clinical picture of a patient without neurological deficits in which white matter hyperintensities are visible on MRI. This term is effectively used in clinical practice, but is more difficult to use in research on the etiology of these lesions. Using the term SCI in research would mean excluding patients with WMHs who happen to have subtle neurological deficits due to extensive

WMHs or WMHs in a critical location, even though the etiology of the WMHs is the same as in patients without neurological deficits. Additionally, since the exact etiology of the lesions is not completely understood, a descriptive term based on imaging findings such as WMHs seems reasonable to use. Therefore, we chose to use the term WMHs and did not exclude patients with neurological deficits due to WMHs.

Patients and Methods

Patients

We prospectively approached all eligible children in two Sickle cell comprehensive care centers (center 1: Emma Children's Hospital, Amsterdam and center 2: Sophia Children's Hospital, Rotterdam). Inclusion criteria were severe SCD, i.e. HbSS or HbS β^0 thalassaemia and age 8-16 years. Exclusion criteria were prior stroke, stenosis of intracranial arteries (as demonstrated by MRI/MRA prior to participation in this study), abnormal or intermediate velocity on transcranial Doppler imaging (according to Adams *et al.*²²), chronic blood transfusion therapy, bone marrow transplantation, contra-indications for MRI and concomitant major health problem. Because the present study was part of a larger study that included a neuropsychological evaluation, we excluded patients with an inability to undergo neurocognitive testing (e.g. insufficient knowledge of the Dutch language). Patients had to be in a steady disease state, i.e. the absence of infection or crisis for >4 weeks prior to study visit.

All patients underwent a neurological examination performed by a trained pediatric neurologist (ME) who was blinded for imaging results. Results were scored according to the Pediatric Stroke Outcome Measure (PSOM). The PSOM yields a score ranging from 0 (no deficits) to 10 (severe deficits on all 5 subscales) (Supplemental Table 1)²³. Focal neurological deficits were described separately. Genotype was tested using high performance liquid chromatography (HPLC) and confirmed by DNA analysis when necessary. Alpha-thalassaemia was tested by DNA analysis. The use of hydroxyurea was recorded. Results of the most recent TCD measurement during a regular hospital visit were collected. The Institutional Review Board of the Academic Medical Center in Amsterdam approved the study, written informed consent was obtained from all parents or legal guardians and from children aged twelve years and older.

<i>Subscales</i>	<i>Outcome</i>
Right sensimotor	0 = no deficit
Left sensimotor	0.5 = mild deficit, normal function
Language production	1 = moderate deficit, decreased function
Language comprehension	2 = severe deficit, missing function
Cognitive/behavioral	

Supplemental Table 1. Pediatric Stroke Outcome Measure. Total score: 0-10

Laboratory parameters

Blood sampling was performed on the day of study visit. Basic hematologic and biochemical parameters were assessed using standard in-house procedures. Percentage of fetal hemoglobin (HbF) was measured using high-performance liquid chromatography (HPLC). Free hemoglobin (free Hb) was measured using spectrophotometry on a Shimadzu UV-2401 PC. Von Willebrand factor (VWF) plasma concentration was measured by enzyme-linked immunosorbent assay (ELISA) (Dakopatts)²⁴. VWF activity was determined on an automated coagulation analyzer (Behring Coagulation System, BCS) with reagents and protocol from the manufacturer (Siemens Healthcare Diagnostics, Marburg, Germany). VWF propeptide was assessed by ELISA using CLB-pro, an antibody against VWF propeptide²⁵. The activated conformation of VWF was measured by semi-automated ELISA on a TECAN Freedom EVO robot (Tecan, Männedorf, Switzerland) using an antibody against active VWF as described previously²⁶. Prothrombin fragment 1 and 2 (F1+2) was measured by ELISA using a mouse anti-human antibody²⁷. Thrombin-antithrombin complex (TAT) was measured by ELISA using a rabbit anti-human antibody (Enzygnost)²⁸. ADAMTS-13 was determined as described previously using a semi-automated assay²⁹. Glucose-6-phosphate dehydrogenase activity (G6PD) was measured in all boys using spectrophotometry.

Magnetic Resonance Imaging

Acquisition

Patients were imaged on a 3.0 Tesla (3T) Intera with a SENSE-8-channel head coil (n=32) or on a 3.0 T Ingenia with a SENSE-15-channel head coil (n=8), both Philips Healthcare, Best, the Netherlands. The MRI scan protocol included both a 2 dimensional (2D) T2-weighted and 2D fluid-attenuated inversion recovery (FLAIR) scan (both 5 mm slice thickness) for the visualization of WMHs, and a time of flight (TOF) MR angiography (MRA) of the intracranial arteries for the visualization of arterial stenosis. Added to this protocol was an ASL sequence with pseudo-continuous ASL labeling strategy (PCASL) and a gradient echo single shot echo-planar imaging (EPI) readout, with the following imaging parameters: resolution = $3 \times 3 \times 7 \text{ mm}^3$; field of view (FOV) = $240 \times 240 \text{ mm}^2$; 17 continuous axial slices; TE/TR = 17/4000 ms; flip angle = 90° ; SENSE = 2.5; labeling duration = 1650 ms; post-labeling delay for the 17 sequentially acquired slices in ascending order = 1525-2014 ms. Seventy-five label and control pairs were acquired, resulting in a scan duration of ten minutes. Background suppression was implemented with two inversion pulses, 1680 ms and 2830 ms after a pre-labeling saturation pulse. The labeling plane was positioned approximately 9 cm caudal to the anterior commissure-posterior commissure line and perpendicular to the carotid and vertebral arteries, based on 2D coronal and sagittal TOF angiograms³⁰.

ASL post-processing: quantification

Matlab 7.12.0 (The MathWorks, Inc., Natick, MA USA) and the SPM8 toolbox (Statistical Parametric Mapping, Wellcome Trust Centre for Neuroimaging, London, UK) were used for offline data processing with custom-built software. After 3D rigid-body motion correction, the control-label pairs were pair-wise subtracted and a robust perfusion-weighted map was created using linear robust regression with Huber's M-estimator³¹. These perfusion-weighted maps were converted into CBF maps using a single compartment quantification model, assuming that the label decays with the T1 of blood^{32,33}. A single M0 value - obtained in a previous study - was used for all participants³⁴.

ASL post-processing: spatial normalization

The 2D T2-weighted anatomical scan was segmented into GM and WM tissue probability maps. All CBF maps were transformed into anatomical space by a rigid-body registration of the averaged control image on the GM tissue probability maps. A two-stage approach was used to spatially normalize anatomical differences and residual EPI geometric distortion differences between subjects. First, the T1 tissue probability maps were spatially normalized using the Diffeomorphic Anatomical Registration

analysis using Exponentiated Lie algebra (DARTEL) algorithm, with the resulting normalization fields applied to the average control images³⁵. Secondly, the average control images were segmented into probability maps that were also normalized using DARTEL. Finally, EPI geometric distortion was corrected by warping the average control images to the average T2. All estimated transformations were applied to the corresponding CBF maps. CBF was calculated for GM and WM separately, for the whole brain and per hemisphere. In addition, we calculated CBF for the total normal appearing WM by excluding the WMHs itself.

White matter hyperintensities

All scans were evaluated by two independent observers (CBLMM and VvdL or HJMMM); discrepancies were resolved by mutual consent. The observers were blinded for all clinical information and study results except for the diagnosis of SCD. We defined WMHs using the Standards for Reporting Vascular changes on Neuroimaging (STRIVE) definition: a white matter hyperintensity of presumed vascular origin being a hyperintensity of variable size in the white matter on the FLAIR scan, without cavitation.³⁶ Incidental findings were described separately.

WMH volume was obtained semi-automatically by the procedure as illustrated in Figure 2. On all FLAIR slices WMHs were visually identified and manually selected as regions of interest (ROIs) (Figure 2a) with a wide margin using ITK-Snap³⁷. These ROIs were used for an intensity-based segmentation. GM was segmented on all FLAIR scans (Figure 2b), and the mean GM intensity of each patient was calculated. All voxels with a signal intensity >1.02 times of the average GM intensity were selected (Figure 2c). All selected voxels within the manually delineated ROIs were labeled as WMH (Figure 2d). Stenosis of intracerebral arteries were rated on the TOF MRA by an experienced neuro-radiologist (CBLMM) as follows: $<25\%$; $25-50\%$; $50-75\%$; $75-99\%$ or occlusion.

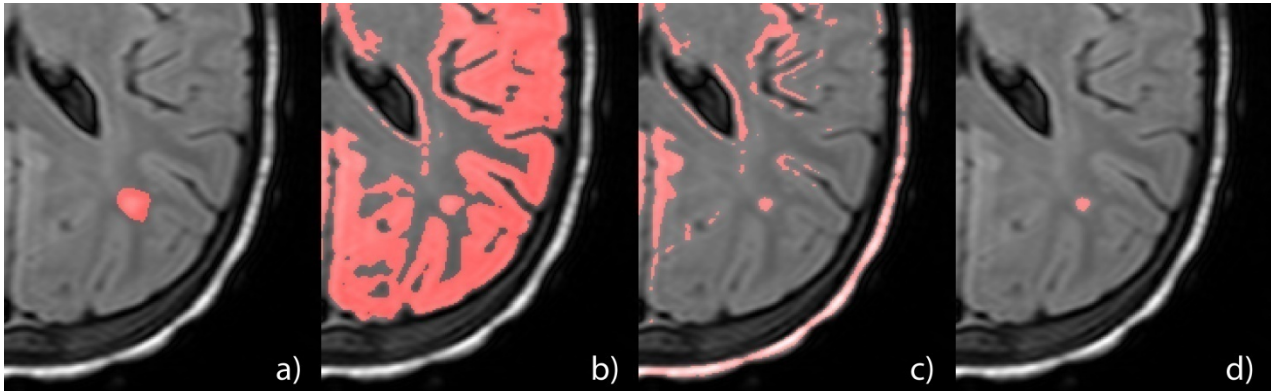


Figure 2. Semi-automatic delineation of white matter hyperintensities. Fluid attenuated inversion recovery (FLAIR) scan. a: Manual delineation of region of interest containing a white matter hyperintensity. b: Automatic segmentation of gray matter. c: Segmentation of voxels with an intensity of >1.02 times the intensity of gray matter. d: Semi-automatic delineation of white matter hyperintensity by selecting voxels within the region of interest.

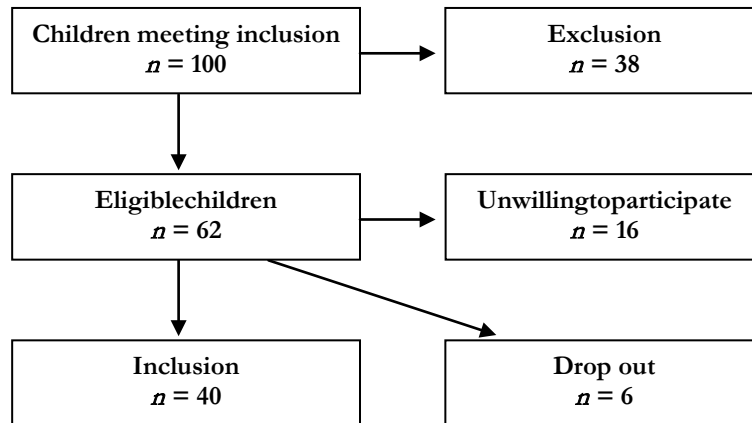
Statistical analysis

For comparison of continuous variables between groups, we used a Student's t-test or a Mann-Whitney U test when data was not normally distributed. For categorical variables, we performed a Fisher's exact test. In patients with WMHs, we investigated the association between potential laboratory risk factors and CBF on one side, and WMH volume on the other side using linear regression analysis. Because the distribution of WMH volume was skewed we used a rank score of WMH volume as the outcome in the linear regression analyses. In addition, we investigated the association between potential laboratory risk factors and CBF using linear regression.

Results

Patient population

We included 40 patients (for inclusion and exclusion, see Supplemental Figure 1). Mean age was 12.1 ± 2.6 years, 58% was male and most patients had homozygous SCD (95%); the remaining patients HbS β^0 thalassemia. A total of fifteen patients (7 with WMHs and 8 without) used hydroxyurea with a mean duration of 3.5 years: 39% of boys and 35% of girls. G6PD deficiency was not present. TCD was normal in all 40 patients.



Supplemental Figure 1. Flow chart illustrating inclusion. Reasons for exclusion: exclusion criteria for MRI. i.e. dental braces (n = 10); patients judged not likely to be compliant by treating hematologist and/or frequent missed appointments (n=9); abnormal or intermediate trans-cranial Doppler (n=4); previous overt stroke and/or chronic blood transfusion therapy (n=10); mental retardation or severe depression (n=3); other major health problem (n=2). Reasons for drop out: non-compliant with appointments (n=3); unable to make appointment due to frequent crisis (n=2); child refused MRI (n=1).

Description of neurological damage

WMHs were present in half of the patients (Table 1); the WMH volume per patient displayed a wide variety. Neurological examination was normal (PSOM score of 0) in 34 patients (85%). Three patients had a focal neurological deficit: one boy had a pyramidal tract syndrome, one girl had a partial visual field deficit and another girl experienced saccadic eye movements. These patients all had a high WMH volume (863 mm³, 15.097 mm³ and 16.343 mm³, respectively). The above mentioned boy also had an abnormal MRA: a 50-75% stenosis of the A1 branch of the left anterior cerebral artery despite normal TCD. One other boy had several intracranial stenosis, despite normal TCD: a 75-99% stenosis of the left internal carotid artery, a 50-75% stenosis of the M1 branch of the left middle cerebral artery, a 25-50% stenosis of the M1 branch of the right middle cerebral artery and a 25-50% stenosis of the A1 branch of the right anterior cerebral artery. This patient had extensive WMHs with a total volume of 1420 mm³; neurological examination was normal. Gray matter involvement was seen in 2 other patients. In one boy we discovered a small (<15 mm) cortical infarct in the occipital lobe with a normal neurological evaluation; this patient had a WMH volume of 697 mm³, stenosis of intracranial arteries could not be evaluated because of motion artifacts on the TOF scan but TCD was normal. One girl had two small (<5mm) cortical infarcts in the frontal and temporal lobe, she did not have any WMHs and neurological examination was normal.

Volume category	median	n	%
WMH volume (mm ³)			
0 mm ³	0 mm ³	20	50%
1-100 mm ³	46 mm ³	7	17%
101-1000 mm ³	503 mm ³	10	25%
>1000 mm ³	15.097 mm ³	3	8%

Table 1. Distribution of white matter hyperintensities. WMHs = white matter hyperintensities

Potential risk factors for WMHs including endothelial and coagulation activation

WMHs occurred more often in boys (75% vs. 40%, $p=0.05$, OR 4.5, 95% CI 1.2 - 17.4) (Table 2). This effect was not mediated by age (12.6 yrs for boys vs. 11.5 yrs for girls, $p=0.22$), G6PD deficiency (not present), HbF (11.3% in boys vs. 9.7% in girls, $p=0.41$) or other laboratory parameters with the exception of LDH (546 U/l in boys vs. 463 U/l in girls, $p=0.02$). We could not demonstrate significant differences in other potential risk factors between patients with WMHs and patients without WMHs. In patients with WMHs, we studied the association between potential risk factors and WMH volume using linear regression analysis (Table 3). A lower HbF was associated with a larger WMH volume (Figure 3) (regression coefficient -0.62, $R^2=0.25$, $p=0.04$). There was a trend towards a negative association between VWF propeptide and WMH volume (regression coefficient -0.11, $R^2=-0.17$, $p=0.08$).

	No WMHs (<i>n</i> =20)	WMHs (<i>n</i> =20)	<i>p</i>
Age (years)	12.2 ± 2.8	12.1 ± 2.5	0.98
Sex, male	8 (40%)	15 (75%)	0.05
Intracranial stenosis	-	2 (10%)	0.49
α thalassemia $\alpha\alpha/\alpha\alpha$	8 (40%)	10 (50%)	0.75
$\alpha\alpha/\alpha-$	11 (55%)	8 (40%)	0.75
$\alpha-/ \alpha-$	-	2 (10%)	0.49
missing	1 (5%)	-	1.00
Hemoglobin (mmol/L)	5.4 ± 0.7	5.2 ± 0.7	0.41
Reticulocytes (%)	9.4 ± 4.4	10.1 ± 5.3	0.67
Leukocytes ($10^9/L$)	9.9 ± 2.2	10.6 ± 4.1	0.51
HbF (%)	11.8 ± 6.0	9.3 ± 4.8	0.18
Free Hb ($\mu\text{mol/L}$)	11.8 ± 9.3	15.0 ± 11.6	0.41
LDH (U/L 37C)	491 ± 85	531 ± 128	0.26
VWF Antigen (%)	178 ± 45	176 ± 41	0.84
VWF Activity (%)	155 ± 47	144 ± 43	0.45
VWF Propeptide (%)	120 ± 37	112 ± 23	0.43
VWF Active conformation (%)	154 ± 36	163 ± 66	0.64
TAT Complex ($\mu\text{g/L}$)	7.0 (5.3 – 12.8)	8.0 (6.5 – 14.7)	0.47
F1+F2 ($\mu\text{mol/L}$)	201 (122 – 371)	178 (98 – 303)	0.65
ADAMTS-13 (%)	99 ± 11	100 ± 32	0.89
Ratio VWF Propeptide/VWF Antigen	0.64 (0.57 – 0.79)	0.62 (0.54 – 0.73)	0.57
Ratio VWF Antigen/ADAMTS-13	1.75 (1.52 – 2.15)	1.81 (1.28 – 2.45)	0.80

Table 2. Potential risk factors for white matter hyperintensities in children with sickle cell disease. Data is presented as count (percentage) for categorical data, mean ± SD for continuous data, or median (interquartile range) for continuous data not normally distributed. F1+2, prothrombin fragment 1+2; LDH, lactate dehydrogenase; SD, standard deviation; TAT, thrombin-antithrombin; VWF, von Willebrand Factor; WMHs, white matter hyperintensities.

	Patients with WMHs		
	(n=20)		
	β #	R ²	p
Hemoglobin (mmol/L)	-1.59	0.04	0.40
Reticulocytes (%)	-0.09	0.01	0.72
Leukocytes (10 ⁹ /L)	-0.14	0.01	0.69
HbF (%)	-0.62	0.25	0.04
Free Hb (μ mol/L)	30.43	<0.01	0.82
LDH (U/L 37C)	<0.01	<0.01	0.94
VWF Antigen (%)	<0.01	<0.01	0.91
VWF Activity (%)	<-0.01	<0.01	0.85
VWF Propeptide (%)	<0.11	0.17	0.08
VWF Active conformation (%)	<0.01	<0.01	0.72
TAT Complex (μ g/L)	0.01	<0.01	0.92
F1+F2 (μ mol/L)	<0.01	<0.01	0.78
ADAMTS-13 (%)	-0.05	0.09	0.25
Ratio VWF Propeptide/VWF Antigen	-12.45	0.14	0.10
Ratio VWF Antigen/ADAMTS-13	1.37	0.05	0.43

Table 3. Association between potential risk factors and white matter hyperintensity volume. F1+2, prothrombin fragment 1+2; LDH, lactate dehydrogenase; TAT, thrombin-antithrombin; VWF, von Willebrand Factor; WMHs, white matter hyperintensities R²explained variance. # Unstandardized regression coefficient. Bold denotes statistical significance ($p < 0.05$).

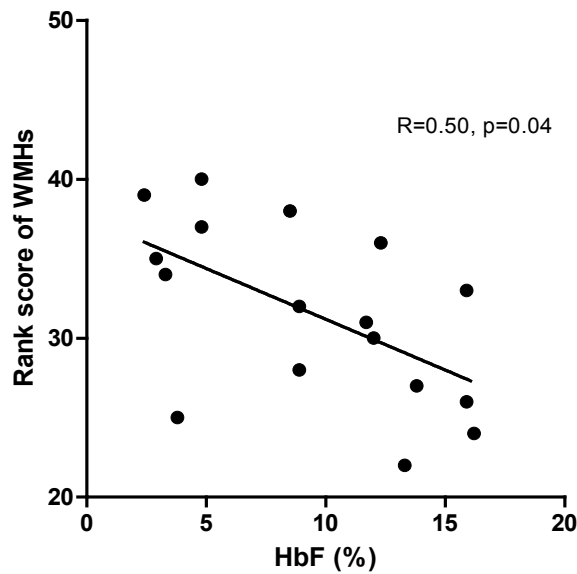


Figure 3. Association between HbF and white matter hyperintensity volume. Patients with white matter hyperintensities were selected. X-axis denotes HbF (%), Y-axis denotes rank score of white matter hyperintensity volume. HbF, fetal hemoglobin; WMHs, white matter hyperintensities.

Cerebral blood flow and its association with WMHs

Total GM and WM CBF did not differ between patients with WMHs or patients without WMHs. In patients with WMHs, there was no association between WMH volume and CBF in any brain region using linear regression analysis ($p > 0.10$ for all associations). CBF did not differ between boys and girls. In patients with WMHs, we calculated CBF in normal appearing WM by excluding the WMHs itself. CBF in normal appearing WM was 35.9 mL/100g/min, compared to mean CBF in WM of 37.3 mL/100g/min in patients without WMHs ($p = 0.41$).

Association between CBF and laboratory parameters including endothelial and coagulation activation

Higher CBF values in GM and WM were both significantly associated with lower Hb (regression coefficient -7.60, $R^2 0.23$, $p < 0.01$ and regression coefficient -2.68, $R^2 0.22$, $p < 0.01$, respectively) and lower HbF (regression coefficient -0.74, $R^2 0.12$, $p = 0.03$ and regression coefficient -0.24, $R^2 0.11$, $p = 0.04$, respectively). Lower CBF in WM was associated with lower ADAMTS13 (regression coefficient 0.07, $R^2 0.15$, $p = 0.03$) and the ratio VWF antigen to ADAMTS13 (regression coefficient -2.33, $R^2 0.13$, $p = 0.04$) (Table 4).

	CBF in GM			CBF in WM		
	$\beta\#$	R ²	<i>p</i>	$\beta\#$	R ²	<i>p</i>
Hemoglobin (mmol/L)	-7.60	0.23	<0.01	-2.68	0.22	<0.01
Reticulocytes (%)	0.65	0.07	0.09	0.20	0.05	0.16
Leukocytes (10 ⁹ /L)	-0.70	0.04	0.22	-0.20	0.03	0.33
HbF (%)	-0.74	0.12	0.03	-0.24	0.11	0.04
Free Hb (μmol/L)	-195.88	0.03	0.32	-120.70	0.09	0.09
LDH (U/L 37C)	0.01	0.01	0.63	<0.01	<0.01	0.79
VWF Antigen (%)	-0.05	0.03	0.31	-0.01	0.02	0.37
VWF Activity (%)	-0.02	0.01	0.67	-0.01	0.01	0.62
VWF Propeptide (%)	0.05	0.01	0.50	0.02	0.01	0.53
VWF Active conformation (%)	0.07	0.08	0.11	0.02	0.04	0.26
TAT Complex (ug/L)	<0.01	<0.01	1.00	0.09	0.08	0.08
F1+F2 (pmol/L)	<0.01	<0.01	0.71	0.01	0.09	0.08
ADAMTS-13 (%)	0.09	0.03	0.36	0.07	0.15	0.03
Ratio VWF Propeptide/VWF Antigen	15.60	0.07	0.12	4.50	0.05	0.21
Ratio VWF Antigen/ADAMTS-13	-4.30	0.06	0.18	-2.33	0.13	0.04

Table 4. Association between laboratory markers and Cerebral Blood Flow. CBF, cerebral blood flow; F1+2, prothrombin fragment 1+2; GM, gray matter; LDH, lactate dehydrogenase; TAT, thrombin-antithrombin; VWF, von Willebrand Factor; WM, white matter. Bold denotes statistical significance ($p < 0.05$). R² explained variance. # Unstandardized regression coefficient.

Discussion

Our results show that male sex is a risk factor of WMHs and that a lower level of HbF is associated with a higher WMH volume. We could not demonstrate an association between endothelial activation and WMHs, but a low level of ADAMTS13 was associated with lower CBF in the WM. CBF was not associated with WMHs. Boys displayed an increased risk for WMHs independent of age, anemia, HbF or G6PD deficiency, although boys did have a higher level of LDH. This is in agreement with previous studies: in a multivariate analysis of 814 patients screened for the SITT, De Baun *et al.* have previously demonstrated that male sex was a risk factor for SCIs, however, their odds ratio of 1.37 is notably lower¹³. Bernaudin *et al.* found a trend towards an increased risk for SCIs in boys ($p = 0.07$) in univariate

analysis in their newborn cohort (n=217), but in multivariate analysis, G6PD deficiency was the only identified risk factor for SCIs¹. Our results confirm that boys seem to be at increased risk for WMHs, perhaps through (X-linked) genetic polymorphisms present in boys.

We demonstrated that a lower level of HbF is associated with a larger WMH volume. This association was significant, even though patients using hydroxyurea were included in the analysis. Before the start of hydroxyurea, the level of HbF would have been lower in these patients, associated with an increased risk to develop WMHs. The fact that we still found an association between HbF and volume of WMHs demonstrates its robustness. The association between the level of HbF and WMH volume has not been reported previously. In the SIT trial, there was a trend towards a lower HbF in patients with SCIs compared to patients without SCIs (11.1% vs. 12.5%, p=0.06)¹³. HbF is one of the most important known modifiers of disease severity in SCD, predicting mortality, pain rates, dactylitis and acute chest syndrome³⁸⁻⁴². Because HbF does not polymerize and reduces the concentration of HbS, high levels can inhibit polymerization and the subsequent detrimental effects such as hemolysis and vaso-occlusion.⁴³ Increasing HbF by using hydroxyurea has been shown to decrease several complications and decrease hemolysis, but it is unclear whether it can protect against the development of WMHs^{44,45}.

We observed a trend towards a lower VWF propeptide in patients with a larger WMH volume. This is in accordance with the results of Colombatti *et al.* who found some evidence for a higher level of endothelial dysfunction in patients with SCIs.¹² Interestingly, recent insights suggest that endothelial dysfunction plays a pivotal role in the occurrence of SCIs in other patient groups such as vascular dementia^{46,47}.

In addition, we investigated the association between WMHs and CBF and did not find any differences in CBF in GM or WM between patients with and without WMHs. CBF in normal appearing WM also did not differ from CBF in the white matter of patients without any WMHs. This may be due to the fact that we performed a cross-sectional study and only investigated patients during steady disease state. Perhaps CBF could become insufficient in our patients during episodes of increased demand. Future studies should therefore focus on the dynamics of CBF in order to elucidate its role in the etiology of WMHs. Besides being associated with Hb and HbF, we observed a positive association between ADAMTS13 levels and CBF in the WM. ADAMTS13 is released from endothelial cells and cleaves large VWF multimeres into smaller units. A (relative) insufficiency of ADAMTS13 may indicate endothelial dysfunction, potentially hampering CBF; however very few studies have explored this. The interaction

between HbF, endothelial dysfunction and CBF in the pathogenesis of WMHs (Figure 1) requires further research but could result in new insights for novel therapeutic targets.

Strengths and Limitations

MRI scanning was performed using a 3T scanner which yields high resolution images, and additionally we used a semi-automatic method to delineate WMHs, leading to a good estimation of the total volume of the WMHs. Instead of only calculating CBF in the GM, we used a state of the art ASL method and were able to quantify CBF in the WM and GM separately. We used a broad panel of markers of endothelial and coagulation activation to investigate the association with WMHs and CBF.

We specifically studied risk factors for WMHs in SCD, regardless of neurological status. We realize this is not in line with most previous studies on SCIs, that mostly defined SCIs as areas of abnormal hyperintensity on MRI of the brain in a patient with no history or physical findings of a focal neurological deficit. Extensive WMHs or a WMH located at a vital location could result in focal neurological deficits and would lead to the exclusion of these patients when using this latter definition of SCIs, while the etiology of the lesions is similar. Because our objective was to study risk factors for WMHs, we did not exclude these patients. As this was an explorative study, we did not perform a correction for multiple testing; this should be taken into account when interpreting the results.

Conclusion

Our study showed that boys have a higher risk of WMHs and that a high HbF concentration seems protective for the development of WMHs. Lower ADAMTS13 levels were associated with lower CBF in the WM, suggesting that endothelial activation could potentially hamper CBF. Our findings suggest that fetal hemoglobin and endothelial dysfunction may be involved in the pathogenesis of WMHs in patients with SCD, possibly mediated through altered CBF.

Reference list

1. Bernaudin F, Verlhac S, Arnaud C, et al. Impact of early transcranial Doppler screening and intensive therapy on cerebral vasculopathy outcome in a newborn sickle cell anemia cohort. *Blood*. 2011;117(4):1130–1140.
2. Casella JF, King AA, Barton B, et al. Design of the Silent Cerebral Infarct Transfusion (SIT) Trial. *Pediatr. Hematol.* 2010;27:69–89.
3. Schatz J, Brown RT, Pascual JM, Hsu L, Debaun MR. Poor school and cognitive functioning with silent cerebral infarcts and sickle cell disease. *Neurology*. 2001;56:1109–1111.
4. Armstrong FD, Thompson RJ, Wang W, et al. Cognitive Functioning and Brain Magnetic Resonance Imaging in Children With Sickle Cell Disease. *Pediatrics*. 1996;97:864–870.
5. Pegelow CH, Macklin E a, Moser FG, et al. Longitudinal changes in brain magnetic resonance imaging findings in children with sickle cell disease. *Blood*. 2002;99(8):3014–8.
6. DeBaun MR, Gordon M, McKinstry RC, et al. Controlled Trial of Transfusions for Silent Cerebral Infarcts in Sickle Cell Anemia. *N. Engl. J. Med.* 2014;371(8):699–710.
7. Manwani D, Frenette PS. Vaso-occlusion in sickle cell disease : pathophysiology and novel targeted therapies. *Blood*. 2013;122(24):3892–3898.
8. Belcher JD, Chen C, Nguyen J, et al. Heme triggers TLR4 signaling leading to endothelial cell activation and vaso-occlusion in murine sickle cell disease. *Blood*. 2014;123(3):377–90.
9. Chen J, Hobbs WE, Le J, et al. The rate of hemolysis in sickle cell disease correlates with the quantity of active von Willebrand factor in the plasma. *Blood*. 2011;117(13):3680–3.
10. Koshy M, Thomas C, Goodwin J. Vascular lesions in the central nervous system in sickle cell disease (neuropathology). *J. Assoc. Acad. Minor. Phys.* 1990;1(3):71–8.
11. Connes P, Verlhac S, Bernaudin F. Advances in understanding the pathogenesis of cerebrovascular vasculopathy in sickle cell anaemia. *Br. J. Haematol.* 2013;161(4):484–98.
12. Colombatti R, De Bon E, Bertomoro A, et al. Coagulation activation in children with sickle cell disease is associated with cerebral small vessel vasculopathy. *PLoS One*. 2013;8(10):e78801.
13. DeBaun MR, Sarnaik S a, Rodeghier MJ, et al. Associated risk factors for silent cerebral infarcts in sickle cell anemia: low baseline hemoglobin, sex, and relative high systolic blood pressure. *Blood*. 2012;119(16):3684–90.
14. Kwiatkowski JL, Zimmerman RA, Pollock AN, et al. Silent infarcts in young children with sickle cell disease. *Br. J. Haematol.* 2009;146:300–305.
15. Oguz KK, Golay X, Pizzini FB, et al. Radiology Sickle Cell Disease : Continuous Arterial Spin-labeling Perfusion MR Imaging in Children 1. *Radiology*. 2003;227:567–574.
16. Arkuszewski M, Krejza J, Chen R, Melhem ER. Sickle cell anemia: reference values of cerebral blood flow determined by continuous arterial spin labeling MRI. *Neuroradiol. J.* 2013;26(2):191–200.
17. Prohovnik I, Hurllet-Jensen A, Adams R, De Vivo D, Pavlakis SG. Hemodynamic etiology of elevated flow velocity and stroke in sickle-cell disease. *J. Cereb. blood flow Metab.* 2009;29(4):803–10.
18. Dowling MM, Quinn CT, Rogers ZR, Buchanan GR. Acute Silent Cerebral Infarction in Children with Sickle Cell Anemia. 2010;(October 2009):461–464.
19. Helton KJ, Paydar A, Glass J, et al. Arterial Spin-Labeled Perfusion Combined With Segmentation Techniques to Evaluate Cerebral Blood Flow in White and Gray Matter of Children With Sickle Cell Anemia. *Pediatr. Blood Cancer*. 2009;52:85–91.
20. Thomas DJ, Marshall J, Russell RW, et al. Effect of haematocrit on cerebral blood-flow in man. *Lancet*. 1977;2(8045):941–3.
21. Gruber EM, Jonas RA, Newburger JW, et al. The effect of hematocrit on cerebral blood flow velocity in neonates and infants undergoing deep hypothermic cardiopulmonary bypass. *Anesth. Analg.* 1999;89(2):322–7.

22. Adams RJ, McKie VC, Hsu L, et al. Prevention of a first stroke by transfusions in children with sickle cell anemia and abnormal results on transcranial Doppler ultrasonography. *N. Engl. J. Med.* 1998;339(1):5–11.
23. Kitchen L, Westmacott R, Friefeld S, et al. The pediatric stroke outcome measure: a validation and reliability study. *Stroke.* 2012;43(6):1602–8.
24. Cejka J. Enzyme Immunoassay for Factor VIII-Related Antigen. *Clin. Chem.* 1982;28(6):1356–1358.
25. Borchiellini A, Fijnvandraat K, Ten Cate J, et al. Quantitative analysis of von Willebrand factor propeptide release in vivo: effect of experimental endotoxemia and administration of 1- deamino-8-D-arginine vasopressin in humans. *Blood.* 1996;88:2951–2958.
26. Hyseni A, Kemperman H, de Lange DW, et al. Active von Willebrand factor predicts 28-day mortality in patients with systemic inflammatory response syndrome. *Blood.* 2014;123(14):2153–6.
27. Pelzer H, Schwarz A, Stüber W. Determination of human prothrombin activation fragment 1 + 2 in plasma with an antibody against a synthetic peptide. *Thromb. Haemost.* 1991;65(2):153–9.
28. Hoek JA, Sturk A, ten Cate JW, et al. Laboratory and clinical evaluation of an assay of thrombin-antithrombin III complexes in plasma. *Clin. Chem.* 1988;34(10):2058–62.
29. Kostousov V, Fehr J, Bombeli T. Novel, semi-automated, 60-min-assay to determine von Willebrand factor cleaving activity of ADAMTS-13. *Thromb. Res.* 2006;118(6):723–31.
30. Aslan S, Xu F, Wang PL, et al. Estimation of labeling efficiency in pseudocontinuous arterial spin labeling. *Magn. Reson. Med.* 2010;63(3):765–71.
31. Maumet C, Maurel P, Ferré J-C, Barillot C. Robust estimation of the cerebral blood flow in arterial spin labelling. *Magn. Reson. Imaging.* 2014;32(5):497–504.
32. Alsop DC, Detre JA, Golay X, et al. Recommended implementation of arterial spin-labeled perfusion MRI for clinical applications: A consensus of the ISMRM perfusion study group and the European consortium for ASL in dementia. *Magn. Reson. Med.* 2014;
33. Wang J, Alsop DC, Li L, et al. Comparison of quantitative perfusion imaging using arterial spin labeling at 1.5 and 4.0 Tesla. *Magn. Reson. Med.* 2002;48(2):242–54.
34. Heijtel DFR, Mutsaerts HJMM, Bakker E, et al. Accuracy and precision of pseudo-continuous arterial spin labeling perfusion during baseline and hypercapnia: a head-to-head comparison with ¹⁵O H₂O positron emission tomography. *Neuroimage.* 2002;92:182–92.
35. Ashburner J. A fast diffeomorphic image registration algorithm. *Neuroimage.* 2007;38(1):95–113.
36. Wardlaw JM, Smith EE, Biessels GJ, et al. Neuroimaging standards for research into small vessel disease and its contribution to ageing and neurodegeneration. *Lancet Neurol.* 2013;12(8):822–838.
37. Yushkevich P a, Piven J, Hazlett HC, et al. User-guided 3D active contour segmentation of anatomical structures: significantly improved efficiency and reliability. *Neuroimage.* 2006;31(3):1116–28.
38. Platt OS, Brambilla DJ, Rosse WF, et al. Mortality in sickle cell disease. *N. Engl. J. Med.* 1994;330(23):1639–1644.
39. Platt OS, Thorington BD, Brambilla DJ, et al. Pain in sickle cell disease. *N. Engl. J. Med.* 1991;325(1):11–6.
40. Bhatnagar P, Keefer JR, Casella JF, et al. Association Between Baseline Fetal Hemoglobin Levels and Incidence of Severe Vaso-Occlusive Pain Episodes in Children With Sickle Cell Anemia. *Pediatr Blood Cancer.* 2013;(April):12–14.
41. Bailey K, Morris JS, Thomas P, Serjeant GR. Fetal haemoglobin and early manifestations of homozygous sickle cell disease. *Arch. Dis. Child.* 1992;67(4):517–20.
42. Castro O, Brambilla DJ, Thorington B, et al. The acute chest syndrome in sickle cell disease: incidence and risk factors. *Blood.* 1994;84(2):643–9.
43. Steinberg MH, Chui DHK, Dover GJ, Sebastiani P, Alsultan A. Perspectives Fetal hemoglobin in sickle cell anemia : a glass half full ? 2014;123(4):481–485.

44. Charache S, Terrin ML, Moore RD, et al. Effect of hydroxyurea on the frequency of painful crises in sickle cell anemia. *N. Engl. J. Med.* 1995;332(20):1317–1322.
45. Wang WC, Ware RE, Miller ST, et al. Hydroxycarbamide in very young children with sickle-cell anaemia : a multicentre , randomised , controlled trial (BABY HUG). *Lancet.* 2011;377(9778):1663–1672.
46. Wardlaw JM, Smith C, Dichgans M. Mechanisms of sporadic cerebral small vessel disease : insights from neuroimaging. *Lancet Neurol.* 2013;12(5):483–497.
47. Lavallée PC, Faïlle D. Circulating Markers of Endothelial Dysfunction and Platelet Activation in Patients with Severe Symptomatic Cerebral Small Vessel Disease. 2013;131–138.

10

**General discussion,
conclusions
and implications**

Part I Inter-vendor reproducibility of arterial spin labeling

Throughout the lines of arterial spin labeling (ASL) developments, reliability assessments of ASL remained a central theme¹⁻⁶ because of its intrinsically low signal-to-noise ratio (SNR)⁷. **Part I** of this thesis can be viewed as a sequel of the previous work of dr. Gevers *et al.*⁸ and dr. Heijtel *et al.*⁹. The first have established that the single-vendor intra- and inter-scanner reproducibility of ASL were sufficient and comparable. The latter have established that the reproducibility of ASL is comparable with H₂O¹⁵-positron emission tomography (PET) when a two-compartment quantification model was used. These findings suggested that the measurement reproducibility of the state-of-the-art ASL sequence is sufficiently high, and that the variability of ASL may be dominated by physiological perfusion fluctuations rather than technical limitations. Since different magnetic resonance imaging (MRI) centers use scanners from different MRI vendors, the next logical step towards large clinical multi-center perfusion studies was to investigate the inter-vendor reproducibility of ASL.

The incentive to study the inter-vendor reproducibility of ASL (**Chapters 2-4**) was the possibility to pool ASL-based cerebral blood flow (CBF) results from two scanners from different MRI manufacturers. Although the labeling strategy implemented in the product sequence of both vendors was the same (pseudo-continuous ASL (PCASL)), the readout was fundamentally different, 3D spiral fast-spin echo (FSE) (General Electric (GE)) versus 2D gradient-echo echo-planar imaging (EPI) (Philips). The first visually appreciable difference between these sequences on both the individual subject level and on the group level was the difference in the spatial smoothing, leading to substantial mean CBF and inter-session variation differences between vendors on a voxel level. However, on a total gray matter (GM) level, there was excellent agreement between the mean CBF of both vendors. In addition, the intra-vendor inter-session variation of both vendors as well as the inter-vendor inter-session variation were comparable on a total GM level, and comparable with the between-weeks variation of several previous reproducibility studies^{1, 8, 10}. These findings led to the encouraging conclusion that baseline CBF values can be compared between fundamentally different sequences from different vendors on a total GM level (**Chapter 2**). This can be attributed to the fact that baseline long-term physiological perfusion fluctuations dominate sequence and hardware differences between vendors. The large differences on a voxel level were mainly attributed to the fundamental differences in readout modules implemented by both vendors. This is a clear obstacle for the comparison of ASL-based data between the different product sequences from the two vendors, which led to the initiation of the study in **Chapter 5**.

Similar to the baseline CBF comparison, the inter-session variation of a pharmacologically induced CBF decrease was comparable between sequences on a total GM level but not on a voxel level (**Chapter 3**). This again implies that on the total GM level, the inter-vendor variability is dominated by normal long-term perfusion fluctuations, which is in agreement with previous studies ^{1,9,11}. However, on a voxel level the readout differences between the product sequences dominated the perfusion variability. We showed that by additional smoothing of the 2D EPI data to achieve the same smoothness as the 3D spiral data, we were able to approach the inter-session variation that was observed for the 3D spiral readout. This is in agreement with the large difference in point spread function (PSF) between the sequences, as can be easily appreciated by visually comparing the CBF maps of both sequences ¹². In addition, it shows the potential benefit of additional spatial smoothing for the analysis of 2D EPI pharmacological ASL (phASL) data ¹³. For the detection of small focal changes - such as in finger tapping functional ASL (fASL) (**Chapter 4**) - however, it remains questionable whether or not additional smoothing removes focal activation regions ¹⁴. The residual variability differences between the 3D spiral data and smoothed 2D EPI data may be explained by the differences in background suppression efficiency. This was indicated in a previous study that studied differences in activation detectability between a 2D and two 3D readouts without background suppression, as well as the same two 3D readouts with background suppression ¹². This study showed that the detectability differences between 2D and 3D readouts themselves were small, but also that the detectability of the 3D readout increased significantly by the use of background suppression. Although we employed background suppression in both the 2D EPI and 3D spiral readouts in our studies, the efficiency of background suppression in a 2D readout steadily decreases with later acquired slices ¹⁵.

Both the mean phASL CBF decrease (**Chapter 3**) as well as the fASL CBF increase (**Chapter 4**) differed between the product sequences, although this difference was not significant for the latter. Interestingly in this respect, was that the main voxel-wise CBF differences between sequences in **Chapter 2 and 3** were found in the posterior watershed area. These regions are known for having the longest transit times (TTs) ^{4,16}. Because the 3D sequence readout has a single post-labeling delay (PLD) whereas the PLD of the 2D EPI sequence increases along an inferior-superior gradient, both sequences differ much in their TT sensitivity. It is most likely that the abovementioned cases of CBF disagreement between the product sequences can be explained by the differences in TT sensitivity between both readout modules. This is in agreement with a previous comparison between the performance of a 3D spiral readout with either a PLD of 1500 or 2500 ms ¹⁷. Regions with long TT showed hypoperfusion when the 1500 ms PLD was used, but not with the 2500 ms PLD. In addition, reproducibility was higher for 2500 ms PLD, suggesting that TT contributes in variability when a short PLD is chosen. From these observations, we

may conclude that TT can influence both the accuracy and the precision of ASL measurements, and that its influence depends upon the employed readout module. This strongly encourages the development of sequences that simultaneously measure CBF and TT without significant penalties in SNR for the CBF measurement^{18,19}.

Using previously proposed methods²⁰, we provided sample size calculations for future phASL studies in **Chapter 3**. We underlined that sample size requirements for the detection of any effect may be small, but that the requirements for detecting differences in an effect are quadratically larger. Although this observation is easily deduced from sample size equations, we believe that it is important to acknowledge this observation when planning future phASL or fASL studies. The same effect was observed for the within-subject coefficient of variation (wsCV) in **Chapters 3 and 4**. Whereas the inter-session variation of the absolute CBF decrease was not very different from baseline inter-session CBF variation in both cases, the small effect size of phASL (~20%) and fASL (~4%) increased the wsCV fivefold and 25-fold respectively. As a consequence, the finger tapping fASL activation (**Chapter 4**) was barely statistically detectable. It should be noted, however, that this low detectability should not discourage the use of ASL to detect task-based CBF changes^{12, 21}. Whereas the temporal resolution of ASL for the 2D EPI sequence was reasonable (8 seconds), it was very low for the 3D spiral sequence (135 seconds). For a fair comparison, the 2D EPI data was averaged to obtain the same temporal resolution. Although the SNR of an individual 2D EPI ASL subtraction is very low, a higher temporal resolution may still benefit statistical modeling. Moreover, current efforts are aimed at increasing the temporal resolution of 3D ASL sequences while retaining its benefits in terms of higher SNR²².

Chapter 5 concerned a triple vendor comparison. Whereas the previous chapters aimed to investigate the penalty of using fundamentally dissimilar standard ASL implementations of different vendors, the study in this chapter aimed to investigate the inter-vendor reproducibility when sequences are optimized to be as identical as possible between the scanners. The first and most apparent result when the near-identical sequences (**Chapter 5**) are compared with the dissimilar sequences (**Chapter 2**), is that both the mean CBF and inter-session variation maps were visually much more comparable between scanners from different vendors for near-identical sequences than for the dissimilar sequences. Likewise, the GM-white matter (WM) CBF ratios were significantly different between dissimilar sequences whereas these ratios were very comparable with near-identical sequences. This was in agreement with our hypothesis that ASL results are much more comparable between vendors when the same readout and similar sequence parameters are used¹².

A main limitation of this study was that scanner hardware differences were too large to create a single identical sequence for the three scanners of the different vendors. The reason for these differences in hardware specifications was that MRI hardware development is ongoing²³, and one scanner was older than the two others. The solution was to split the triple vendor comparison into two dual vendor comparison studies. For scanners with similar hardware specifications it would have been possible to create the same near-identical sequence for the scanners from all three vendors. However, this main limitation led to an important serendipitous finding. Because the hardware specifications of one scanner were flexible, it participated in both comparisons. Consequently, the results of these slightly different sequences could be compared on the same vendor. Whereas the total GM inter-session variation of study 2 was comparable with the inter-session variation in **Chapter 2**, and with other previous between-weeks reproducibility studies^{1,8}, the inter-session variation of study 1 was twice as high as in study 2. In other words, the precision was more comparable between identical sequences employed on scanners from different vendors than between slightly less identical sequences on the same scanner. The same was true for the accuracy. The quantitative agreement seemed much less affected by vendor effects (differences in scanner hardware and software) than by sequence effects, which were mainly differences in echo time and inter-pulse time during labeling. These results demonstrate the importance of keeping sequence parameters identical for future multi-center ASL studies. In addition, the same message is very important for clinical single-site ASL studies. Scanner hardware and software are often updated halfway in an ongoing clinical study, and these results provide strong evidence that it is very important to keep sequence parameters as identical as possible within the limitations created by such scanner updates.

Part II Clinical applicability of arterial spin labeling

Despite its potential relevance as a micro-vascular biomarker²⁴⁻²⁶, ASL-based WM CBF measurements were previously not deemed feasible for two main reasons. Firstly, because of too low SNR due to longer TT than in GM, and secondly because of too low spatial resolution to acquire pure WM signal, i.e. which is not contaminated by signal from the GM²⁷. Recently, SNR improvements rendered the detection of WM perfusion signal possible in the majority of WM voxels²⁸. However, WM voxels with the highest and most reliably measured perfusion signal are situated in the juxtacortical peripheral WM, whereas signal in deep central WM voxels are not measurable even after 10 minutes of scanning²⁸. These findings raise the question to what extent they are due to a real perfusion gradient from the peripheral to central WM, or rather to the spatial extent of signal contamination of GM CBF²⁷. Signal contamination can be expected to result from a combination of acquisition PSF, motion and

interpolation in the post-processing stage^{12, 14, 29}. Moreover, as the SNR of ASL within the WM remains relatively poor³⁰, it is important to balance between including as many voxels as possible into a WM region of interest (ROI) to increase the statistical power of WM CBF on the one hand, and excluding as many peripheral WM voxels to exclude GM signal contamination on the other hand³¹.

In **Chapter 6**, perfusion signal of WM voxels medial to the cortical GM (inward contamination) were compared with perfusion signal of voxels lateral to the cortical GM (outward contamination) within a single slice. This analysis is based on the assumption that the extent of inward and outward GM signal contamination is similar. Our analyses showed that significant outward GM signal contamination stretched across 3 voxels. Therefore, the conclusion was that a typical WM mask should be eroded three-fold to create a WM ROI that holds as many relatively uncontaminated WM voxels as possible. However, it should be acknowledged that the spatial extent of signal contamination may differ much between studies or even between subjects, because of differences in acquisition, subject motion and post-processing methods^{12, 14, 29}. Therefore, the proposed three-voxel erosion guideline should be customized to the data under investigation. Nevertheless, after three-voxel erosion the WM signal was still significantly larger than the signal outside the GM (i.e. cerebrospinal fluid (CSF), bone and air). This observation confirms previous research^{28, 30} and shows the possibility to significantly detect uncontaminated perfusion signal in the WM with ASL. However, this signal could still be too weak to be able to make statistical inferences in group analyses.

There is accumulating evidence that TT measurements may both significantly improve the quantification of CBF^{7, 32} and provide additional information that could even be more valuable than CBF in some clinical cases³³⁻³⁶. One way to estimate TT is to calculate the ratio of ASL sequences with and without vascular crushing, which is known as flow encoding arterial spin tagging (FEAST)³⁷. In **Chapters 7 and 8**, FEAST was applied with slightly adapted parameters, to measure TT as well as both crushed and non-crushed CBF. The application of vascular crushing removes some of the macro-vascular contribution to CBF, which may be less of interest than the pure micro-vascular tissue perfusion signal³⁸. On the other hand, when macro-vascular signal is removed this will also reduce the available SNR³⁷. On the individual subject level it is important to retain as most SNR as possible, especially in elderly with neurodegenerative or cerebrovascular disease. Therefore, crushing is not recommendable for clinical applications of ASL on the single subject level⁷. For group analyses, it may be a different case, as we showed in **Chapter 7**. In this study, correlations with age or gender were stronger for crushed CBF-values than without crushing. It should be noted that the applied crushing was moderate (i.e. velocity encoding cutoff 5 cm/s), removing only signal in the largest vessels with minor SNR penalty. When

vascular crushing is applied to completely remove macro-vascular perfusion signal, a lower velocity cutoff is used (e.g. velocity cutoff 1-3 cm/s) and the resulting SNR penalty may be too severe for applications in elderly patients ³⁷. Therefore, if any crushing is applied, the consensus paper recommended to apply moderate crushing (4 cm/s) ⁷ which is close to the velocity cutoff that was used in these chapters. The observation that slight crushing increased statistical power, suggests that it can be advantageous to decrease the influence of macro-vascular perfusion fluctuations on the reproducibility of the ASL measurement - even at the expense of some SNR.

It could be argued that with optimal sequence timing - i.e. labeling duration and PLD - macro-vascular contribution is minimal and crushing may not be required. In this respect, the mean PLD applied in these chapters was relatively low (1800 ms vs. 2000 ms as recommended in elderly patients) ⁷. However, TT can be expected to vary more in elderly patients than in healthy volunteers, because of differences in vessel tortuosity, vascular resistance and cerebral autoregulation deficiency ³⁹. Therefore, it may remain difficult - if not impossible - to exactly confine ASL timing parameters to the subject that is being scanned. The physiological correlations with the estimated TT were even stronger than with the crushed or non-crushed CBF measurements - not only for the correlations with age and gender (**Chapter 7**) but also with white matter lesion (WML) volume (**Chapter 8**). There could be good physiological reasons for this observation, including the fact that the preferential location of WML is in regions with the longest TT , such as watershed areas ⁴⁰. However, to which extent these stronger correlations with crushed CBF and TT had physiological origins, or were merely due to a decrease in the effect of macro-vascular perfusion fluctuations on the measurement variability, cannot be differentiated from our data. Interestingly, a recent study found lower measurement variability for TT than for CBF, using a multi-PLD PCASL sequence ⁴¹. This suggests that the stronger correlations with TT are at least partly due to higher stability of TT compared to CBF measurements. It is noteworthy that new ASL techniques are currently under development that can simultaneously measure both CBF and TT - some even without sacrificing SNR for the single time point CBF map ⁴¹⁻⁴³. Moreover, these techniques enable a more absolute quantification of TT , whereas the quantification of FEAST-based TT depends much on PLD and CBF velocity differences between subjects and brain regions ^{37, 38}. These new ASL techniques are probably preferable over FEAST for clinical research applications, and can be expected to enhance the value of ASL even further ⁷.

Despite these limitations of FEAST in terms of absolute quantification, we were able to construct TT maps that resemble the known anatomy of the cerebral vasculature ⁴⁴. Therefore, the spatial accuracy of FEAST is at least sufficient to create a population-based TT gradient. These maps can be helpful in

future ASL research for the definition of vascular ROIs, if hypothesized perfusion effects are restricted to certain flow territories only, or if spatial averaging is required when an anatomical structure is too small considering ASL limitations in terms of SNR or spatial smoothing⁷. Potential applications include the investigation of a vascular component to degeneration of the dementia-relevant regions precuneus and hippocampus, which are supplied by the distal anterior and posterior cerebral arteries^{45, 46}. Alternatively, if no T^* measurements are available, our ROI-based T^* values can be used to improve CBF quantification for regional T^* variation in the elderly.

In **Chapters 8 and 9**, we investigated correlations between CBF measured within GM, normal appearing WM (NAWM) and WML ROIs and WML volume, as well as with other clinical and hematological parameters. These measurements were performed in elderly with hypertension (**Chapter 8**) and children with sickle cell disease (SCD) (**Chapter 9**). It has been suggested that the WML in both populations share a similar cerebrovascular etiology⁴⁷. In **Chapter 8**, GM CBF was higher than NAWM CBF, which was higher than WML CBF. Interestingly, the ratios between GM, NAWM and WML CBF were comparable to ratios that were previously reported with contrast-based perfusion MRI^{40, 48, 49}. Although SNR may be too low for sufficient precision of ASL-based WM CBF measurements in the elderly, the accuracy of ASL as compared to contrast-based perfusion MRI appears sufficient within the WM. The fact that WM CBF was correlated with hematological parameters in children with SCD (**Chapter 9**) shows that WM CBF measurements can be sufficiently reliable for clinical correlations. This can be explained by the shorter T^* and higher CBF in children with SCD, leading to higher SNR for ASL-based WM CBF measurements. Furthermore, physiological perfusion fluctuations are lower for WM than for GM CBF, which may also increase statistical power¹¹. These findings show potential for ASL-based perfusion measurements within the NAWM and WML ROIs in children with SCD.

The clinical question in **Chapter 8** was whether WML volume is associated with either isolated focal or also with more general perfusion deficits, using the methodologies that were introduced in **Chapters 6 and 7**. Both hypotheses are deemed plausible^{25, 26, 50, 51} but not yet fully elucidated. Hence, it is hitherto unknown which of these two hypotheses should be given priority in terms of further research or treatment development. In our study, WML volume was correlated with WML CBF but not with NAWM CBF or GM CBF. As abovementioned, the fact that CBF was lower within WML regions than in regions with NAWM is in agreement with previous literature based on MRI perfusion measurements with exogenous contrast agents^{40, 48, 49}. The correlation between WML CBF and WML volume can - at least partly - be attributed to various degrees of ASL signal contamination from the NAWM into the WML, especially considering the large spatial extent of signal contamination as discussed in **Chapter 6**.

To what extent the WML CBF is truly correlated to WML volume cannot be differentiated with these data.

The absence of a correlation between GM CBF and WML volume in **Chapter 8** disagrees with some previous studies^{26, 51, 52}. Possible explanations include that the strength of this correlation depends upon the study population, techniques used for the detection of WML and measurement of CBF, the presence of perfusion confounders and the type of statistical analysis. Future research should aim at disentangling effects generated by the multitude of diseases that are associated with aging, such as cardiovascular disease, large- and small vessel cerebrovascular disease and neurodegeneration. Although the studied cohort was restricted to community dwelling elderly with hypertension without any serious medical conditions, the abovementioned diseases can still be expected to be present in such a population. Another question that is left to be answered is whether the correlation between GM CBF and WML volume found in other populations is of a causal nature or that the two are simply synchronous consequences of a worsening condition of the cerebral vasculature.

In **Chapter 9**, these WML are discussed in the context of children with SCD. Similar to WML in the elderly, two hypotheses exist that could explain the development of WML. The first relates to endothelial dysfunction^{61, 62}. In SCD, sickled red blood cells and other inflammatory mediators induce the activation of the endothelium, leading to impaired vasodilation and increased adhesiveness of the endothelium⁶³. Markers of endothelial dysfunction, such as ADAMTS13, have been shown to be correlated with WML in SCD⁶⁴. Our findings show that this marker is also correlated to CBF. The second pathophysiological hypothesis is related to the loss of cerebrovascular reactivity⁵³: the severe chronic anemia in these children can apparently be mostly compensated by increased CBF due to increased cardiac output and cerebral vasodilation^{54, 55}. However, this means that CBF cannot be increased much more in periods of increased demand for oxygen and nutrients to sustain cerebral metabolism. In other words, the cerebrovascular reactivity is reduced in these children, and moments of transient ischemia may lead to the development of WML^{53, 56}. Fetal hemoglobin (HbF) is a type of hemoglobin that does not polymerize and reduces the concentration of pathological hemoglobin S (HbS)^{58, 59}. Our results showed that children with lower fetal hemoglobin (HbF) levels had both higher CBF and higher WML volume. These findings could suggest that children with lower HbF levels require a higher compensatory CBF increase to sustain their cerebral metabolism. In addition, they suggest that low HbF levels and high CBF lead to more WMLs development, possibly as a result of a more impaired cerebrovascular reactivity. Therefore, although we did not find a direct correlation between CBF and WML volume, these findings are in agreement with the cerebrovascular reactivity hypothesis⁵⁷. It should

be noted that part of the investigated population was treated with hydroxyurea therapy. This therapy increases the level of HbF, which is known to reduce several symptoms of this disease with less side effects than chronic blood transfusion therapy⁶⁰. Our finding that CBF is inversely correlated with HbF implicates that less compensatory CBF increase is required with higher HbF levels. Hence, cerebrovascular reactivity can potentially be restored by increasing HbF levels. From these findings we can hypothesize that patients with high baseline CBF benefit the most by increasing HbF levels with hydroxyurea therapy. In this respect, ASL could potentially develop as a non-invasive biomarker.

Conclusions

Part I Inter-vendor reproducibility of ASL

- 1 On a voxel level, CBF measurements from different vendors are only comparable when the same readout modules are used (**Chapters 2-5**).
- 2 Differences between 2D and 3D ASL sequences can be mainly explained by differences in T^* sensitivity, PSF and efficiency of background suppression (**Chapters 2-4**).
- 3 Differences in ASL sequence parameters should be avoided, since even slight differences in ASL sequence parameters can have a large effect upon the reproducibility (**Chapter 5**).

Part II Clinical applicability of ASL

- 4 Uncontaminated WM perfusion signal can be detected with ASL, if tissue masks are carefully eroded to minimize GM contamination (**Chapter 6**).
- 5 The statistical power of ASL may be increased by moderate vascular crushing, suggesting that removing macro-vascular perfusion variability can be more important than holding on to sufficient SNR (**Chapter 7**).
- 6 Information from T^* measurements may carry important diagnostic value and simultaneous measurements of CBF and T^* should be carried out when possible (**Chapters 7-8**).
- 7 WML volume is correlated with WML CBF but not with normal appearing WM or GM CBF in elderly with hypertension, suggesting that WML development is the result of local rather than systemic perfusion disturbances (**Chapter 8**).
- 8 WM CBF is correlated with clinically relevant hematological parameters in children with SCD, alluding to the possible development of ASL-based CBF measurements as a non-invasive biomarker in this population (**Chapter 9**).

Implications

The conclusions of the inter-vendor reproducibility studies (**Part I**) have the following implications for the development of ASL for clinical studies. We have demonstrated the importance of keeping ASL sequence parameters identical, in order to be able to pool ASL-based CBF data (**Chapters 2-5**). An important practical single-center example is the update of scanner hardware or software in the middle of a cross-sectional or longitudinal clinical trial, which may lead to or require small changes in ASL sequence parameters. These results encourage investigators to carefully tweak sequence parameters to keep them as identical as possible between the scans before and after the scanner update. The same should be attempted when multi-center studies are being planned. When this is not possible - e.g. when pooling data from existing multi-center ASL studies where product sequences have been used - investigators are encouraged to acknowledge the effects of using different sequences. Main examples that result from different readout modules are discussed in this thesis, including 'TT' sensitivity (**Chapters 2-3**), PSF (**Chapter 2**) and background suppression efficiency (**Chapters 2-4**). For clinical practice, absolute quantitative agreement between ASL sequences may not be required. Therefore, slight sequence differences may be less of an issue here and we recommend instead to only focus on using the same readout when visually comparing CBF maps between different clinical centers. Alternatively, it may be helpful to remove data smoothness differences (**Chapter 3**) that result from the differences in PSF between product sequences. This could be easily implemented as post-processing option in medical imaging software.

The conclusions of the clinical applicability studies (**Part II**) have the following implications for the development of ASL for clinical studies. We have demonstrated the possibility to estimate the effective spatial extent of GM signal contamination within acquired data (**Chapter 6**). We showed the possibility to measure uncontaminated WM signal, but also highlighted the importance to acknowledge this spatial extent of signal contamination. The findings of **Part I** imply that, as ASL technology advances, the reliability of ASL will at some point be limited by physiological perfusion fluctuations rather than measurement precision. These findings are reinforced by the findings in elderly with hypertension in **Chapter 7**, implying that it can be more important to reduce physiological perfusion fluctuations than to hold on to sufficient SNR in large clinical studies. Although it has been shown for individual clinical cases, the results of **Chapters 7** and **8** are the first to imply that 'TT' measurements can be more important than CBF measurements in large clinical studies. This finding encourages research physicians to focus on more perfusion parameters than CBF only and stimulate the current development of sequences that can simultaneously measure CBF and 'TT'. **Chapters 8** and **9** provide examples on how

ASL perfusion measurements can bridge the research gap between clinical or hematological parameters and accumulated cerebral pathology such as WML.

When the study subjects and findings of this thesis are compared with previous ASL theses, we can conclude that ASL steadily advances towards a more stable position within clinical research. In this respect, the limitations of ASL are shifting from fundamental sequence development limitations to sequence choices by MRI vendors, physiological perfusion fluctuations and the confounding effect of TT. Current developments aimed at WM perfusion measurements, the simultaneous measurement of CBF and TT and the reduction of the influence of physiological perfusion fluctuations are expected to increase the clinical value of ASL even further. Future efforts aimed at the creation of normal and pathological perfusion templates may eventually enable the development of ASL as clinical and psychopharmacological biomarker.

Reference list

1. Chen Y, Wang DJ, Detre JA. Test-retest reliability of arterial spin labeling with common labeling strategies. *J Magn Reson Imaging* 2011; **33(4)**:940-949.
2. Kilroy E, Apostolova L, Liu C, Yan L, Ringman J, Wang DJ. Reliability of two-dimensional and three-dimensional pseudo-continuous arterial spin labeling perfusion MRI in elderly populations: Comparison with 15o-water positron emission tomography. *J Magn Reson Imaging* 2013.
3. Liu T, Wierenga C, Mueller B, F-BIRN. Reliability and Reproducibility of Arterial Spin Labeling Perfusion Measures Assessed with a Multi-Center Study. In: International Society of Magnetic Resonance in Medicine; 2008. p. 3338.
4. Petersen ET, Mouridsen K, Golay X. The QUASAR reproducibility study, Part II: Results from a multi-center Arterial Spin Labeling test-retest study. *Neuroimage* 2010; **49(1)**:104-113.
5. Wu WC, Jiang SF, Yang SC, Lien SH. Pseudocontinuous arterial spin labeling perfusion magnetic resonance imaging--a normative study of reproducibility in the human brain. *Neuroimage* 2011; **56(3)**:1244-1250.
6. Xu G, Rowley HA, Wu G, Alsop DC, Shankaranarayanan A, Dowling M, *et al.* Reliability and precision of pseudo-continuous arterial spin labeling perfusion MRI on 3.0 T and comparison with 15O-water PET in elderly subjects at risk for Alzheimer's disease. *NMR Biomed* 2010; **23(3)**:286-293.
7. Alsop DC, Detre JA, Golay X, Gunther M, Hendrikse J, Hernandez-Garcia L, *et al.* Recommended implementation of arterial spin-labeled perfusion MRI for clinical applications: A consensus of the ISMRM perfusion study group and the European consortium for ASL in dementia. *Magn Reson Med* 2014.
8. Gevers S, van Osch MJ, Bokkers RP, Kies DA, Teeuwisse WM, Majoie CB, *et al.* Intra- and multicenter reproducibility of pulsed, continuous and pseudo-continuous arterial spin labeling methods for measuring cerebral perfusion. *J Cereb Blood Flow Metab* 2011; **31(8)**:1706-1715.
9. Heijtel DF, Mutsaerts HJ, Bakker E, Schober P, Stevens MF, Petersen ET, *et al.* Accuracy and precision of pseudo-continuous arterial spin labeling perfusion during baseline and

- hypercapnia: a head-to-head comparison with $(1)(5)\text{O}$ $\text{H}(2)\text{O}$ positron emission tomography. *Neuroimage* 2014; **92**:182-192.
10. Floyd TF, Ratcliffe SJ, Wang J, Resch B, Detre JA. Precision of the CASL-perfusion MRI technique for the measurement of cerebral blood flow in whole brain and vascular territories. *J Magn Reson Imaging* 2003; **18(6)**:649-655.
 11. Parkes LM, Rashid W, Chard DT, Tofts PS. Normal cerebral perfusion measurements using arterial spin labeling: reproducibility, stability, and age and gender effects. *Magn Reson Med* 2004; **51(4)**:736-743.
 12. Vidorreta M, Wang Z, Rodriguez I, Pastor MA, Detre JA, Fernandez-Seara MA. Comparison of 2D and 3D single-shot ASL perfusion fMRI sequences. *Neuroimage* 2012; **66C**:662-671.
 13. Skup M. Longitudinal fMRI analysis: A review of methods. *Stat Interface* 2010; **3(2)**:232-252.
 14. Ridgway GR, Litvak V, Flandin G, Friston KJ, Penny WD. The problem of low variance voxels in statistical parametric mapping; a new hat avoids a 'haircut'. *Neuroimage* 2012; **59(3)**:2131-2141.
 15. Ghariq E, Chappell MA, Schmid S, Teeuwisse WM, van Osch MJ. Effects of background suppression on the sensitivity of dual-echo arterial spin labeling MRI for BOLD and CBF signal changes. *Neuroimage* 2014; **103C**:316-322.
 16. Hendrikse J, Petersen ET, van Laar PJ, Golay X. Cerebral border zones between distal end branches of intracranial arteries: MR imaging. *Radiology* 2008; **246(2)**:572-580.
 17. Wu B, Lou X, Wu X, Ma L. Intra- and interscanner reliability and reproducibility of 3D whole-brain pseudo-continuous arterial spin-labeling MR perfusion at 3T. *J Magn Reson Imaging* 2013.
 18. Petersen ET, De Vis JB, Van den Berg CAT, Hendrikse J. Turbo-QUASAR: a signal-to-noise optimal arterial spin labeling and sampling strategy. In: International Society for Magnetic Resonance in Medicine; 2013.
 19. Teeuwisse WM, Schmid S, Ghariq E, Veer IM, van Osch MJ. Time-encoded pseudocontinuous arterial spin labeling: Basic properties and timing strategies for human applications. *Magn Reson Med* 2014.
 20. Murphy K, Harris AD, Diukova A, Evans CJ, Lythgoe DJ, Zelaya F, *et al.* Pulsed arterial spin labeling perfusion imaging at 3 T: estimating the number of subjects required in common designs of clinical trials. *Magn Reson Imaging* 2011; **29(10)**:1382-1389.
 21. Edlow BL, Giacino JT, Wu O. Functional MRI and outcome in traumatic coma. *Curr Neurol Neurosci Rep* 2013; **13(9)**:375.
 22. Gunther M, Oshio K, Feinberg DA. Single-shot 3D imaging techniques improve arterial spin labeling perfusion measurements. *Magn Reson Med* 2005; **54(2)**:491-498.
 23. Koretsky AP. Early development of arterial spin labeling to measure regional brain blood flow by MRI. *Neuroimage* 2012; **62(2)**:602-607.
 24. Yamaji S, Ishii K, Sasaki M, Imamura T, Kitagaki H, Sakamoto S, *et al.* Changes in cerebral blood flow and oxygen metabolism related to magnetic resonance imaging white matter hyperintensities in Alzheimer's disease. *J Nucl Med* 1997; **38(9)**:1471-1474.
 25. Brickman AM, Zahra A, Muraskin J, Steffener J, Holland CM, Habeck C, *et al.* Reduction in cerebral blood flow in areas appearing as white matter hyperintensities on magnetic resonance imaging. *Psychiatry Res* 2009; **172(2)**:117-120.
 26. Zhang Q, Stafford RB, Wang Z, Arnold SE, Wolk DA, Detre JA. Microvascular Perfusion Based on Arterial Spin Labeled Perfusion MRI as a Measure of Vascular Risk in Alzheimer's Disease. *J Alzheimers Dis* 2012; **32(3)**:677-687.
 27. van Gelderen P, de Zwart JA, Duyn JH. Pitfalls of MRI measurement of white matter perfusion based on arterial spin labeling. *Magn Reson Med* 2008; **59(4)**:788-795.
 28. van Osch MJ, Teeuwisse WM, van Walderveen MA, Hendrikse J, Kies DA, van Buchem MA. Can arterial spin labeling detect white matter perfusion signal? *Magn Reson Med* 2009; **62(1)**:165-173.

29. Dai W, Carmichael OT, Lopez OL, Becker JT, Kuller LH, Gach HM. Effects of image normalization on the statistical analysis of perfusion MRI in elderly brains. *J Magn Reson Imaging* 2008; **28(6)**:1351-1360.
30. Wu WC, Lin SC, Wang DJ, Chen KL, Li YD. Measurement of cerebral white matter perfusion using pseudocontinuous arterial spin labeling 3T magnetic resonance imaging--an experimental and theoretical investigation of feasibility. *PLoS One* 2013; **8(12)**:e82679.
31. Pohmann R. Accurate, localized quantification of white matter perfusion with single-voxel ASL. *Magn Reson Med* 2010; **64(4)**:1109-1113.
32. Wu WC, St Lawrence KS, Licht DJ, Wang DJ. Quantification issues in arterial spin labeling perfusion magnetic resonance imaging. *Top Magn Reson Imaging* 2010; **21(2)**:65-73.
33. MacIntosh BJ, Graham SJ. Magnetic resonance imaging to visualize stroke and characterize stroke recovery: a review. *Front Neurol* 2013; **4**:60.
34. Donahue J, Sumer S, Wintermark M. Assessment of collateral flow in patients with cerebrovascular disorders. *J Neuroradiol* 2013.
35. MacIntosh BJ, Swardfager W, Robertson AD, Tchistiakova E, Saleem M, Oh PI, *et al*. Regional Cerebral Arterial Transit Time Hemodynamics Correlate with Vascular Risk Factors and Cognitive Function in Men with Coronary Artery Disease. *AJNR Am J Neuroradiol* 2014.
36. Al-Bachari S, Parkes LM, Vidyasagar R, Hanby MF, Tharaken V, Leroi I, *et al*. Arterial spin labelling reveals prolonged arterial arrival time in idiopathic Parkinson's disease. *Neuroimage Clin* 2014; **6**:1-8.
37. Wang J, Alsop DC, Song HK, Maldjian JA, Tang K, Salvucci AE, *et al*. Arterial transit time imaging with flow encoding arterial spin tagging (FEAST). *Magn Reson Med* 2003; **50(3)**:599-607.
38. Chen Y, Wang DJ, Detre JA. Comparison of arterial transit times estimated using arterial spin labeling. *MAGMA* 2012; **25(2)**:135-144.
39. Brown WR, Thore CR. Review: cerebral microvascular pathology in ageing and neurodegeneration. *Neuropathol Appl Neurobiol* 2011; **37(1)**:56-74.
40. Makedonov I, Black SE, MacIntosh BJ. Cerebral small vessel disease in aging and Alzheimer's disease: a comparative study using MRI and SPECT. *Eur J Neurol* 2013; **20(2)**:243-250.
41. Mezue M, Segerdahl AR, Okell TW, Chappell MA, Kelly ME, Tracey I. Optimization and reliability of multiple postlabeling delay pseudo-continuous arterial spin labeling during rest and stimulus-induced functional task activation. *J Cereb Blood Flow Metab* 2014; **34(12)**:1919-1927.
42. Teeuwisse WM, Schmid S, Ghariq E, Veer IM, van Osch MJ. Time-encoded pseudocontinuous arterial spin labeling: Basic properties and timing strategies for human applications. *Magn Reson Med* 2014; **72(6)**:1712-1722.
43. Sousa I, Vilela P, Figueiredo P. Reproducibility of the quantification of arterial and tissue contributions in multiple postlabeling delay arterial spin labeling. *J Magn Reson Imaging* 2014; **40(6)**:1453-1462.
44. Nowinski WL, Chua BC, Marchenko Y, Puspitsari F, Volkau I, Knopp MV. Three-dimensional reference and stereotactic atlas of human cerebrovasculature from 7Tesla. *Neuroimage* 2011; **55(3)**:986-998.
45. Szabo K, Forster A, Jager T, Kern R, Griebe M, Hennerici MG, *et al*. Hippocampal lesion patterns in acute posterior cerebral artery stroke: clinical and MRI findings. *Stroke* 2009; **40(6)**:2042-2045.
46. Cavanna AE, Trimble MR. The precuneus: a review of its functional anatomy and behavioural correlates. *Brain* 2006; **129(Pt 3)**:564-583.
47. Van der Land V., Zwanenburg JJ, Biemond BJ, Hendrikse J, Mutsaerts HJMM, Engelen M, *et al*. Cerebral small vessel disease in patients with sickle cell disease: initial findings with ultra-high field 7T MRI. In: Annual Meeting and Exposition. New Orleans: Blood; 2013.

48. Sachdev P, Wen W, Shnier R, Brodaty H. Cerebral blood volume in T2-weighted white matter hyperintensities using exogenous contrast based perfusion MRI. *J Neuropsychiatry Clin Neurosci* 2004; **16(1)**:83-92.
49. O'Sullivan M, Lythgoe DJ, Pereira AC, Summers PE, Jarosz JM, Williams SC, *et al.* Patterns of cerebral blood flow reduction in patients with ischemic leukoaraiosis. *Neurology* 2002; **59(3)**:321-326.
50. Erten-Lyons D, Woltjer R, Kaye J, Mattek N, Dodge HH, Green S, *et al.* Neuropathologic basis of white matter hyperintensity accumulation with advanced age. *Neurology* 2013; **81(11)**:977-983.
51. Benedictus MR, Binnewijzend MA, Kuijjer JP, Steenwijk MD, Versteeg A, Vrenken H, *et al.* Brain volume and white matter hyperintensities as determinants of cerebral blood flow in Alzheimer's disease. *Neurobiol Aging* 2014; **35(12)**:2665-2670.
52. Bastos-Leite AJ, Kuijjer JP, Rombouts SA, Sanz-Arigita E, van Straaten EC, Gouw AA, *et al.* Cerebral blood flow by using pulsed arterial spin-labeling in elderly subjects with white matter hyperintensities. *AJNR Am J Neuroradiol* 2008; **29(7)**:1296-1301.
53. Prohovnik I, Hurllet-Jensen A, Adams R, De VD, Pavlakis SG. Hemodynamic etiology of elevated flow velocity and stroke in sickle-cell disease. *J Cereb Blood Flow Metab* 2009; **29(4)**:803-810.
54. Arkuszewski M, Krejza J, Chen R, Melhem ER. Sickle cell anemia: reference values of cerebral blood flow determined by continuous arterial spin labeling MRI. *Neuroradiol J* 2013; **26(2)**:191-200.
55. Oguz KK, Golay X, Pizzini FB, Freer CA, Winrow N, Ichord R, *et al.* Sickle cell disease: continuous arterial spin-labeling perfusion MR imaging in children. *Radiology* 2003; **227(2)**:567-574.
56. Dowling MM, Quinn CT, Rogers ZR, Buchanan GR. Acute silent cerebral infarction in children with sickle cell anemia. *Pediatr Blood Cancer* 2010; **54(3)**:461-464.
57. Steinberg MH, Chui DH, Dover GJ, Sebastiani P, Alsultan A. Fetal hemoglobin in sickle cell anemia: a glass half full? *Blood* 2014; **123(4)**:481-485.
58. Connes P, Verlhac S, Bernaudin F. Advances in understanding the pathogenesis of cerebrovascular vasculopathy in sickle cell anaemia. *Br J Haematol* 2013; **161(4)**:484-498.
59. Bailey K, Morris JS, Thomas P, Serjeant GR. Fetal haemoglobin and early manifestations of homozygous sickle cell disease. *Arch Dis Child* 1992; **67(4)**:517-520.
60. Charache S, Terrin ML, Moore RD, Dover GJ, Barton FB, Eckert SV, *et al.* Effect of hydroxyurea on the frequency of painful crises in sickle cell anemia. Investigators of the Multicenter Study of Hydroxyurea in Sickle Cell Anemia. *N Engl J Med* 1995; **332(20)**:1317-1322.
61. Belcher JD, Chen C, Nguyen J, Milbauer L, Abdulla F, Alayash AI, *et al.* Heme triggers TLR4 signaling leading to endothelial cell activation and vaso-occlusion in murine sickle cell disease. *Blood* 2014; **123(3)**:377-390.
62. Chen J, Hobbs WE, Le J, Lenting PJ, de Groot PG, Lopez JA. The rate of hemolysis in sickle cell disease correlates with the quantity of active von Willebrand factor in the plasma. *Blood* 2011; **117(13)**:3680-3683.
63. Manwani D, Frenette PS. Vaso-occlusion in sickle cell disease: pathophysiology and novel targeted therapies. *Hematology Am Soc Hematol Educ Program* 2013; **2013**:362-369.
64. Colombatti R, De BE, Bertomoro A, Casonato A, Pontara E, Omenetto E, *et al.* Coagulation activation in children with sickle cell disease is associated with cerebral small vessel vasculopathy. *PLoS One* 2013; **8(10)**:e78801.

11

Summary

Samenvatting

Summary

This summary concerns the thesis *Arterial spin labeling, inter-vendor reproducibility and clinical applicability*. Maintenance of adequate cerebral perfusion is of vital importance for the health, growth and repair of brain tissue. Arterial spin labeling (ASL) is a perfusion magnetic resonance imaging (MRI) technique that non-invasively measures cerebral blood flow (CBF). Its non-invasiveness has considerable research advantages: it is possible to repeat CBF measurements as frequently as desired and its measurements can be applied in vulnerable populations. ASL relies on the use of blood water protons as its endogenous label: blood is labeled in proximal arteries in the neck and after a post-labeling delay (PLD) - during which blood travels to the brain parenchyma - the brain is imaged. After the subtraction with a brain image without previous labeling, the resulting image is proportional to CBF. Since its inception, ASL has matured to a whole-brain perfusion technique that is available on all major MRI systems. Its accuracy and precision are comparable with existing invasive perfusion modalities and clinical and psychopharmacological research applications of ASL are rapidly evolving. Large clinical multi-center ASL studies may extend our understanding of the pathophysiology of many common neurological and psychiatric disorders. The first aim of this thesis was to investigate the inter-vendor reproducibility of ASL. The second aim of this thesis was to investigate several clinical applicabilities of ASL.

The first part of this thesis concerns the inter-vendor reproducibility of ASL. The ASL product sequences of two major MRI vendors were compared in **Chapters 2-4**. Throughout these chapters, the inter-session variation was comparable on a total gray matter (GM) level but not on a voxel level. In addition, the mean of baseline CBF measurements (**Chapter 2**) showed excellent agreement between the sequences on a total GM level, but again not on a voxel level. This led to the conclusion that on a total GM level, long-term physiological perfusion fluctuation dominates differences between sequences and scanners. The fact that CBF data from smaller regions of interest (ROIs) were not comparable between the different sequences could be explained by fundamental differences between the 2D EPI and 3D spiral readout modules, including differences in effective PLD leading to differences in transit time (TT) sensitivity, the extent of point spread function and efficiency of background suppression. Measurements of pharmacologically induced (**Chapter 3**) and task-based (**Chapter 4**) CBF changes were not in agreement with the different sequences. This could be attributed to differences in effective PLD between the 2D EPI and 3D spiral readouts leading to differences in TT sensitivity. In **Chapter 5**, pseudo-continuous ASL sequences were implemented on three major MRI vendors with the same readout module. Because of scanner hardware limitations, two dual vendor comparison studies were performed with slightly different sequence parameters, with three vendors in total, one vendor joining

both studies. Whereas the mean and inter-session variation of CBF were comparable on a voxel level between different vendors with identical sequence parameters, this was not the case when the slightly different sequences from the two studies were compared on the same vendor. Together with the results in **Chapters 2-4**, these results show the importance to keep sequences in multi-center ASL studies as identical as possible.

The second part of this thesis is focused on the clinical applicability of ASL. Despite their potential relevance for clinical studies, white matter (WM) CBF measurements with ASL are cumbersome. The definition of a WM ROI requires a delicate balance between including many voxels to counterbalance its low signal-to-noise ratio, and excluding peripheral voxels to avoid signal contamination from the GM. In **Chapter 6**, the spatial extent of GM contamination was investigated for a 2D EPI readout in elderly with mild cognitive complaints. The results show that significant WM perfusion signal can be measured, but also that the WM ROI should be carefully eroded to avoid GM contamination. In **Chapter 7**, the statistical benefits in terms of correlations with age and gender are shown for modest vascular crushing in a large population of elderly with hypertension, suggesting that the removal of macro-vascular perfusion variability outweighs the signal-to-noise ratio (SNR) decrease on a group level. Within the same population, correlations with age, gender (**Chapter 7**) and WM lesion (WML) volume (**Chapter 8**) were much larger with TT than with CBF. These findings encourage simultaneous measurements of CBF and TT in large clinical perfusion studies. Within the same population of elderly with hypertension, WML volume was correlated with WML CBF but not with normal appearing WM or GM CBF. This suggests that WML development is predominantly related to local rather than systemic perfusion disturbances. In children with sickle cell disease (SCD) (**Chapter 9**), CBF disturbances are believed to play a key role in the pathophysiology of WML. ASL-based CBF measurements were correlated with hematological parameters that are both involved in the pathogenesis of WML and they key targets in SCD treatment. This alludes to the possible development of ASL-based CBF measurements as a non-invasive predictor or biomarker of treatment response.

The main implication of this thesis is that investigators should strive to keep sequence parameters as identical as possible between different ASL datasets, whether this concerns a single-center scanner hardware update or pooling different multi-center ASL datasets. Differences in TT sensitivity, point spread function and background suppression between sequences should be acknowledged. For clinical practice, slight sequence differences may be less of an issue and we recommend instead to focus on sequence differences that are visually apparent when CBF maps are compared between different clinical centers. It may be helpful to remove data smoothness differences that result from point spread function

differences between product sequences. Furthermore, as ASL techniques advance, it becomes more important to reduce the influence of physiological perfusion fluctuations than to hold on to sufficient SNR in large clinical studies. TT measurements can provide information additional to CBF and simultaneous CBF and TT measurements are encouraged in clinical studies. Finally, ASL perfusion measurements can elucidate the relation between clinical or hematological parameters and accumulated cerebral pathology such as WML.

Samenvatting

Deze samenvatting betreft het proefschrift *Arterial spin labeling, inter-vendor reproducibility and clinical applicability*. Behoud van cerebrale perfusie is van wezenlijk belang voor de gezondheid, groei en het herstel van hersenweefsel. Arterial spin labeling (ASL) is een relatief nieuwe magnetic resonance imaging (MRI) techniek die op non-invasieve wijze cerebrale doorbloeding (cerebral blood flow, CBF) meet. Omdat ASL non-invasief is kan deze perfusiemeting zo vaak als gewenst herhaald worden en kan de meting worden toegepast bij kwetsbare patiënten. ASL is gebaseerd op het gebruik van bloed-water protonen als endogeen label. Het bloed wordt eerst gelabeld in proximale arteriën in de hals. Na een post-labeling delay (PLD) - waarin het gelabelde bloed naar het hersenweefsel stroomt - wordt een afbeelding verkregen van de hersenen. Van deze afbeelding wordt een afbeelding van de hersenen waarbij niet voorafgaand is gelabeld afgetrokken, resulterend in afbeelding gewogen voor CBF. In de laatste twintig jaar is ASL geëvolueerd tot een volwaardige perfusiemeting van de complete hersenen, die beschikbaar is op de meest voorkomende MRI-systemen. De nauwkeurigheid en precisie van ASL zijn vergelijkbaar met bestaande invasieve perfusiemetingen. Klinische en psychofarmacologische onderzoekstoepassingen van ASL zijn volop in ontwikkeling. Grote klinische multicenter ASL studies kunnen de pathofysiologische kennis van veelvoorkomende neurologische of psychiatrische ziektebeelden doen vergroten. Het eerste doel van dit proefschrift was het bestuderen van de reproduceerbaarheid van ASL tussen verschillende MRI merken (inter-vendor). Het tweede doel van dit proefschrift was om de klinische toepasbaarheid van ASL te onderzoeken.

Het eerste deel van dit proefschrift behelst de inter-vendor reproduceerbaarheid van ASL. ASL-series van twee veelgebruikte MRI merken werden vergeleken in **hoofdstukken 2-4**. In deze hoofdstukken was de inter-sessie variatie vergelijkbaar op totaal grijze stof (GS) niveau maar niet op voxel niveau. Uit **hoofdstuk 2** blijkt een grote overeenkomst tussen het gemiddelde van baseline CBF-metingen tussen de ASL-series op totaal GS niveau, maar wederom niet op voxel niveau. Dit leidt tot de conclusie dat - op een totaal GS niveau - lange termijn perfusiefluctuaties groter zijn dan verschillen tussen ASL-series. Het feit dat CBF-data in kleinere gebieden niet vergelijkbaar waren tussen de verschillende series kan worden verklaard door fundamentele verschillen tussen 2D EPI en 3D spiral readout strategieën. Men denke aan verschillen in effectieve PLD die leiden tot verschillen in transit time (TT)-gevoeligheid, het bereik van de puntspreidfunctie en efficiëntie van achtergrondruisonderdrukking. De gemiddeld gemeten farmacologisch geïnduceerde (**hoofdstuk 3**) en op taak gebaseerde (**hoofdstuk 4**) CBF-veranderingen kwamen niet overeen tussen de verschillende ASL-series. Dit kan worden toegeschreven aan verschillen in effectieve PLD tussen 2D EPI en 3D spiraal readout strategieën, die leiden tot verschillen in TT-

gevoeligheid. In **hoofdstuk 5** werden pseudo-continue ASL-series geïmplementeerd met dezelfde 2D EPI readout strategie op scanners van drie veelgebruikte MRI merken. Vanwege beperkingen van de scanner-apparatuur werden twee aparte studies uitgevoerd waarin twee merken werden vergeleken, met minimaal verschillende ASL-serie instellingen. Eén merk participeerde in beide studies. Terwijl het gemiddelde en de inter-sessie variatie van CBF op voxel niveau tussen verschillende fabrikanten met identieke ASL-serie instellingen vergelijkbaar waren, was dit niet het geval wanneer de minimaal verschillende ASL-series van de twee aparte studies werden vergeleken op het merk dat aan beide studies deelnam. In combinatie met de resultaten van **hoofdstukken 2-4**, tonen deze resultaten aan dat van belang is de ASL-serie instellingen zo identiek mogelijk te houden bij multi-center ASL studies.

Het tweede deel van dit proefschrift is gericht op de klinische toepasbaarheid van ASL. Hoewel CBF-metingen met ASL in de witte stof (WS) zeer relevant kunnen zijn voor klinisch onderzoek, is de toepassing uitdagend. De definitie van een witte stof gebied vereist een subtiële balans tussen enerzijds het insluiten van zo veel mogelijk voxels om te compenseren voor de lage signaal-ruisverhouding, terwijl anderzijds perifere WS voxels zoveel mogelijk moeten worden uitgesloten om de inmenging van GS signaal (GS contaminatie) te voorkomen. In **hoofdstuk 6** werd het bereik van GS contaminatie onderzocht voor een 2D EPI readout strategie in ouderen met milde cognitieve klachten. De resultaten tonen aan dat significant perfusiesignaal kan worden gemeten in de WS, maar ook dat het WS gebied behoedzaam moet worden geërodeerd om GS contaminatie te voorkomen. In **hoofdstuk 7** werden de statistische voordelen getoond van milde vaatsuppressie in een grote populatie van ouderen met hypertensie, uitgedrukt in correlaties met leeftijd en geslacht. Deze voordelen van vaatsuppressie suggereren dat het verminderen van macro-vasculaire perfusievariabiliteit opweegt tegen de verminderde signaal-ruisverhouding op groepsniveau. Binnen dezelfde populatie waren correlaties met leeftijd en geslacht (**hoofdstuk 7**) en WS laesie (WSL) volume (**hoofdstuk 8**) groter met TT dan met CBF. Deze resultaten moedigen de gelijktijdige meting van CBF en TT aan voor grote klinische perfusiestudies. In dezelfde populatie van ouderen met hypertensie was het WSL volume gecorreleerd met WSL CBF, maar niet met CBF gemeten in normaal lijkende WS of GS (**hoofdstuk 8**). Dit suggereert dat de ontwikkeling van WSL eerder het gevolg van lokale dan van systemische perfusiestoornissen is. Perfusiestoornissen worden geacht een hoofdrol te spelen in de pathofysiologie van kinderen met sikkelcelziekte (**hoofdstuk 9**). CBF was gecorreleerd met hematologische parameters die betrokken zijn bij de pathogenese van WSL en waarvan de modificatie een groot deel van de behandeling van deze ziekte beslaat. Dit doet vermoeden dat CBF-metingen met ASL in de toekomst mogelijk als non-invasieve biomarker kunnen dienen voor patiënten met sikkelcelziekte.

De voornaamste implicatie van dit proefschrift is dat ASL-serie instellingen zo identiek mogelijk moeten worden gehouden tussen verschillende ASL datasets. Dit geldt zowel bij vernieuwingen van scanner apparatuur halverwege ASL studies als voor het samenvoegen van multicenter ASL datasets. Verschillen in TT-gevoeligheid, puntspreidfunctie en achtergrondruisonderdrukking tussen ASL-series dienen in acht te worden genomen. Voor de klinische praktijk is het wellicht niet zo belangrijk om verschillen in ASL-serie instellingen zo klein mogelijk te houden, maar het is des te belangrijker om de ASL-series tussen klinische centra visueel zo goed mogelijk overeen te laten komen. Zo is het aan te bevelen om visuele verschillen in smoothness te reduceren met post-processing software. Een andere implicatie van dit proefschrift – voor grote klinische studies – is dat, bij voortschrijdende ontwikkeling van de ASL meting, het steeds belangrijker wordt om fysiologische perfusievariatie te verminderen en minder belangrijk om de signaal-ruisverhouding zo hoog mogelijk te houden. Vervolgens kunnen TT-metingen toegevoegde waarde hebben bovenop CBF-metingen. Daarom is de ontwikkeling van ASL-series die gelijktijdig CBF en TT meten van groot belang voor klinische studies. Tenslotte kunnen ASL perfusiemetingen ingezet worden om de pathofysiologische kennis omtrent het ontstaan van WSL te vergroten.

List of abbreviations

List of abbreviations

%CBF↓	relative CBF decrease
3CV	triple Vendor Comparison

A

AC-PC line	anterior commissure-posterior commissure line
ACA	anterior cerebral artery
AD	Alzheimer's disease
AMC	academic medical center
ANOVA	analysis of variance
ASL	arterial spin labeling
ATT	arterial transit time

B

BMI	body mass index
BPF	brain parenchymal fraction
BOLD contrast	blood-oxygen-level dependent contrast

C

CASL	continuous ASL
CBF	cerebral blood flow
CBV	cerebral blood volume
CI	confidence interval
CLEAR	constant level appearance
CMRO ₂	cerebral metabolic rate of oxygen
CPP	cerebral perfusion pressure
CSF	cerebrospinal fluid
CV	coefficient of variation
CVD	cardiovascular disease
CVR	cerebrovascular resistance

D

DARTEL	diffeomorphic anatomical registration analysis using exponentiated lie algebra
DM	diabetes mellitus
DTI	diffusion tensor imaging

E

ELISA	enzyme-linked immunosorbent assay
EPI	echo-planar imaging

F

FA	flip angle
fASL	functional ASL
FEAST	flow encoding arterial spin tagging
FHWM	full width at half maximum
FLAIR	fluid attenuated inversion recovery
fMRI	functional MRI
FOV	field of view
FSE	fast spin echo
FT	finger tapping

G

G6PD	glucose-6-phosphate dehydrogenase
GE	General Electric
GLM	general linear model
GM	gray matter

H

Hb	hemoglobin
HbF	fetal hemoglobin
HbS	hemoglobin S
HPLC	high-performance liquid chromatography

I

ICC	intraclass correlation coefficient
ICV	intracranial volume
IQR	inter quartile range

L

LDH	lactate dehydrogenase
LOA	limits of agreement

M

MC	medical center
MCA	middle cerebral artery
MCI	mild cognitive impairment
MMSE	mini mental state examination
MRA	magnetic resonance angiography
MRI	magnetic resonance imaging

N

NAWM	normal appearing white matter
------	-------------------------------

O

OEF	oxygen extraction fraction
OR	odds ratio

P

PASL	pulsed ASL
PCA	posterior cerebral artery
PCASL	pseudo-continuous ASL
PD	proton density
PET	positron emission tomography
phASL	pharmacological ASL
PreDIVA	prevention of dementia by intensive vascular care
PLD	post-labeling delay
PSF	point spread function

PV	partial volume
R	
R	rest
RF	radiofrequency
RR	blood pressure
ROI	region of interest
S	
SCD	sickle cell disease
SCI	silent cerebral infarct
SENSE	sensitivity encoding
SD	standard deviation
SITT	Silent Infarct Transfusion Trial
SPIR	spectral pre-saturation by inversion recovery
SPM	statistical parametric mapping
SPSS	statistical package for the social sciences
STRIVE	Standards for Reporting Vascular changing on Neuroimaging
SVD	small vessel disease
SNR	signal-to-noise ratio
T	
T	Tesla
T1	longitudinal relaxation time
T2	transverse relaxation time
T1w	T1-weighted
TAT	thrombin-antithrombin complex
TCD	transcranial Doppler
TE	echo time
TOF	time of flight
t-PA	tissue plasminogen activator
TR	repetition time

V

VESPA	VEndor SPecific features of Asl
VU	Vrije Universiteit
VWF	Von Willebrand factor

W

WM	white matter
WMH	white matter hyperintensity
WML	white matter lesion
wsCV	within-subject coefficient of variation

Portfolio

Portfolio

Name: Henri J.M.M. Mutsaerts
 PhD period: April 2011 - March 2015
 Promotor: Prof. dr. C.B.L.M. Majoie
 Co-promotor: Dr. ir. A.J. Nederveen

General courses	Year	Workload (ECTS)
BROK course	2011	0.9
Systematic Reviews	2011	0.3
Clinical data management	2012	0.3

Specific courses

ESMRMB Perfusion MRI school Oxford	2011	1.0
In Vivo NMR	2011	1.0
COST AID ASL school Verona	2013	1.0
EIBIR Summer course Neurology Imaging	2013	1.0

Conferences

COST	2013 (2x), 2014 (2x)	2.0
ESMRMB	2012, 2013	0.5
ISMRM Benelux	2012, 2013, 2014	0.75
ISMRM	2012, 2013, 2014	3.0
ISMRM perfusion workshop	2012	0.5
NICA	2013	0.25
ESMRMB Brainstorm Session Vienna	2014	0.5

Teaching

PhD student (0.5 year)	2014	1.0
Bachelor student internship (2x11 weeks)	2014	1.0
MD student, research assistant (2.5 years)	2012, 2013, 2014	10.0

Poster presentations (2.5 ECTS)

Intra-scan reproducibility of total white matter perfusion in dementia using pseudo-continuous arterial spin labeling

ISMRM 2012, Melbourne

Blood T1 measurements in children with sickle cell disease ESMRMB 2013, Toulouse

Inter-vendor reproducibility of pseudo-continuous arterial spin labeling at 3T ESMRMB 2013, Toulouse

Dual-vendor comparison of arterial spin labeling with same labeling and readout modules ISMRM 2014, Milan

Inter-vendor reproducibility of arterial spin labeling cerebral blood flow measurements at 3T ISMRM 2014, Milan

Oral presentations (4.0 ECTS)

Intra-scan reproducibility of total white matter perfusion in dementia using pseudo-continuous arterial spin labeling

ESMRMB 2012, Lisbon

VEndor SPecific features and reproducibility of Arterial Spin Labeling: the VESPA study ISMRM perfusion workshop 2012, Amsterdam

Inter-vendor reproducibility of pseudo-continuous arterial spin labeling at 3 Tesla COST AID Action 2013, Brussels

Multi-vendor reliability of arterial spin labeling perfusion MRI using a near-identical sequence: implications for multi-center studies COST AID Action 2014, Milan

Whole brain arterial transit times in the elderly estimated using arterial spin labeling ISMRM 2013, Salt Lake City

Whole brain arterial transit times in the elderly estimated using arterial spin labeling ISMRM Benelux 2013, Rotterdam

ASL toolbox for post-processing, quality assurance and statistical analysis COST AID Action 2014, Dubrovnik

Circadian modulation of cerebral blood flow COST AID Action 2014, Dubrovnik

List of publications

International reviewed manuscripts

Mutsaerts HJMM, Steketee RME, Heijtel DFR, Kuijer JPA, Van Osch MJP, Majoie CBLM, Smits M, Nederveen AJ *Inter-vendor reproducibility of arterial spin labeling at 3 Tesla*. PlosOne 2014. In press

Mutsaerts HJMM, Richard E, Heijtel DF, Van Osch MJ, Majoie CB, Nederveen AJ *Gray matter contamination in arterial spin labeling white matter perfusion measurements in patients with dementia*. NeuroImage Clin. 4; 2014: 139-144

Heijtel DF, **Mutsaerts HJMM**, Bakker E, Schöber P, Steven MF, Petersen ET, Van Berckel BN, Majoie CB, Booij J, Van Osch MJ, Van Bavel E, Boellaard R, Lammertsma AA, Nederveen AJ *Accuracy and precision of pseudo-continuous arterial spin labeling perfusion during baseline and hypercapnia: a head-to-head comparison with ¹⁵O H₂O positron emission tomography*. NeuroImage 92; 2014: 182-92

Van der Land V, Hijmans CT, De Ruiter M, **Mutsaerts HJMM**, Cnossen MH, Engelen M, Majoie CB, Nederveen AJ, Grootenhuys MA, Fijnvandraat K *Volume of white matter hyperintensities is an independent predictor of intelligence quotient and processing speed in children with sickle cell disease*. Br J Haematol. 2014. In press

Mutsaerts, HJMM, Palm-Meinders IH, De Craen AJM, Reiber JHC, Blauw GJ, Van Buchem MA, Van der Grond J, Box FMA *Carotid artery wall shear stress is associated with cerebral infarcts and periventricular white matter lesions*. Stroke 42(12); 2011: 3497-501

Mutsaerts HJMM, Out M, Goedhart PT, Ince C, Hardeman MR, Romijn JA, Rabelink TJ, Reiber JHC, Box FMA *Improved viscosity modeling in patients with type 2 diabetes mellitus by accounting for enhanced red blood cell aggregation tendency*. Clinical Hemorheology and Microcirculation 44(4); 2010: 303-313

Articles in submission

Mutsaerts HJMM, Van Osch MJP, Zelaya FO, Wang DJJ, Nordhøy W, Wang Y, Wastling S, Fernandez-Seara M, Petersen ET, Pizzini FB, Fallatah S, Hendrikse J, Geier O, Günther M, Golay X, Nederveen AJ, Bjørnerud A, Groote IR *Multi-vendor reliability of arterial spin labeling perfusion MRI using an identical sequence: implications for multi-center studies*.

Mutsaerts HJMM, Steketee RME, Heijtel DFR, Kuijer JPA, Van Osch MJP, Majoie CBLM, Smits M, Nederveen AJ *Reproducibility of pharmacological ASL using sequences from different vendors: implications for multi-center drug studies*.

- Mutsaerts HJMM**, Van Dalen JW, Heijtel DFR, Majoie CBLM, Richard E, Nederveen AJ *Cerebral perfusion measurements in the elderly using arterial spin labeling.*
- Steketee RME, **Mutsaerts HJMM**, Bron EE, Van Osch MJP, Majoie CBLM, Van der Lugt A, Nederveen AJ, Smits M *Assessing feasibility of multicenter quantitative functional arterial spin labeling (fASL) in the motor cortex.*
- Van Dalen JW, **Mutsaerts HJMM**, Nederveen AJ, Vrenken H, Steenwijk M, Caan M, Majoie BLM, Van Gool P, Richard E *White matter hyperintensities in hypertension are not related to general perfusion deficits.*
- Heijtel DFR*, Schmid S*(joined 1st), **Mutsaerts HJMM**, Boellaard R, Lammertsma AA, Nederveen AJ, Van Osch MJP *Comparison of velocity and acceleration selective arterial spin labeling with ¹⁵O-H₂O positron emission tomograph.*
- Van der Land V, **Mutsaerts HJMM**, Engelen M, Heijboer H, Kuijpers TW, Nederkoorn PJ, Cnossen MH, Majoie CBLM, Nederveen AJ, Fijnvandraat K *Risk factor analysis of cerebral white matter hyperintensities in children with sickle cell disease*
- Steketee RME, Bron EE, Meijboom R, Houston GC, Klein S, **Mutsaerts HJMM**, Mendez Orellana CP, De Jong FJ, Van Swieten JC, Van der Lugt A, Smits M *Early-stage differentiation between presenile Alzheimer's disease and frontotemporal dementia using arterial spin labeling MRI.*
- Heijtel DFR, Petersen ET, **Mutsaerts HJMM**, Bakker E, Schober P, Stevens MF, Van Berckel BNM, Majoie CBLM, Booij J, Van Osch MJP, Van Bavel E, Boellaard R, Lammertsma AA, Nederveen AJ *Quantitative agreement between ¹⁵O-H₂O PET and model-free QUASAR MRI derived cerebral blood flow and arterial blood volume measurements.*
- Reneman L, Schagen S, Mulder M, **Mutsaerts HJMM**, Hageman G, De Ruiter M, *Cognitive impairment and associated loss in brain white microstructure in aircrew members exposed to engine oil fumes: is there an aviation safety concern?*
- Strang, AC, Van Wijk DF, **Mutsaerts HJMM**, Stroes ESG, Nederveen AJ, Rotmans JI, Rabelink TJ, Box FMA *Regression of carotid atherosclerosis relates to wall shear stress and pulse pressure in patients with type 2 diabetes mellitus.*
- Van der Land V, Zwanenburg JJ, Fijnvandraat K, Biemond BJ, Hendrikse J, **Mutsaerts HJMM**, Engelen M, Visser F, Nederveen AJ, Majoie CBLM, Luijten PR, Nederkoorn PJ *Cerebral Small Vessel Disease in Patients With Sickle Cell Disease - Initial findings with Ultra-High Field 7T MRI.*

Curriculum Vitae

Curriculum Vitae

Op 4 november 1983 ben ik geboren te 's-Hertogenbosch. Mijn middelbare schooltijd bracht ik door op het Gymnasium Juvenaat H.H. te Bergen op Zoom. Na mijn eindexamen als eerste lichting van de tweede fase studeerde ik Geneeskunde aan de Universiteit Leiden.

Tijdens mijn studie heb ik onder begeleiding van dr. FMA Box en prof. dr. ir. JHC Reiber onderzoek gedaan op de afdeling radiologie van het Leids Universitair Medisch Centrum (LUMC). Dit onderzoek resulteerde in publicaties in *Stroke* en *Clinical Hemorheology and Microcirculation*. Mijn interesse voor de medische beeldvorming was gewekt. Verder heb ik buiten Nederland klinische ervaring opgedaan in een huisarts-stage in Durham, Verenigd Koninkrijk en twee chirurgie-stages in Kaapstad, Zuid-Afrika. Bestuurlijke ervaring heb ik opgedaan door het organiseren van het Sempre Crescendo gala en het Leids Internationaal Medisch Studenten Congres en door het meelopen met de raad van bestuur van het LUMC. Na een senior co-schap radiologie in het LUMC behaalde ik in maart 2011 mijn artsexamen.

In april 2011 begon ik aan mijn promotietraject als arts-onderzoeker op de afdeling radiologie van het Academisch Medisch Centrum te Amsterdam, onder supervisie van prof. dr. CBLM Majoie en dr. ir. AJ Nederveen. Door de deelname aan een Europese COoperation in Science and Technology (COST)-actie heb ik onderzoekservaring in het buitenland mogen opdoen. Naast vele bijeenkomsten in binnen en buitenland, heb ik in het Oslo University Hospital te Oslo gewerkt, het Institute of Social Sciences te Oslo en in het Institute of Psychiatry van het King's College London. Hiernaast heb ik een zomercursus in Dubrovnik en een brainstorm-sessie in Wenen mogen meemaken. Deze internationale ervaringen hebben mijn promotietijd verrijkt.

Naast de medische wetenschap vormt muziek een rode draad in mijn leven.

Acknowledgments

Dankwoord

Dankwoord

Van 2011 tot 2015 ben ik met groot genoegen als arts-onderzoeker werkzaam geweest op de afdeling Radiologie van het AMC, hetgeen resulteerde in dit proefschrift. Hierbij ben ik geholpen door een groot aantal mensen. Een aantal hiervan benoem ik hieronder expliciet. Het is echter goed mogelijk dat ik hierbij onbedoeld een aantal mensen passeer. Daarom wil ik allereerst graag iedereen bedanken die een bijdrage heeft geleverd aan de totstandkoming van dit proefschrift, in welke hoedanigheid dan ook.

Graag betuig ik mijn dank aan alle gezonde vrijwilligers en patiënten die hebben deelgenomen aan de studies die beschreven zijn in dit proefschrift.

Hooggeachte professor Majoie, beste Charles, dank dat je mij als promotor hebt begeleid. Je interesse en uitgebreide kennis van de vasculaire neuroradiologie hebben mij veel geholpen. Je goede onderzoeksideeën hebben vaak uitkomst geboden en mij data vanaf een ander perspectief doen zien.

Zeer geachte heer Nederveen, beste Aart, zeer veel dank voor de grote reikwijdte aan mogelijkheden die jij mij geboden hebt om mijzelf als zelfstandig wetenschapper én als mens te ontwikkelen. Onze analytische, filosofische en ethische dialogen hebben mijn denkraam verruimd. De wijze waarop jij - met schijnbaar grenzeloze energie - wetenschap, management, religie en gezinsleven combineert is bewonderenswaardig.

Hooggeachte professor Van Bavel, hooggeachte professor Booij, zeer geachte mevrouw Reneman en zeer geachte heer Hendrikse van het AMC Amsterdam en UMC Utrecht, dank voor Uw besluit in mijn commissie plaats te nemen. Dear Professor Golay (University College London) and dear Professor Bjørnerud (Oslo University Hospital), I am very grateful for your decision to join my dissertation committee.

Dear co-authors, many thanks for your help and our fruitful collaboration. Zeer geachte heer Van Osch, beste Thijs, dank voor je onverzadigbare steun bij het herschrijven en bij rebuttals. Zeer geachte mevrouw Smits, beste Marion, dank voor onze enerverende gesprekken. Jouw enthousiasme voor onderzoek binnen de neuroradiologie is besmettelijk. Zeer geachte heer Richard, beste Edo, dank voor je hulp om tijdig een overschot aan analytisch divergeren te signaleren en weer te convergeren naar een praktisch klinisch doel. Zeer geachte mevrouw Fijnvandraat, beste Karin, zeer geachte mevrouw Schouten - Van Meeteren, beste Netteke en zeer geachte heer Biemond, beste Bart, dank voor jullie samenwerking en het mogelijk maken van klinisch onderzoek in het AMC.

Zeer geachte heer Groote, beste Inge, dank voor het mogelijk maken van mijn wetenschapsbezoeken aan Oslo. Jouw humor en filosofie geeft kleur aan de wetenschap en is voor mij een bron van inspiratie. Hopelijk lukt het ons in de toekomst de samenwerking tussen Amsterdam en Oslo verder te ontplooien.

Dear Mr. Zelaya, estimado Fernando, many thanks for organizing a wonderful research experience for me in London. I am looking forward to future research discussions and cooperations.

The work presented in several chapters of this thesis was founded within the European COoperation in Science and Technology (COST)- action Arterial spin labeling In Dementia BM1103. Dear international collaborators of this COST action, I am grateful to the fruitful and educative discussions that we had on our meetings, as well as for your contribution to a beautiful international ASL study.

Ik bedank graag de laboranten van de afdeling Radiologie van het AMC - in het bijzonder Sandra en Raschel - voor alle hulp en samenwerking.

Beste paranymfen, dank voor jullie vriendschap en het mij bijstaan.

Beste collegae onderzoekers, dank voor alle gezelligheid, humor, goede sfeer en samenwerking. Goed succes met jullie carrières als arts, onderzoeker of beide.

Beste Joena, Matthan en Paul, dank voor jullie enorme hulp en logistieke steun. Jullie zijn één van de belangrijkste redenen dat Z0 zo succesvol is.

Beste Sanna, dank voor het mij op weg helpen met ASL. Beste Dennis, dank voor onze samenwerking en het mij bijstaan op momenten dat ik wat minder handig was. Beste Rebecca, Veronica, Jan-Willem, Tanja, Sophie, Anouk en Kerim, dank voor de gezellige samenwerking en kleine kopjes koffie. Beste Folkert, dank dat jij de was wilt doen. Beste Lena, fijn om te zien dat het ASL onderzoek bij jou in goede handen is.

Beste Steffie, dank voor je enorme hulp bij de PIANO-studie. Jouw glimlach, assertiviteit en enthousiasme opent veel deuren.

Ik ben zeer erkentelijk voor de geweldige familie en vrienden die ik om mij heen heb. I am very grateful for being surrounded by wonderful family and friends. Je suis très reconnaissant pour avoir merveilleux famille et amis. Lieve Pappie en Mammie, dank dat jullie altijd voor Joep, Marjolein en mij klaarstaan - hier zijn geen woorden voor. Lieve Mammie, jij hebt je carrière in kunstgeschiedenis opgeofferd voor onze opvoeding. Lieve Ninette en Thieu, George en Xandra, dank dat jullie er voor mij zijn. Lieve Joep en Marjolein, dank voor de gezelligheid. Lieve Bonnemamman, dank voor alle keren dat ik bij jou in België heb mogen logeren. Jouw huis en tuin hebben mij een oase van rust geboden om ongestoord op mijn proefschrift te kunnen concentreren. Hoe jij jarenlang onophoudelijk voor Bonpapa hebt gezorgd na zijn herseninfarct en vasculaire dementie heeft mij doen realiseren waar wij wetenschappers ons onderzoek eigenlijk voor doen.

Beste Teun, ik zou eigenlijk willen zeggen dat onze roadtrips en gezamenlijke humor mij geleerd hebben het leven niet zo serieus te nemen. Maar dat is wellicht niet gepast als dankwoord in een promotieboekje.

Beste Pieter, Patrick en Cyriaan, dank voor jullie hulp bij mijn beslissing het hart voor de muziek en het brein voor de wetenschap te reserveren.

Dear Daphne and Richard, thank you for the music!

Statements pertaining to the thesis:

Stellingen behorende bij het proefschrift:

Arterial spin labeling perfusion MRI - Inter-vendor reproducibility & clinical applicability

- 1 On a voxel level, CBF measurements from different vendors are only comparable when the same readout modules are used (**Chapters 2-5**).
- 2 Differences between 2D and 3D ASL sequences can be mainly explained by differences in transit time sensitivity, point spread function and efficiency of background suppression (**Chapters 2-4**).
- 3 Differences in ASL sequence parameters should be avoided, since even slight differences in ASL sequence parameters can have a large effect upon the reproducibility (**Chapter 5**).
- 4 Uncontaminated white matter perfusion signal can be detected with ASL, if tissue masks are carefully eroded to minimize gray matter contamination (**Chapter 6**).
- 5 The statistical power of ASL may be increased by moderate vascular crushing, suggesting that removing macro-vascular perfusion variability can be more important than holding on to sufficient signal-to-noise ratio (**Chapter 7**).
- 6 Information from transit time measurements may carry important diagnostic value and simultaneous measurements of CBF and transit time should be carried out when possible (**Chapters 7-8**).
- 7 White matter lesion volume is correlated with white matter lesion CBF but not with CBF within the normal appearing white matter or gray matter in elderly with hypertension, suggesting that white matter lesion development is the result of local rather than systemic perfusion disturbances (**Chapter 8**).
- 8 WM CBF is correlated with clinically relevant hematological parameters in children with sickle cell disease, alluding to the possible development of ASL-based CBF measurements as a non-invasive biomarker in this population (**Chapter 9**).
- 9 Good coffee decreases both perfusion and confusion (**opinion**).
- 10 Similarities between white matter lesion characteristics in sickle cell disease and small vessel disease warrant combined research efforts between neuroradiologists, pediatric hematologists and neurologists (**opinion**).
- 11 White matter lesions are simply a consequence of evolution: regions that are least important for brain function survival are perfused last (but also least) (**opinion**).